



**HAL**  
open science

# Study on novel photochromic systems based on chromophores with six-membered ring as central ethene bridge

Yuheng Yang

► **To cite this version:**

Yuheng Yang. Study on novel photochromic systems based on chromophores with six-membered ring as central ethene bridge. Other. École normale supérieure de Cachan - ENS Cachan; East China University of science and technology (Shanghai, Chine), 2012. English. NNT : 2012DENS0023 . tel-00846636

**HAL Id: tel-00846636**

**<https://theses.hal.science/tel-00846636>**

Submitted on 19 Jul 2013

**HAL** is a multi-disciplinary open access archive for the deposit and dissemination of scientific research documents, whether they are published or not. The documents may come from teaching and research institutions in France or abroad, or from public or private research centers.

L'archive ouverte pluridisciplinaire **HAL**, est destinée au dépôt et à la diffusion de documents scientifiques de niveau recherche, publiés ou non, émanant des établissements d'enseignement et de recherche français ou étrangers, des laboratoires publics ou privés.

**THESE DE DOCTORAT  
DE L'ECOLE NORMALE SUPERIEURE DE CACHAN**

Présentée par

Monsieur Yuheng YANG

**pour obtenir le grade de**

**DOCTEUR DE L'ECOLE NORMALE SUPERIEURE DE CACHAN**

Domaine : Chimie

**Sujet de la thèse :**

**Etude de nouveaux systèmes photochromes basés sur des chromophores comportant un cycle à six atomes au niveau du pont éthène central**

**Study on Novel Photochromic Systems Based on Chromophores with Six-membered Ring as Central Ethene Bridge**

Thèse présentée et soutenue à Shanghai le 05 juin 2012 devant le jury composé de :

Yongfeng ZHOU	Professeur des Universités	Président
Guoyue SHI	Professeur des Universités	Rapporteur
Pei YU	Chargé de Recherches CNRS, HDR	Rapporteur
Weihong ZHU	Professeur des Universités	Co-Directeur de thèse
Keitaro NAKATANI	Professeur des Universités	Co-Directeur de thèse

**Cotutelle :**

Institute of Fine Chemicals  
East China University of Science and Technology  
230 Meilong Road, 200237 Shanghai (P.R. China)

Laboratoire de Photophysique et Photochimie Supramoléculaires et Macromoléculaires  
CNRS UMR 853 I  
Ecole Normale Supérieure de Cachan  
61, avenue du Président Wilson, 94235 CACHAN CEDEX (France)

---

## Study on Novel Photochromic Systems Based on Chromophores with Six-membered Ring as Central Ethene Bridge

### Abstract

Photochromism is defined as a light-induced reversible transformation of chemical species between two forms that have different absorption spectra. Molecules that are capable to interconvert reversibly interconverting between two isomers that differ in color are termed as photochromic compounds. Up to date, photochromic systems have become of increasing interest due to their applications in ophthalmic lenses and smart molecular materials acting as photoresponsive self-assemblies, molecular switches, logic gates and information storage. Particularly, bisthiénylenes (BTEs) are one of the most promising families due to their thermal irreversibility and outstanding fatigue resistance among various photochromic systems, in which the 1,3,5-hexatriene section can adopt an appropriate conformation to undergo the conrotatory  $6\pi$ -electron photocyclization, yielding a closed isomer.

Up to date, the rational design of symmetric or asymmetric BTEs have been mainly carried out on the right and left sides of aryl groups. In contrast, the central ethene bridges for the versatility in BTE architectures reported so far have been mostly confined to the cyclopentene unit or its strong electron-withdrawing analogs such as perfluoro-cyclopentene, maleic anhydride or maleic imide. As alternatives to this, several research groups have investigated the use of six-membered ethenes as BTE central bridge. However, due to the strong aromaticity of six-membered ring, thermal back reaction could be observed at room temperature and at dark. Since the ethene bridge with six-membered ring has its own advantages such as higher quantum yield in ring closure and longer absorption wavelength, we envision that the six-membered ring with non-aromaticity as the central ethene bridge might widely extend the diversity in the thermally irreversible photochromic systems.

In chapter 1, general introduction to the main parameters and definitions of organic photochromic compounds are given, such as photochromic reaction, isobestic point, ring closure reaction and ring opening reaction under the irradiation of UV and Visible light, photostationary state and fatigue resistance. Photochromic reactions can be divided into the two following catalogues: *cis-trans* isomerization and electrocyclic ring cyclizations. *Cis-trans* isomerization include azo-benzene and sterically crowded alkenes. Electrocyclic ring cyclizations include fulgides, spiropyran, spirooxazine and diarylethene. The photochromic performance and development of diarylethene photochromic system will be

discussed in detail as it is the major component of this thesis.

Chapter 2 mainly deals with BTTE with benzobisthiadiazole as central ethene bridge. Impressively, *c*-BTTE (the closed isomer of BTTE) exhibits excellent thermal stability and photochromic performance in various solvents. No obvious thermal back reaction could be observed even at elevated temperature in toluene at 80 °C. BTTE forms a typical D- $\pi$ -A system due to the strong electron accepting capability of benzobisthiadiazole and moderate donating ability of thiophene rings. Hence, the fluorescence of BTTE could be modulated by both solvato- and photochromism. Furthermore, BTTE shows excellent photochromic performance and thermal stability in single crystal state. By the introduction of strong electron withdrawing group of benzobisthiadiazole, high bistability and fluorescence switches could be achieved both in solution and crystal state, distinctly eliminating the bias against six-membered ethene bridge with thermal back reaction. This provides a new route to the bistable photochromic system based on six-membered ethene bridge.

Up to now, an insight into photochromic compounds with six-membered ring has seldom been involved. Accordingly, in chapter 3, we systematically report the synthesis and photochromic properties of three ethene bridges with different degrees in aromaticity (BTE-NA, BTA and BTTA). The relationship between aromaticity of the central ethene bridge and thermal stability has been well studied. The fluorescence of these three compounds can be well modulated by both solvato- and photo-chromism due to the strong internal charge transfer character. As demonstrated, an extremely low aromatic property of the central ethene bridge with benzobisthiadiazole unit finally leads to the thermally irreversible photochromic system (BTTA). Moreover, the small energy barrier between the parallel and anti-parallel conformers and great difference in absorption between BTTA and *c*-BTTA allow the full conversion from BTTA to *c*-BTTA.

A current challenge is the development in efficient strategies for the design of switchable nonlinear optical (NLO) materials. Accordingly, in chapter 4, benzothiadiazole was introduced as photoswitchable unit to modulate the changes of second harmonic generation, reflecting NLO properties. Most molecules with large first hyperpolarizability values  $\beta$  comprise  $\pi$  systems that are asymmetrically endcapped with donor and acceptor moieties. However, it costs tedious and hard manipulation of organic synthesis. To circumvent this, donor groups were directly linked to benzothiadiazole. Due to the difference in D- $\pi$ -A structure before and after irradiation, NLO signal is expected to change.

**Keywords:** Photochromism, bithienylethene, chromophore, benzothiadiazole, benzobisthiadiazole, aromaticity

## Table of Contents

Chapter 1	General Introduction to Organic Photochromic Compounds .....	1
1.1	Molecular devices.....	1
1.2	Molecular switches.....	1
1.3	Photochromism.....	2
1.4	Classifications of photochromic systems .....	4
1.4.1	Cis-Trans isomerization.....	5
1.4.2	Electrocyclization reactions.....	6
1.5	Diarylalkenes .....	7
1.5.1	Ring closing reaction.....	7
1.5.2	Quantum yield .....	9
1.5.3	Thermal stability.....	10
1.5.4	Fatigue resistance .....	10
1.6	Bisthienylethenes with different ethene bridges.....	11
1.6.1	Bisthienylethenes based on five-membered ethene bridge .....	11
1.6.2	Photochromic system based on tetraazaporphyrin and phthalocyanine .....	12
1.6.3	Benzothiophene as central ethene bridge .....	14
1.6.4	Imidazole based central ethene bridge .....	17
1.6.5	Thiazole as central ethene bridge .....	22
1.6.6	Oligothienoacene and thiophene bridged photochromic system.....	25
1.6.7	Miscellaneous photochromic systems .....	29
1.7	Photochromic diarylethene based on six-membered ring .....	31
1.8	Preview .....	34
Chapter 2	Unprecedented Stability of a Photochromic Bisthienylethene Based on Benzobisthiadiazole as Six-membered Ethene Bridge.....	36
2.1	Introduction .....	36
2.2	Experiment section .....	37
2.2.1	Instruments and Reagents.....	37
2.2.2	Synthetic route to the target and intermediate molecules.....	37
2.2.3	Preparation of target and intermediate molecules .....	38
2.2.4	UV-Vis spectra of BTTE.....	43

2.2.5	<sup>1</sup> H NMR changes of BTTE before and after irradiation.....	47
2.2.6	Emission spectra of BTTE before and after irradiation.....	48
2.2.7	The fluorescence decay of BTTE in various solvents .....	54
2.2.8	Thermal stability of BTTE in various solvents .....	56
2.2.9	Photochromism of BTTE in crystal state .....	58
2.3	Conclusions .....	60

### Chapter 3 Aromaticity-Controlled Thermal Stability of Photochromic Systems

#### Based on Six-Membered Ring as Ethene Bridges: Photochemical and Kinetic

Studies .....	62
3.1 Introduction .....	62
3.2 Experimental Section.....	63
3.2.1 Instruments and Reagents.....	63
3.2.2 Synthetic route to the target and intermediate molecules.....	63
3.2.3 Preparation of target and intermediate molecules .....	65
3.3 Results and discussion.....	72
3.3.1 Molecular design and synthesis.....	72
3.3.2 <sup>1</sup> H NMR, <sup>13</sup> C NMR and Mass characterization.....	73
3.3.3 UV-Vis absorption of BTE-NA, BTA and BTTA .....	81
3.3.4 <sup>1</sup> H NMR changes of BTE-NA, BTA and BTTA before and after irradiation.....	85
3.3.5 Fluorescence changes of BTE-NA, BTA and BTTA before and after irradiation.....	88
3.3.5 Thermal stability of BTE-NA, BTA and BTTA in various solvents .....	95
3.3.6 DFT calculation of BTE-NA, BTA and BTTA.....	98
3.3.7 Photochromic behavior of BTE-NA, BTA and BTTA in bulky crystal and sol-gel system.....	100
3.4 Conclusions .....	105

### Chapter 4 Nonlinear Optical Materials Based on Benzothiadiazole .....

4.1 Introduction .....	106
4.2 Experiment section .....	106
4.2.1 Instruments and Reagents.....	106
4.2.2 Synthetic route to the target and intermediate molecules.....	107
4.3 Results and discussion.....	110
4.3.1 Molecular design and synthesis.....	110

---

4.3.2 $^1\text{H}$ NMR, $^{13}\text{C}$ NMR and Mass characterization.....	111
4.3.3 UV-Vis absorption spectra of BTC, BTT and BTA.....	115
4.3.4 Emission spectra of BTC, BTT and BTA before and after irradiation .....	119
4.3.5 Second harmonic generation signal changes of BTC, BTT and BTA before and after irradiation .....	122
4.4 Conclusions .....	126
Chapter 5 Photochromic System Based on 2,1,3-Benzothiadiazole .....	127
5.1 Iridium complex utilizing a benzothiadiazole based photochromic unit as ligand .....	127
5.1.1 Instruments and Reagents.....	127
5.1.2 Synthetic route to the target and intermediate molecules.....	127
5.2 NLO photoswitchable system based on benzothiadiazole as central ethene bridge with extended system.....	129
5.2.1 Molecule design and synthesis .....	129
5.2.2 Synthetic route to the target molecule .....	129
5.3 Optical properties and photochromism .....	133
5.4 Conclusions .....	136
Chapter 6 Conclusions.....	137





## Chapter 1 General Introduction to Organic Photochromic Compounds

### 1.1 Molecular devices

A device is a tool or machine that is designed for a particular purpose to perform a specific task or function<sup>[1]</sup>. A molecular device, as the name implies, is composed of molecules that are designed to accomplish a specific function. Although the construction of molecular-scale devices might seem unthinkable, they already exist. The human body is a collection of molecular devices or machines that work together to power our motions (i.e. muscles), repair damage, and control our senses, thoughts and emotions<sup>[2]</sup>. Molecular devices have been fabricated on the molecular scale that mimics rotors<sup>[3]</sup>, gears<sup>[4]</sup>, shuttles<sup>[5]</sup> and ratchets<sup>[6]</sup>. Molecular devices can also be used as sensors, logic gates and switches.<sup>[7]</sup>

Recently, the area of molecular electronics has attracted much attention.<sup>[8]</sup> The forces driving the miniaturization of electronic devices include cost, reliability and performance speed. Silicon-based microelectronic devices have revolutionized our world over the past several decades.<sup>[9]</sup> Advances in lithographic techniques used to fabricate the circuits on these silicon-based devices have led to the development of faster processors and computer chips with smaller device features making them more sophisticated. However, the “scaling down” approach to manufacture these miniaturized integrated devices, which involves engineers, chemists and physicists to manipulate smaller and smaller pieces of matter, has intrinsic limitations. An alternative approach to make micro- or nanoscale devices is to start at the bottom, using molecules and atoms, and “build up”. Manufacturing devices at the molecular or atomic level will circumvent the limitations encountered when attempting to construct nanoscale materials mechanically. Incorporating highly functionalized molecules into specific devices will lead to advantages in both size and efficiency.<sup>[10]</sup>

Chemists are able to design and synthesize large molecules and supramolecules using processes such as self-assembly<sup>[11]</sup>. However, a more important issue than just being able to construct the molecular architecture of the device is the ability to control the functions that the molecular device performs, or the properties that they display. Therefore, elements must be programmed within the molecular framework that allows the properties and functions of the molecules to be turned “on” or turned “off” when desired.

### 1.2 Molecular switches

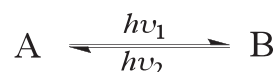
The ability to modulate or regulate the molecular shape and electronic properties using an external trigger is of central importance to the development of molecular scale devices.<sup>[12]</sup> Molecular switches are compounds that reversibly interconvert between two different states

using an external stimulus such as heat, chemical reagents, photons or electrons.<sup>[13]</sup> Inducing changes in molecular systems by introducing chemical substances are the least appealing of these external stimuli since waste is produced upon their consumption and byproducts may be difficult to remove. Photons (light) and electrons (electricity) are the most desirable stimuli to trigger changes in molecular systems since they can be introduced in a more controllable fashion and generally do not result in the production of undesirable byproducts, when properly designed and handled.

Molecules which experience a color change upon exposure to external light, heat or electrical stimuli are termed photochromic, thermochromic and electrochromic compounds, respectively.<sup>[14]</sup> The main focus of this thesis is the design of novel photochromic molecules based on six-membered ring with bistable states. Therefore, the next section will discuss the processes that occur in photochromic systems, outline the important desirable properties of photochromic molecules as well as highlight examples of existing photochromic system with different ethene bridges, in the case of bithienylethenes(BTEs)

### 1.3 Photochromism

Photochromism is defined as a light-induced reversible transformation of a chemical species between two forms that have different absorption spectra.<sup>[15-16]</sup> Molecules that are capable to interconvert reversibly interconverting between two isomers that differ in color are termed as photochromic compounds. For example, the two isomers A and B can reversibly interconvert between the two forms by irradiating with appropriate wavelength of light. Irradiation of isomer A with one wavelength of light ( $h\nu_1$ ) results in a photoisomerization reaction producing isomer B. The reverse reaction is carried out by irradiation of isomer B with a different wavelength of light ( $h\nu_2$ ).



Equation 1.1

The wavelength of light used to interconvert between the two states is dependent on the absorption spectra of each isomer. A desirable property of photochromic molecules is the possibility to independently address each state. Therefore, each isomer should have well-separated absorption bands. Figure 1.1 shows a typical absorption spectrum of a photoinduced transformation between two isomers, A and B, which differ in color. Upon irradiation of A at  $h\nu_1$ , the absorption band in the UV region decreases and an absorption band appears in the visible region due to the formation of isomer B. Irradiation of B at a wavelength in the visible spectra region ( $h\nu_2$ ) results in the reverse isomerization back to

isomer A.

The wavelength at which the absorption spectra intersect in the photochemical isomerization reaction is called the *isobestic point* (Figure 1.1). The isobestic point corresponds to a wavelength in the absorption spectra where the molar absorptivities of A and B are equal. Consequently, the absorbance remains at a constant value during all the course of the photoreaction. Photochemical isomerization is always accompanied by the rearrangement of chemical bonds. During the photoisomerization processes, undesirable side-reactions may occur. The presence of an isobestic point during the photochemical reaction implies that there is only photoisomerization between two forms. However, this is only true if there are not other species generated in photoreaction that do not absorb at the wavelength of light where the isobestic point is present. In this thesis, when an isobestic point is present in the UV-Vis absorption spectra, it refers to the photochemical transformation as a “clean” conversion between the two isomers.

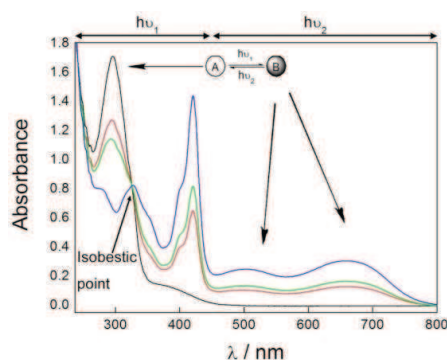


Fig. 1.1 UV-Vis absorption spectrum of a photochromic compound before and after irradiation

Ideally, the two isomers, A and B, of a photochromic system should absorb in well-separated regions so that each isomer can be irradiated independently. However, the two isomers of organic photochromic compounds frequently have absorption bands in the same region where light is used to induce one of the photochemical transformations. In Figure 1.1, both isomers, A and B, absorb light at wavelengths in the region labeled  $h\nu_1$ . Therefore, upon irradiating with a wavelength of light in that region, a photochemical equilibrium is set up where there are competing photoisomerization (i.e.  $A \rightarrow B$ , and  $B \rightarrow A$ ). The point at which the equilibrium is reached is called the photostationary state (PSS). The photostationary state is indicated by the quantum yields ( $\Phi$ ) of the competing photoisomerization reactions at the irradiation wavelength and the concentrations and molar absorptivities ( $\epsilon$ ) of the species in solution (Equation 1.2).

$$\Phi_{A \rightarrow B}[A]\epsilon_A = \Phi_{B \rightarrow A}[B]\epsilon_B \quad \text{Equation 1.2}$$

The PSS can be calculated by determining the ratio of the amount of isomer B at the equilibrium ( $B_f$ ) to the initial amount of isomer A ( $A_i$ ). The PSS is usually reported as a percentage of the isomer formed associated with the wavelength of light used to induce the transformation. Therefore, upon irradiating isomer A with a wavelength of light ( $h\nu_l$ ) producing isomer B, the photostationary state would be:

$$\text{PSS}(\%) = (B_f/A_i) \times 100\% \quad \text{Equation 1.3}$$

If a wavelength of light is used to induce the photoisomerization reaction where only one of the isomers absorbs (form B in [Figure 1.1](#)), irradiation results in complete isomerization to the other form and a PSS corresponding to 100% A isomer.

Since the two isomers of photochromic compounds have different color, they are promising candidates to be incorporated into device applications such as variable transmission filters, optical memory media and display.<sup>[17]</sup> However, the property changes that occur between the two isomers or photochromic compounds is not only limited to color. Changes in other chemical or physical properties such as refractive index, electrical conductivity, viscosity and fluorescence may also accompany the photoisomerization reactions. Therefore, photochromic compounds have the potential to be used in a variety of different optoelectronic device applications such as light-emitting diodes, waveguides, liquid crystal displays and optical memory media.

#### 1.4 Classifications of photochromic systems

Considering practical use in device applications such as optical storage systems, photochromic compounds should meet certain requirements as follows:<sup>[18-19]</sup>

1. Thermal stability: interconversion of the isomers must not occur at the temperature of operation.
2. Photofatigue resistance: photochemical integrity over repetitive cycles must be maintained to allow for multiple write-erase cycles.
3. High efficiency of the photoreaction: both forward and reverse photoreactions must proceed with high yield.
4. Detectability: the two isomers must differ in properties that are easily measured for reading and differentiation purposes.
5. Synthetic modification: there must be the ability to readily incorporate a variety of functional groups without compromising the molecular photochromism.

The following section will highlight several known photochromic compounds, especially

focusing on the advantages and disadvantages with respect to the above mentioned properties.

Generally, there are two general classes of photochromic systems based on the photoinduced transformations: (1) *cis-trans* isomerization and (2) electrocyclic photocyclization.

#### 1.4.1 *Cis-Trans* isomerization

Azobenzenes are a member of photochromes that reversibly undergo light-induced *cis-trans* isomerization (Figure 1.2).<sup>[20-21]</sup> The *trans* to *cis* isomerization of the N=N double bond in azobenzenes is induced by irradiation with light. The reverse isomerization reaction from the *cis* to *trans* isomer occurs by either irradiation with light or by thermal reversion. The thermal instability of the *cis* isomer is a severe drawback of this photochromic system, especially for applications that hinge on the bistability of both isomers such as optical data storage. Also, the difference in the UV-Vis absorption spectra of the two forms do not differ significantly, which lowers the ability to both address and detect each isomer upon the photoreaction. However, an appealing quality of azobenzenes is that synthetic modifications can be made to the system by introducing a variety of substituents onto the benzene ring of the molecular scaffold.

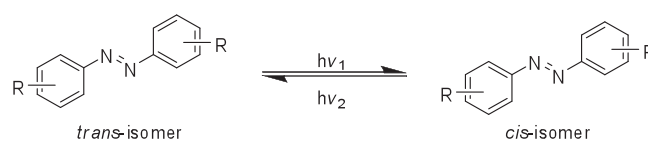


Fig. 1.2 Photoisomerization and thermal back reaction of azobenzene triggered by light and heat

Another class member of photochromic systems relying on *cis-trans* isomerization is sterically crowded alkenes.<sup>[22]</sup> These molecules are unique with respect to the fact that they adopt a non-planar helical shape due to the steric interactions between the groups that are attached to the central double bond. Upon irradiation with light, they undergo not only the *cis-trans* isomerization, but also the simultaneous inversion of the helical structure (Figure 1.3). This has made them particularly appealing for use as chiroptical molecular switches. These molecules show favorable properties of fatigue resistance and thermal stability. The drawbacks of this photochromic system are that the synthesis of such sterically crowded molecules tends to be tedious, and the photoreactions exhibit slow response times.

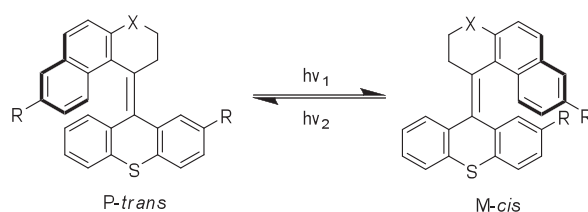


Fig. 1.3 Photoisomerization of bulky alkene triggered by alternation of UV and Vis light

#### 1.4.2 Electrocyclization reactions

A second class of photochromic systems is molecules, which undergo reversible electrocyclization reactions. In general, the systems that will be discussed here contain  $6\pi$ -electrons arranged as a 1,3,5-hexatriene. Irradiation with an appropriate wavelength results in a ring-closing reaction that produces a 1,3-cyclohexadiene derivative (Figure 1.4). The reverse ring-opening reaction occurs by irradiation with another wavelength of light.

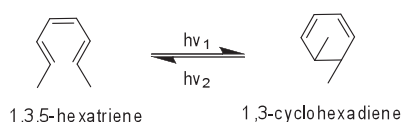
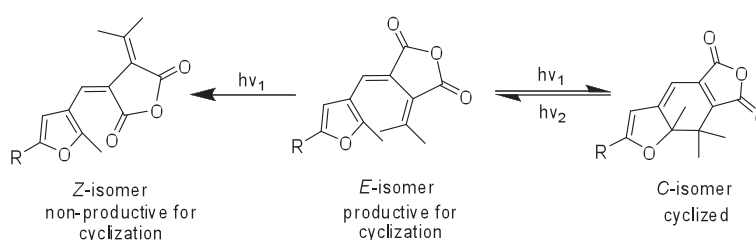


Fig. 1.4 Ring closure reaction of 1,3,5-hexatriene under irradiation of UV light

Fulgides undergo reversible ring-opening and ring-closing reaction upon irradiation with light of appropriate wavelengths.<sup>[23]</sup> Irradiation of the colorless ring-open (*E*-isomer) with UV light produces the colored ring-closed (*C*-isomer). This process is reversible since irradiation of the ring-closed *C*-isomer with visible light regenerates the original *E*-isomer (Scheme 1.1). Both ring-open and ring-closed isomers are thermally stable, making this class of photochromic molecules appealing for use in device applications such as optical memory media where bistability is a necessity to maintain the integrity of the data stored. Both isomers are easily addressed and detected due to the large differences in their UV-Vis absorption profiles.



Scheme. 1.1 Ring closure reaction of fulgide irradiated at 365 nm with the side reaction of *E-Z* isomerization causes a decrease of the fatigue resistance

The major problem associated with fulgides is that in addition to the two photochemically active forms (colorless *E*-form and colored *C*-form), photochemical *E-Z* isomerization also occurs when irradiated with UV light. The *Z*-form is a non-productive isomer for photocyclization, and is subject to photofatigue. Cyclization of the same solution of fulgide results in the increase of the *Z*-isomer which cannot undergo the ring-cyclization process.

Spiropyran derivatives also undergo a reversible photoisomerization process between a closed (colorless) spiropyran form and an open (colored) merocyanine form (Figure 1.5).<sup>[24]</sup> Specifically, the spiropyrans have several drawbacks such as low thermal stability of the merocyanine (open) form and low fatigue resistance. Spiropyran were originally used as the coloring agent in ophthalmic lenses, however, these compounds are photodegraded over time in the presence of sunlight, a serious shortcoming for the use in this application. The lack of thermal stability for spiropyrans accompanied by the low fatigue resistance severely limits their application to any optical device applications.

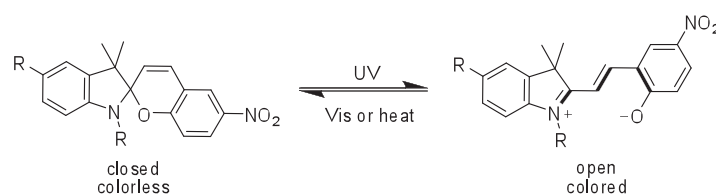


Fig. 1.5 Photoisomerization of spiropyran under UV irradiation due to the breaking of C-O bond

## 1.5 Diarylalkenes

Diarylalkenes interconvert between their colorless ring-open isomer and colored ring-closed isomer by alternate irradiation with UV and visible light (Figure 1.6)<sup>[25-26]</sup>. These compounds, like the fulgides and spiropyran, are members of photochromic compounds that undergo a  $6\pi$ -electrocyclization reaction. However, the photofatigue resistant properties of diarylalkenes are far superior to that of both fulgides and spiropyran. Along with fatigue resistance, the thermal stability of both ring-open and ring-closed isomers makes them particularly appealing for use in optoelectronic devices and optical memory media. The research presented in this thesis is primarily focused on the photochromic diarylalkene. Therefore, the next sections discuss in detail the photochromism of diarylethene.

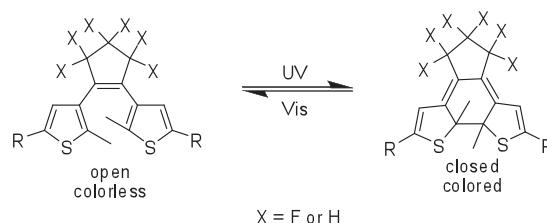


Fig. 1.6 Photofatigue resistance of perfluorocyclopentene or cyclopentene bithiophenes under alternative irradiation of UV and visible light

### 1.5.1 Ring closing reaction



The ring-open form of the photochromic bisthiénylenes (BTEs) can exist in two conformations: (1) the parallel conformation with two rings in mirror symmetry and (2) the anti-parallel conformation where the molecule has a  $C_2$  axis of symmetry (Figure 1.7). The photoisomerization of BTE occurs via a conrotatory ring-closing reaction of the photoexcited anti-parallel ring-open form.<sup>[18-19]</sup>

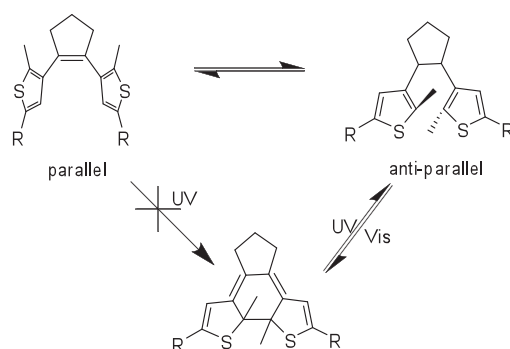


Fig. 1.7 Photochromic compounds using cyclopentene as central ethene bridge have two conformers (parallel and anti-parallel conformers). Pericyclic reaction can only happen in anti-parallel conformer under the irradiation of UV light

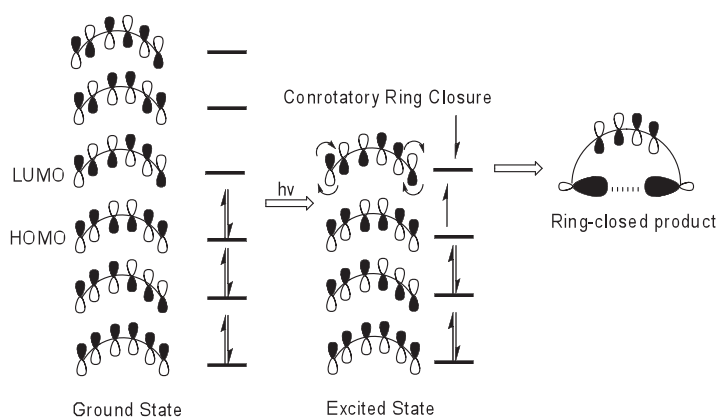


Fig. 1.8 Frontier theory and reaction pathway of 1,3,5-hexatriene

The frontier molecular orbital diagram of the 1,3,5-hexatriene system, which is the simplest molecular framework of BTE, is shown in Figure 1.8. Upon light-activation of the ring-open form, an electron is promoted from the ground state HOMO into the LUMO. To preserve the  $\pi$ -orbital symmetry, the ring-closure can only occur via a conrotatory process, where both reacting orbitals turn in the same direction.<sup>[27]</sup> The disrotatory ring-closing reaction (reacting orbitals turn in the opposite direction), which would occur through the parallel conformation, is thermally allowed from the ground state. However, it does not occur practically due to steric hindrance of the central methyl substituent. Additionally, the ground state energy of the ring-closed isomer that would be produced upon disrotatory ring-closure is

higher in energy than the ground state energy of the ring-open form, and thus, would not be stable<sup>[18]</sup>.

Since the photoinduced cyclization reactions of systems containing a 1,3,5-hexatriene only practically occur in a conrotatory fashion, these electrocyclization reactions are highly stereospecific. However, since the conrotatory ring closure can occur in either a clockwise or counterclockwise direction with equal probability, ring closure of BTEs produces both *RR* and *SS* stereoisomers (Figure 1.9)

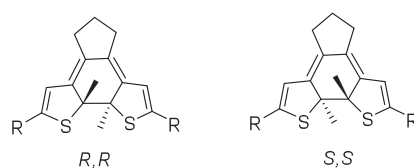


Fig. 1.9 Chiral structure of 1,3,5-hexatriene after ring closure reaction

### 1.5.2 Quantum yield

The efficiencies of photochemical isomerization reactions of BTEs are measured by determination of the photoreaction quantum yield ( $\Phi$ ).<sup>[28]</sup> The photoreaction quantum yield is the fraction of molecules that undergo the isomerization reaction after excitation using light. Since the BTEs requires only a single photon absorption to undergo the ring-closing/ring-opening reactions, the general equation for calculation the quantum yield for the isomerization reactions of BTEs is :

$$\Phi = \text{number of molecules that isomerize} / \text{number of photons absorbed} \quad \text{Equation 1.4}$$

As mentioned previously, the BTEs can adopt both parallel and anti-parallel conformations. In general, the ratio of the two conformational isomers is 1:1. The interconversion rate between the two conformations was estimated to be slower than their excited state lifetimes. Therefore, excitation of both isomers occur simultaneously, and only the anti-parallel conformer photocyclizes. As a result, assuming that there is an equal ratio of the two conformations, the quantum yield of BTEs does not exceed 0.5. Increasing the ratio of anti-parallel conformation of the ring-open isomer has resulted in an increase in the quantum yield of the ring-closing reaction. This has been accomplished by (1) introducing bulky substituent at the reactive carbon centers of the thiophene heterocycles (2- and 2'- position)<sup>[29]</sup> or (2) inclusion of a bithienyl inside the cavity of a cyclodextrin<sup>[30]</sup>.

When bulky isopropyl groups were incorporated at the 2- and 2'-position of the thiophene ring instead of methyl groups, an increase in the anti-parallel conformation was observed and the cyclization quantum yield increased from 0.35 to 0.52. However, the

ring-closed isomer was found to be thermally unstable. The cyclization quantum yield of a BTEs in the presence of  $\beta$ -cyclodextrin was 1.5 times larger than without the cyclodextrin. This was attributed to the inclusion of only the reactive anti-parallel conformer inside the cyclodextrin cavity.

### 1.5.3 Thermal stability

Thermal stability is of great importance in commercial application. A key property that controls the thermal stability of the ring-closed isomer of diarylethene is the type of aromatic ring employed.<sup>[19]</sup> Upon ring-closure, the aromaticity of aryl rings is lost. The major driving force for the thermal reversion back to the ring-open isomer is the rearomatization of the aryl rings. The ring-closed forms of diarylethene possessing pyrrole rings, which have high aromatic stabilization, are thermally unstable, and return back to the ring-open form in the dark. Diarylethene possessing thiophene rings have shown to exhibit extreme thermal stability over extended periods of time (>3 months at 80 °C). This is due to the low aromatic stabilization energy of the thiophene ring (4.7 kcal/mol). As demonstrated, BTEs are excellent photochromic systems due to the high thermal stability, which have become the leading candidates for application in optoelectronics and optical storage.

### 1.5.4 Fatigue resistance

For practical application in devices, photochromic compounds must reversibly interconvert between the two isomers over multiple cycles. During the photo-reactions, however, undesirable side-reactions may take place, resulting in a degradation in chemical structures over numerous ring-closing/ring-opening cycles.<sup>[19]</sup> Capability to undergo a high cycle numbers is termed as photo-fatigue resistance. The repeatable cycle number for BTEs is defined as the performed number of ring-closing/ring-opening cycles when the corresponding absorbance of the ring-open isomer has decreased to 80% of the first cycle. BTEs have shown to exhibit exceptional fatigue resistance. In particular, BTEs containing benzothiophene rings can undergo more than 13000 cycles (in methylcyclohexane) without significant degradation (Figure 1.10).<sup>[26]</sup> In comparison, the bis(phenylthiophene)dithienylperfluorocyclopentene derivative can only be cycled less than 500 times (in hexane) in the presence of air due to the formation of oxidized products. Although the bis(phenylthiophene) derivative was not as robust as the bis(benzothiophene) derivative, the fatigue resistance is still greater than other systems, such as fulgides.

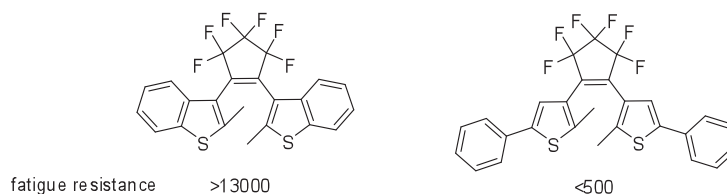


Fig. 1.10 Fatigue resistance of benzothiophene and 2-phenyl-thiophene substituted photochromic compounds using perfluorocyclopentene as central ethene bridge

## 1.6 Bisthienylethenes with different ethene bridges

Concerning the fatigue resistance and thermal stability, BTEs are the most promising candidates for the commercial application. However, up to date, the modification of BTEs mainly focused on the symmetric and asymmetric synthesis of the organic framework. In contrast, the center ethene bridges for the versatility in BTE architectures reported so far have been mostly confined to the cyclopentene unit or its strong electron-withdrawing analogs, such as perfluoro-cyclopentene, maleic anhydride or maleic imide (Figure 1.11).<sup>[31]</sup> The introduction of the strong electron withdrawing groups guarantees the photochromic property, and fatigue resistance as well as thermal stability.

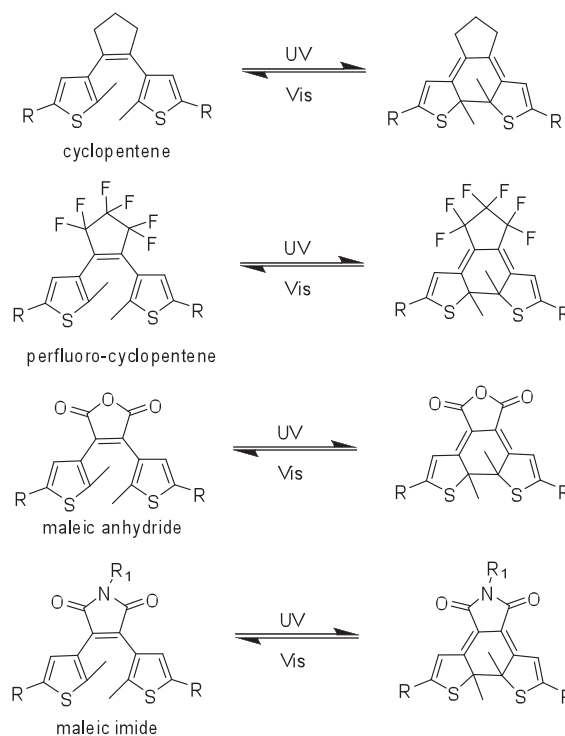


Fig. 1.11 Photochromic compounds utilizing cyclopentene or strong electron withdrawing groups such as perfluorocyclopentene, maleic anhydride and maleimide as central ethene bridge

### 1.6.1 Bisthienylethenes based on five-membered ethene bridge

Generally speaking, BTE compounds utilize heterocyclic rings as central ethene bridge. When a 1,3,5-hexatriene structure without such a ring is adopted, electrocyclization occurs with *Z-E* transformation when excited with UV irradiation (Figure 1.12),<sup>[32]</sup> thus suppressing the fatigue resistance and the photocyclization. When heterocyclic rings are introduced, the undesirable photo-generated byproduct can be completely eliminated.

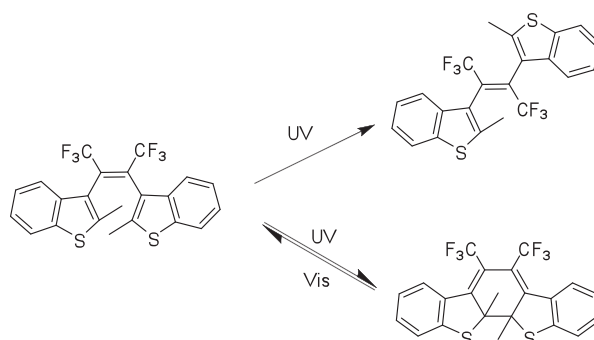


Fig. 1.12 Decreased fatigue resistance of non-cyclic ethene bridge due to the *Z-E* isomerization after UV irradiation

The absorption peaks of the closed-ring isomers are shifted to longer wavelengths upon decreasing the center bridge ring size. The closed-ring form without center ring structure has an absorption maximum at 449 nm. The maximum at 510 nm for the closed-ring form of center six-membered center ring derivative is shifted to 526 nm for the center five-membered center ring derivative, and further to 532 nm for the center four-membered ring derivative (Figure 1.13).<sup>[19]</sup> Consequently, it is suggested that the ring size controls the planarity, thus affecting the extent of  $\pi$ -conjugation in the closed-ring isomers. Obviously, the cyclization quantum yield was dependent on the ring size, and the highest value was observed for the six-membered ring derivative. Taking the two factors into account, the absorption maximum of the closed-ring form and the cyclization quantum yield, the five-membered ring is the most appropriate cycloalkene structure. Up to now, the central ethene bridge of BTEs has been mostly confined to perfluoro-cyclopentene due to the excellent fatigue resistance and thermal stability.

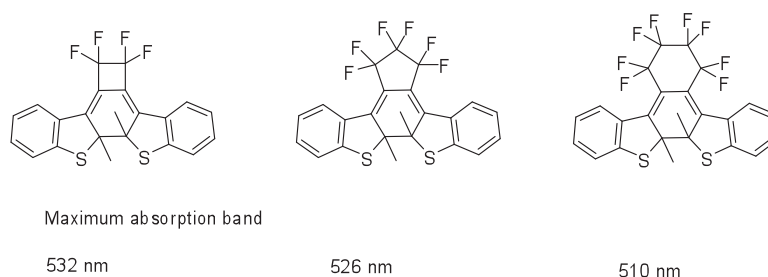


Fig. 1.13 Maximum UV-Vis absorption of photochromic compounds using cyclic rings as central ethene bridge in hexane

### 1.6.2 Photochromic system based on tetraazaporphyrin and phthalocyanine

Tian and coworkers reported a photochromic compound based on tetraazaporphyrin

(Figure 1.14),<sup>[33]</sup> which exhibits excellent photochromic property in  $\text{CHCl}_3$ . The photochromic units at opposite position could undergo cyclization reaction at the same time upon excitation at 365 nm. Even after prolonged UV irradiation, additional cyclization was not observed until complete photo-damage of the compounds. Excitation energy from the excited open-ring unit to the closed-ring through the macrocycle is considered to suppress the further photocyclization. The conversion yield from ring-open to ring-closed form is close to unity as deduced from percentage of quenched fluorescence. Interestingly, the compound exhibits excellent photochromic reaction in  $\text{CHCl}_3$  while no UV-Vis absorption changes could be recorded in ethanol under prolonged irradiation, indicating that the photochromic reaction could be modulated by the polarity of solvents. One of the drawbacks in this system is the slower responding time with respect to other systems.

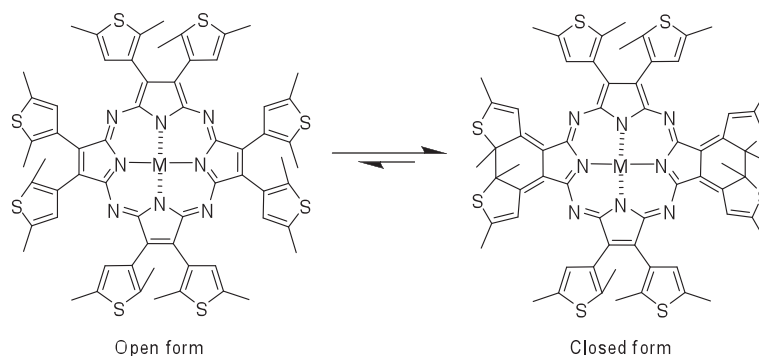


Fig. 1.14 Photochromic compounds using tetraazaporphyrin ring as central ethene bridge

Similarly, Tian and coworkers reported a series of photochromic compounds based on phthalocyanine (Figure 1.15).<sup>[34]</sup> In contrast, the photochromic reaction was barely affected by the solvent polarity (DMSO,  $\text{CHCl}_3$ ,  $\text{CH}_2\text{Cl}_2$ , EtOH). However, the central coordinated metal ions in phthalocyanine unit have a great effect on the modulation of photochromic behavior. It takes 9 h and 1.5 h to reach the PSS with Mg and Zn as central metal ions, respectively. Interestingly, no obvious UV-Vis absorption changes could be recorded for compounds without metal ion after prolonged irradiation. Excitation energy from the excited open-ring unit to the closed-ring through the macrocycle is considered to suppress further photocyclization. The drawbacks for this system are the difficulties in the manipulation of organic synthesis along with the slow responding time.

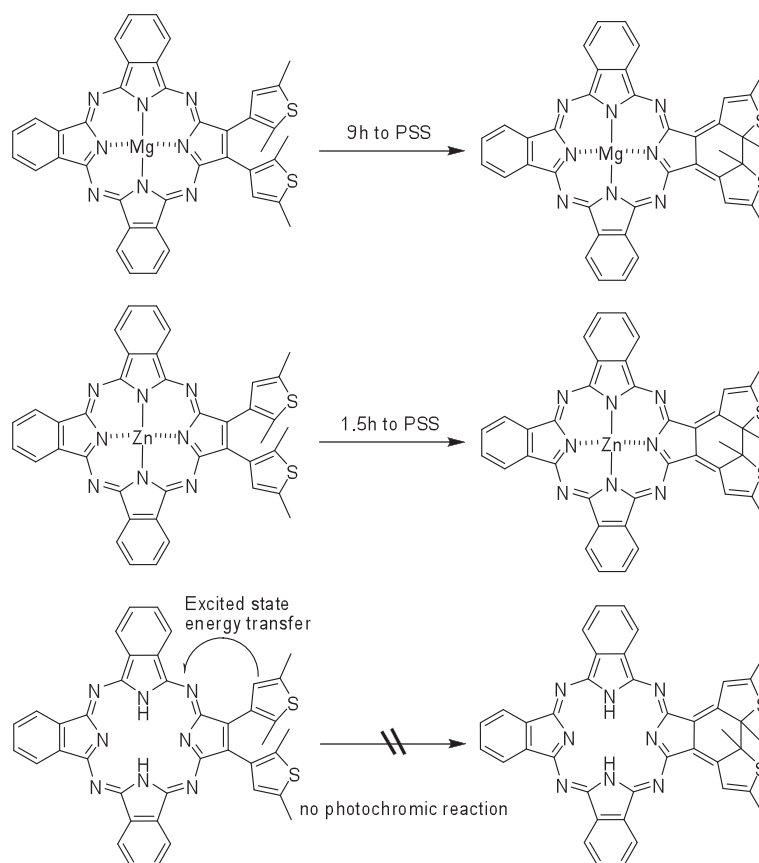


Fig. 1.15 Photochromic system based on phthalocyanine. The photochromic properties can be tuned by chelating with different metals

### 1.6.3 Benzothiophene as central ethene bridge

Recently, Kawai and coworker<sup>[35]</sup> reported a triangular dithiazolyl-azaindole derivative with high sensitivity. Benzothiophene derivative 1a, benzopyrrole derivative 2a, both showed photochromism with quantum yields of 98 and 90% in hexane, respectively, and 54 and 90% in methanol, respectively. Because both molecules are composed of similar molecular units, and display dual non-covalent intramolecular interactions, one may expect similar photochromic reactivity. Indeed, the photochromic quantum yield of 2a was similar to that of 1a in hexane (90% for 2a and 98% for 1a), whereas that of 1a was significantly suppressed in methanol. The difference between  $\Phi_{o-c}$  of the two compounds in methanol suggests that the CH/N interaction in 2a might be stronger than the S/N interaction in 1a, and that the reactive C2-symmetric conformation of 2a persists even in methanol. In methanolic solution, 1a showed no marked temperature-dependent  $^1\text{H}$  NMR shifts, and almost no specific regulation of conformation with the intramolecular interaction. In hexane, both 2a and 1a are mostly in the reactive conformation, and show high  $\Phi_{o-c}$ . Here, the slight difference in  $\Phi_{o-c}$  of 2a ( $\Phi_{o-c} = 0.90$ ) and of 1a ( $\Phi_{o-c} = 0.98$ ), may thus be explained, not from the viewpoint of population ratio of the reactive and non-reactive conformations, but by the reactivity of the reactive

conformation (Figure 1.16).

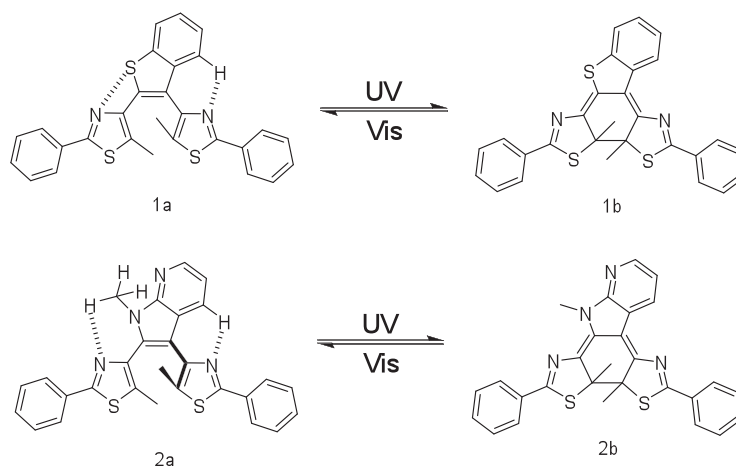


Fig. 1.16 Photochromic systems based on benzothiophene and benzopyrrole. Through the intramolecular hydrogen bonding, the increased fraction of the photo-active conformer enhances the photocyclization reaction quantum yield.

Similarly, Li and coworkers synthesized and investigated a photochemical active triangle terarylene based on benzothiophene.<sup>[36]</sup> Its photochromic reactivity can be strongly suppressed by selected oxidization of the sulfur atoms in the molecules by mCPBA. Reactivated photochromic reactivity was obtained by deoxidization of the *S,S*-dioxide moieties by NaBH<sub>4</sub>. The suppressed photoactivity of the oxidation state was attributed to the stronger intramolecular hydrogen bonding interactions (Figure 1.17). Accordingly, A gated photochromism could be achieved before and after oxidation of the bridge.

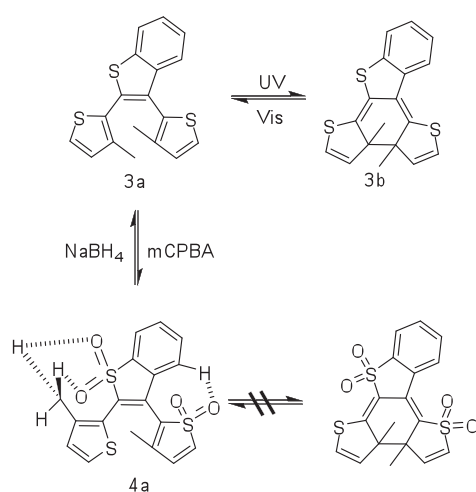
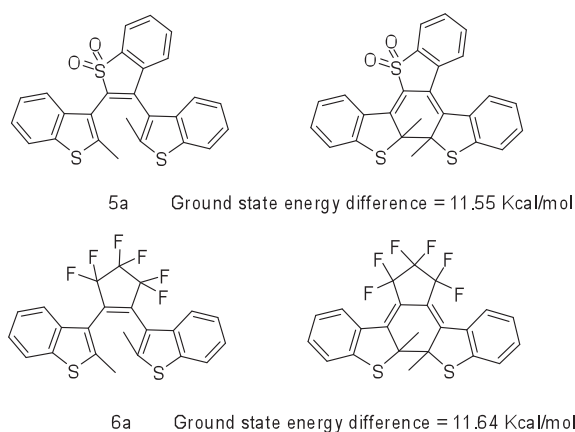


Fig. 1.17 Photochromic compounds using benzothiophene as central ethene bridge. A gated photochromism could be achieved before and after oxidation of the bridge

Kwang-Hyun Ahn and coworkers<sup>[37]</sup> found a photochromic terarylene derivative 5a,



which has a readily synthesized sulfone group at the upper benzothiophene ring using Suzuki coupling reaction (Figure 1.18), with good photochromic properties. Interestingly, the closed form of the compound 5a shows a good photostability as well as a thermal stability with respect to its reduced analog, providing a method to enhance the photostability of versatile photochromic terarylenes. From the calculation, it was found that the energy difference between open- and closed-ring isomers of the oxidized terarylene 5a (11.55 kcal/mol) is similar to that of diarylethene 6a (11.64 kcal/mol). One of the drawbacks of this system is the difficulties in asymmetric synthesis that limits the application in nonlinear optics (NLO)..



**Fig. 1.18** Excellent photo-fatigue resistance and thermal stability of photochromic system by utilizing the oxidation state of benzothiophene (benzo[*b*]thiophene-1,1-dioxide unit) as central ethene bridge, comparable with perfluorocyclopentene analogues.

Recently, Zhu and coworkers reported a photochromic terarylene (BTO) containing benzo[*b*]thiophene-1,1-dioxide unit as central ethene bridge, exhibiting good thermal stability and fatigue resistance both in solution and bulk crystals (Figure 1.19).<sup>[38]</sup> When triggered by chemical ions, protons or light, BTO can behave as absorbance and fluorescence switch, leading to a multi-addressable system. The color changes of BTO upon adding Cu<sup>2+</sup> and Hg<sup>2+</sup> ions with different competition are arisen from their relative binding stoichiometry and association affinities. Moreover, the conversion yield of BTO can be modulated by chemical ions. Impressively, an increase in conversion yield was observed by adding Hg<sup>2+</sup> to the solution of BTO, that is, the conversion yield and cyclization quantum yield are increased from 77.6% and 28.5% (for BTO only) to 99.8% and 43.1% (BTO-Hg<sup>2+</sup>), respectively.

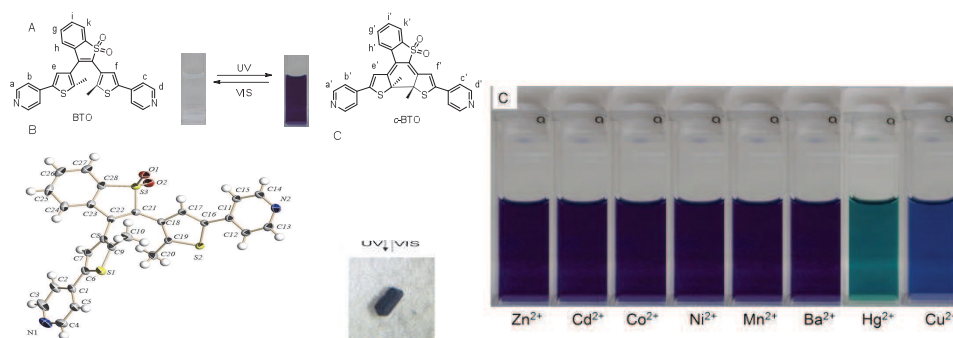


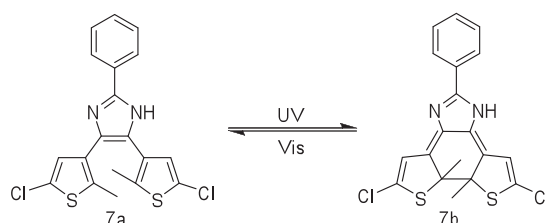
Fig. 1.19 Photochromic properties of BTO in solution and crystal state with different response to the metal ions in THF

Photochromic systems based on benzothiophene as central ethene bridge show excellent fatigue resistance as well as thermal stability. Wide occurrence of intra- or intermolecular interactions could be observed when the bridge was selectively oxidized or the side aryl was replaced by thiazole, which could greatly affect the photochromic behaviors and UV-Vis or fluorescence response. However, the asymmetric nature of the central ethene bridge causes difficulties in the manipulations on organic modifications.

#### 1.6.4 Imidazole based central ethene bridge

Imidazole group has outstanding complexing abilities. So far, imidazole ring has only been used as side aryl substituent in photochromic systems due to its good affinity with proton and reactivity with base. However, few groups reported utilization of imidazole as central ethene bridge, and further complexation between metal ions.

Recently, Chen and coworkers explored a new class of diarylethenes with a imidazole bridge unit, showing outstanding photochromic properties under the alternation of UV/Vis irradiation (Figure 1.20).<sup>[39]</sup> It is found that electronic properties of substituent in the imidazole bridge unit have a great effect on both photochromism and fluorescence of diarylethenes because of intramolecular charge transfer. Both “turn-on” and “turn-off” fluorescent diarylethenes systems can be achieved by simple modification with different substituents, which provides an accessible strategy for fluorescence switchers. Up to now, the fluorescence turn-on photochromic compounds are extremely rare in diarylethene system, especially for the closed forms.



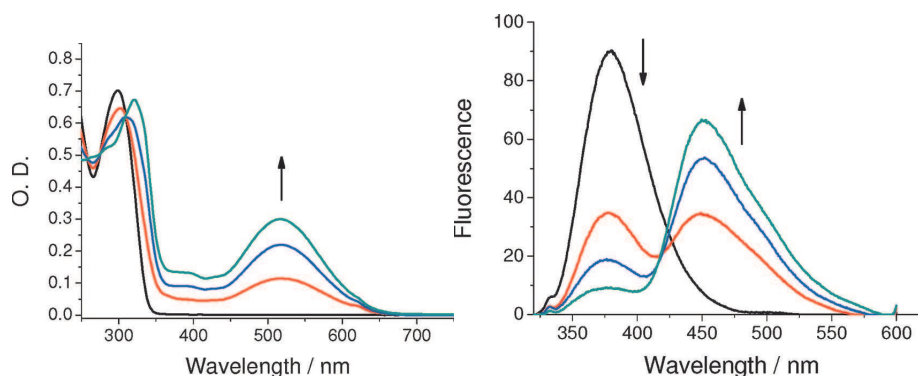


Fig. 1.20 Fluorescence increase after UV irradiation of a photochromic compound using imidazole as central ethene bridge

Yam and coworkers synthesized a series of chelating *N*-pyridyl-imidazol-2-ylidene tetracyanoruthenates (II), achieved through the use of the pyridylimidazolium ligand precursors under acidic condition (Figure 1.21).<sup>[40]</sup> The lowest-energy excited state of these complexes has been assigned as the  $^3\text{MLCT}$  state in both room-temperature solution and the low-temperature glass state. The *N*-heterocyclic carbene ligands are found to be more  $\sigma$ -donating and less  $\pi$ -accepting than their bipyridyl analogues, as revealed by photophysical and electrochemical studies. Substituents on the pyridine ring have been found to affect the electronic absorption and emission spectra of the complexes remarkably, whereas introduction of the dithienylethene moiety on the imidazolium ring had little effect on the energy of the transitions, but would offer an additional competing pathway for the deactivation of the  $^3\text{MLCT}$  excited state. With the incorporation of the metal center, the photochromic reaction has been accomplished by means of a sensitizing mechanism that involves the triplet excited state, which would extend the excitation source to lower-energy visible light. Such coordination with a metal center further provides the tuning of the center ethene bridge.

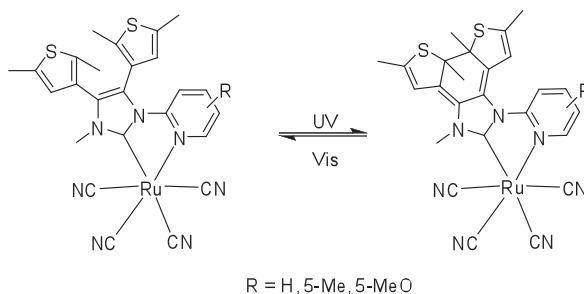


Fig. 1.21 Tunable photochromic reaction pathway through a triplet state using imidazole complex as central ethene bridge

Moreover, Yam and coworkers synthesized a series of BTEs-containing imidazolium salts utilizing ring-closing or C-N cross-coupling reactions (Figure 1.22).<sup>[41]</sup> These

imidazolium salts and imidazoles undergo a photocyclization reaction upon photoirradiation in the UV region, and the reverse reaction takes place upon excitation at the visible region. The closed form of the imidazolium salt undergoes nucleophilic addition with anionic nucleophiles at 2-position of the five-membered ring to generate the neutral product, whereas the open form is found to be essentially inert towards nucleophiles. This significant difference between the open and closed forms has been attributed to their differences in aromaticity. As a result, a reversible photogated switch in reactivity can be obtained in these systems.

A series of half-sandwich type *N*-heterocyclic carbene-ruthenium(II) complexes  $[(\eta^6\text{-mesitylene})\text{Ru}(\text{NHC-L})\text{Cl}]\text{PF}_6$  containing the BTEs moiety (Figure 1.23) was also developed.<sup>[42]</sup> These complexes show photochromic properties upon photo-irradiation. However, they exhibit a low quantum yield in the photochromic reaction, which is attributed to an efficient deactivation of the excited state.

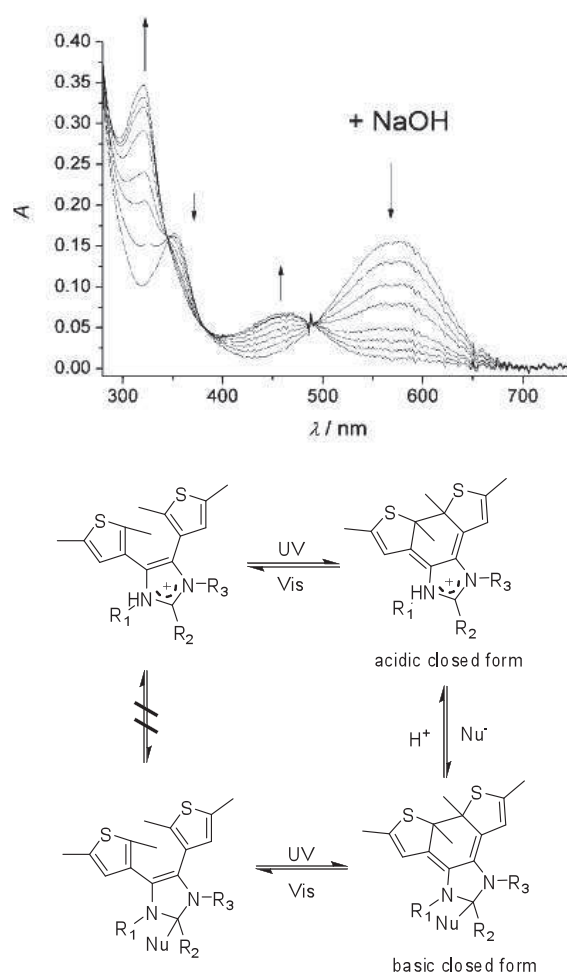


Fig. 1.22 Behavior of a photochromic system bearing an imidazole central bridge towards a nucleophile: reaction scheme and spectral response.

Different attempts have been made to design photochromic compounds that show

absorption and reactivity in the near-infrared (NIR) region in order to enhance the semiconductor diode laser susceptibility for applications in optical memory storage. One commonly employed approach to achieve NIR absorption is to increase the extent of  $\pi$ -conjugation of the thiophene moiety so as to red-shift the absorption maxima. However, the synthesis is usually tedious and non-trivial, and the wavelength shift would eventually reach its convergence limit. Recently, Yam and coworkers reported diarylethene derivatives that function as ligands for incorporation into transition metal complexes, in which photochromic perturbation of the diarylethene moiety upon coordination to the metal center has been observed (Figure 1.24).<sup>[43]</sup> Indeed, the incorporation of diarylethene derivatives as ligands into transition metal complex systems can extend the absorption peak to longer wavelength through a planarity enhancement of the  $\pi$ -conjugated system, thus realizing an alternative and versatile route toward NIR photochromic materials. Furthermore, in this way, the photochromic behavior can also be sensitized through indirect excitation into the relevant excited state of metal complex unit.

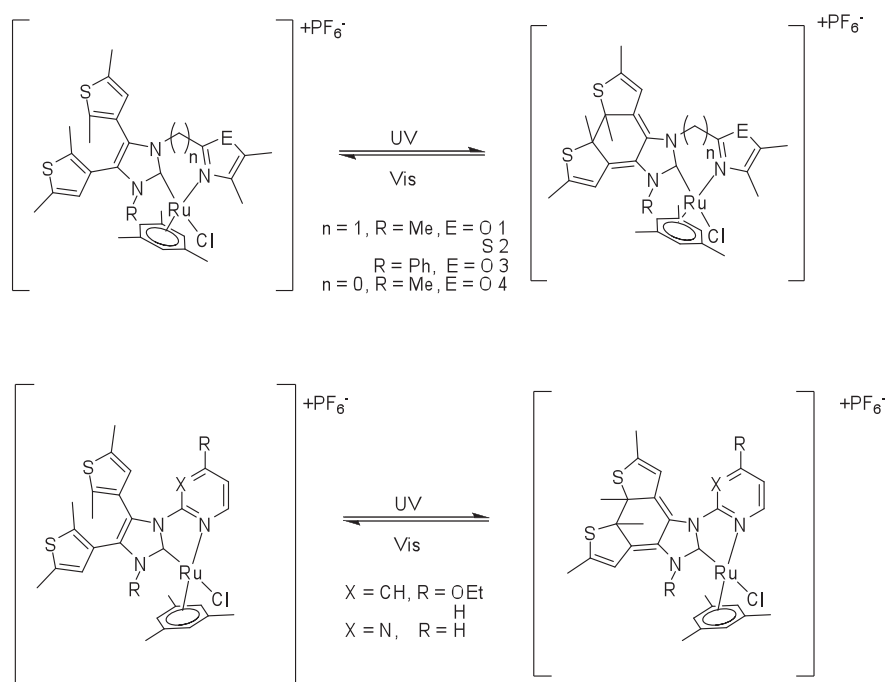


Fig. 1.23 Photochromic reaction of *N*-heterocyclic carbene-ruthenium(II) complexes  $[(\eta^6\text{-mesitylene})\text{Ru}(\text{NHC-L})\text{Cl}]\text{PF}_6$  containing BTEs moiety

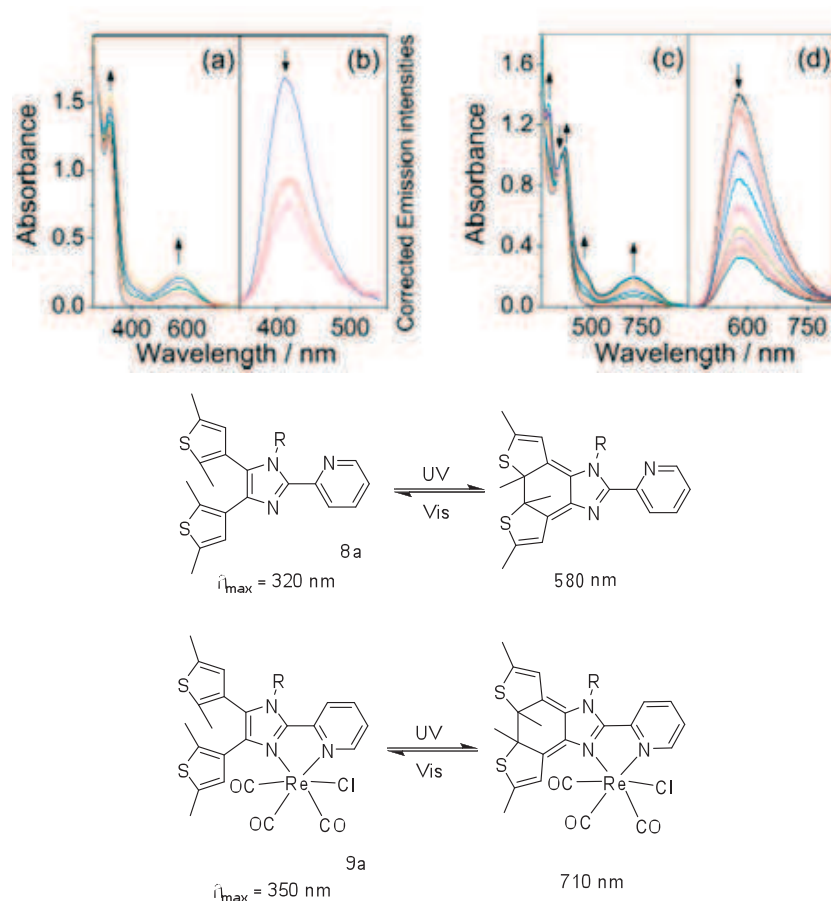


Fig. 1.24 (a) UV-vis absorption and (b) corrected emission spectral changes of 8a in chloroform upon IL excitation at 320 nm at 298 K. (c) UV-vis absorption and (d) corrected emission spectral changes of 9a in chloroform upon MLCT excitation at 410 nm at 298 K.

Yam and coworkers also reported a series of diarylethene-containing nitrogen-containing heterocyclic carbene (NHC) complexes of Au(I), Ag(I) and Pd(II) and their imidazolium salt precursors (Figure 1.25).<sup>[44]</sup> Incorporation of the diarylethene moiety into the core of imidazolium salt generates ionic liquids and novel NHC complexes with photoswitchable functional properties, such as switchable catalytic, regio-, or enantioselective activities, as well as physical and optical properties, giving rise to electronic and conformational/steric changes.

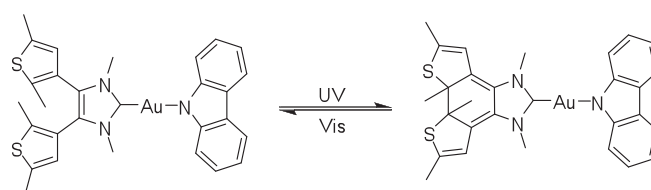


Fig. 1.25 Photochromic system based on carbene

### 1.6.5 Thiazole as central ethene bridge

The attachment of thiazole to the ethene bridge could result in the thermal reversible reaction due to the comparatively large aromaticity in the heterocyclic ring. However, the wide occurrence of intra- or intermolecular interactions between thiazole and hydrogen provides extra force to fix the conformation, which could to some extent increase the amount of anti-parallel conformer and thus enhance the photochromic behavior as well as the cyclization quantum yield.

Kawai and coworkers firstly reported novel photochromic triangle terarylenes based on thiazole bridged unit (Figure 1.26).<sup>[45]</sup> Fairly high photochemical coloration reactivity is observed with photochemical quantum yield as high as 0.6 for a 4,5-dithienyl thiazole derivative. Introduction of phenylethynyl groups into the molecular structure allows systematic control of thermal cycloreversion time constant over 105 times, and a half-lifetime shorter than 2 s is achieved at 303 K. Thus, a novel molecular engineering concept for systematic control of thermal bleaching reaction rate is presented without taking bulky functional groups on reaction center.

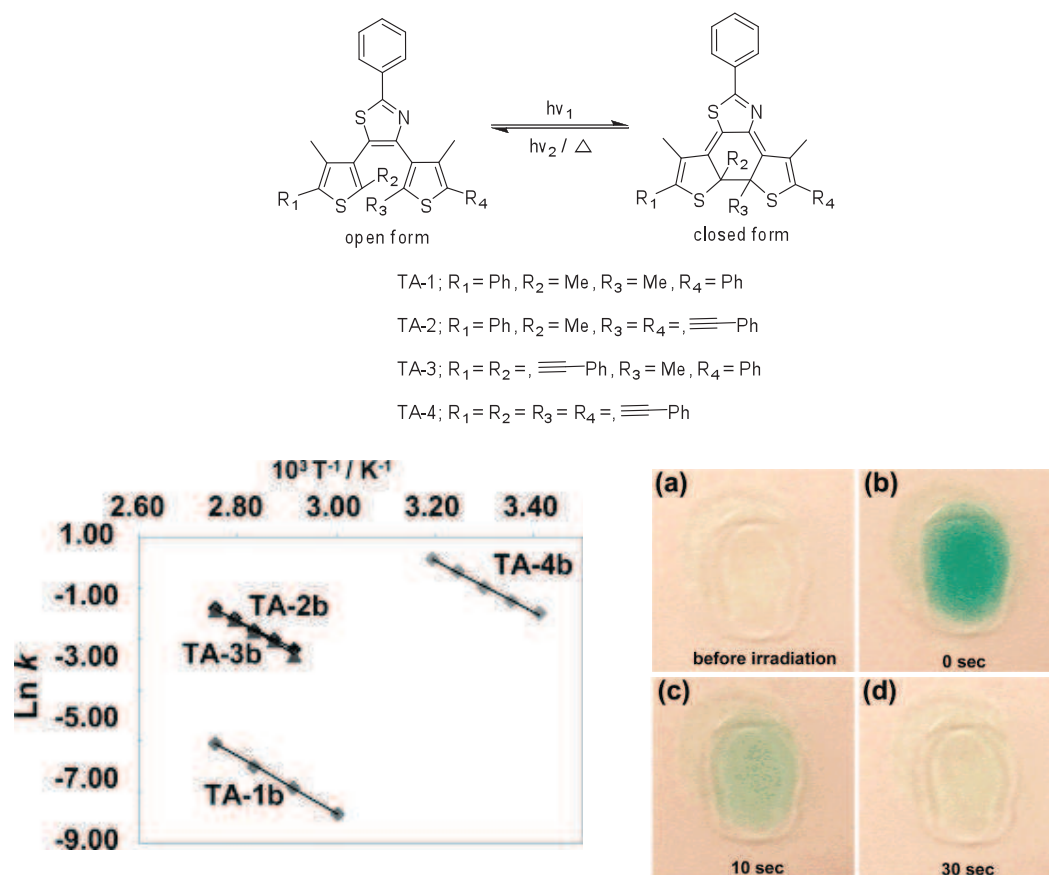


Fig. 1.26 Top: Photochromic compound based on a thiazole bridged unit; Left: Arrhenius plots of the thermal cycloreversion rate constant of TA-1, TA-2, TA-3, and TA-4 in toluene; Right: Photochromic coloration and spontaneous bleaching of TA-4 dispersed in PMMA film at room temperature

To further investigate the different in side aryl substituents, Kawai and coworkers developed triangle terarylenes with the substitution of one or three thiazole groups as aryl units (Figure 1.27).<sup>[46]</sup> The thiazole-containing compounds 10 and 11 show relatively high photocyclization quantum yields. Interestingly, the monothiazolyl-substituted terarylene 10 exhibited reversible photochromism even in the crystalline phase, whereas terthiazole 11 did not. This difference was explained in terms of conformational differences in the crystalline phase as revealed by X-ray crystallographic analyses. The thermal stabilities of the ring-closed isomers were greatly enhanced by the introduction of thiazole groups, which possess smaller aromatic stabilization energy than that of thiophene. Mono- and tri-thiazolyl substituted compounds (10 and 11) had half-lifetimes 30 times and 2600 times longer, respectively, than that of trithiophene-substituted.

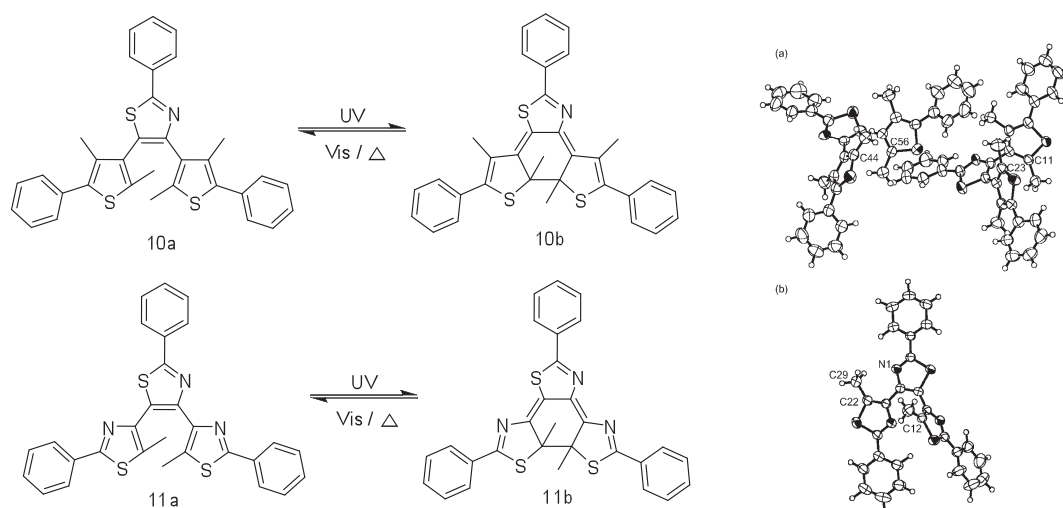


Fig. 1.27 Thiazole bridged photochromic compounds with different aryl substituents showing different photochromic behavior in both solution and bulky crystal state.

Recently, Kawai and coworkers reported a photochromic compound where the reactivity of terarylenes is controlled through a host-guest interaction, and involves a molecular folding process (Figure 1.28).<sup>[47]</sup> A thieno-[3,2,*b*]pyridine unit is introduced into a photochromic terarylene structure as an aryl unit to form a guest-interacting site. Thienopyridine-containing terarylenes showed solvent-dependent photochromic reactivity in solution. A terarylene moiety that contains two thienopyridyl units showed a significantly high photocoloration reactivity as high as 88% of photocyclization quantum yield in methanol, whereas that value was only 24% in hexane. A temperature-dependent <sup>1</sup>H NMR spectroscopic study in different solvents indicated an interconversion between photochromic-reactive and unreactive conformations. In methanol, the intermolecular interaction between terarylene species and



solvent molecules slows the rate of interconversion, and increases the population of the photochromic-active form, whereas the unreactive conformation is dominant in hexane. Structural studies of crystals structural studies demonstrated the perfect regulation of molecular folding between a photochromic-active form and an unreactive conformation by changing recrystallization solvents. Single crystals obtained from solutions in methanol showed reversible photochromic reactivity, whereas recrystallization from solutions in hexane lead to unactive crystals. X-ray crystallographic studies of single crystals from solutions in methanol demonstrated that the photochromic molecules bind a solvent methanol molecule at the guest-interacting site to regulate the molecular conformation into a photochromic-active form in collaboration with specific intramolecular interactions, whereas crystals from hexane are in the unreactive conformation.

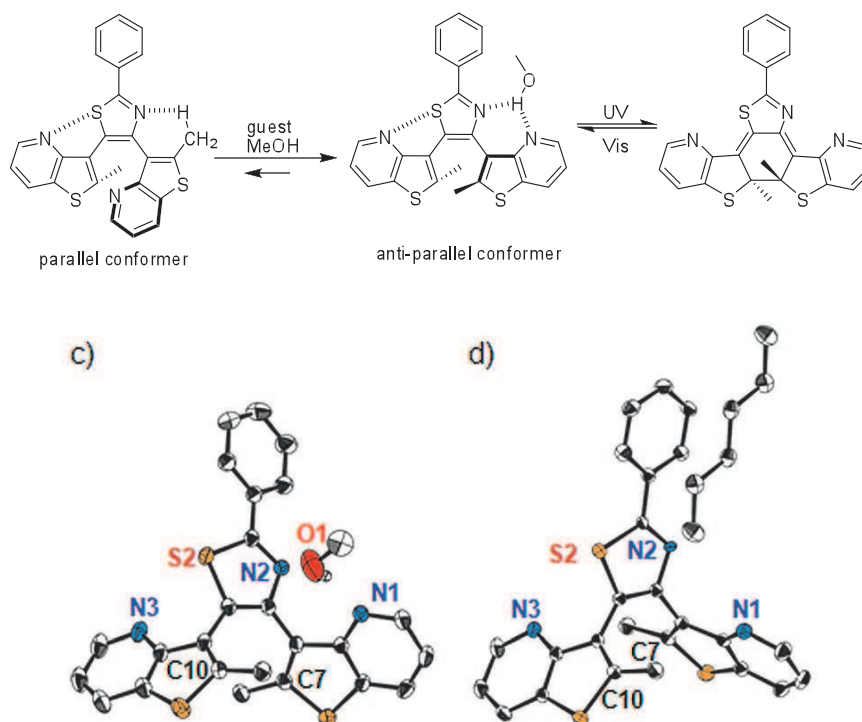


Fig. 1.28 Thiazole bridged photochromic compounds with modulated behavior in solvent and crystal state

To further extend the application of photochromism, Kawai and coworkers studied a photoresponsive molecule containing a terarylene type structure and a methoxy group as a leaving unit, which shows a relatively high fluorescence quantum yield after UV-light irradiation, indicating the possibility of future application as an active material in write-once type optical data-storage systems (Figure 1.29).<sup>[48]</sup>

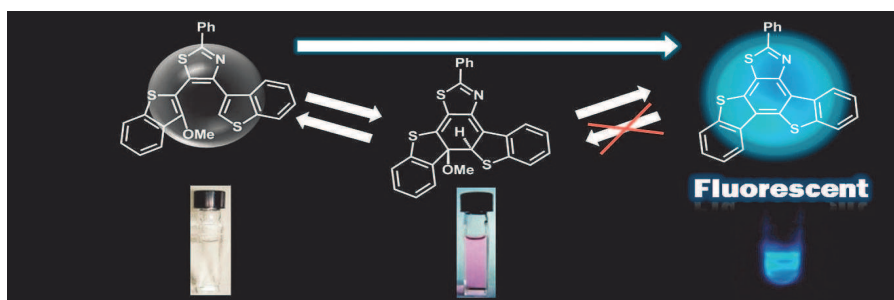


Fig. 1.29 Photochromic terarylene having a methoxy group and hydrogen as the leaving units at the photochemical reaction center carbon atoms

### 1.6.6 Oligothiеноacene and thiophene bridged photochromic system

Thiophene unit is well known for its conductivity and electron donating ability potentially utilized in optoelectronic materials. Due to the lower aromaticity of thiophene, it has been selected and widely used as side aryl. However, the introduction of thiophene heterocyclic ring as central ethene bridge has rarely been considered.

Unlike the commonly encountered poor processability of the fused thiophene systems, compounds 12-14 have good solubility in common organic solvents, which is attributed to the presence of the solubilizing 2,5-dimethylthiophene substituents (Figure 1.30).<sup>[49]</sup> Compared with 12 and 13, the lower absorption energy for 14 is in line with the more extended  $\pi$ -conjugation for dithienothiophene. However, for compounds 13 and 14, which consist of two diarylethene moieties, photocyclization could only take place at one of the diarylethene moieties even upon prolonged irradiation. This could be reflected in the  $^1\text{H}$  NMR spectra as well as the observation of the very well defined isosbestic point and the close resemblance of the UV-Vis absorption spectral changes of 13 and 14 on UV excitation. This may be attributed to the presence of the lower-lying excited state in the 8a,8b-dimethyl-1,8-dithia-as-indacene moiety (closed form moiety), which quenches the reactive excited state via an effective intramolecular pathway.

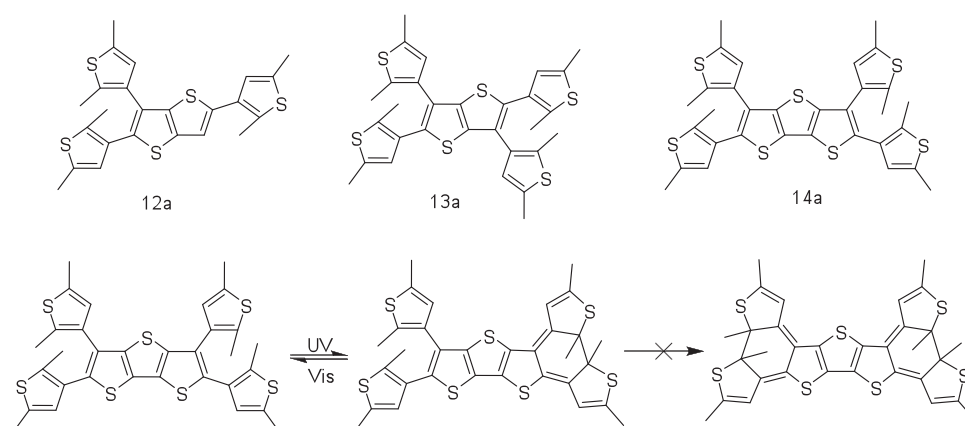
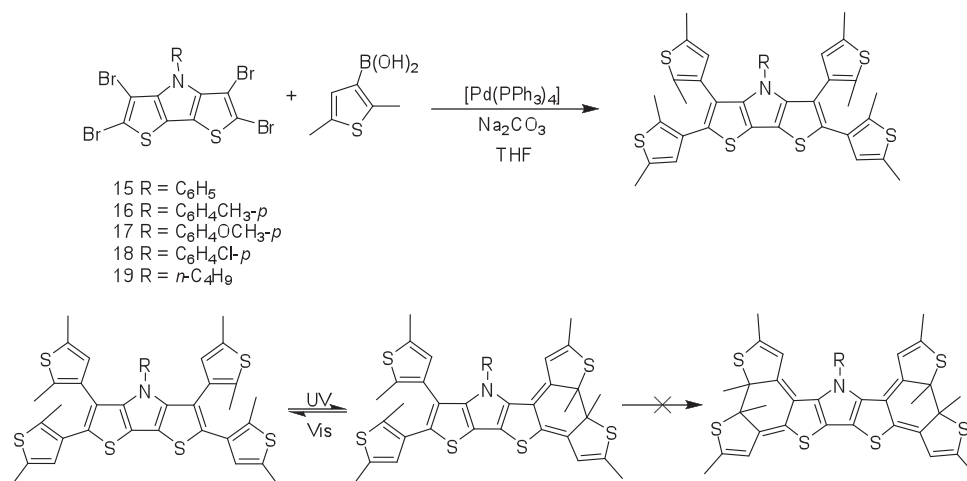


Fig. 1.30 Oligothiеноacene bridged photochromic system

Due to the insolubility of oligothiеноacene in various organic solvents, Yam and coworkers recently introduced dithieno[3,2-*b*:2',3'-*d*]pyrroles as central ethene bridge (Figure 1.31).<sup>[50]</sup> All 15-19 show excellent photochromic behavior in benzene. Interestingly, the crystal of 17a exhibits both parallel and anti-parallel conformers. The photochromic reaction could only occur from one side of the system due to the intramolecular energy transfer.

Fig. 1.31 Photochromic diarylethene-containing dithieno[3,2-*b*:2',3'-*d*]pyrroles

$\beta$ -diketonate is well-known as *O,O*-donor ligands for transition-metal centers and lanthanides. Yam and coworkers recently reported a series of  $\beta$ -diketonate diarylethenefunctionalized ligands (Figure 1.32).<sup>[51]</sup> The <sup>1</sup>H NMR spectrum of 20a shows that the enol form predominates in both CD<sub>2</sub>Cl<sub>2</sub> and C<sub>6</sub>D<sub>6</sub>, with a population of *ca.* 95% in the enol form, which is stabilized by an intramolecular hydrogen bond. 20a in its open form was found to dissolve in benzene to give a pale-yellow solution with an intense absorption band at *ca.* 368 nm, corresponding to the intraligand (IL)  $\pi \rightarrow \pi^*$  transition of 1-(2-thiophenyl)-1,3-butanedione moiety, with mixing of the  $\pi \rightarrow \pi^*$  transitions of dimethylthiophene moieties. Upon coordination to the boron(III) center, the IL absorption band was red-shifted from 368 nm to 415-434 nm. The red shift is attributed to the strong electron-accepting ability of boron, which decreases both the HOMO and LUMO energy levels, with the LUMO being lowered by a greater amount because it is more localized on the  $\beta$ -diketone core; the result is a decrease in the transition energy. UV excitation of 20a produced a new absorption band at *ca.* 630 nm, which is ascribed to the absorption of the closed form. Both 21a and 22a show NIR photochromic behavior upon excitation at  $\lambda < 420$  nm, with four absorption bands at *ca.* 298, 355, 506, and 758 nm in 2a, and three absorption

bands at ca. 297, 543, and 810 nm in 3a. 4a showed no photochromic behavior, with only photodegradation after prolonged UV irradiation.

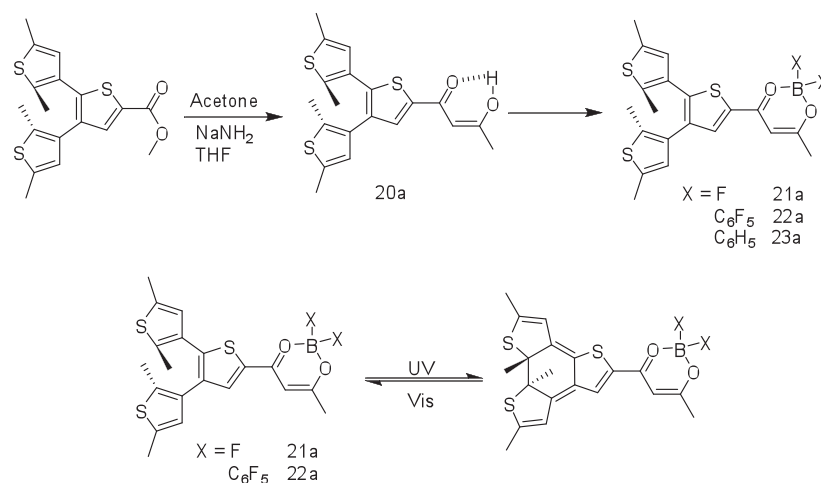


Fig. 1.32 Photochromic system based on  $\beta$ -diketonate diarylethene-functionalized ligands

Yam and coworkers studied the electrochemical, photophysical and photochromic behavior of cyclometalated platinum(II) complexes  $[\text{Pt}(\text{C}^{\wedge}\text{N})(\text{O}^{\wedge}\text{O})]$  (24a28a and 24b28b), where  $\text{C}^{\wedge}\text{N}$  is a cyclometalating 2-(2-thienyl)pyridyl (thpy) or 2-(2-thienothienyl)pyridyl (tthpy) ligand containing the photochromic BTEs unit and  $\text{O}^{\wedge}\text{O}$  is a  $\beta$ -diketonato ligand of acetylacetonato (acac) or hexafluoroacetylacetonato (hfac) (Figure 1.33).<sup>[52]</sup> The electrochemical studies reveal that the first quasi-reversible reduction couple, the nature of lowest unoccupied molecular orbital (LUMO) of the complexes, is sensitive to the nature of the ancillary  $\text{O}^{\wedge}\text{O}$  ligands. Upon photoexcitation, complexes 24a26a and 24b26b exhibit drastic color changes, ascribed to the reversible photochromic behavior, which is found to be sensitive to the substituents on pyridyl ring and the extent of  $\pi$ -conjugation of the  $\text{C}^{\wedge}\text{N}$  ligand as well as the nature of the ancillary ligand. The thermal bleaching kinetics of complex 24a has been studied in toluene at various temperatures, and the activation barrier for the thermal cycloreversion of the complexes has been determined. Density functional theory (DFT) calculations have been performed to provide an insight into the electrochemical, photophysical and photochromic properties.

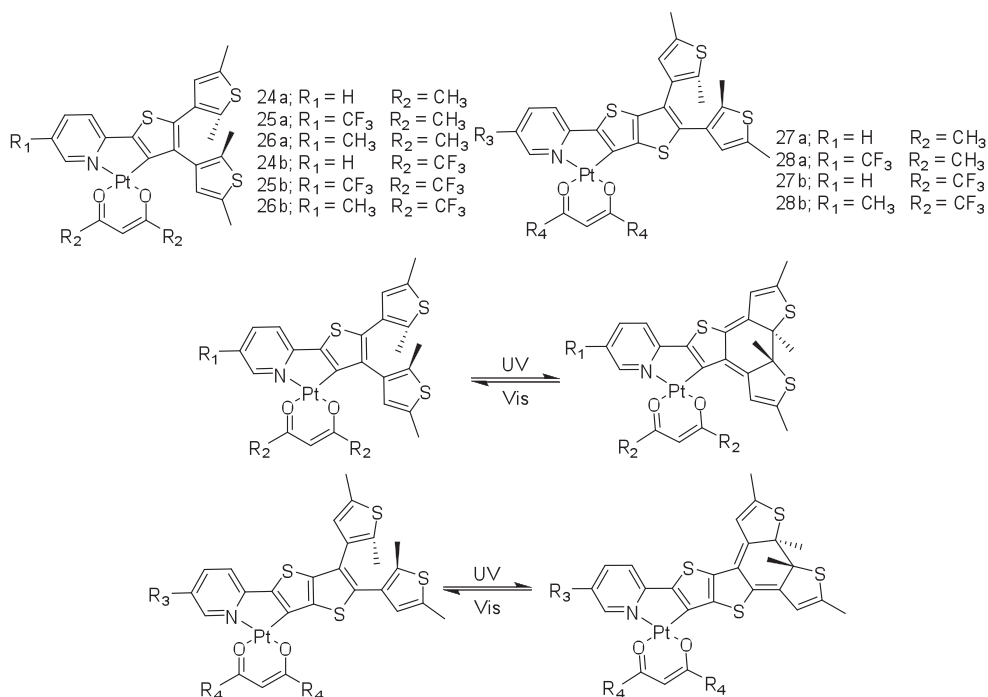


Fig. 1.33 Diarylethene-containing cyclometalated platinum(II) complexes: tunable photochromism via metal coordination and rational ligand design

Recently, Chen and coworkers reported a series photochromic compounds based on 2,5-dihydrothiophene (Figure 1.34).<sup>[53]</sup> The authors focus mainly on the organic synthesis, and the study of UV-Vis and fluorescence is not very much described in detail. The UV-Vis absorption of closed form corresponding to 2,5-dihydrothiophene bridged compounds are approximately 40 nm shorter than that of thiophene derivatives. The absorption wavelengths and the molar absorptivity can be modulated with different substituents.

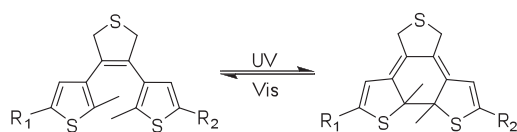


Fig. 1.34 Photochromic system based on 2,5-dihydrothiophene

Photochromic materials with gated properties serve as an important development in nondestructive readout and for practical applications. In gated photochromism, the photochromic property is suppressed or blocked by controlling multiphoton excitation, intramolecular hydrogen bonds, oxidation/reduction, acid/base, and chemical reactions, and temperature, or an external stimulus, which is required to “unlock” or reactivate the photochromic reactivity. Recently, Yam and coworkers developed triarylborane-based materials for potential applications in optoelectronic and anion-sensing.<sup>[54]</sup> The vacant  $p_\pi$  orbital of boron in triarylborane allows for conjugation with an organic  $\pi$  system, and serves

as a strong Lewis acid. After binding with a Lewis base, the trigonal planar geometry of the boron center is changed to tetrahedral, thus interrupting the electron delocalization and the  $\pi$ -conjugation with a significant change in photochromic behavior.

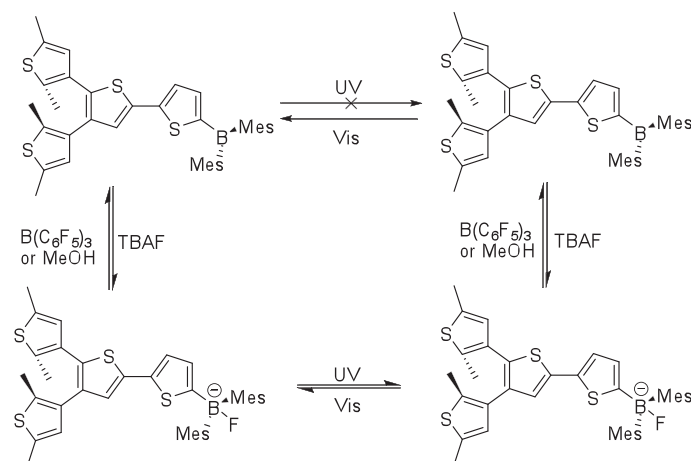
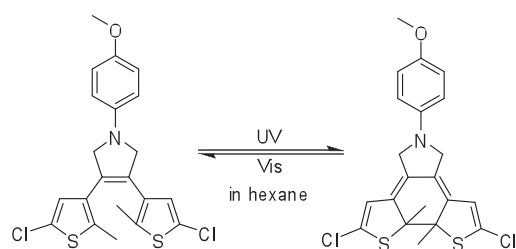


Fig. 1.35 Gated photochromism in triarylborane-containing dithienylethenes utilizing thiophene as central ethene bridge

### 1.6.7 Miscellaneous photochromic systems

Chen and coworkers recently reported symmetric and nonsymmetric diarylethenes with a 2,5-dihydropyrrole bridging unit (Figure 1.36).<sup>[55]</sup> Both symmetric and nonsymmetric diarylethenes with 2,5-dihydropyrrole bridging units undergo reversible ring-opening and ring-closing photoisomerization in nonpolar solvents with UV/vis light, and some of them exhibit good fatigue resistance, and no marked degradation is detected after 10 cycles of on/off switching. In polar solvents, however, photochromic diarylethenes with 2,5-dihydropyrrole bridging units produce 3,4-diarylpyrrole derivatives instead of the ring-closing isomer of diarylethenes with UV light irradiation. A class of *N*-substituted 3,4-diphenylethenes with 2,5-dihydropyrrole bridging units were prepared and used as templates to investigate the conversion reactions.



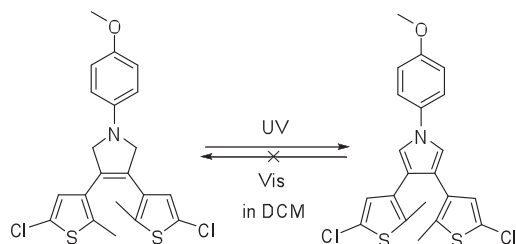


Fig. 1.36 Photochromic systems based on 2,5-dihydropyrrole

Belser and coworkers reported on BTEs derivatives containing a cyclobutene-1,2-dione skeleton. No photochromic reaction could be observed when both ketone are not protected or when only one of them is protected. The system could undergo a  $6\pi$  electrocyclic reaction upon excitation when both ketone functions are protected. However, fatigue is noticeably detected after 10 cycles of alternative irradiation with UV and Vis light (Figure 1.37).<sup>[56]</sup>

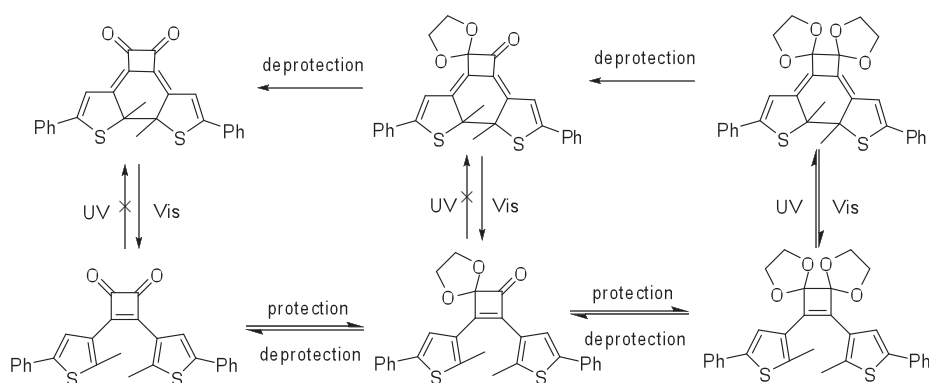


Fig. 1.37 Gated photochromism based on cyclobutene-1,2-dione skeleton

Yokoyama and coworkers have synthesized a novel thermally irreversible photochromic system based on  $6\pi$ -electrocyclization with three easily modifiable functional groups (Figure 1.38)<sup>[57]</sup>. Bisarylindenone 30a with thiazole as side aryl showed photochromic back-and-forth reactions with visible light of different wavelengths. The photochromic and absorption spectral properties can be switched by its acetalization. Significantly, the photocyclization quantum yield of acetal 31a, i.e., 0.81 in hexane, is extremely appealing for  $6\pi$ -electrocyclization in solution. Achievement of the large quantum yield may be explained by the intramolecular interactions of nitrogen and hydrogen atoms to fix the conformation in favor of photochemical cyclization. Interestingly, 29a did not show any photochromic behavior even under prolonged reaction.

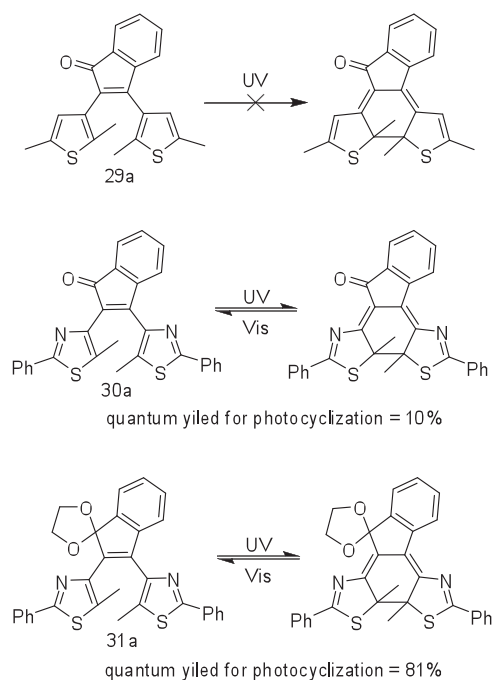


Fig. 1.38 Photochromic bisarylidenone and its acetal

### 1.7 Photochromic diarylethene based on six-membered ring

Up to date, photochromic systems have been mainly confined to five-membered heterocyclic rings. However, the exploitation of six-membered ethene bridges has been limited and scarcely reported. However, six-membered ethene bridges have their own advantages such as longer absorption wavelength of the closed isomer and a higher quantum yield. Unfortunately, most of the six-membered ethene bridges exhibit some aromaticity, which limit the commercial application due to the lack of bistable state.

Although a number of photochromic compounds are known, most of the studies are directed toward the molecular design and synthesis of the organic framework of the diarylethenes, while studies on the exploitation of these diarylethenes as ligands to form metal complexes are extremely rare. The combination of the diarylethene ligands and metal complex systems has shown novel properties. Recently, Yam and coworkers reported the syntheses, crystal structure, and sensitized photochromic properties of a versatile diarylethene containing 1,10-phenanthroline ligand (32a) and its rhenium(I) complex,  $[\text{Re}(\text{CO})_3(\text{L1})\text{Cl}]$  (33a) (Figure 1.39)<sup>[58]</sup>, which unlike most other studies in which the diarylethene ligands are derived from the attachment of donor atoms or groups as pendants to the bis(thienyl)perfluorocyclopentene core, the present design involves the ligand itself directly forming part of the diarylethene framework, which is extremely rare. Both 32a and 33a show two well-resolved sets of  $^1\text{H}$  NMR signals, corresponding to the parallel and antiparallel



conformations, commonly found in diarylethene systems. The cyclization quantum yield for 32a and 33a in benzene are 33% and 65%, respectively. Due to the strong aromaticity of the central ethene bridge, both 32b and 33b show some thermal back reaction with half life of 143 h and 78 h. The complexation with metal ions greatly enhanced the photochromic behavior.

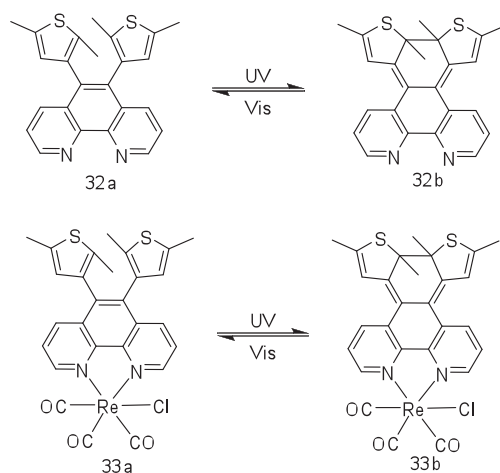


Fig. 1.39 Diarylethene-containing 1,10-phenanthroline ligand and its rhenium(I) complex

Recently, Branda and coworkers reported a novel molecular switching system showing reactivity-gated photochromism. Based on butadiene, it undergoes a [4 + 2] cycloaddition reaction with a dienophile to produce the photoresponsive 1,2-bisthiénylene backbone (Figure 1.40).<sup>[59]</sup> The reversible change in color, when samples are irradiated with appropriate wavelengths of light, occurs only after the Diels-Alder cycloaddition reaction takes place. An improved system is based on cyclic diene 35, which eliminates the rotational freedom in the butadiene fragment and is more suitable for developing dosimetry applications. This novel example of reactivity-gated photochromism has the potential to significantly impact dosimetry applications and the concept of controlled release of chemical species.

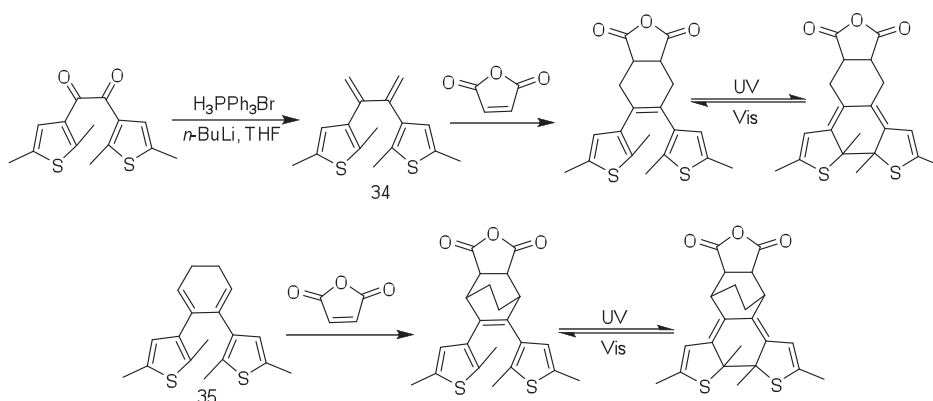


Fig. 1.40 Reactivity-gated photochromism of 1,2-bisthiénylenes

Yokoyama and coworkers recently synthesized three dual mode fluorescence switching molecules based on 3,4-bisthiazolylcoumarins (Figure 1.41).<sup>[60]</sup> Among them, under the basic conditions, 7-hydroxy-3,4-bis(5-methyl-2-phenyl-4-thiazolyl)coumarin changed its fluorescence intensity (quantum yield of 0.25 at pH 9.48 in buffered aqueous solution containing methanol) by photochromism as well as by changes of the pH of the medium. The fluorescence intensity ratio of the photostationary state compared to the open form was 1.5% at pH 9.48, while the fluorescence intensity of the open form at pH 7.58 was 14-fold that at pH 6.05. These results show that the fluorescence intensity can be modulated by both the photochromic reactions and the medium's pH.

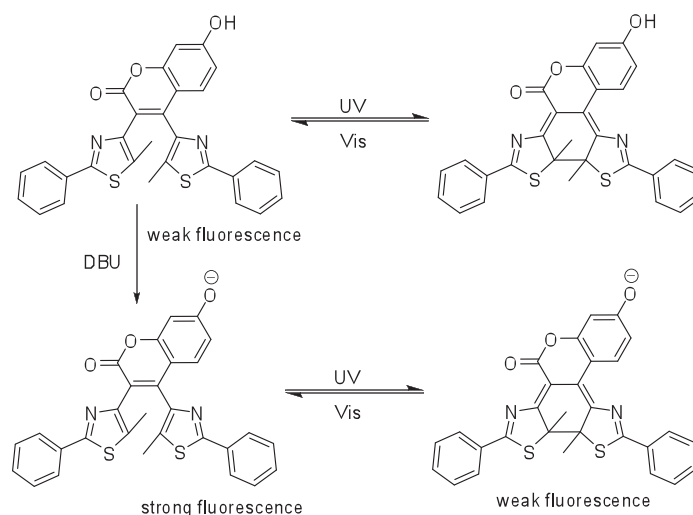
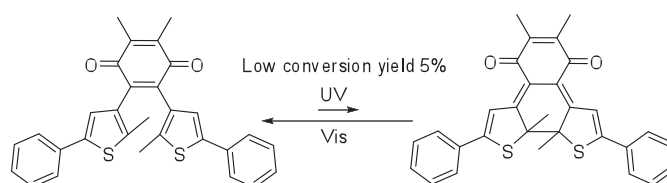


Fig. 1.41 3,4-Bisthiazolylcoumarin based photochromic compound modulated by pH and photochromic reaction

Liebeskind and coworkers recently reported a novel photochromic system based on benzoquinone (Figure 1.42).<sup>[61]</sup> 1a isomerized slowly under the irradiation of UV light. Usually, the conversion yield for this series will not exceed 5-30%. When Lewis acid was introduced, the open ring form was converted to intermediate 2, which could be fully converted to the closed ring form when treated with triethylamine. The closed ring form could be fully reverted with irradiation at visible light.



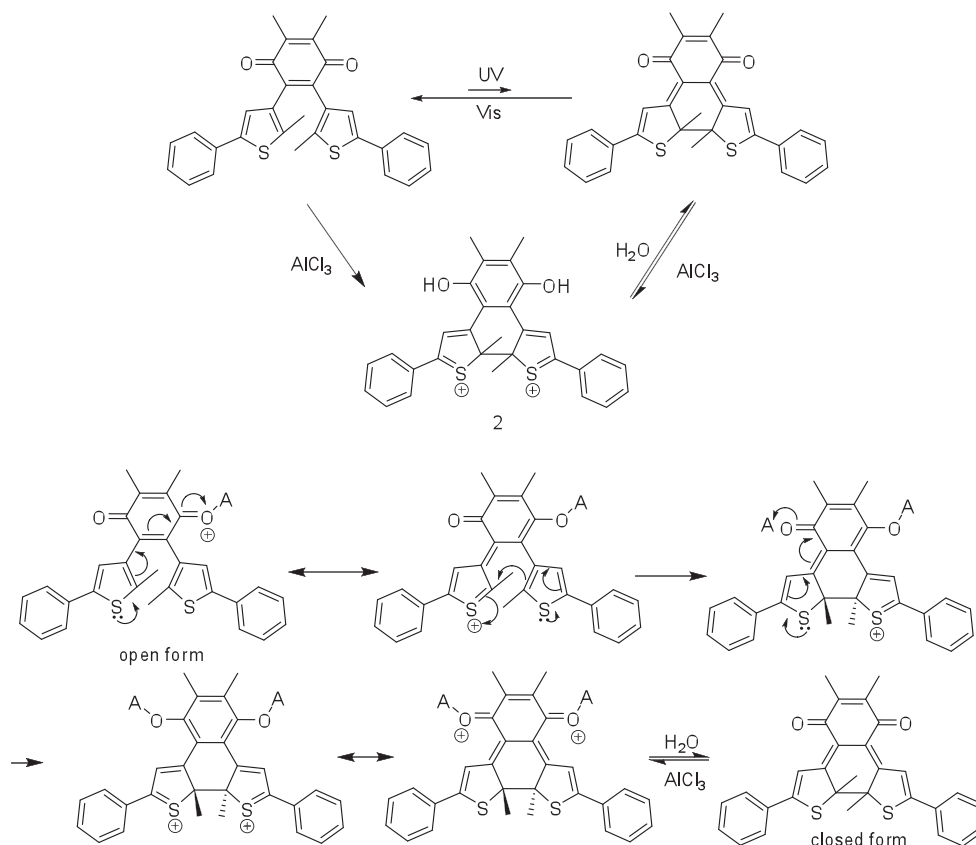


Fig. 1.42 Benzoquinone bridged photochromism and mechanism of color changes

## 1.8 Preview

As demonstrated above, up to date, the reported photochromic systems with six-membered ring as central ethene bridge are limited. Thus, the work presented in this thesis will mainly focus on the tailoring and the modifications of central ethene bridge with different functionalized groups.

In chapter 2, we incorporated high polar and electron-withdrawing chromophores of benzobisthiadiazole units as a novel family of six-membered ethene bridge to realize good photochromic performances with excellent fatigue resistance in solution as well as in crystal state. The fluorescence can be modulated by both solvato- and photochromism due to the strong electron mobilization before and after irradiation. Additionally, a lower aromaticity of the center ethene moiety in BTEs leads to a higher thermal stability of the closed form.

In chapter 3, we systematically reported the synthesis and photochromic properties of three ethene bridges with different degrees in aromaticity (BTE-NA, BTA and BTTA). Obvious thermal stability evolution and fluorescence modulation by solvato- and photo-chromism were observed in six-membered ethene bridged photochromic systems. An extremely low aromatic property of the center ethene bridge with benzobisthiadiazole unit

finally leads to the unexpected thermally irreversible photochromic system (BTTA). Small energy barrier between the parallel and anti-parallel conformers allows the full conversion from BTTA to *c*-BTTA. For the first time, the three ethene bridges with different degrees in aromaticity give a systematical comparison in the thermal stability evolution for their corresponding closed forms.

In chapter 4, benzothiadiazole was introduced directly as central ethene bridge as well as acceptor to form a D- $\pi$ -A structure and to achieve efficient photoswitchable nonlinear optical (NLO) materials. The strategy for the designing of NLO switchable system was based on the difference in efficiency in D- $\pi$ -A structure before and after irradiation caused by the coplanarity between the donor and the benzothiadiazole ring. However, due to the strong  $\pi\cdots\pi$  interaction and planarity of benzothiadiazole ring, the compounds adopt centrosymmetric packing in single crystal state, thus resulting in the absence of any bulk second harmonic generation..

In chapter 5, photochromic molecules based on 2,1,3-benzothiadiazole as ethene bridge are developed. New molecule bearing such a six-membered ethene bridge, and end groups such as pyridine or triphenylamine were synthesized. They were designed respectively for complexation and NLO properties. The compounds obtained are photochromic, however neither complexation nor NLO activity were evidenced.

## Chapter 2 Unprecedented Stability of a Photochromic Bisthienylethene Based on Benzobisthiadiazole as Six-membered Ethene Bridge

### 2.1 Introduction

Photochromic systems are of increasing interest due to their applications in ophthalmic lenses<sup>[62]</sup> and smart molecular materials acting as photoresponsive self-assemblies, molecular switches, logic gates and information storage.<sup>[63-70]</sup> Particularly, bisthienylethenes (BTEs)<sup>[71-75]</sup> have become one of the most promising families due to their thermal irreversibility and outstanding fatigue resistance among various photochromic systems, in which the 1,3,5-hexatriene section can adopt an appropriate conformation to undergo the conrotatory  $6\pi$ -electron photocyclization. Up to date, the rational design of symmetric or asymmetric BTEs have been mainly carried out on the right and left sides of aryl groups.<sup>[76-81]</sup> In contrast, the center ethene bridges for the versatility in BTE architectures reported so far have been mostly confined to the cyclopentene unit or its strong electron-withdrawing analogs such as perfluoro-cyclopentene, maleic anhydride or maleic imide. As alternatives to this, a few research groups have investigated the use of six-membered ethenes as BTE center bridge, such as 1,10-phenanthroline<sup>[58,82]</sup> and cyclohexene obtained via a [4 + 2] cycloaddition of butadiene with a dienophile<sup>[59]</sup>, to perform photochromism. Recently, we have incorporated highly polar and electron-withdrawing chromophores like 2,1,3-benzothiadiazole (Figure 2.1) or naphthalimide units to build novel series of six-membered ethene bridge and to realize good photochromic performance with moderate fatigue resistance in solution or in organogel systems.<sup>[83-84]</sup> Moreover, their fluorescence can be modulated by solvato- and photochromism, eventually leading to a combined NOR and INHIBIT logic operation system. However, the two building blocks bear aromaticity to some extent, which can facilitate the undesirable thermal back reaction at dark due to the large loss of aromatic stabilization energy upon photocyclization from the open to the closed form.

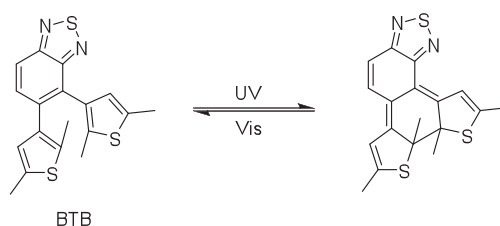


Fig. 2.1 Photochromic compound BTB based on 2,1,3-benzothiadiazole as central ethene bridge

Accordingly, a lower aromaticity of the center ethene moiety in BTEs is expected to lead to a higher thermal stability of the closed form. Since the ethene bridge with a six-membered ring has its own advantages such as higher quantum yield in ring closure and longer absorption wavelength, we envision that the six-membered ring with non-aromaticity as the center ethene bridge might widely extend the diversity in the thermally irreversible photochromic systems. With this in mind, and following up the preceding molecule (BTB, Figure 2.1), we report herein on an original BTE photochromic system (BTTE, Figure 1) based on benzo[1,2-*c*:3,4-*c'*]bis[1,2,5]thiadiazole (abbreviated as benzobisthiadiazole) chromophore as a novel six-membered center ethene bridging unit, which is expected to have a low aromaticity, and yield a thermally stable closed form *c*-BTTE (Figure 2.2).

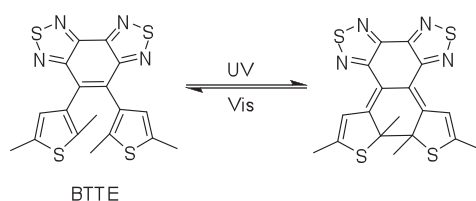


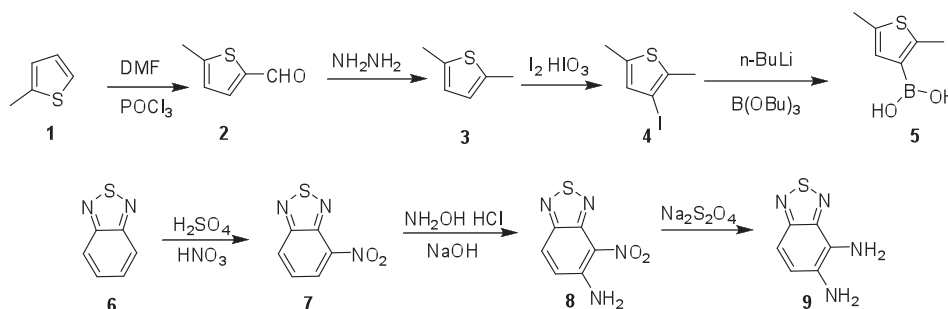
Fig. 2.2 Photochromic compound BTTE based on benzobisthiadiazole as central ethene bridge

## 2.2 Experiment section

### 2.2.1 Instruments and Reagents

$^1\text{H}$  NMR and  $^{13}\text{C}$  NMR spectra were recorded on JEOL spectrometers. MS were recorded on a Waters ESI mass spectroscopy. Absorption and fluorescence spectra were recorded on UVIKON 933 (Kontron instruments) and FluoroMax-3 (Horiba Jobin-Yvon), respectively. Fluorescence lifetime measurements were measured (see Appendix I for detailed information). The photochromic property was evidenced and characterized by following *in situ* the absorption spectra under continuous irradiation (see Appendix I for detailed information).

### 2.2.2 Synthetic route to the target and intermediate molecules



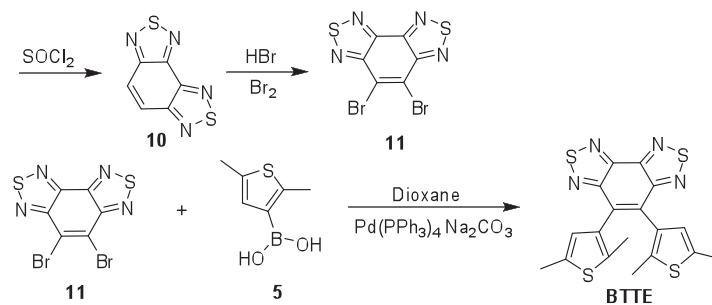
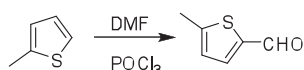


Fig 2.3 Synthetic routes of novel BTTEs with Benzobisthiadiazole as ethene bridges

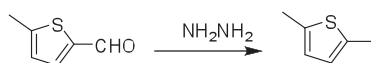
## 2.2.3 Preparation of target and intermediate molecules

### 2.2.3.1 5-Methyl-thiophene-2-carbaldehyde



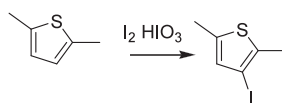
In a 100 mL two necked flask were added (49 g, 0.5 mol) 2-methylthiophene and dried DMF (47 g, 0.625 mol).  $\text{POCl}_3$  (98 g, 0.625 mol) was introduced slowly in an ice bath. The resulting mixture was allowed to stir at room temperature for 3 h until the solution turn red. After refluxing for another 1 h, the resulting mixture was then poured into crushed ice (500 mL). The solution was neutralized with  $\text{K}_2\text{CO}_3$  and extracted with Dichloromethane. The solvent was removed under vacuum and distilled under reduced pressure (1 mmHg) to yield 62 g yellow liquid. Yield: 99%

### 2.2.3.2 2,5-Dimethyl-thiophene



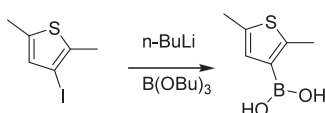
To a 100 mL two necked flask were added 5-Methyl-thiophene-2-carbaldehyde (11.7 g, 0.093 mol), 85% Hydrazine hydrate (11.4 mL) and 35 mL ethylene glycol. The mixture was refluxed for 30 min. The residual amount of water and Hydrazine hydrate were removed under vacuum.  $\text{KOH}$  (15.4 g, 0.28 mol) were introduced by portion. Then, the resulting mixture was allowed to reflux for 30 min. The crude product was distilled under reduced pressure to give mixture of oil and water. The oil phase was separated from water and dried with  $\text{Na}_2\text{SO}_4$  to yield a transparent liquid 5.04 g. Yield: 50%.

### 2.2.3.3 2,5-Dimethyl-3-iodo-thiophene



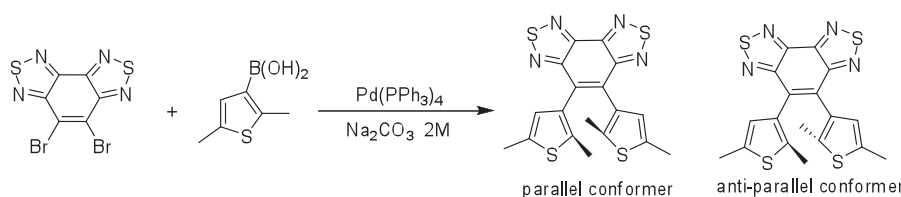
To a 100 mL two necked flask were added 2,5-Dimethyl-thiophene (4.1 g, 0.036 mol), Acetic acid (12 mL), water (4.45 mL),  $\text{CCl}_4$  (2.0 mL),  $\text{H}_2\text{SO}_4$  (0.21 mL),  $\text{I}_2$  (3.3 g, 0.065 mol) and  $\text{HIO}_3$ . The mixture was reacted at 80 °C for 3 h. After reaction, the mixture was poured into water and treated with  $\text{Na}_2\text{S}_2\text{O}_3$ . The oil phase was separated from water and further dried with  $\text{Na}_2\text{SO}_4$ . The crude product was purified under reduced pressure to give 2,5-Dimethyl-3-iodo-thiophene 6.2 g. Yield: 73%.  $^1\text{H NMR}$  (400 MHz,  $\text{CDCl}_3$ ): 6.60 (s, 1 H), 2.39 (s, 3 H), 2.36 (s, 3 H).

#### 2.2.3.4 2,5-Dimethyl-thiophyl-boric acid



To a 100 mL fire dried Schlenk tube was added 2,5-Dimethyl-3-iodo-thiophene (2.0 g, 8.4 mmol) and dried THF (25 mL). The solution was cooled to -78 °C. 1.6 M BuLi (5.6 mL, 8.9 mmol) was introduced dropwise through syringe. After 30 min,  $\text{B}(\text{OBu})_3$  (2.2 g, 9.6 mmol) was added. The resulting mixture was kept at -78 °C for 2 h. After reaction, 3 M HCl 12 mL were added to quench the reaction. The water phase was extracted with ether for three times. The ether phase was extracted with 10% NaOH (15 mL) for three times. The resulting base solution was neutralized by 10% HCl to give a white solid 0.8 g. Yield: 60%

#### 2.2.3.5 BTTE



To a 100 mL two necked flask charged with nitrogen was added Benzo[1,2-*c*:3,4-*c'*]bis[1,2,5]thiadiazole (0.19 g, 0.54 mmol), 2 M  $\text{Na}_2\text{CO}_3$  30 mL, 15 mL dioxane,  $\text{Pd}(\text{PPh}_3)_4$  (0.1 g). The mixture was allowed to reflux for 15 min, then,



2,5-dimethylthiophen-3-ylboronic acid (0.69 g, 4.42 mmol) dissolved in 20 mL dioxane was introduced. The resulting mixture was allowed to reflux under the protection of nitrogen at dark for 40 h. Then, the reactive mixture was poured into H<sub>2</sub>O and extracted with ethyl acetate. The organic layer was separated and dried (Na<sub>2</sub>SO<sub>4</sub>). After concentration, the compound was purified by column chromatography on silica (petroleum: dichloromethane = 130:80 v/v) to give a pale yellow solid 0.14 g. Yield: 66.7%. <sup>1</sup>H NMR (400 MHz, CDCl<sub>3</sub>, ppm): 1.96 (s, 3 H, -CH<sub>3</sub>, anti-parallel conformer), 2.09 (s, 3 H, -CH<sub>3</sub>, parallel conformer), 2.42 (s, 3 H, -CH<sub>3</sub>, parallel conformer), 2.46 (s, 3 H, -CH<sub>3</sub>, anti-parallel conformer), 6.42 (s, 1 H, thiophene-H, parallel conformer), 6.69 (s, 1 H, thiophene-H, anti-parallel conformer). <sup>13</sup>C NMR (CDCl<sub>3</sub>, 75 MHz): 14.59, 14.70, 15.39, 127.49, 131.07, 131.22, 131.37, 131.59, 135.76, 135.95, 136.06, 136.70, 147.53, 157.20, 157.51. HRMS (TOF MS ES<sup>+</sup> for [M + H]<sup>+</sup>): calcd. for C<sub>18</sub>H<sub>15</sub>N<sub>4</sub>S<sub>4</sub>, 415.0180; found 415.0186.

Pure closed form: <sup>1</sup>H NMR (400 MHz, CDCl<sub>3</sub>, ppm): 2.18 (s, 6 H, -CH<sub>3</sub>), 2.29 (s, 6 H, -CH<sub>3</sub>), 7.45 (s, 2 H, thiophene-H).

## 2.3 Results and Discussion

### 2.3.1 Molecule design and synthesis

Figure 2.3 illustrate the synthetic route to the intermediate and target molecules. The important ethene bridge BBT was obtained through 5 steps starting from 2-methylthiophene. Generally speaking, all 5 steps were classic organic reaction with cheap starting materials and reagents, mild conditions and comparative high yields. Actually, it's difficult to obtain BBT due to the mixture of reagent, mono-substituted and fully substituted benzo[1,2-*c*:3,4-*c'*]bis[1,2,5] thiadiazole as a result of short reaction time at the beginning. The ratio between reagent and mono substituted benzo[1,2-*c*:3,4-*c'*]bis[1,2,5] thiadiazole was found to be 1: 20 after 16 h monitored by <sup>1</sup>H NMR. After prolonged reaction for 80 h and addition of another portion of Br<sub>2</sub>, BBT was easily obtained by removing extra Br<sub>2</sub> with water, and recrystallized from CHCl<sub>3</sub>. The target molecule could be obtained by typical Suzuki coupling. Mono substituted BBT could be suppressed by controlling the ratio between BBT and 2,5-dimethyl-thiophyl-boric acid, which finally facilitate the separation process. Dioxane was used for the Suzuki coupling instead of THF in order to increase the reactivity and temperature.

As a matter of fact, the greatly enhanced ground-state energy difference (Hückel rule) between the open and closed forms finally results in the thermal instability of the closed form in BTEs due to the strong aromaticities of six-membered ethene bridges.<sup>[18]</sup> Considering that benzobisthiadiazole is a highly electro-withdrawing group, we herein synthesized a novel photochromic BTTE system based on the benzobisthiadiazole unit, showing excellent thermal

stability for the closed form in various solvents from nonpolar to polar, and even at elevated temperatures. Since the ethene bridge with six-membered ring has its own advantages such as higher quantum yield in ring closure and longer absorption wavelength, we envision that the six-membered ring with low or non-aromaticity as the center ethene bridge might widely extend the diversity in the thermally irreversible photochromic systems.

### 2.3.2 $^1\text{H}$ NMR, $^{13}\text{C}$ NMR and Mass characterization

The following are the characterizations of important intermediates and target molecule:

Interestingly, BTTE shows two well-resolved sets of methyl proton signals in  $^1\text{H}$  NMR, corresponding to the parallel (2.09, 2.42 ppm) and anti-parallel (1.96, 2.46 ppm) conformations, commonly found in BTE systems (Figure 2.4).<sup>[82]</sup> In general, the two conformations, parallel (photochromic inactive) and antiparallel (photochromic active) conformations in most BTEs would undergo very fast single bond rotation resulting in only one set of time-averaged  $^1\text{H}$  NMR signals. Only for those diarylethenes bearing substituents, the rotation of aryl groups can be slowed down, resulting in two sets of  $^1\text{H}$  NMR signals. As integrated from  $^1\text{H}$  NMR, the ratio between parallel and antiparallel conformations of BTTE in  $\text{CDCl}_3$  is 55 to 45 (Figure 2.5). Due to the different conformers, the  $^{13}\text{C}$  NMR of BTTE appears to be quite complicated. The carbon atom of methyl groups give three signals corresponding to parallel and anti-parallel conformers and a mixture of the signal coming from both conformers.

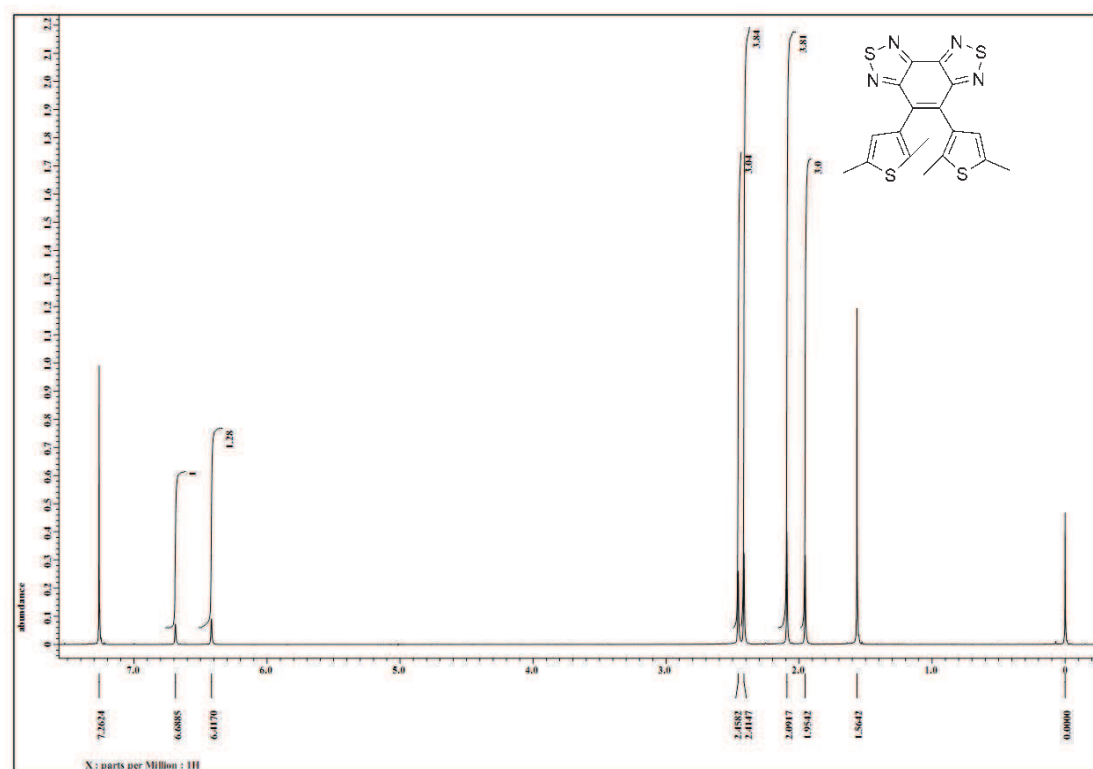


Fig. 2.4  $^1\text{H}$  NMR spectrum of BTTE in  $\text{CDCl}_3$

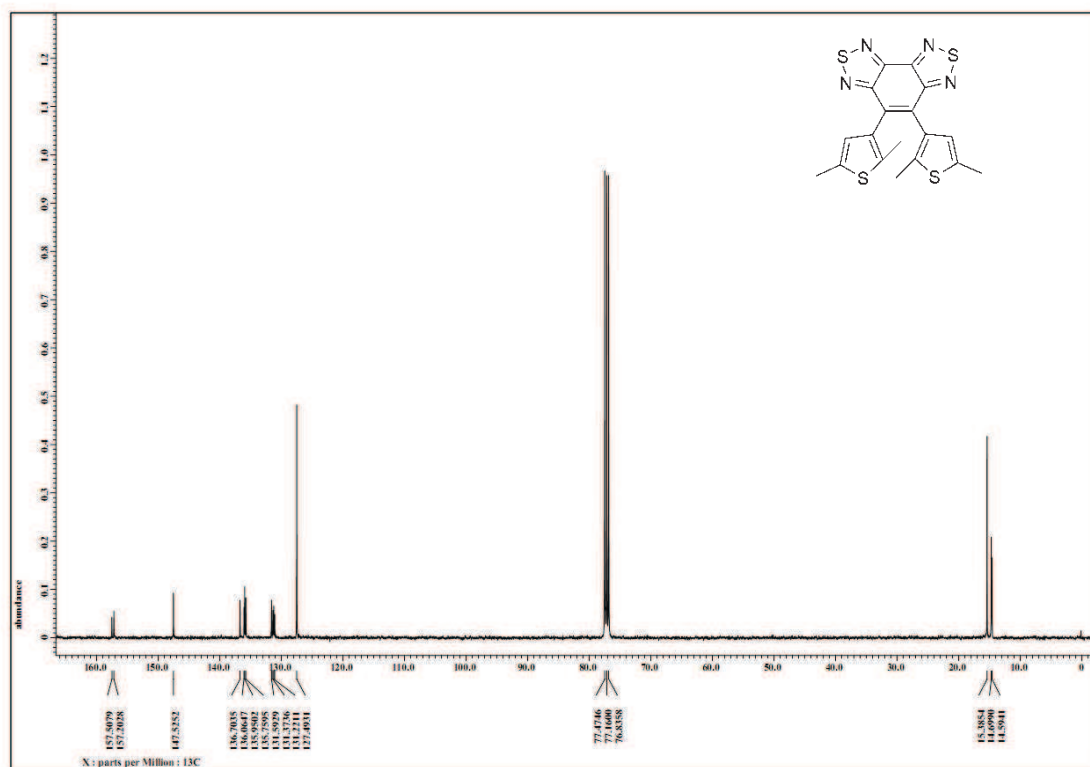


Fig. 2.5  $^{13}\text{C}$  NMR spectrum of BTTE in  $\text{CDCl}_3$

HRMS of BTTE (Figure 2.6) shows an apparent molecular ion peak corresponding to  $[\text{M} + \text{H}]^+$ . The calculated value for  $[\text{M} + \text{H}]^+$  is 415.0180, which is in accordance with an observed value of 415.0186

**Single Mass Analysis**

Tolerance = 5.0 mDa / DBE: min = -1.5, max = 100.0

Element prediction: Off

Number of isotope peaks used for i-FIT = 2

**Monoisotopic Mass, Even Electron Ions**

19 formula(e) evaluated with 1 results within limits (up to 1 best isotopic matches for each mass)

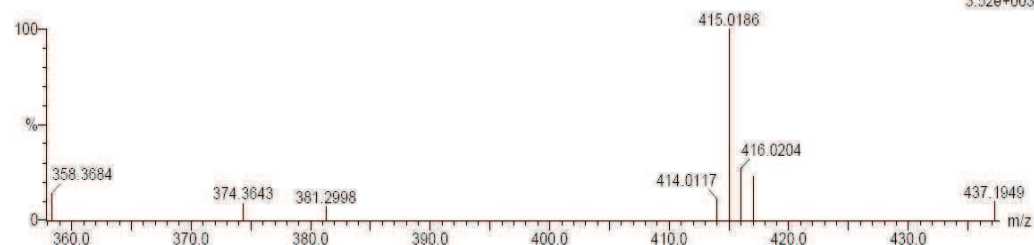
Elements Used:

C: 0-20 H: 0-15 N: 0-4 S: 0-4

ZHU-WH

ZWH-YYH-6 60 (1.921) Cm (57.60)

1: TOF MS ES+  
3.52e+003



Minimum: -1.5  
Maximum: 5.0 50.0 100.0

Mass	Calc. Mass	mDa	PPM	DBE	i-FIT	i-FIT (Norm)	Formula
415.0186	415.0180	0.6	1.4	13.5	0.1	0.0	C16 H15 N4 S4

Fig. 2.6 HRMS of BTTE

Under the condition of elevated temperature, the two sets of the signals disappeared and a time averaged signal was created (Figure 2.7). Only when the temperature reaches 160 °C could the signal be fully converted by extrapolation of the NMR data.

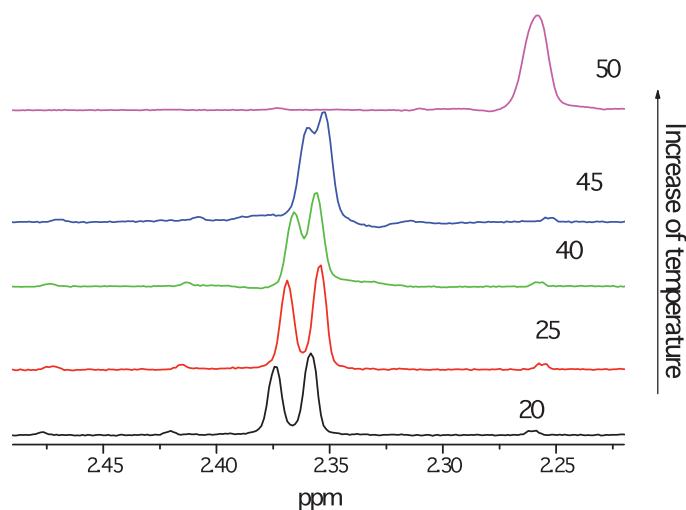


Fig. 2.7 Influence of the temperature on  $^1\text{H}$  NMR of BTTE in  $\text{CD}_3\text{CN}$  (numbers are temperature in  $^\circ\text{C}$ )

Further investigation reveals that the ratio between parallel conformer and anti-parallel conformer is scarcely affected by the variation of temperature (Table 2.1). No intra- or inter-molecular hydrogen bonding could be observed in *o*-BTTE evidence by  $^1\text{H}$  NMR at elevated temperature and in  $\text{CD}_3\text{OD}$ .

Table 2.1 Variation of the molar fractions of parallel and anti-parallel conformers affected by the increase of the temperature in  $\text{CD}_3\text{CN}$

Temperature	Molar fractions of parallel (left) and anti-parallel (right) conformers
20 $^\circ\text{C}$	45.6 / 54.4
25 $^\circ\text{C}$	44.8 / 55.2
30 $^\circ\text{C}$	44.05 / 55.95
35 $^\circ\text{C}$	45.24 / 54.76
40 $^\circ\text{C}$	44.24 / 55.76
45 $^\circ\text{C}$	45.66 / 54.34
50 $^\circ\text{C}$	43.86 / 56.14

#### 2.2.4 UV-Vis spectra of BTTE

BTTE exhibits a colourless solution with an intense absorption band at *ca.* 288 nm and another moderate absorption band at *ca.* 361 nm in various solvents (Table 2.5). The

absorption band at 361 nm is composed of HOMO→LUMO  $\pi$ - $\pi^*$ , HOMO-1→LUMO  $\pi$ - $\pi^*$ , HOMO-2→LUMO  $n$ - $\pi^*$  transitions through the comparison of UV-Vis absorption and calculated spectra by TD-DTF (Gaussian03, B3LYP, 6-31g(d,p)) (Tables 2.2 and 2.3). As expected, upon light irradiation at 365 nm, the solution of BTTE quickly turns brown with an intense absorption band at 382 nm (HOMO→LUMO+2 transition) and two moderate low lying bands at 455 (HOMO→LUMO+1 transition) and 585 nm (HOMO→LUMO transition) (Figure 2.9 B and Table 2.4), indicative of the appearance of the closed form (*c*-BTTE) produced by the characteristic photocyclization (Figure 2.9 A). The significant bathochromic shift in absorption bands of the closed forms relative to their open forms is mainly due to the extended  $\pi$ -conjugation across the whole moiety. The clear isobestic point strongly indicates that the photochromic reaction through excited state is simply composed of open and closed isomers. Upon absorption of photons, the transition occurs within  $10^{-15}$  s, thus its rate is three magnitudes faster than the rotation and reorientation of chromophore. Hence, the transition is recognized to be vertical, and the absorption should be barely affected by the solvent polarity (Figure 2.9 B-F). Moreover, the absorption bands in the visible region are gradually bleached as a result of the photochromic back reaction upon irradiation at 575 nm. The typical photochromic properties of BTTE and *c*-BTTE are summarized in Table 2.6. Particularly, BTTE exhibits comparatively larger ring-closure quantum yields in polar solvents than that in low polar solvents (from 14.5% in toluene to 42.1% in acetonitrile), which is rarely observed in diarylethene photochromic systems.<sup>[86-87]</sup> Detailed mechanism will be discussed in the following section.

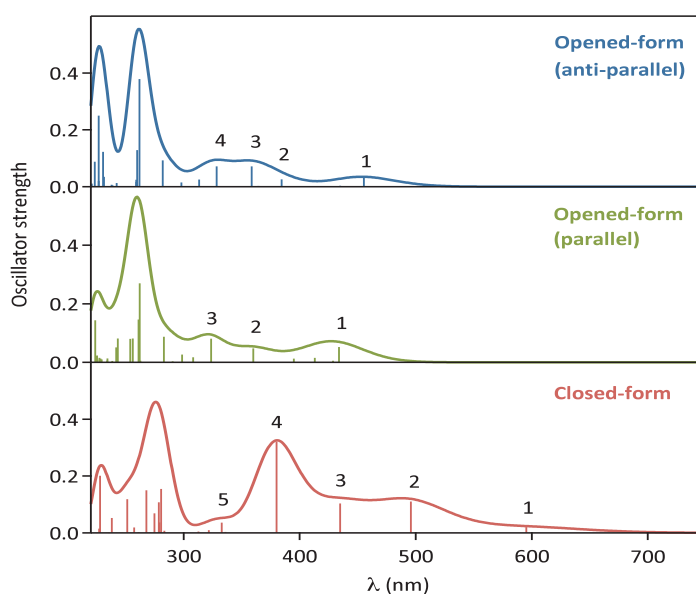


Fig. 2.8 Franck-Condon electronic transitions of BTTE calculated by TD-DFT (using  $3000\text{ cm}^{-1}$  gaussian bandwidth)

**Table 2.2** Composition of main electronic transitions of BTTE, open form (anti-parallel conformer)

Open form (anti-parallel conformer) (HOMO = 107 / LUMO = 108)	Character
Transition 1: (HOMO)→(LUMO) 100%	$\pi$ - $\pi^*$ transition, charge-transfer character
Transition 2: (HOMO-1)→(LUMO) 100%	$\pi$ - $\pi^*$ transition, charge-transfer character
Transition 3: (HOMO-2)→(LUMO) 91%	n- $\pi^*$ transition, charge-transfer character
Transition 4: (HOMO-3)→(LUMO) 98%	n- $\pi^*$ transition, charge-transfer character

**Table 2.3** Composition of main electronic transitions of BTTE open form (parallel conformer)

Open form (parallel conformer) (HOMO = 107 / LUMO = 108)	Character
Transition 1: (HOMO)→(LUMO) 95%	$\pi$ - $\pi^*$ transition, charge-transfer character
Transition 2: (HOMO-2)→(LUMO) 100%	n- $\pi^*$ transition, charge-transfer character
Transition 3: (HOMO-3)→(LUMO) 91%	n- $\pi^*$ transition, charge-transfer character

**Table 2.4** Composition of the main electronic transitions of BTTE, closed form (c-BTTE)

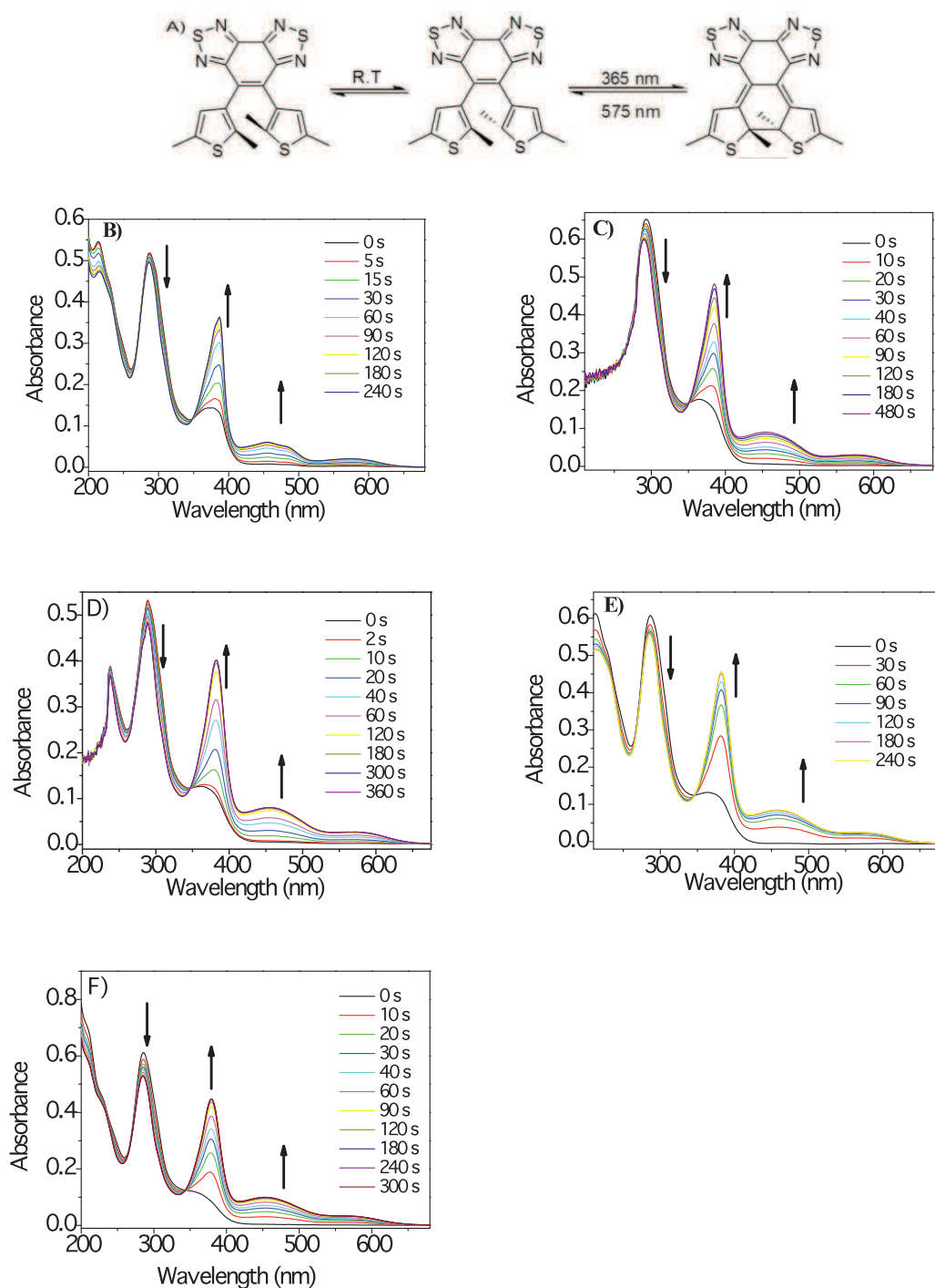
Closed form (HOMO = 107 / LUMO = 108)	Character
Transition 1: (HOMO)→(LUMO) 100%	$\pi$ - $\pi^*$ transition, almost no charge-transfer
Transition 2: (HOMO)→(LUMO+1) 100%	$\pi$ - $\pi^*$ transition, slight charge-transfer
Transition 3: (HOMO)→(LUMO+2) 81% (HOMO-1)→(LUMO) 19%	$\pi$ - $\pi^*$ transition, slight charge-transfer
Transition 4: (HOMO)→(LUMO+2) 12% (HOMO-1)→(LUMO) 88%	$\pi$ - $\pi^*$ transition, slight charge-transfer
Transition 5: (HOMO-1)→(LUMO+1) 78% (HOMO)→(LUMO+3) 22%	$\pi$ - $\pi^*$ transition, slight charge-transfer $\pi$ - $\pi^*$ transition, no charge-transfer

**Table 2.5** Absorption of BTTE and c-BTTE in various solvents with the cyclization quantum yields

Solvents	BTTE ( $\lambda_{\max}$ , nm)	c-BTTE <sup>[a]</sup> ( $\lambda_{\max}$ , nm)	$\Phi_{O-C}$ (%) <sup>[b]</sup>
Cyclohexane	287, 375	284, 387, 453, 485, 575	15.0
Toluene	293, 366	284, 380, 455, 581	14.5
THF	288, 361	289, 382, 455, 585	26.4
Ethanol	285, 364	284, 382, 458, 587	27.5
Acetonitrile	285, 357	284, 379, 454, 576	42.1

[<sup>a</sup>] Pure closed form was separated on silica gel eluted with petroleum ether: dichloromethane = 130:80 v/v.

[<sup>b</sup>] Cyclization quantum yield was measured for 365 nm UV irradiation in various solvents.



**Fig. 2.9** (A) Photographic images and structural changes of BTTE under the alternate irradiation of UV and visible light in THF ( $2.09 \times 10^{-4} \text{ mol}\cdot\text{L}^{-1}$ ); UV absorption spectra changes of BTTE upon irradiation at 365 nm in B) cyclohexane ( $2.10 \times 10^{-5} \text{ mol}\cdot\text{L}^{-1}$ ); C) toluene ( $2.69 \times 10^{-5} \text{ mol}\cdot\text{L}^{-1}$ ); D) THF ( $2.09 \times 10^{-5} \text{ mol}\cdot\text{L}^{-1}$ ); E) ethanol ( $2.49 \times 10^{-5} \text{ mol}\cdot\text{L}^{-1}$ ); F) acetonitrile ( $2.31 \times 10^{-5} \text{ mol}\cdot\text{L}^{-1}$ ).

### 2.2.5 $^1\text{H}$ NMR changes of BTTE before and after irradiation

Generally speaking, there are great differences in  $^1\text{H}$  NMR before and after irradiation at 365 nm due to the structure change after isomerization. Thus,  $^1\text{H}$  NMR is an important tool to study the photochromic reaction.<sup>[88-90]</sup>

The existence of *c*-BTTE is evidenced by  $^1\text{H}$  NMR signals. The two sets of well-resolved signals were converted into one set of methyl proton signals on thiophene rings (moved from 1.96 and 2.09 ppm, 2.42 and 2.46 ppm to 2.29 and 2.18 ppm, respectively). The simultaneous disappearance of the two sets of signals indicates that a slow interconversion between parallel and anti-parallel conformations takes place in the system, and that the chemical environment of the two sets of methyl groups becomes identical after the cyclization reaction. Interestingly, in contrast to the two thiophene protons (6.42, 6.69 ppm) in the open form of BTTE, the thiophene protons shifted downfield to 7.45 ppm in the closed form, which can be attributed to the possible formation of intramolecular hydrogen bonding between the proton on thiophene and nitrogen atom on the benzobisthiadiazole unit upon photocyclization (Figure 2.10).

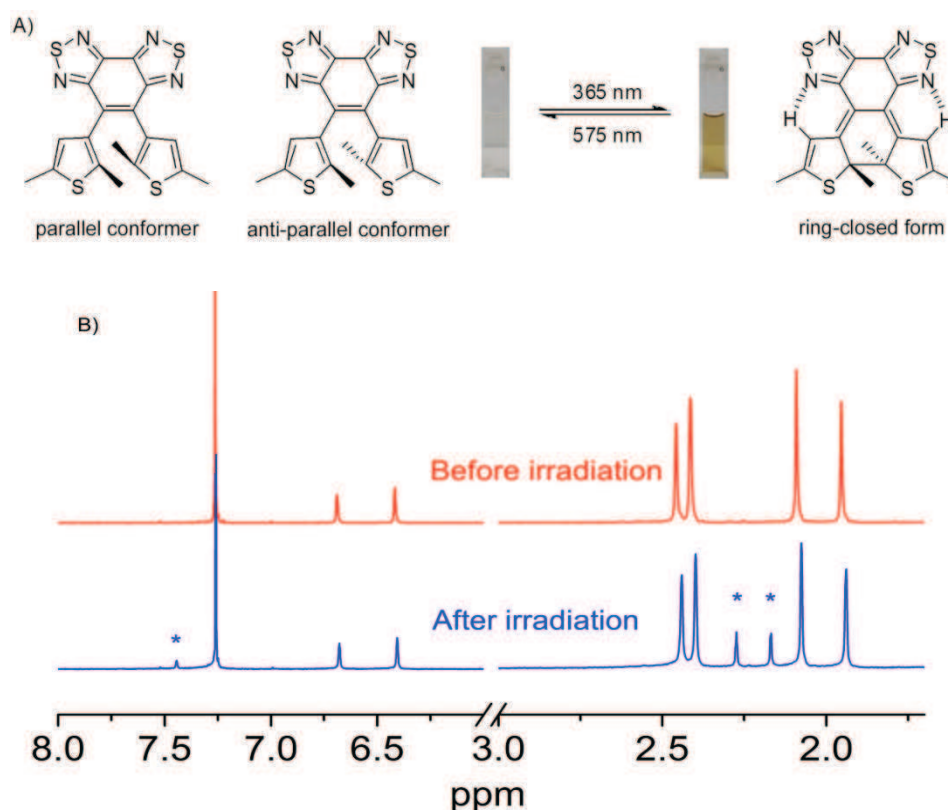
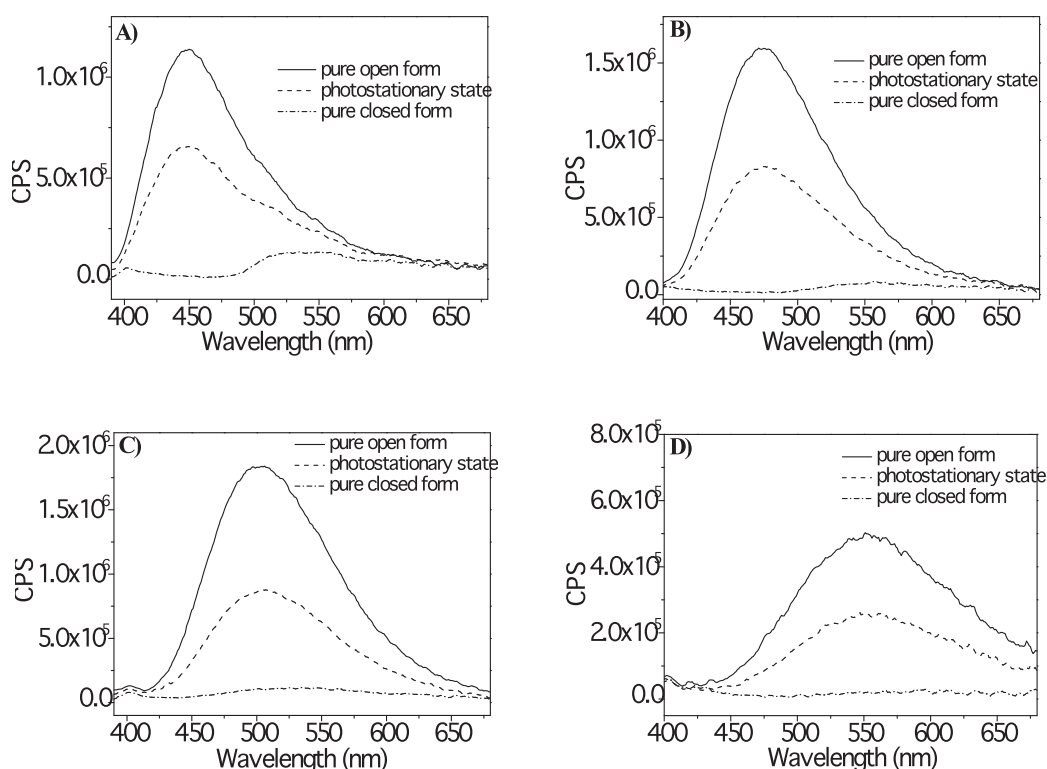


Fig. 2.10 (A) Photographic images and structural changes of BTTE under the alternate irradiation of UV and visible light in THF ( $2.09 \times 10^{-4} \text{ mol}\cdot\text{L}^{-1}$ ), and (B)  $^1\text{H}$  NMR signal changes of BTTE upon UV irradiation in  $\text{CDCl}_3$ .



### 2.2.6 Emission spectra of BTTE before and after irradiation

According to the parameters listed in Table 2.5, the absorption of BTTE is barely affected by the solvent polarity. The absorption band of *o*-BTTE and *c*-BTTE remain at 375 nm and 575, 587 nm, respectively, from nonpolar (hexane) to polar solvent (acetonitrile). However, BTTE shows noticeable fluorescence in various solvents, the emission wavelength and intensity of which could be modulated through both solvato- and photochromism. As a matter of fact, pure *c*-BTTE was separated successfully. Upon irradiation at the maximum absorption band of *c*-BTTE at 585 nm, no obvious fluorescence could be recorded (Figure 2.11), indicating that *c*-BTTE is a non-fluorescent compound. The fluorescence of BTTE was quenched by 48% excited at the isobestic point of 347 nm after irradiation at 365 nm in THF until the photostationary state was reached. The percentage of quenched fluorescence is fully compatible with the conversion yield 53% (Table 2.6). Thus, it could be concluded that the quenched fluorescence is simply due to the disappearance of *o*-BTTE and non-fluorescent property of *c*-BTTE.



**Fig. 2.11** Spectral changes of fluorescence (A, B, C, D) of the pure open and closed forms in cyclohexane ( $3.20 \times 10^{-5} \text{ mol}\cdot\text{L}^{-1}$ ), toluene ( $2.69 \times 10^{-5} \text{ mol}\cdot\text{L}^{-1}$ ), THF ( $2.35 \times 10^{-5} \text{ mol}\cdot\text{L}^{-1}$ ), and ethanol ( $1.26 \times 10^{-5} \text{ mol}\cdot\text{L}^{-1}$ ). Excitation for fluorescence at the isosbestic point (respectively 348, 351, 357, 346 nm). The PSS were obtained by irradiating solutions with 365 nm light until no further spectral changes were observed. Pure closed form was separated by column chromatography eluted with petroleum ether:dichloromethane = 130:80 v/v.

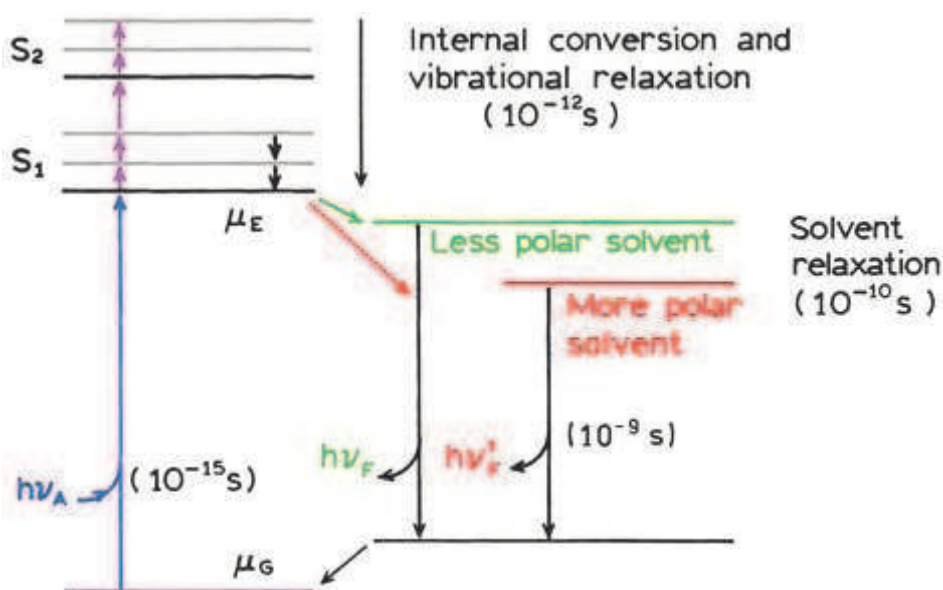
Table 2.6 Photochromic and fluorescent properties of BTTE in various solvents

	Cyclohexane	Toluene	THF	Ethanol	Acetonitrile
BTTE: $\lambda_{em}$ (nm)	449	475	504	553	542
$\Phi_{o-c}$ <sup>[a]</sup>	15.0	14.5	26.4	27.5	42.1
$\Phi_{c-o}$ <sup>[a]</sup>	7.7	5.9	7.4	6.2	6.8
$\alpha_{PSS}$ (%) <sup>[a]</sup>	36.2	43.0	53.0	51.1	58.1
$\tau_1$ (ns) / $f_1$ <sup>[b]</sup>	-	0.24 / 0.76	0.60 / 0.92	1.22 / 0.90	1.39 / 0.97
$\tau_2$ (ns) / $f_2$ <sup>[b]</sup>	-	0.12 / 0.24	0.22 / 0.08	0.07 / 0.10	0.17 / 0.03
$\Phi_F$ (%) <sup>[c]</sup>	0.36	0.51	0.80	1.04	1.33

<sup>[a]</sup>  $\Phi_{o-c}$ ,  $\Phi_{c-o}$  and  $\alpha_{PSS}$  are depicted as the ring-closure quantum yield at 365nm, the ring-opening quantum yield at 575nm and the conversion yield at 365nm, respectively.

<sup>[b]</sup> The decay curves were analyzed by a two-exponential function:  $I_F(t) = A_1 \times \exp(-t/\tau_1) + A_2 \times \exp(-t/\tau_2)$ . The fractions of intensity  $f_i$  corresponding to the time-constants  $\tau_1$  and  $\tau_2$  were calculated by the following equation:  $f_i = A_i \tau_i / \sum A_j \tau_j$ .

<sup>[c]</sup>  $\Phi_F$  is the fluorescence quantum yield.


 Fig. 2.12 Jablonski diagram for fluorescence with solvent relaxation<sup>[93]</sup>.

Emission from fluorophores generally occurs at wavelengths that are longer than those at which absorption occurs. This loss of energy is due to a variety of dynamic processes that occur following light absorption (Figure 2.12). The fluorophore is typically excited to the first singlet state ( $S_1$ ), usually to an excited vibrational level within  $S_1$ . The excess vibrational energy is rapidly lost to the solvent. If the fluorophore is excited to the second singlet state ( $S_2$ ), it rapidly decays to the  $S_1$  state in  $10^{-12}$  s due to internal conversion. Solvent effects shift

the emission to still lower energy due to stabilization of the excited state by the polar solvent molecules. Typically, the fluorophore has a larger dipole moment in the excited state ( $\mu_E$ ) than in the ground state ( $\mu_G$ ). Following excitation the solvent dipoles can reorient or relax around  $\mu_E$ , which lowers the energy of the excited state. As the solvent polarity is increased, this effect becomes larger, resulting in emission at lower energies or longer wavelengths. In general, only high polar fluorophores display a large sensitivity to solvent polarity. Nonpolar molecules, such as unsubstituted aromatic hydrocarbons, are much less sensitive to solvent polarity. Fluorescence lifetimes (1–10 ns) are usually much longer than the time required for solvent relaxation. For fluid solvents at room temperature, solvent relaxation occurs in 10–100 ps. For this reason, the emission spectra of fluorophores are representative of the solvent relaxed state. Examination of Figure 2.12 and Figure 2.13 reveals why absorption spectra are less sensitive to solvent polarity than emission spectra. Absorption of light occurs in about  $10^{-15}$  s, a time too short for the fluorophore or solvent to move. Absorption spectra are less sensitive to solvent polarity because the molecule is exposed to the same local environment in the ground and excited states. In contrast, the emitting fluorophore is exposed to the relaxed environment, which contains solvent molecules oriented around the dipole moment of the excited state.

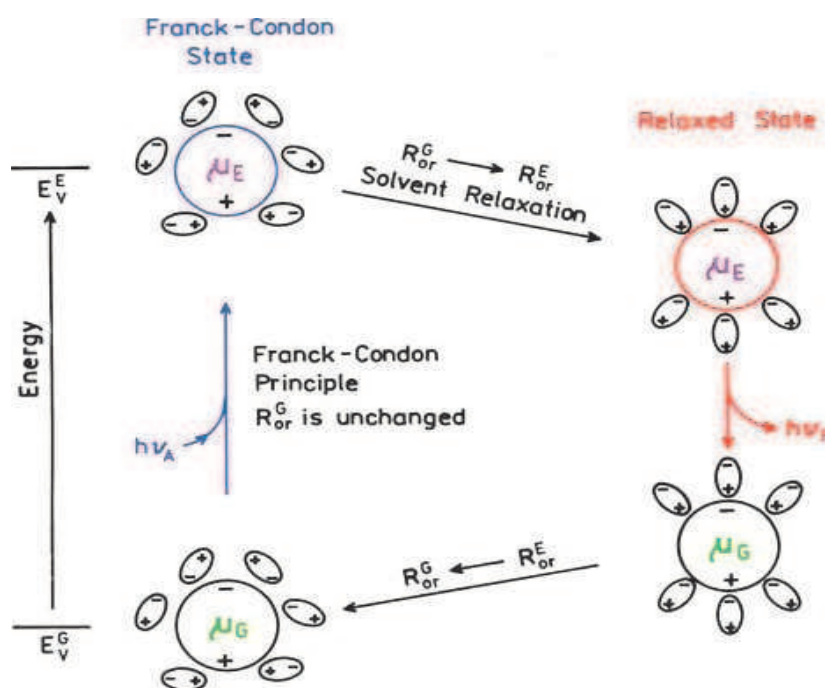
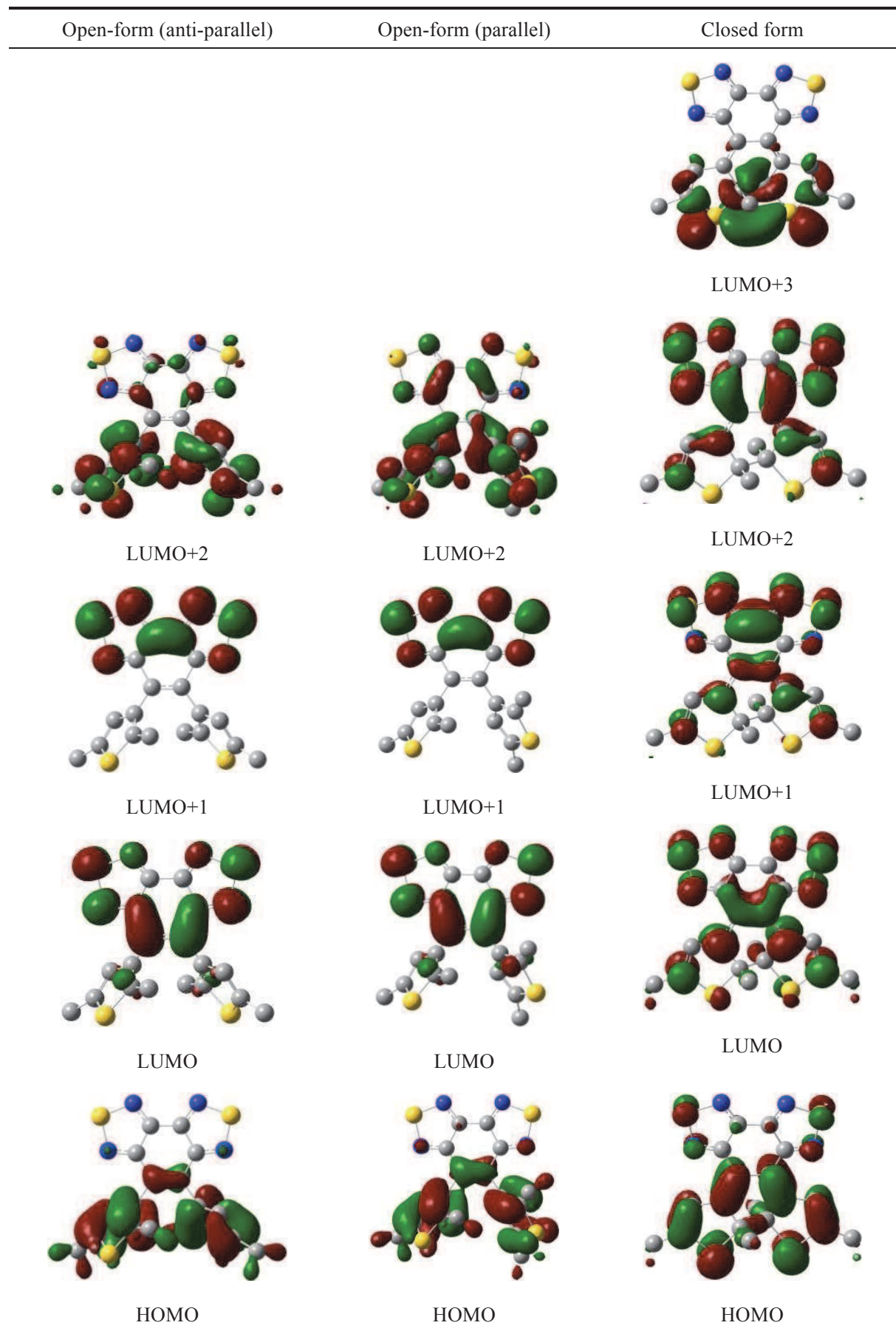
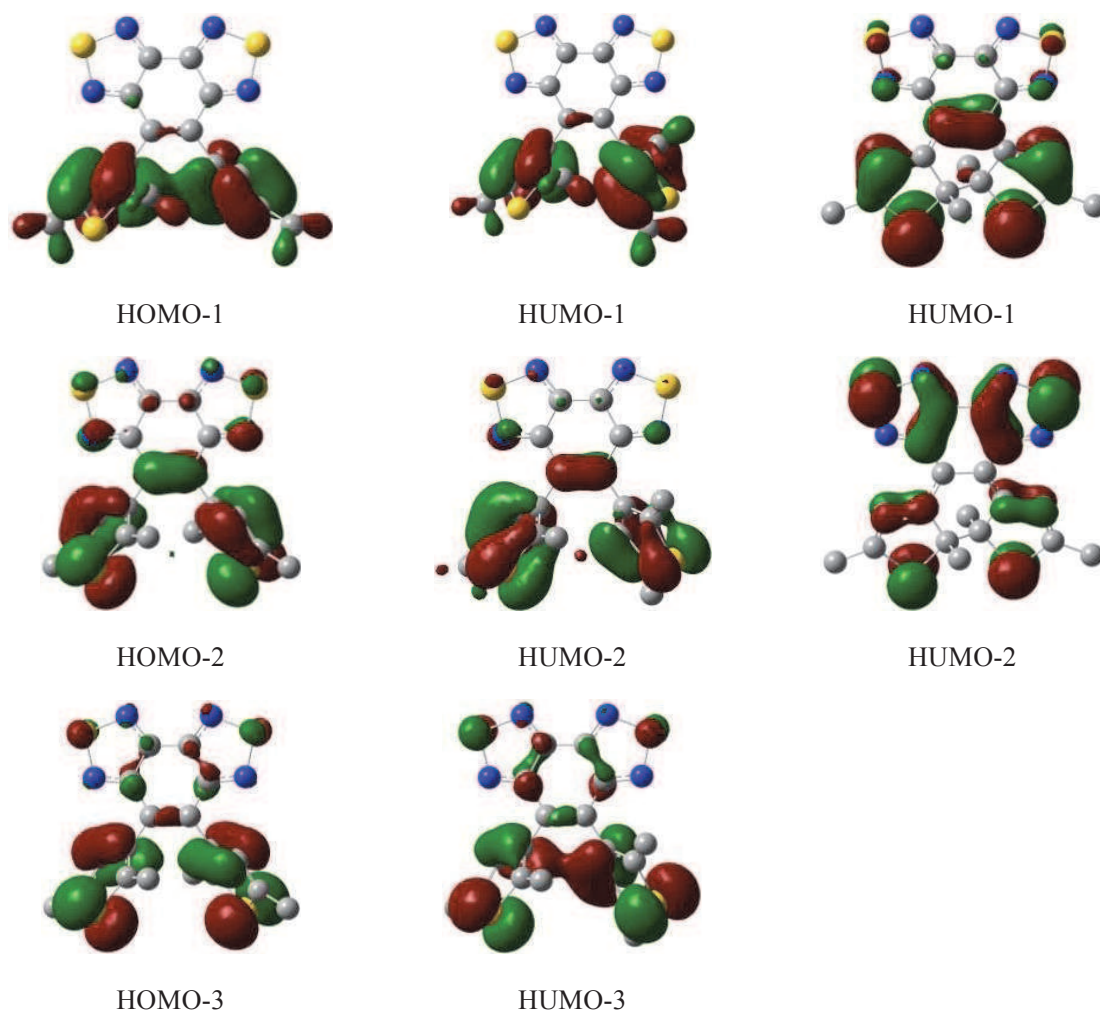


Fig. 2.13 Effects of the electronic interactions and orientation reaction fields on the energy of a dipole in a dielectric medium,  $\mu_E > \mu_G$ . The smaller circles represent the solvent molecules and their dipole moments<sup>[93]</sup>.

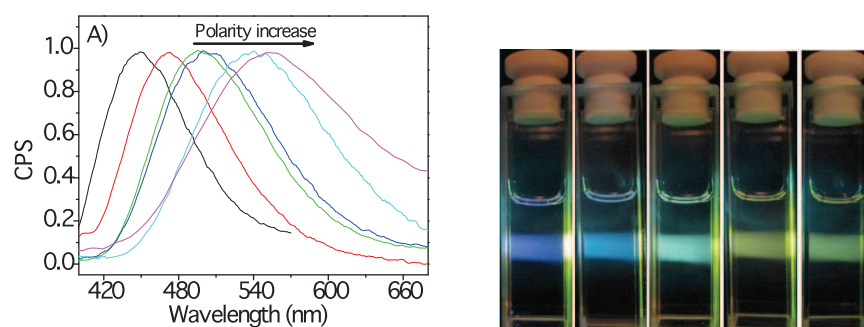
Table 2.7 Molecular orbitals of BTTE involved in the main electronic transitions





Note: Molecular orbitals were drawn with an iso-coefficient of 0.03

According to the DFT calculation listed in [Table 2.7](#), a large charge transfer exists between the HOMO-LUMO orbital of BTTE. When excited from the ground state to the excited state, the dipole moment was greatly enhanced. As mentioned above, the enhanced dipole moment can be stabilized in polar solvents; hence, the energy gap between HOMO-LUMO is lowered to a longer emission wavelength. On the other hand, in nonpolar solvent, the enhanced dipole moment cannot be stabilized, thus, the emission wavelength is shorter ([Figure 2.14](#)).



**Fig. 2.14** A) Normalized fluorescence spectra in various solvents (from left to right, cyclohexane,

chloroform, THF, acetonitrile, DMF, and ethanol); B) Photographic fluorescence images of BTTE in different solvents ( $2.0 \times 10^{-5} \text{ mol}\cdot\text{L}^{-1}$ ). From left to right: hexane, toluene, THF, ethanol, and acetonitrile.

To further investigate the effect of solvatochromism on the excited state of BTTE, we studied the Lippert-Mataga plots of BTTE in various solvents. The interaction between BTTE and solvents can affect the energy gap between HOMO-LUMO, which can be expressed in wavenumber ( $\text{cm}^{-1}$ ) as a function of dielectric constant ( $\epsilon$ ) and refractive index ( $n$ ), and described by Lippert-Mataga equation<sup>[91-92]</sup>:

$$\begin{aligned} \bar{\nu}_A - \bar{\nu}_F = \Delta\bar{\nu} &= \frac{2}{hca^3} \left( \frac{\epsilon - 1}{2\epsilon + 1} - \frac{n^2 - 1}{2n^2 + 1} \right) (\mu_e - \mu_g)^2 + const \\ &= \frac{2\Delta f}{hca^3} \Delta\mu^2 + const \end{aligned} \tag{Equation 2.1}$$

In this equation  $h$  ( $= 6.6256 \times 10^{-27} \text{ erg}$ ) is Planck's constant,  $c$  ( $= 2.9979 \times 10^{10} \text{ cm/s}$ ) is the speed of light, and  $a$  is the radius of the cavity in which the fluorophore resides (this parameter could be obtained through DFT calculation or averaged crystal radius).  $\nu_A$  and  $\nu_F$  are the wavenumbers ( $\text{cm}^{-1}$ ) of the absorption and emission, respectively. Equation 2.1 is only an approximation, but there is reasonable correlation between the observed and calculated energy losses in non-protic solvents. By non-protic solvents we mean those without hydroxyl groups, or other groups capable of hydrogen bonding. The Lippert-Mataga equation is an approximation in which the polarizability of the fluorophore and higher-order terms are neglected. These terms would account for second order effects, such as the dipole moments induced in the solvent molecules resulting by the excited fluorophore, and vice versa.

Table 2.8 Spectral Properties of BTTE in various solvents

Solvents	$\lambda_{\text{max}}^{\text{abs}}$ (nm)	$\lambda_{\text{max}}^{\text{Em}}$ (nm)	Stokes shift ( $\text{cm}^{-1}$ )	$\Delta f$
Cyclohexane	375	449	4395	0.001
Chloroform	365	497	7374	0.185
THF	361	504	7860	0.209
DMF	363	549	8931	0.276
Ethanol	364	553	9389	0.298
Acetonitrile	357	542	9500	0.304

From the values shown in Table 2.8, we obtained the Lippert-Mataga plot of BTTE (Figure 2.15). It could be evidenced that the excited BTTE has a higher dipole moment than the ground state BTTE, which is probably due to the photoinduced charge transfer from electron rich thiophene rings to the electron deficient benzobisthiadiazole moiety. Hence,

BTTE exhibits different emission spectra in various solvents<sup>[93]</sup>.

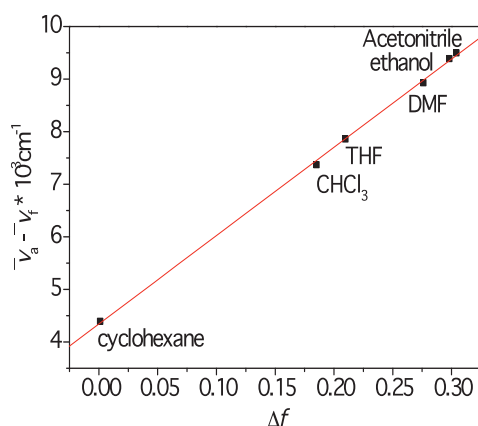
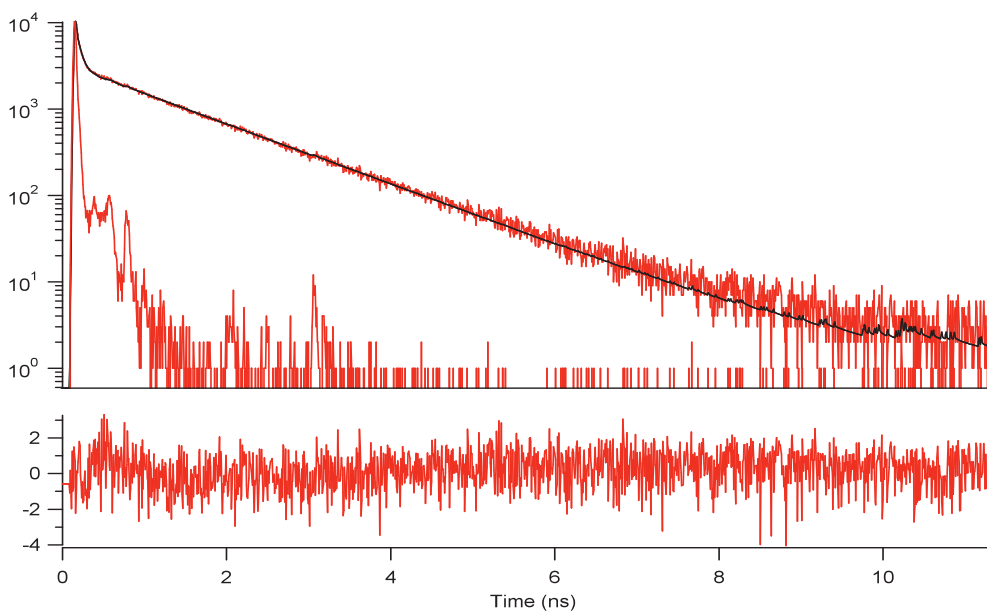
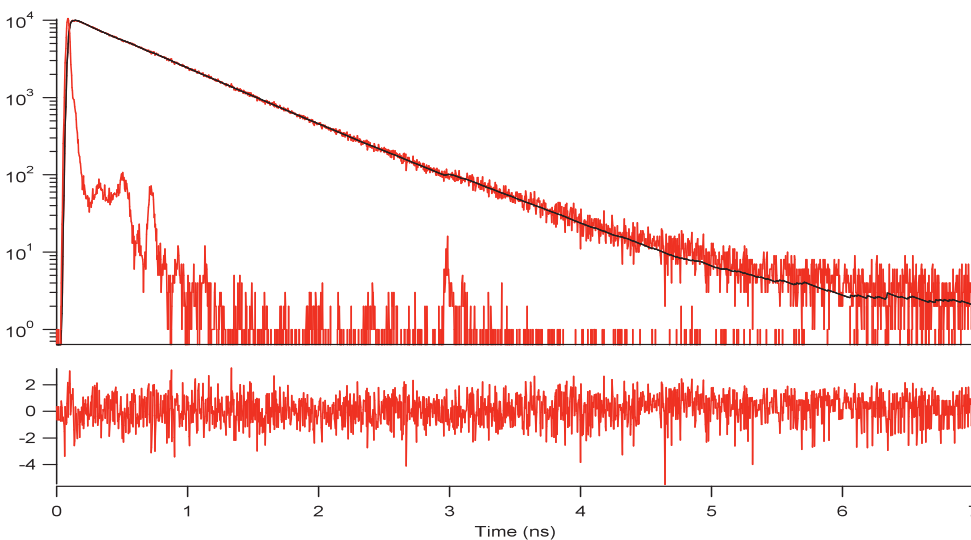
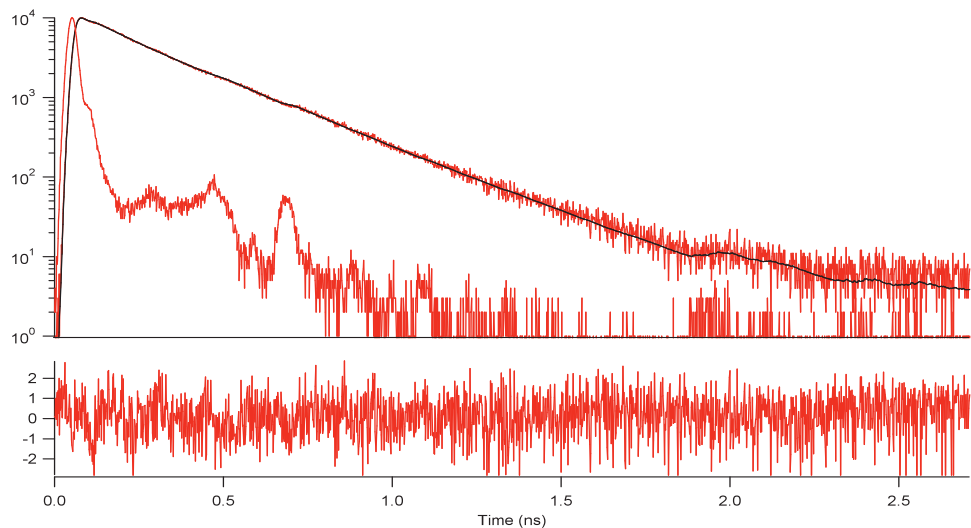


Fig. 2.15 Lippert-Mataga plot of BTTE

### 2.2.7 The fluorescence decay of BTTE in various solvents

In order to gain further insight into the photochromic and fluorescent properties of BTTE, fluorescence decays were acquired in several solvents by the time-correlated single photon counting technique. In all investigated solvents (toluene, THF, ethanol and acetonitrile), the fluorescence decay curves were successfully analyzed by means of a biexponential function ( $\chi^2_{\text{R}} < 1.2$ ). In these solvents, the long time-constant  $\tau_1$  increases together with the solvent polarity (from 0.24 ns in toluene to 1.39 ns in acetonitrile), whereas the short time-constant  $\tau_2$  remains almost unchanged, in the range of 0.07–0.22 ns (Table 2.6). The corresponding fractions of intensity ( $f_i$ ) show that the emission arises predominantly from the long lifetime, with an increasing contribution for the more polar solvents. It may be concluded that the long decay-time corresponds to a population of molecules in their parallel conformation, known to be non-photochromic, but noticeably fluorescent. By increasing the solvent polarity, the fluorescence quantum yield of BTTE becomes higher, the fluorescence spectrum shows a red-shift (vide supra) and the lifetime  $\tau_1$  becomes longer. These observations are consistent with a mostly fluorescent parallel conformation bearing perpendicular thiophene rings with respect to the benzobisthiadiazole moiety, which could significantly enhance the intramolecular charge transfer (ICT) efficiency in excited states. On the other hand, the short decay-time  $\tau_2$  may correspond to the photochromic but weakly fluorescent anti-parallel conformation. Its fluorescence contribution ( $f_2$ ) decreases with an increase in the solvent polarity, which is fully compatible with the increasing ring-closure quantum yield ( $\Phi_{\text{o-c}}$ , Table 2.6). Indeed, for the photochromic-active conformation, it is reasonable to assert that the ring-closure reaction occurring from the excited state is in competition with the radiative pathway to the ground state.





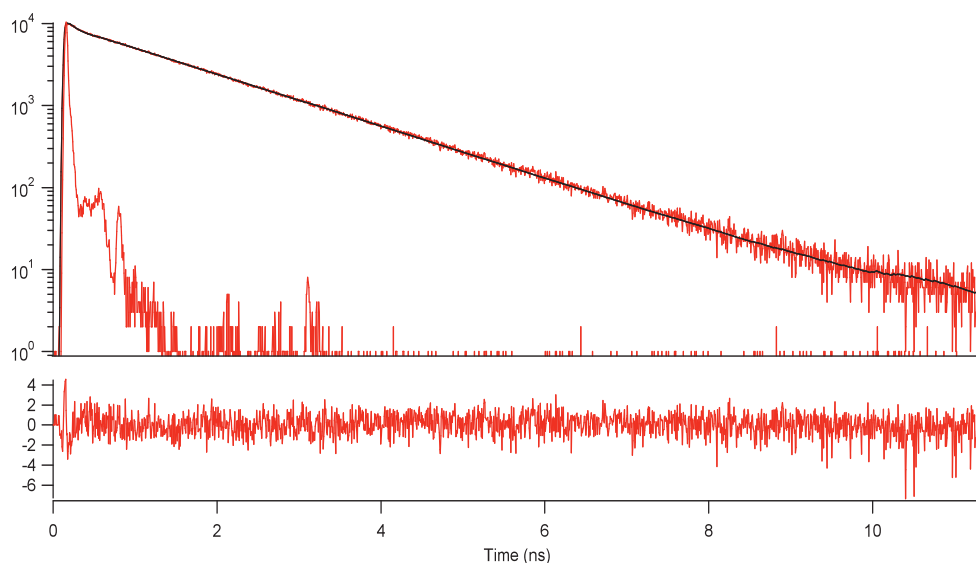
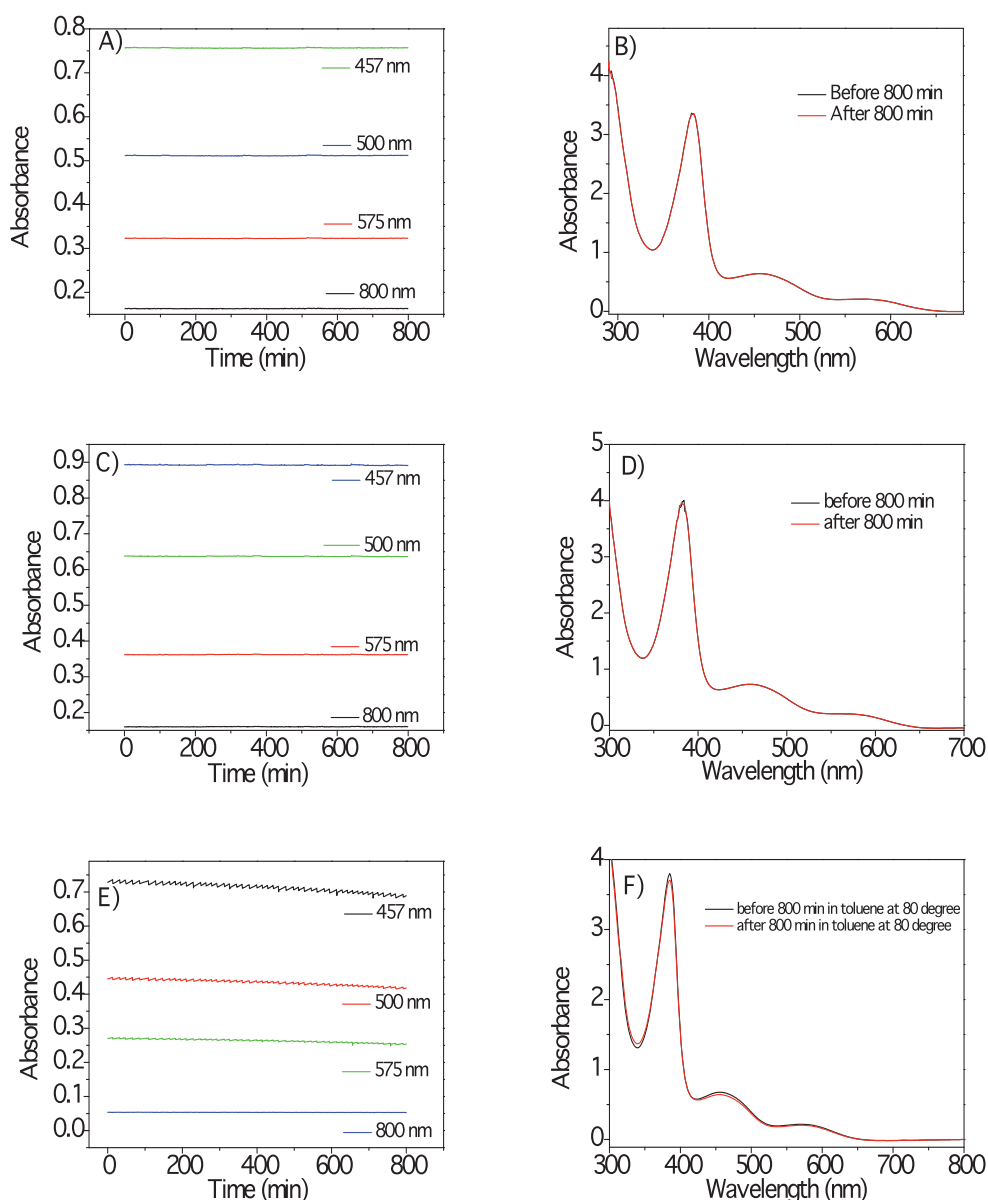


Fig. 2.16 Fluorescence decay of BTTE in various solvents (From top to bottom: toluene, THF, ethanol and acetonitrile)

### 2.2.8 Thermal stability of BTTE in various solvents

Generally in BTE derivatives, an aromatic character of six-membered ethene favors the undesirable thermal back reaction at dark due to the large loss of aromatic stabilization energy upon photocyclization. In contrast, *c*-BTTE preserves very promising thermal stability with almost flat decays, and does not show any thermal back reaction in various solvents like cyclohexane, THF and even in ethanol at dark and room temperature (Figures 2.17). Actually, the pure closed form was successfully separated on silica gel eluted with petroleum ether: dichloromethane. At elevated temperature (80 °C) in toluene, *c*-BTTE shows only 5.4% decrease of its absorbance at 457 nm after 800 min (Figures 2.17). In contrast with *c*-BTB (Figure 2.1) containing benzothiadiazole unit as the bridge, <sup>[84]</sup> the thermal stability of *c*-BTTE is not affected by solvent polarity: *c*-BTB is stable at room temperature only in low polar solvents such as cyclohexane and hexane, showing first-order decay in polar solvents such as THF ( $k = 3.17 \times 10^{-5} \text{ min}^{-1}$ ) and acetonitrile ( $k = 2.95 \times 10^{-4} \text{ min}^{-1}$ ). Moreover, the fatigue resistance of BTTE was also studied: upon alternating UV (365 nm) and visible light (575 nm) irradiation in degassed THF, BTTE can be repeatedly toggled between the open-form and closed-form, keeping intact without any obvious degradation. Thus, by the introduction of the uncommon benzobisthiadiazole six-membered ring as ethene bridge, BTTE can provide the photochromic performances of parent BTEs, such as the widely known five-membered hexafluorocyclopentene-based counterparts.



**Fig. 2.17** Absorbance monitoring at room temperature of BTTE after reaching the PSS by UV irradiation A, B) in THF,  $2.09 \times 10^{-4} \text{ mol}\cdot\text{L}^{-1}$ ; C, D) in ethanol,  $2.49 \times 10^{-4} \text{ mol}\cdot\text{L}^{-1}$ ; E, F) in toluene at  $80^\circ\text{C}$ . The noise on the data is due to the evaporation and the condensation of the solvent. No obvious back reaction was observed at 457nm, 500nm, 575nm and 800nm after 800 min

To gain insight into the geometry, the molecular orbitals and eventually the role of the highly polar and remarkably electron-withdrawing benzobisthiadiazole unit on the previously mentioned properties, quantum chemical calculations (DFT) were performed with Gaussian 09 program and compared to the reference compound BTB.<sup>[94]</sup> The geometries were optimized with PBE0 functional<sup>[95]</sup> and 6-31G(d,p) basis set. On the basis of optimized structures, more accurate energy determination can be achieved by performing single-point calculations with the larger basis set 6-311+g(d,p). The solvent effect is taken into account

within the polarizable continuum model<sup>[96]</sup> in the single-point calculations (Table 2.9 and Figure 2.18). For instance, the energy of the open-ring isomer corresponding to the reference of BTB is -8.768 kcal/mol lower than the closed-ring isomer in THF. While for BTTE, the open-ring isomer is more stable only by -4.607 kcal/mol as opposed to the closed-ring isomer in THF. Accordingly, during the course of photocyclization, the destabilization energy of BTTE destruct aromaticity is lower than for BTB.<sup>[97]</sup> Here, such relative low energy difference between the open form and closed form preserves excellent thermal stability, and does not show any thermal back reaction at dark at room temperature in a variety of solvents.

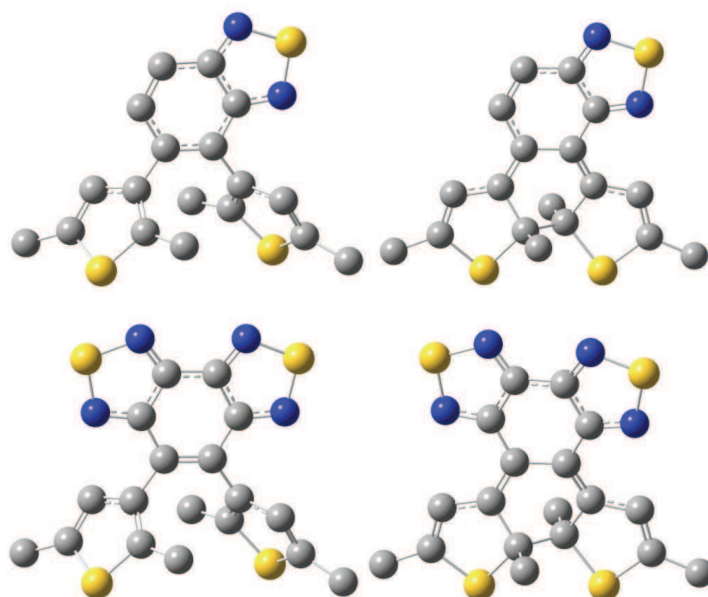


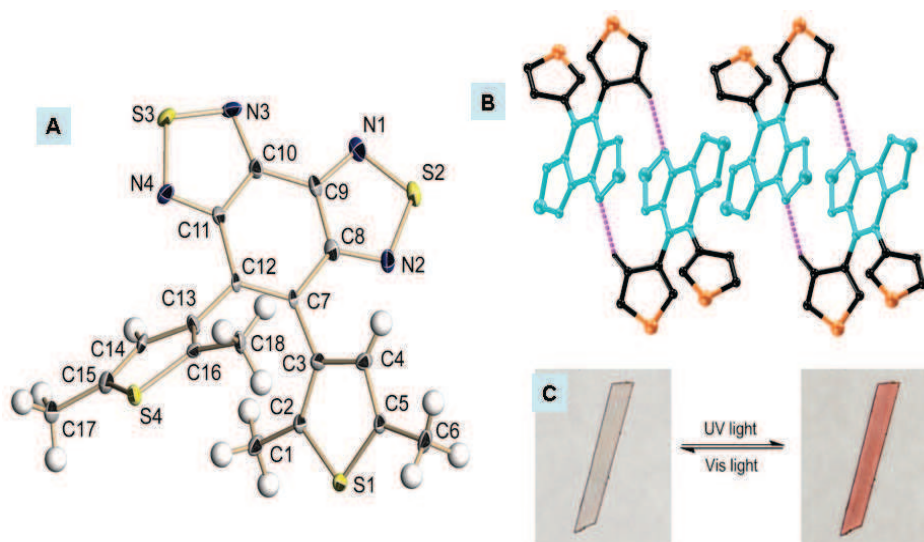
Fig. 2.18 The optimized ground state geometries for the open-ring and closed-ring isomers of BTB and BTTE.

Table 2.9 The optimized ground state energies for the open-ring and closed-ring isomers of BTB and BTTE

	THF
BTB	-1998.4856915 a.u.
<i>c</i> -BTB	-1998.4717193 a.u.
$\Delta E$	-8.768 kcal/mol
BTTE	-2504.7519347 a.u.
<i>c</i> -BTTE	-2504.7445946 a.u.
$\Delta E$	-4.607 kcal/mol

### 2.2.9 Photochromism of BTTE in crystal state

Single crystals of BTTE were grown by slow evaporation from THF-H<sub>2</sub>O solution and the X-ray crystallographic data of the open form were collected. Only the anti-parallel conformer exists in the single crystals (Figure 2.19A), although BTTE adopts both anti-parallel and parallel configurations in solution as evidenced by <sup>1</sup>H NMR. The resolved structure reveals that no intramolecular hydrogen bonding interaction exists in the crystal lattice. In contrast, the benzobisthiadiazole rings are assembled into a 1D chain by  $\pi\cdots\pi$  stacking interactions and intermolecular hydrogen bonds (Figure 2.19B). Notably, in the single crystal state,<sup>[98-99]</sup> the distance between the photoactive carbon atoms (C2 $\cdots$ C16) is 3.451 Å, the shortest among reported BTE systems and meeting the prerequisites for a molecule to undergo photochromic reaction in crystalline phase.<sup>[100-101]</sup> Indeed, bulk crystals of BTTE can be easily colored with typical photochromic behaviors, and the reaction is fully reversible (Figure 2.19C). In addition, the bond lengths of C11-C12 (1.491 Å) and C7-C8 (1.483 Å) are indicative of a single bond character, while the C7-C12 distance (1.395 Å) is clearly a double bond. Apparently, the benzobisthiadiazole chromophore shows almost no aromaticity, and the center bridge linking the two thiophene units is typical of a double bond, ensuring the 1,3,5-hexatriene section to adopt an appropriate conformation to undergo the conrotatory 6 $\pi$ -electron photocyclization. As Irie et al.<sup>[97]</sup> have demonstrated that a low aromaticity correlates well with the thermal stability of the closed form, these features of BTTE explain the excellent thermal stability of the closed-ring isomer.



**Fig. 2.19** A) ORTEP representation of the crystal structure of BTTE with displacement ellipsoids shown at the 50% probability level. Selected bond lengths (Å): C11-C12, 1.491(3); C7-C8, 1.483(3); C7-C12, 1.395(3); C2 $\cdots$ C16, 3.451(6). B) View of one-dimensional structure of BTTE formed by cooperative hydrogen bonding and  $\pi\cdots\pi$  stacking interactions. Methyl groups and non-hydrogen-bonded hydrogen atoms are omitted for clarity. Selected bond lengths and bond angles: N $\cdots$ H, 2.65 Å; S $\cdots$ H-C, 151°; N $\cdots$ C, 3.488(6) Å. Interplane ( $\pi\cdots\pi$ ) angle, 0°; S $\cdots$ centroid (benzene), 3.55 Å; centroid (thiadiazole) $\cdots$ centroid

(thiadiazole), 3.43 Å. C) Photographic color changes of BTTE in single crystal state by alternate 365 and 575 nm irradiations.

Table 2.10 Crystal and Structure Determinations Data of BTTE

Compounds	BTTE
Empirical formula	C <sub>18</sub> H <sub>14</sub> N <sub>4</sub> S <sub>4</sub>
Formula weight	414.61
Temp, K	-173(1)
Crystal system	triclinic
Space group	P-1
<i>a</i> , Å	7.679(2)
<i>b</i> , Å	8.799(2)
<i>c</i> , Å	14.555(4)
$\alpha$ , deg	99.149(7)
$\beta$ , deg	99.196(7)
$\gamma$ , deg	109.666(7)
Volume, Å <sup>3</sup>	890.0(4)
<i>Z</i>	2
density(calc), mg/mm <sup>3</sup>	1.547
crystal size, mm <sup>3</sup>	0.10 × 0.07 × 0.01
index ranges	-11 ≤ <i>h</i> ≤ 10, -13 ≤ <i>k</i> ≤ 9, -18 ≤ <i>l</i> ≤ 21
reflections collected	13351
independent reflections	4947 [ <i>R</i> <sub>int</sub> = 0.0727]
GOF on <i>F</i> <sup>2</sup>	1.139
final <i>R</i> indices [ <i>I</i> ≥ 2σ( <i>I</i> )]	<i>R</i> <sub>1</sub> = 0.0943, <i>wR</i> <sub>2</sub> = 0.2451
Largest diff. peak and hole / e Å <sup>-3</sup>	1.19 and -0.96

### 2.3 Conclusions

In conclusion, a novel photochromic BTEs BTTE based on benzobisthiadiazole as six-membered ethene bridge has been synthesized and studied. This compound possesses several merits as: i) an excellent photochromic performance in both solution and single crystals; ii) an extremely low aromatic property of the center ethene bridging unit of benzobisthiadiazole arising from the high polarity and electron-withdrawing tendency of the

benzobisthiadiazole unit; iii) an unprecedented thermal stability in a variety of solvents from nonpolar cyclohexane to polar ethanol among BTE bearing a six-membered ethene bridge, correlated to the limited loss of aromatic stabilization energy upon photocyclization, and iv) a convenient fluorescence modulation of BTTE with photochromism and solvatochromism. This compound opens up a new way in the molecular design of BTE-based bistable systems.

## Chapter 3 Aromaticity-Controlled Thermal Stability of Photochromic Systems Based on Six-Membered Ring as Ethene Bridges: Photochemical and Kinetic Studies

### 3.1 Introduction

Due to the strong aromaticities of six-membered ethene bridges, the greatly enhanced ground-state energy difference (Hückel rule) between the open and closed forms finally results in the thermal instability of the closed form in BTEs<sup>[97]</sup>, which could limit the commercial application of BTEs.<sup>[102-107]</sup> In Chapter 2, we studied a novel photochromic BTE system based on the specific benzobisthiadiazole unit, showing excellent thermal stability for the closed form in various solvents from nonpolar to polar, and even at elevated temperature.<sup>[116]</sup> Since the ethene bridge with six-membered ring has its own advantages such as higher quantum yield in ring closure and longer absorption wavelength compared to five-membered analogues, we envision that the six-membered ring with low or non-aromaticity as the center ethene bridge might widely extend the diversity in the thermally irreversible photochromic systems.<sup>[108-116]</sup> However, up to now, a deep insight into the ethene bridges has seldom been given. Accordingly, herein we systematically report the synthesis and photochromic properties of three ethene bridges with different degree in aromaticity (BTE-NA, BTA and BTTA, Scheme 1), which is expected to achieve obvious thermal stability evolution, and realize the fluorescence modulation by solvato- and photo-chromism in the six-membered ethene bridged photochromic systems. As expected, an extremely low aromatic property of the center ethene bridge with benzobisthiadiazole unit finally leads to the unexpected thermally irreversible photochromic system (BTTA). Moreover, the small energy barrier between the parallel and anti-parallel conformers allows the full conversion from BTTA to c-BTTA. For the first time, three ethene bridges with different degrees in aromaticity give a systematical comparison in the thermal stability evolution for their corresponding closed forms. This work contributes to the understanding of aromaticity-controlled thermal stability of photochromic systems based on six-membered ring as ethene bridges, and broadening novel building blocks for the photochromic BTE systems (Figure 3.1).

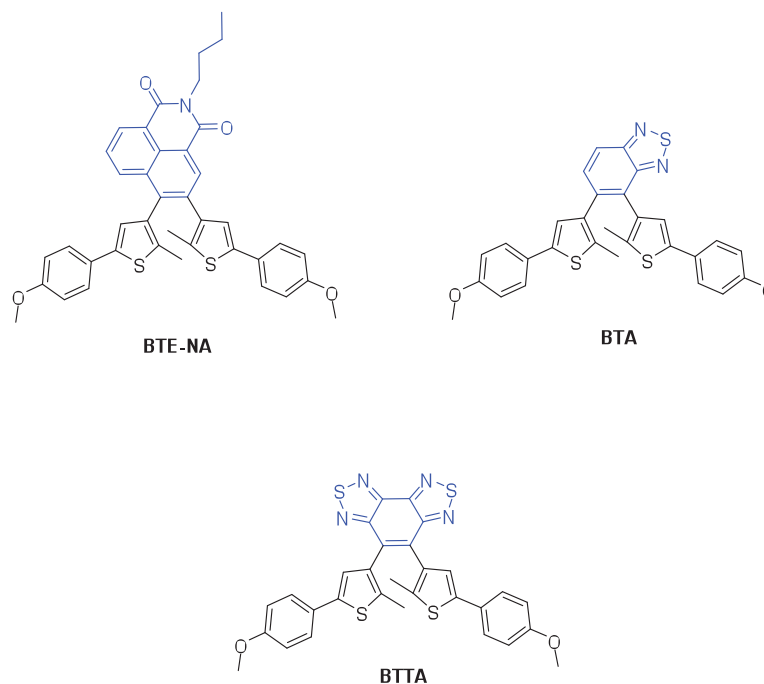


Fig. 3.1 Naphthalimide, benzothiadiazole, benzobisthiadiazole with different degree of aromaticities were utilized as central ethene bridge.

## 3.2 Experimental Section

### 3.2.1 Instruments and Reagents

$^1\text{H}$  NMR and  $^{13}\text{C}$  NMR spectra were recorded on Bruker Avance III 400 MHz spectrometers with tetramethylsilane (TMS) as an internal reference recorded at room temperature.  $\text{CDCl}_3$  and  $d_6$ -benzene were used as solvents. HRMS were recorded on a Waters LCT Premier XE spectrometer with methanol or acetonitrile as solvents. Absorption and fluorescence spectra were recorded on Varian Cary 500 and FluoroMax-3 (Horiba Jobin-Yvon), respectively. The photochromic property was evidenced and characterized by following *in situ* the absorption spectra under continuous irradiation (see Appendix I for detailed information). 4-bromo-*N*-butyl-3-iodo-1,8-naphthalimide,<sup>[83]</sup> 4,5-dibromo-2,1,3-benzothiadiazole,<sup>[84]</sup> 4,5-dibromobenzo[1,2-*c*:3,4-*c'*]bis[1,2,5]thiadiazole<sup>[116]</sup> and 5-(4-methoxyphenyl)-2-methylthiophen-3-ylboronic acid were prepared according to established method.<sup>[83]</sup> All other reagents were of analytical purity and dried before use.

### 3.2.2 Synthetic route to the target and intermediate molecules



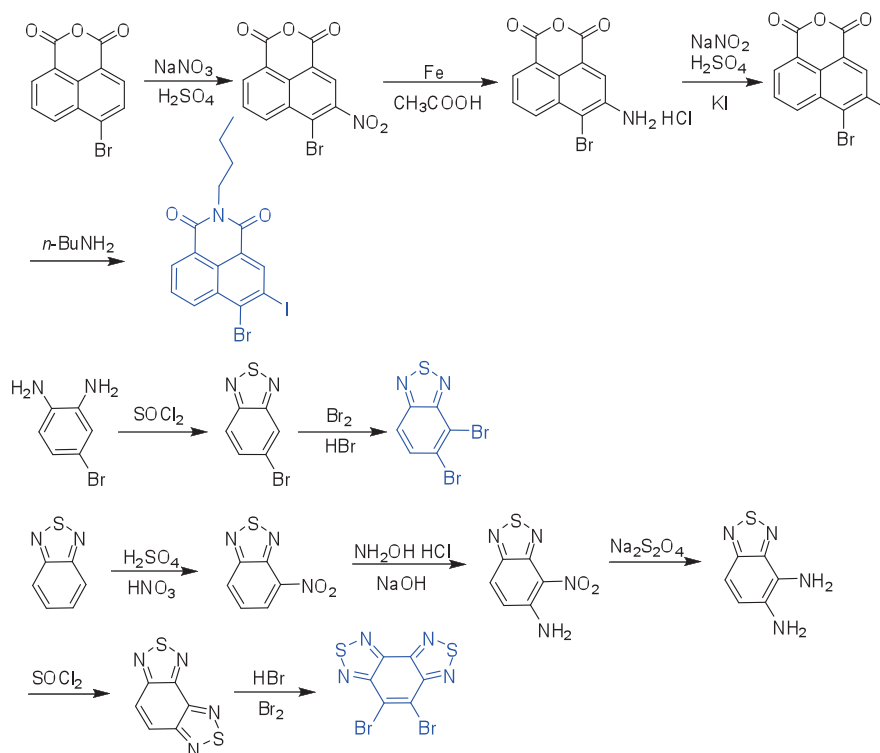


Fig. 3.2 Synthetic routes to Naphthalimide, benzothiadiazole, benzobisthiadiazole as central ethene bridge.

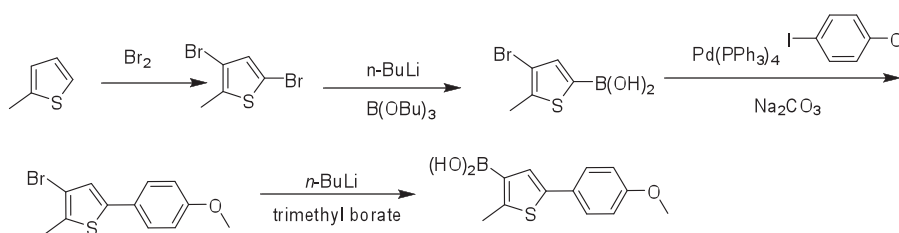
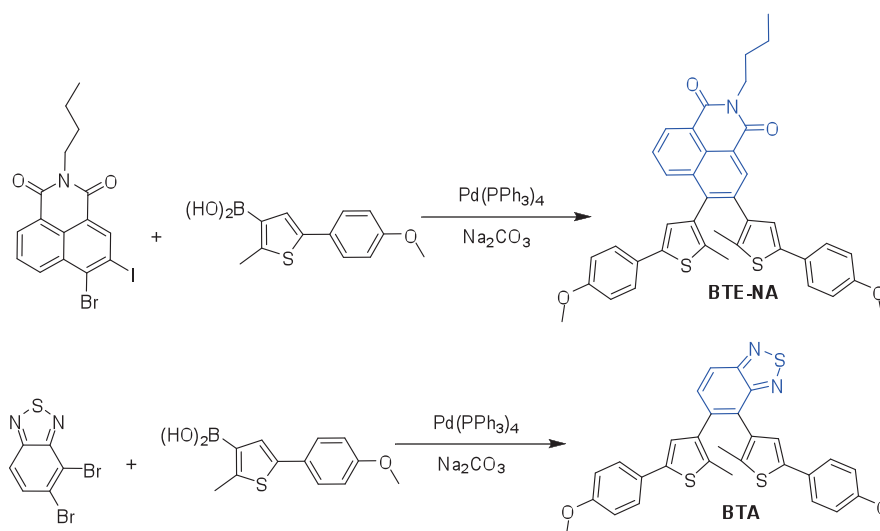


Fig. 3.3 Synthetic route to 5-(4-methoxyphenyl)-2-methylthiophen-3-ylboronic acid.



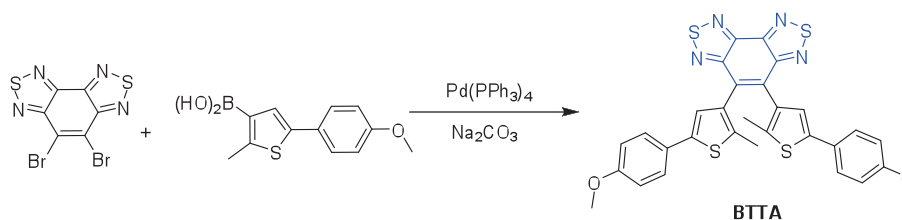


Fig. 3.4 Synthetic routes to BTE-NA, BTA and BTTA.

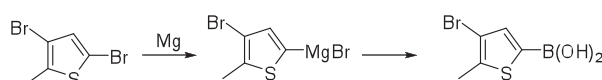
### 3.2.3 Preparation of target and intermediate molecules

#### 3.2.3.1 3,5-Dibromo-2-methylthiophene



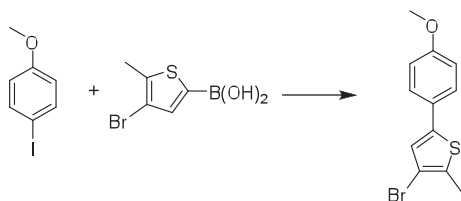
To a 500 mL single necked flask was added 2-methylthiophene (10.0 g, 10.2 mmol) and 230 mL acetic acid. Br<sub>2</sub> (33.2 g, 20.8 mmol) was introduced slowly in an ice bath. The resulting mixture was allowed to stand overnight (15 h) at room temperature. The solution was poured into 1000 mL of water and extracted with dichloromethane and neutralized with NaHCO<sub>3</sub> (aq) until the organic layer turned yellow. The solvent was removed under vacuum and the crude product was distilled under reduced pressure 54-56°C/1 mm Hg to yield an orange liquid 19.2 g. Yield: 73.5%

#### 3.2.3.2 4-bromo-5-methyl-2-thiophenyl boric acid



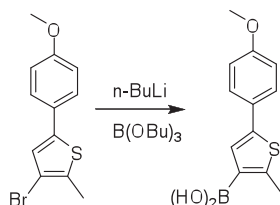
To a fire dried three necked flask was added Mg (0.3 g, 12.12 mmol), a piece of I<sub>2</sub> and 10 mL THF. 3,5-Dibromo-2-methylthiophene dissolved in 10 mL THF was introduced slowly to initiate the reaction. After initiation, the remaining solution was added within 1 h. The reaction is exothermic and the mixture was allowed to stand at room temperature for 3 h. The resulting mixture was introduced to a Schlenk tube through syringe and cooled to -78 °C. Trimethyl borate (2 mL 17.84 mmol) was introduced and the resulting mixture was kept at -78 °C for another 2 h. Then the mixture was warmed to room temperature to stay overnight. 1 M HCl was added to quench the reaction. The water phase was extracted with ether for three times. The ether phase was extracted with 10% NaOH for three times. The resulting base solution was neutralized by 10% HCl to give a white solid 1.8 g. Yield: 83.4%

## 3.2.3.3 3-Bromo-5-(4-methoxyphenyl)-2-methylthiophene



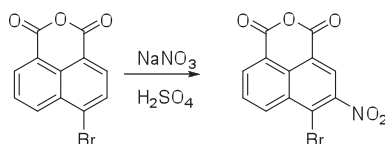
To a 100 mL single necked flask was added 4-Bromo-5-methyl-2-thiophenyl boric acid (1.50 g, 6.80 mmol), 4-iodoanisole (1.59 g, 6.80 mmol), Pd(PPh<sub>3</sub>)<sub>4</sub> (0.15 g), THF 30 mL, 2 M Na<sub>2</sub>CO<sub>3</sub> 20 mL. The reaction was refluxed for 15 h under the protection of argon. The mixture was poured into water and extracted with dichloromethane. The organic phase was separated and dried with Na<sub>2</sub>SO<sub>4</sub>. The crude product was purified by chromatographer eluted by (ether: ethyl acetate = 5: 1 v/v). The resulting solid was further purified by recrystallization with methanol to give a white solid 1.29 g. Yield: 67.1% <sup>1</sup>H NMR (400 MHz, CDCl<sub>3</sub>): 2.40 (s, 3 H, -CH<sub>3</sub>), 3.83 (s, 3 H, -OCH<sub>3</sub>), 6.89 (d, *J* = 8.8 Hz, 2 H, -Ph-H), 6.98 (s, 1 H, Thiophene-H), 7.42 (d, *J* = 8.8 Hz, 2 H, -Ph-H). <sup>13</sup>C NMR (100 MHz, CDCl<sub>3</sub>, ppm): 14.77, 55.38, 109.62, 114.35, 124.48, 126.40, 126.68, 132.57, 141.10, 159.41.

## 3.2.3.4 5-(4-methoxyphenyl)-2-methylthiophen-3-ylboronic acid



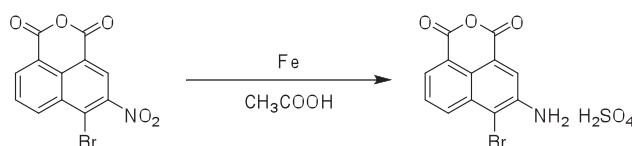
To a fire dried Schlenk tube was added 3-Bromo-5-(4-methoxyphenyl)-2-methylthiophene (0.21 g, 0.74 mmol) and 20 mL dried THF. The mixture was cooled to -78 °C and 1.6 M BuLi (0.3 mL, 2.9 mmol) was introduced dropwise. After 1 h, tributyl borate 0.27 mL was introduced. The resulting mixture was kept at -78 °C for another 3 h. After the reaction, the solvent was removed under vacuum and crude product was used directly without further treatment.

## 3.2.3.5 3-Nitro-4-bromo-1,8-naphthalic anhydride



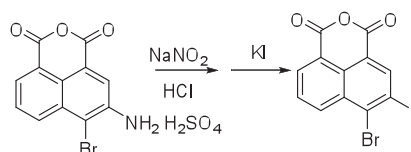
To a 250 mL three necked flask was added 4-bromo-1,8-naphthalic anhydride (6.41 g, 23.2 mmol) dissolved in 45 mL concentrated sulfuric acid kept at an ice bath.  $\text{NaNO}_3$  (2.1 g, 24.7 mmol) was added by portion within 1 h. The reactive mixture was stirred at 0-5 °C for 2.5 h and another 30 min at room temperature. The resulting mixture was poured into crushed ice to yield 6.8 g of a yellow solid. The crude product was recrystallized from acetic acid to give needle like crystal 5.42 g. Yield: 73%.

### 3.2.3.6 3-Amino-4-bromo-1,8-naphthalic anhydride hydrochloric acid salt



To a 100 mL single necked flask was added 3-Nitro-4-bromo-1,8-naphthalic anhydride (5 g, 15.6 mmol), Fe powder (5.6, 0.1 mol) as reducing agent and acetic acid (50 mL). The mixture was refluxed for 6 h under the protection of argon. The reactive mixture was poured into diluted sulfuric acid to yield bright yellow solid 4.0g. The crude product was used without further treatment. Yield: 95%.

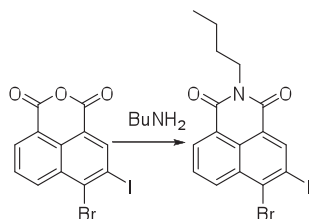
### 3.2.3.7 4-Bromo-3-iodo-1,8-naphthalic anhydride



To a three necked flask equipped with mechanical stirrer was added 3-Amino-4-bromo-1,8-naphthalic anhydride hydrochloric acid salt (5.0 g, 18 mmol), sulfuric acid 40 mL, water 80 mL. The mixture was stirred for 3 h to ensure well the suspension of the reactant.  $\text{NaNO}_2$  (1.6 g, 23 mmol) in 33 mL water was added slowly in an ice bath. The reactive mixture was stirred at 0 °C for another 3 h. Subsequently, KI in 50 mL water (12.4 g, 75 mmol) was introduced slowly and the mixture was further stirred for 2 h. Then, the solid was filtered and washed with  $\text{NaHSO}_3$  (aq). The crude product was refluxed in a mixture of

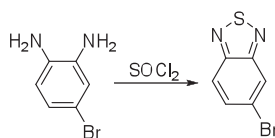
acetonitrile 15 mL and triethylamine 1 mL for 4 h to give a white solid 2.5 g. Yield: 40%.

### 3.2.3.8 4-Bromo-*n*-butyl-3-iodo-1,8-naphthalimide



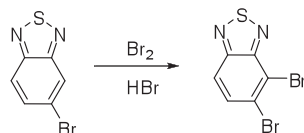
To a 100 mL single necked flask was added 4-Bromo-3-iodo-1,8-naphthalic anhydride (1 g, 2.5 mmol), *n*-butylamine 0.6 mL and dioxane 30 mL. The reactant was refluxed under the protection of argon for 3 h. The crude product was purified by chromatography eluted by (CCl<sub>4</sub>: CH<sub>2</sub>Cl<sub>2</sub> = 20: 1 v/v) to yield a white powder 0.5 g. Yield: 41%. <sup>1</sup>H NMR (400 MHz, CDCl<sub>3</sub>): 0.96 (t, *J* = 7.2 Hz, 3 H, -CH<sub>2</sub>CH<sub>3</sub>), 1.39 (m, 2 H, -CH<sub>2</sub>CH<sub>3</sub>), 1.66 (m, 2 H, -NCH<sub>2</sub>CH<sub>2</sub>-), 4.14 (t, *J* = 7.4 Hz, 2 H, -NCH<sub>2</sub>-), 7.80 (t, *J* = 7.7 Hz, 1 H, naphthalene-H), 8.63 (m, 2 H, naphthalene-H), 8.93 (s, 1 H, naphthalene-H). <sup>13</sup>C NMR (100 MHz, CDCl<sub>3</sub>, ppm): 13.84, 20.34, 30.12, 40.48, 101.79, 122.53, 123.25, 127.71, 129.08, 131.75, 131.79, 134.85, 137.02, 140.81, 162.53, 163.23.

### 3.2.3.9 5-Bromo-2,1,3-benzothiadiazole



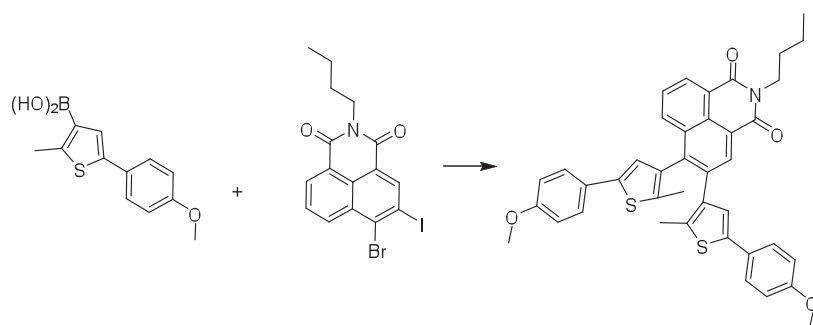
To a 500 mL single necked flask was added 4-bromobenzene-1,2-diamine (5.0 g, 26.7 mmol), dried dichloromethane 150 mL and triethylamine (11 g, 109 mmol). SOCl<sub>2</sub> (6.4 g, 54 mmol) was introduced slowly in an ice bath. Subsequently, the reactive mixture was refluxed for 4 h. The solvent was removed under vacuum to give a black solid. The crude product was purified by chromatography eluted with ether: ethyl acetate = 6: 1 to give a white solid 4.2 g. Yield: 73%.

### 3.2.3.10 4,5-Dibromo-2,1,3-benzothiadiazole<sup>[85]</sup>



To a single necked flask was added 5-Bromo-2,1,3-benzothiadiazole (4.2 g, 19.5 mmol), hydrobromic acid 30 mL. Br<sub>2</sub> (1.2 mL, 23.3 mmol) was added within 2 h when heated. Another portion of 1.2 mL Br<sub>2</sub> was introduced and then the reactive mixture was refluxed for another 5 h. The reaction should be stopped immediately to avoid the formation of tri-substituted by-product. The reactive mixture was poured into crushed ice and filtered. The crude product was recrystallized from methanol to give 2.1 g of a white powder. Yield: 36%. <sup>1</sup>H NMR (400 MHz, CDCl<sub>3</sub>): 7.80 (d, *J* = 9.2 Hz, 1 H, -Ph-H), 7.85 (d, *J* = 9.2 Hz, 1 H, -Ph-H).

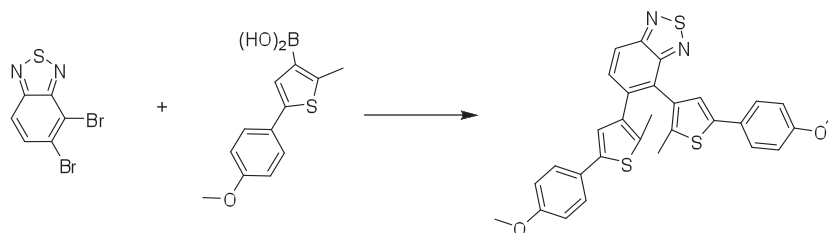
### 3.2.3.11 BTE-NA



4-bromo-N-butyl-3-iodo-1,8-naphthalimide (0.68 g, 1.5 mmol) was dissolved in dioxane (100 mL), Pd(PPh<sub>3</sub>)<sub>4</sub> (0.35 g) was added, and the resulting mixture was stirred for 15 min at room temperature. Then aqueous Na<sub>2</sub>CO<sub>3</sub> (100 mL, 2.0 mol L<sup>-1</sup>) was added. The reactive mixture was heated and refluxed at a temperature of 60 °C and the solution of 5-(4-methoxyphenyl)-2-methylthiophen-3-ylboronic acid (0.74 g, 3.0 mmol) was added dropwise via a syringe. Subsequently the mixture was refluxed for 24 h, and cooled to room temperature. The reactive mixture was poured in H<sub>2</sub>O and extracted with ether. The organic layer was separated and dried with Na<sub>2</sub>SO<sub>4</sub>. After concentration, the compound was purified by column chromatography on silica gel (CCl<sub>4</sub> : ethyl acetate = 20: 1 v/v) to yield a yellow solid (340 mg, yield 35%). <sup>1</sup>H NMR (400 MHz, CDCl<sub>3</sub>, ppm): 0.98 (t, *J* = 7.6 Hz, 3 H, -CH<sub>2</sub>CH<sub>3</sub>), 1.44 (m, 2 H, -CH<sub>2</sub>CH<sub>3</sub>), 1.72 (m, 2 H, -NCH<sub>2</sub>CH<sub>2</sub>-), 1.99 (s, 3 H, -CH<sub>3</sub>), 2.34 (s, 3 H, -CH<sub>3</sub>), 3.80 (s, 3 H, -OCH<sub>3</sub>), 3.84 (s, 3 H, -OCH<sub>3</sub>), 4.21 (t, *J* = 7.6 Hz, 2 H, -NCH<sub>2</sub>-), 6.72 (s, 1 H, thiophene-H), 6.81 (d, *J* = 8.8 Hz, 1 H, -Ph-H), 6.89 (d, *J* = 8.8 Hz, 1 H, -Ph-H),

6.97 (s, 1 H, Thiophene-H), 7.30 (d,  $J = 8.8$  Hz, 2 H, -Ph-H), 7.44 (d,  $J = 8.8$  Hz, 2 H, -Ph-H), 7.70 (t,  $J = 7.6$  Hz, 1 H, naphthalene-H), 8.17 (d,  $J = 8.4$  Hz, 1 H, naphthalene-H), 8.62 (d,  $J = 7.2$  Hz, 1 H, naphthalene-H), 8.67 (s, 1 H, naphthalene-H).  $^1\text{H}$  NMR (400 MHz,  $d_6$ -benzene, ppm): 0.90 (t,  $J = 7.6$  Hz, 3 H,  $-\text{CH}_2\text{CH}_3$ ), 1.39 (m, 2 H,  $-\text{CH}_2\text{CH}_3$ ), 1.82 (s, 3 H,  $-\text{CH}_3$ ), 1.87 (m, 2 H,  $-\text{NCH}_2\text{CH}_2-$ ), 2.13 (s, 3 H,  $-\text{CH}_3$ ), 3.22 (s, 3 H,  $-\text{OCH}_3$ ), 3.26 (s, 3 H,  $-\text{OCH}_3$ ), 4.36 (t,  $J = 7.2$  Hz, 2 H,  $-\text{NCH}_2-$ ), 6.69 (d,  $J_1 = 8.4$  Hz, 2 H, -Ph-H), 6.73 (d,  $J_1 = 8.8$  Hz, 2 H, -Ph-H), 6.84 (s, 1 H, Thiophene-H), 6.94 (s, 1 H, Thiophene-H), 7.40 (d,  $J = 8.4$  Hz, 2 H, -Ph-H), 7.45 (d,  $J = 8.8$  Hz, 2 H, -Ph-H), 7.99 (d,  $J = 8.4$  Hz, 1 H, naphthalene-H), 8.63 (d,  $J = 6.8$  Hz, 1 H, naphthalene-H), 8.91 (s, 1 H, naphthalene-H).  $^{13}\text{C}$  NMR (100 MHz,  $\text{CDCl}_3$ , ppm): 13.91, 14.06, 14.17, 20.45, 30.29, 40.33, 55.36, 55.41, 114.21, 114.35, 121.83, 122.83, 124.29, 125.09, 126.84, 126.93, 127.17, 127.21, 127.56, 130.92, 131.72, 133.07, 133.46, 134.57, 134.94, 135.73, 136.46, 137.38, 139.73, 139.94, 140.72, 158.98, 159.23, 164.08, 164.34. HRMS (TOF MS  $\text{ESI}^+$  for  $[\text{M} + \text{H}]^+$ ): calcd. for  $\text{C}_{40}\text{H}_{36}\text{NO}_4\text{S}_2$ , 658.2086; found 658.2089.

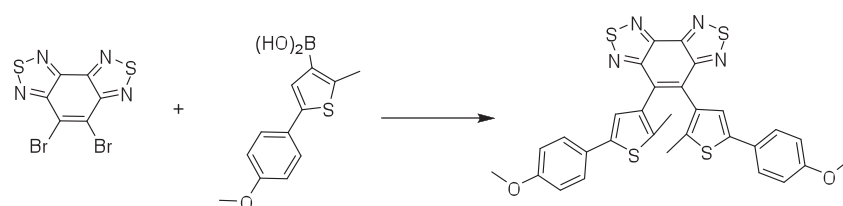
### 3.2.3.12 BTA



4,5-Dibromo-2,1,3-benzothiadiazole (0.238 g, 0.81 mmol) was dissolved in dioxane (60 mL),  $\text{Pd}(\text{PPh}_3)_4$  (0.20 g) was added, and the resulting mixture was stirred for 15 min at room temperature. Then aqueous  $\text{Na}_2\text{CO}_3$  (40 mL,  $2.0 \text{ mol L}^{-1}$ ) was added. The reactive mixture was heated and refluxed at a temperature of  $60^\circ\text{C}$  and the solution of 5-(4-methoxyphenyl)-2-methylthiophen-3-ylboronic acid (0.595 g, 2.40 mmol) was added dropwise via a syringe. Subsequently the mixture was refluxed for 24 h, and cooled to room temperature. The reactive mixture was poured in  $\text{H}_2\text{O}$  and extracted with ether. The organic layer was separated and dried with  $\text{Na}_2\text{SO}_4$ . After concentration, the compound was purified by column chromatography on silica gel ( $\text{CCl}_4$  : ethyl acetate = 40: 1 v/v) to yield a yellow solid (250 mg, yield 57%).  $^1\text{H}$  NMR (400 MHz,  $\text{CDCl}_3$ , ppm): 2.07 (s, 3 H,  $-\text{CH}_3$ ), 2.23 (s, 3 H,  $-\text{CH}_3$ ), 3.81 (s, 3 H,  $-\text{OCH}_3$ ), 3.82 (s, 3 H,  $-\text{OCH}_3$ ), 6.85 (m, 5 H, -Ph-H), 7.04 (s, 1H, Thiophene-H), 7.36 (d,  $J = 8.8$  Hz, 2 H, -Ph-H), 7.42 (d,  $J = 8.8$  Hz, 2 H, -Ph-H), 7.71 (d,  $J = 9.2$  Hz, 1 H, -Ph-H), 8.02 (d,  $J = 8.8$  Hz, 1 H, -Ph-H).  $^1\text{H}$  NMR (400 MHz,  $d_6$ -benzene, ppm): 1.98 (s, 3 H,  $-\text{CH}_3$ ), 2.03 (s, 3 H,  $-\text{CH}_3$ ), 3.22 (s, 3 H,  $-\text{OCH}_3$ ), 3.23 (s, 3 H,  $-\text{OCH}_3$ ), 6.68 (d,  $J$

= 6.0 Hz, 2 H, -Ph-H), 6.71 (d,  $J = 6.0$  Hz, 2 H, -Ph-H), 6.95 (s, 1 H, Thiophene-H), 7.34 (d,  $J = 8.8$  Hz, 1 H, -Ph-H), 7.44 (d,  $J = 8.8$  Hz, 2 H, -Ph-H), 7.47 (d,  $J = 8.8$  Hz, 2 H, -Ph-H), 7.79 (d,  $J = 8.8$  Hz, 1 H, -Ph-H).  $^{13}\text{C}$  NMR (100 MHz,  $\text{CDCl}_3$ , ppm): 14.23, 14.53, 55.37, 114.18, 114.27, 119.95, 124.30, 124.98, 126.83, 126.94, 127.10, 127.41, 128.27, 133.25, 133.76, 135.17, 136.59, 136.66, 137.46, 140.00, 140.16, 154.26, 155.16, 158.93, 159.06. HRMS (TOF MS  $\text{ESI}^+$  for  $[\text{M} + \text{H}]^+$ ): calcd. for  $\text{C}_{30}\text{H}_{25}\text{N}_2\text{O}_2\text{S}_3$ , 541.1078; found 541.1078.

### 3.2.3.13 BTTA

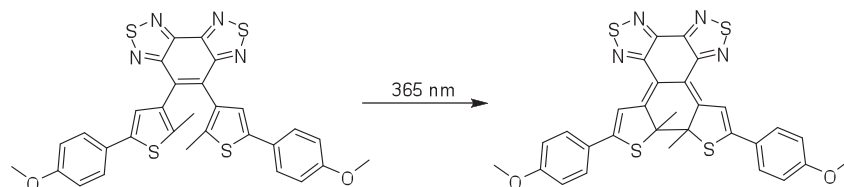


BBT (0.369 g, 1.05 mmol) was dissolved in dioxane (60 mL),  $\text{Pd}(\text{PPh}_3)_4$  (0.20 g) was added, and the resulting mixture was stirred for 15 min at room temperature. Then aqueous  $\text{Na}_2\text{CO}_3$  (40 mL,  $2.0 \text{ mol L}^{-1}$ ) was added. The reactive mixture was heated and refluxed at a temperature of  $60^\circ\text{C}$  and the solution of 5-(4-methoxyphenyl)-2-methylthiophen-3-ylboronic acid (0.78 g, 3.15 mmol) was added dropwise via a syringe. Subsequently the mixture was refluxed for 24 h, and cooled to room temperature. The reactive mixture was poured in  $\text{H}_2\text{O}$  and extracted with ether. The organic layer was separated and dried with  $\text{Na}_2\text{SO}_4$ . After concentration, the compound was purified by column chromatography on silica gel ( $\text{CCl}_4$  : ethyl acetate = 4: 1 v/v) to yield a yellow solid (270 mg, yield 43%).  $^1\text{H}$  NMR (400 MHz,  $\text{CDCl}_3$ , ppm): 2.10 (s, 3 H,  $-\text{CH}_3$ , anti-parallel conformer), 2.20 (s, 3 H,  $-\text{CH}_3$ , parallel conformer), 3.81 (s, 3 H,  $-\text{OCH}_3$ , parallel conformer), 3.83 (s, 3 H,  $-\text{OCH}_3$ , anti-parallel conformer), 6.84 (d,  $J = 8.4$  Hz, 2 H, -Ph-H, parallel conformer), 6.88 (d,  $J = 8.8$  Hz, 2 H, -Ph-H, anti-parallel conformer), 6.92 (s, 1 H, Thiophene-H, parallel conformer), 7.13 (s, 1 H, Thiophene-H, anti-parallel conformer), 7.38 (d,  $J = 8.8$  Hz, 2 H, -Ph-H, parallel conformer), 7.44 (d,  $J = 8.4$  Hz, 2 H, -Ph-H, anti-parallel conformer).  $^1\text{H}$  NMR (400 MHz,  $d_6$ -benzene, ppm): 1.98 (s, 3 H,  $-\text{CH}_3$ , anti-parallel conformer), 2.04 (s, 3 H,  $-\text{CH}_3$ , parallel conformer), 3.22 (s, 3 H,  $-\text{OCH}_3$ , parallel conformer), 3.26 (s, 3 H,  $-\text{OCH}_3$ , anti-parallel conformer), 6.69 (d,  $J = 8.4$  Hz, 2 H, -Ph-H, parallel conformer), 6.74 (d,  $J = 8.4$  Hz, 2 H, -Ph-H, anti-parallel conformer), 7.05 (s, 1 H, Thiophene-H, parallel conformer), 7.25 (s, 1 H, Thiophene-H, anti-parallel conformer), 7.48 (d,  $J = 8.4$  Hz, 2 H, -Ph-H, parallel conformer), 7.51 (d,  $J = 8.8$  Hz, 2 H, -Ph-H, anti-parallel conformer).  $^{13}\text{C}$  NMR (100 MHz,  $\text{CDCl}_3$ , ppm): 14.85, 55.37, 114.24, 124.43, 124.57, 126.93, 127.03, 127.09, 130.75, 130.91, 132.42, 132.57, 137.07,



137.85, 140.33, 140.54, 147.48, 156.85, 157.15, 159.09. HRMS (TOF MS ESI<sup>+</sup> for [M]<sup>+</sup>): calcd. for C<sub>30</sub>H<sub>22</sub>N<sub>4</sub>O<sub>2</sub>S<sub>4</sub>, 598.0626; found 598.0626.

### 3.2.3.14 *c*-BTTA



BTTA (150 mg, 0.25 mmol) was dissolved in 30 mL benzene and irradiated continuously at 365 nm with an input power of 0.54 mW for 7 h. After the reaction, the solvent was removed under vacuum and separated by chromatography on aluminum oxide eluted with CCl<sub>4</sub>: dichloromethane = 4: 1 to yield *c*-BTTA 140 mg. Yield: 93.3%. <sup>1</sup>H NMR (400 MHz, *d*<sub>6</sub>-benzene, ppm): 2.50 (s, 6 H, -CH<sub>3</sub>), 3.19 (s, 6 H, -OCH<sub>3</sub>), 6.66 (d, *J* = 8.8 Hz, 4 H, -Ph-H), 7.64 (d, *J* = 8.8 Hz, 4 H, -Ph-H), 8.48 (s, 2 H, Thiophene-H).

## 3.3 Results and discussion

### 3.3.1 Molecular design and synthesis

Figure 3.4 illustrates the synthetic route to the three target molecules. BTE-NA, BTA and BTTA were obtained via 4-bromo-1,8-naphthalic anhydride, 4-bromobenzene-1,2-diamine and benzothiadiazole as starting materials by four, two and five steps, respectively. Generally speaking, all the synthetic routes were classic organic reactions with cheap starting materials and reagents, mild conditions and comparatively high yields. It is difficult to obtain and purify 4-bromo-3-iodo-1,8-naphthalic anhydride during the organic manipulation as the reaction was carried out in solid phase. Thus, pre-process of raw material to have a well suspended mixture could to some extent guarantee the reaction to proceed smoothly with a considerable yield. 4,5-dibromo-2,1,3-benzothiadiazole was easily synthesized by conventional bromination. However, the reaction span has to be controlled precisely to avoid the appearance of 4,5,7-tribromo-2,1,3-benzothiadiazole. The target molecules were obtained through classic Suzuki coupling between 5-(4-methoxyphenyl)-2-methylthiophen-3-ylboronic acid and 4-bromo-*N*-butyl-3-iodo-1,8-naphthalimide, 4,5-dibromo-2,1,3-benzothiadiazole and BBT, respectively. The mono-substituted byproduct could be suppressed by controlling the ratio. Dioxane was used for the Suzuki coupling instead of THF in order to increase the reactivity and temperature, which finally facilitates the separation process.

Naphthalimide, benzothiadiazole and benzobisthiadiazole are excellent candidates for the acceptor moieties due to their attractive photo-physical property and their strong electron withdrawing capability. As shown in Figure 3.1, we designed novel BTE derivatives with these building blocks based on the following points: i) considering similar strong electron-withdrawing properties of perfluoro-cyclopentene, maleic anhydride or maleic imide, the remarkably electron-withdrawing units of naphthalimide, benzothiadiazole and benzobisthiadiazole are supposed to assure good photochromism with considerable bistability, high cyclization quantum yield and fatigue resistance; ii) naphthalimide, benzothiadiazole and benzobisthiadiazole are essentially well-known fluorescent building blocks in the design of functional materials such as sensors, OLEDs, NLO materials and solar cells.<sup>[117-123]</sup> Thus, the electron-withdrawing groups and the electron-donating anisole can form an efficient Donor- $\pi$ -Acceptor (D- $\pi$ -A) system with significant charge transfer between HOMO and LUMO upon excitation to realize the fluorescence modulation by both photochromism and solvatochromism,<sup>[93]</sup> iii) the three ethene bridges with different degrees in aromaticity can give a systematical comparison in the thermal stability evolution for their corresponding closed forms.

### 3.3.2 $^1\text{H}$ NMR, $^{13}\text{C}$ NMR and Mass characterization

The followings are the characterizations of important intermediates and target molecule.

Figure 3.5 illustrates the  $^1\text{H}$  NMR spectrum of 4-bromo-*N*-butyl-3-iodo-1,8-naphthalimide. The chemical shift at 0.97 ppm corresponds to the hydrogen atoms of the end methyl groups of butyl. The multiplet was the result of coupling between neighbouring proton. The chemical shift on butyl depends on the distance from the naphthalimide ring. The closer to the ring, the lower the field of the signal. The signal of methylene directly connected with anhydride was even at 4.14 ppm. The signal at 8.93 ppm is the proton on the side of iodine both affected by the ring and iodine substituent.

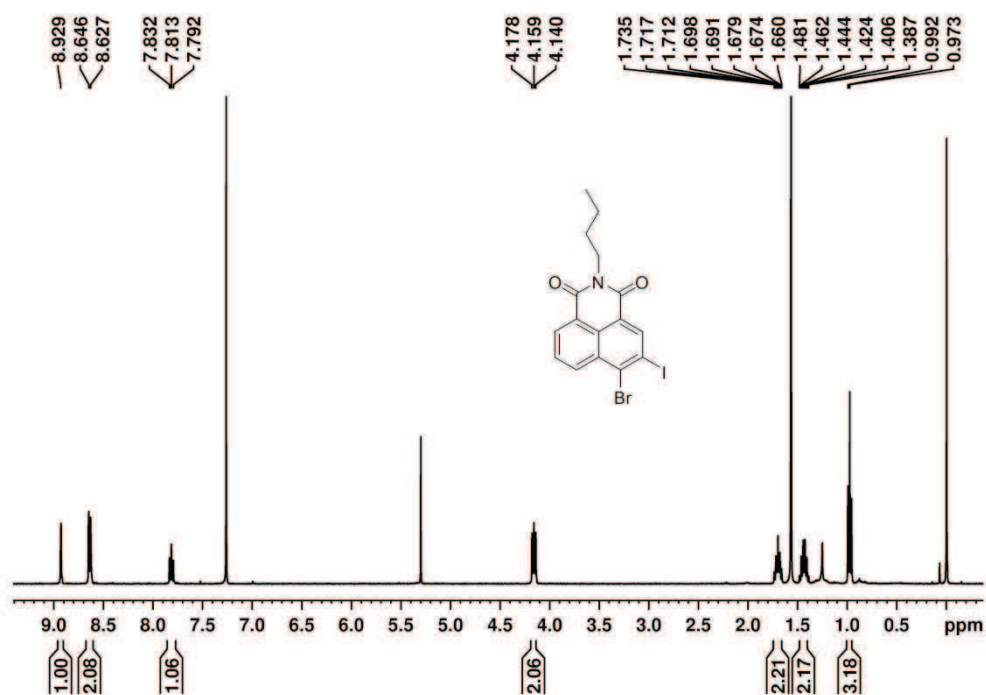


Fig. 3.5  $^1\text{H}$  NMR spectrum of 4-bromo-*n*-butyl-3-iodo-1,8-naphthalimide in  $\text{CDCl}_3$

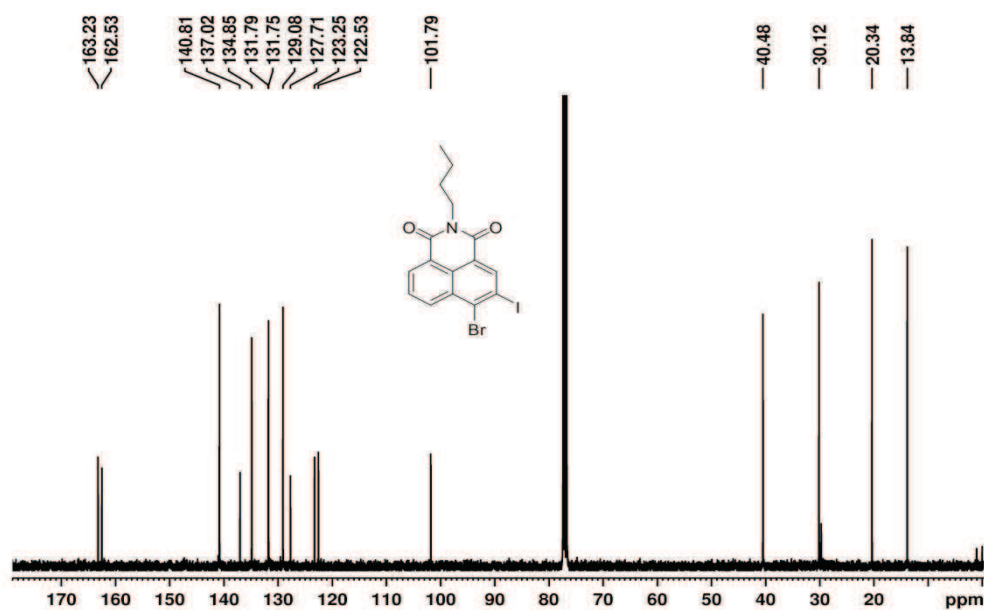


Fig. 3.6  $^{13}\text{C}$  NMR spectrum of 4-bromo-*n*-butyl-3-iodo-1,8-naphthalimide in  $\text{CDCl}_3$

Figure 3.6 shows the  $^{13}\text{C}$  NMR of 4-bromo-*N*-butyl-3-iodo-1,8-naphthalimide. Four are at high field and others are at low field. The total number of the signal is 16, which is in accordance with total carbon species within the molecule.

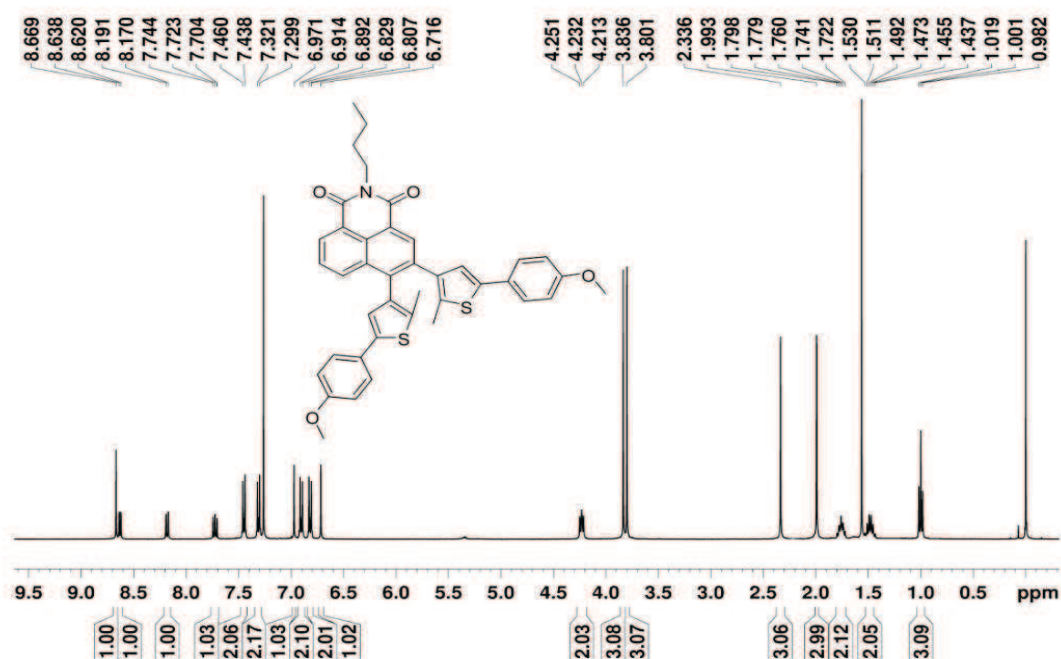


Fig. 3.7  $^1\text{H}$  NMR spectrum of BTE-NA in  $\text{CDCl}_3$

Figure 3.7 illustrates the  $^1\text{H}$  NMR spectrum of BTE-NA in  $\text{CDCl}_3$ . The signals of the protons of the butyl group exhibit the same behavior as those of 4-bromo-*N*-butyl-3-iodo-1,8-naphthalimide. The donating groups were introduced, all the signals on naphthalimide shifted upfield due to the shielding effect. The parallel and anti-parallel conformers in BTE-NA change quickly so that time-averaged signals of both are seen. The methyl on thiophene rings at (1.99, 2.34 ppm) are due to the asymmetric nature of the ethene bridge.

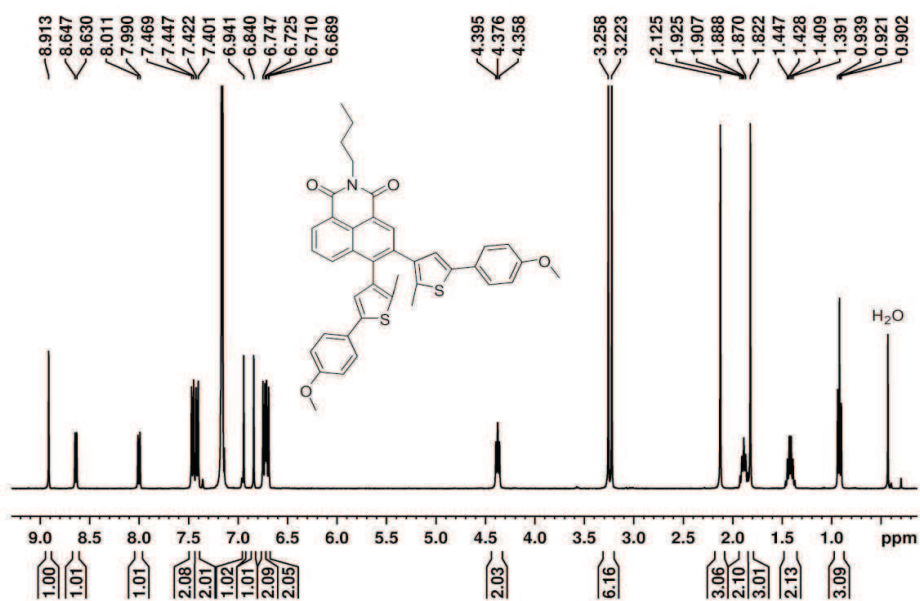


Fig. 3.8  $^1\text{H}$  NMR spectrum of BTE-NA in  $d_6$ -benzene. Note:  $H_f$  overlaps with the residual peaks of

*d*<sub>6</sub>-benzene.

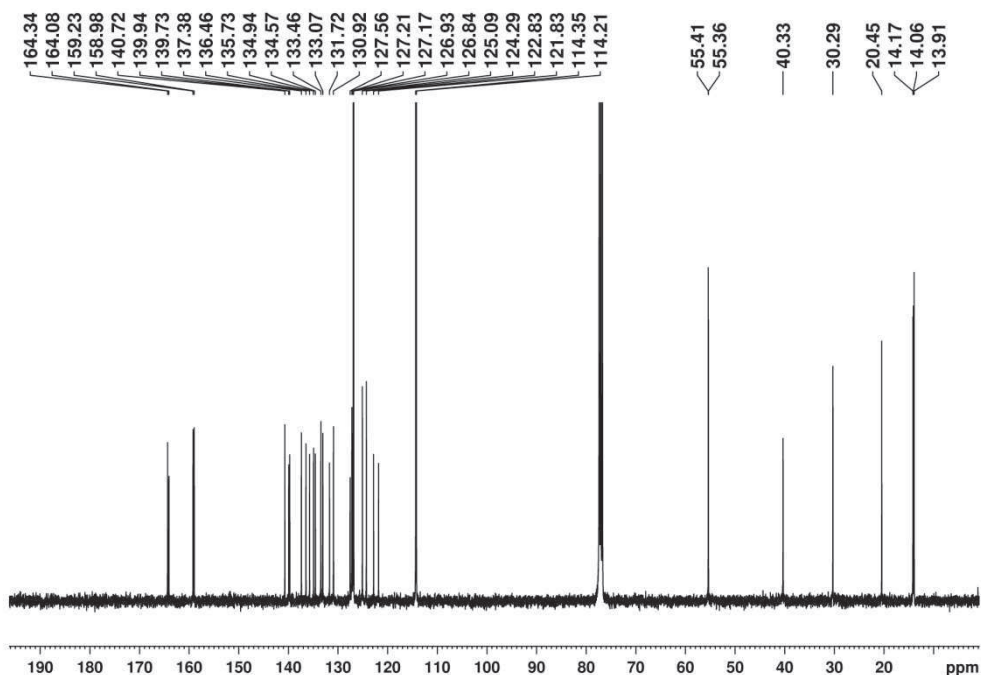


Fig. 3.9 <sup>13</sup>C NMR spectrum of BTE-NA in CDCl<sub>3</sub>

Figure 3.9 illustrates the <sup>13</sup>C NMR of BTE-NA. Eight are at high field and others are at low field. The total number of the signals is 35, which is in accordance with the total number of carbon species within the molecule.

Elemental Composition Report

Page 1

Single Mass Analysis

Tolerance = 50.0 mDa / DBE: min = -1.5, max = 100.0  
 Element prediction: Off  
 Number of isotope peaks used for i-FIT = 2

Monoisotopic Mass, Even Electron Ions

71 formula(e) evaluated with 10 results within limits (up to 1 closest results for each mass)

Elements Used:

C: 0-40 H: 0-40 N: 0-5 O: 0-4 S: 0-2

ZHU-WH

ECUST institute of Fine Chem

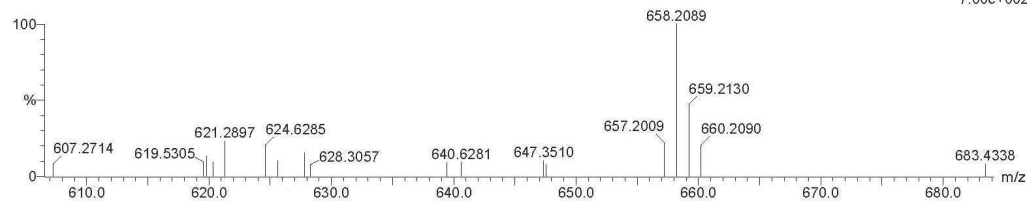
ZWH-YY-1026 14 (0.521) Cm (14:20)

28-Oct-2011

16:00:31

1: TOF MS ES+

7.00e+002



Minimum:

Maximum: 50.0 50.0 -1.5 100.0

Mass	Calc. Mass	mDa	PPM	DBE	i-FIT	i-FIT (Norm)	Formula
658.2089	658.2086	0.3	0.5	23.5	7.3	0.0	C40 H36 N O4 S2

Fig. 3.10 High resolution mass spectra of BTE-NA

RMS of BTE-NA shows an apparent molecular ion peak corresponding to [M + H]<sup>+</sup>. The calculated value for [M + H]<sup>+</sup> is 658.2086, which is in accordance with the observed value of

658.2089.

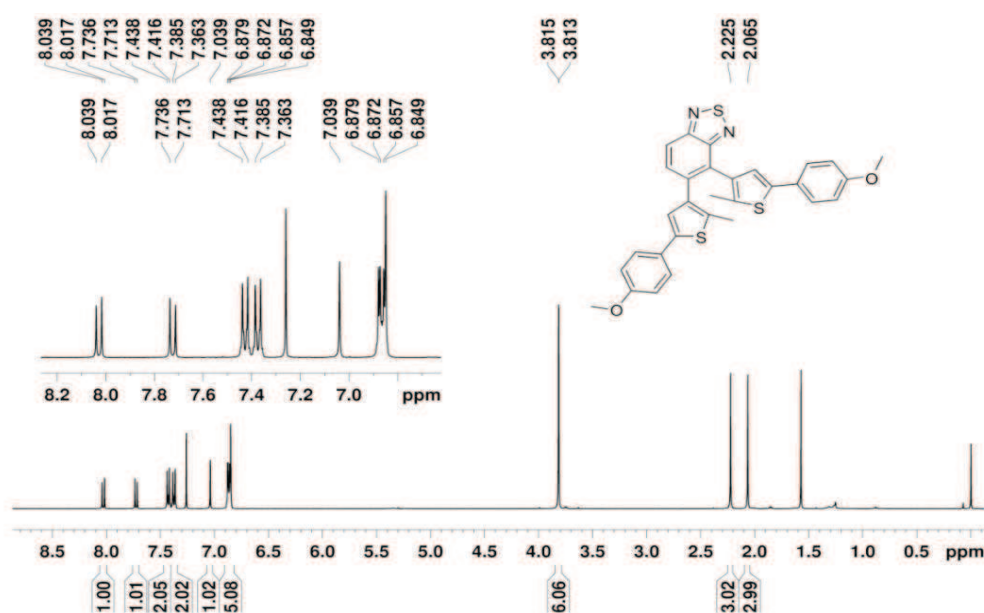


Fig. 3.11  $^1\text{H}$  NMR spectrum of BTA in  $\text{CDCl}_3$

Figure 3.11 illustrates the  $^1\text{H}$  NMR of BTA in  $\text{CDCl}_3$ . The chemical shift difference of the protons (at 7.71 and 8.02 respectively) on 2,1,3-benzothiadiazole become large after introduction of electron donating groups. Due to the interaction between the two protons, the signal of these two proton exhibit typical d peaks. Due to the far distance of methoxy groups away from 2,1,3-benzothiadiazole, the chemical shifts are almost the same at 3.813 and 3.815 ppm, respectively. The parallel and anti-parallel conformers in BTA change quickly so that time-averaged signals of both are seen. The methyl signals on the thiophene rings at 2.07 and 2.23 ppm are due to the asymmetric nature of the ethene bridge.

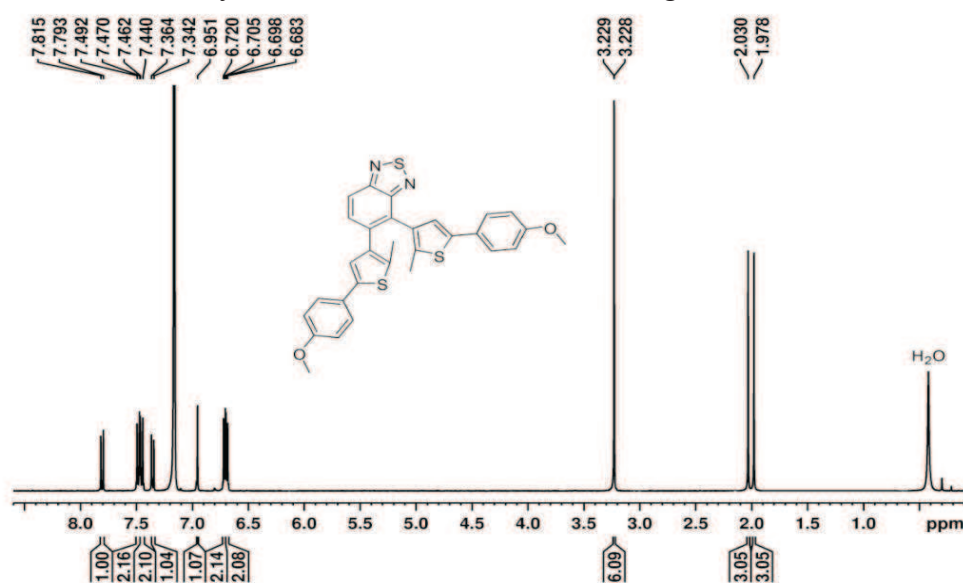


Fig. 3.12  $^1\text{H}$  NMR spectrum of BTA in  $d_6$ -benzene. Note:  $H_p$  overlaps with the residual peaks of  $d_6$ -benzene.

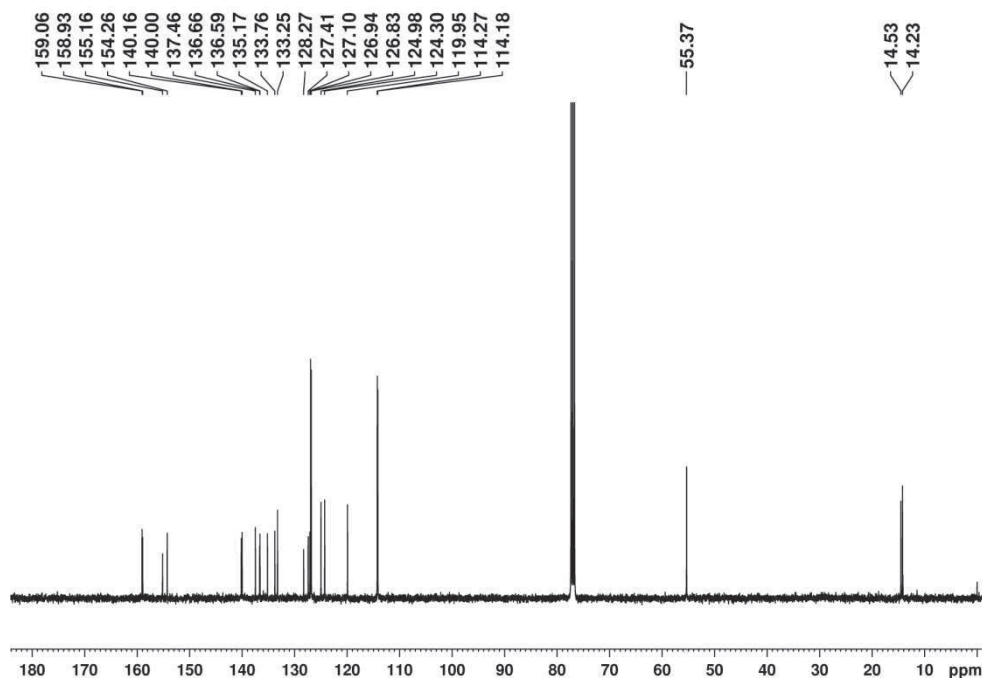


Fig. 3.13 <sup>13</sup>C NMR spectrum of BTA in CDCl<sub>3</sub>

Figure 3.13 illustrates the <sup>13</sup>C NMR of BTA. Three are at high field and others are at low field. The total number of the signal is 25, which is in accordance with total carbon species within the molecule.

Elemental Composition Report

Single Mass Analysis

Tolerance = 50.0 mDa / DBE: min = -1.5, max = 100.0  
 Element prediction: Off  
 Number of isotope peaks used for i-FIT = 2

Monoisotopic Mass, Even Electron Ions

101 formula(e) evaluated with 19 results within limits (up to 1 closest results for each mass)

Elements Used:

C: 0-40 H: 0-40 N: 0-2 O: 0-2 S: 0-3

ZHU-WH

ECUST institute of Fine Chem

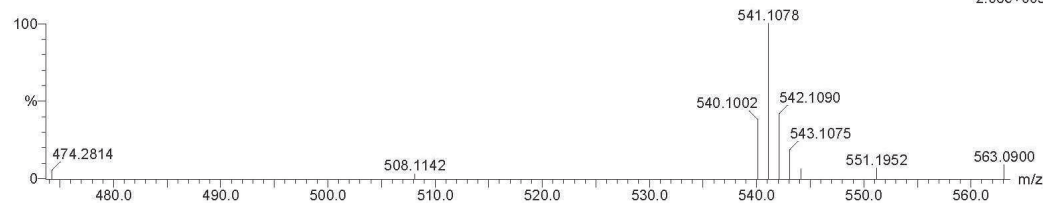
07-Sep-2011

17:59:36

1: TOF MS ES+

2.06e+003

ZW-YY-0907 12 (0.446) Cm (11:16)



Mass	Calc. Mass	mDa	PPM	DBE	i-FIT	i-FIT (Norm)	Formula
541.1078	541.1078	0.0	0.0	19.5	9.8	0.0	C30 H25 N2 O2 S3

Fig. 3.14 High resolution mass spectra of BTA

HRMS of BTA shows an apparent molecular ion peak corresponding to  $[M + H]^+$ . The calculated value for  $[M + H]^+$  is 541.1078, which is in accordance with the observed value of

541.1078.

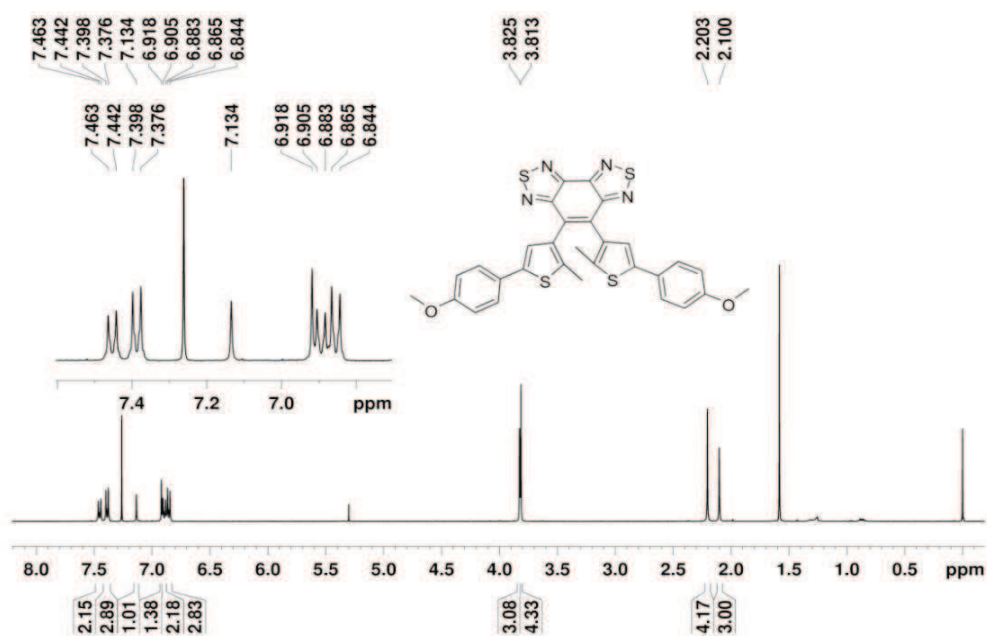
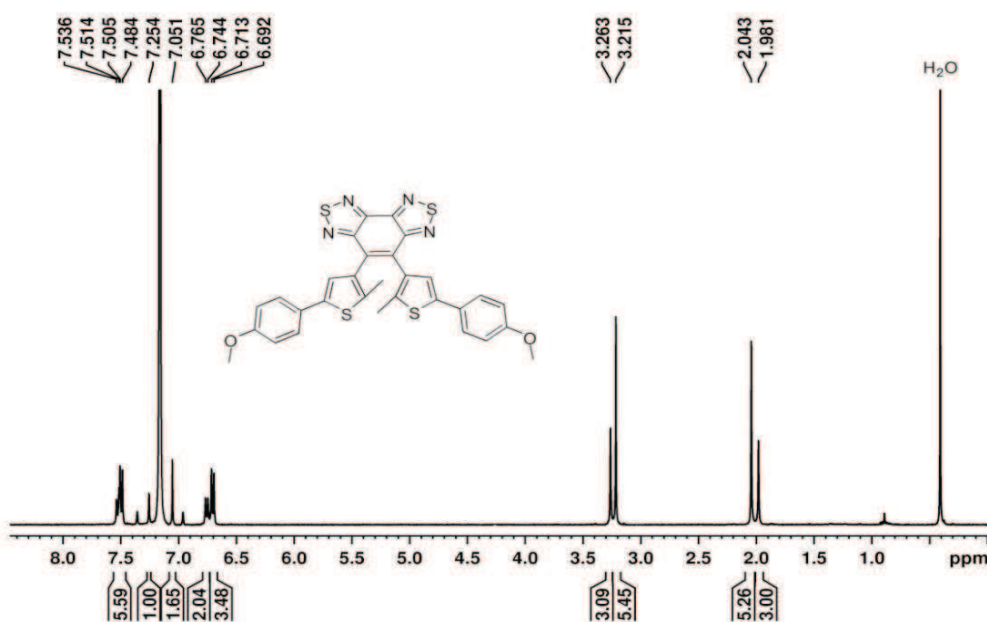

 Fig. 3.15  $^1\text{H}$  NMR spectrum of BTTA in  $\text{CDCl}_3$ 

 Fig. 3.16  $^1\text{H}$  NMR spectrum of BTTA in  $d_6$ -benzene.

Figure 3.16 illustrates the  $^1\text{H}$  NMR spectrum of BTTA in  $d_6$ -benzene. It shows two well-resolved sets of signals for the methyl protons which correspond to the parallel ( $\delta = 2.04$  ppm) and antiparallel ( $\delta = 1.98$  ppm) conformers. In fact, the two conformations, parallel (photochromic inactive) and antiparallel (photochromic active) conformers, undergo very fast single-bond rotation in BTE-NA and BTA, thereby resulting in only one set of time-averaged



signals in the  $^1\text{H}$  NMR spectra. Only in the cases of BTEs with large energy barrier between two conformers can the rotation of the aryl groups be slowed down sufficiently to give two sets of signals.<sup>[58,82]</sup> As found by the area integration in  $^1\text{H}$  NMR spectra, the ratio between the parallel and antiparallel conformers of BTTA in  $d_6$ -benzene is 64:36 while the ratio is 58:42 in  $\text{CDCl}_3$ , indicating that the solvent has a great effect on the equilibrium between the conformers.

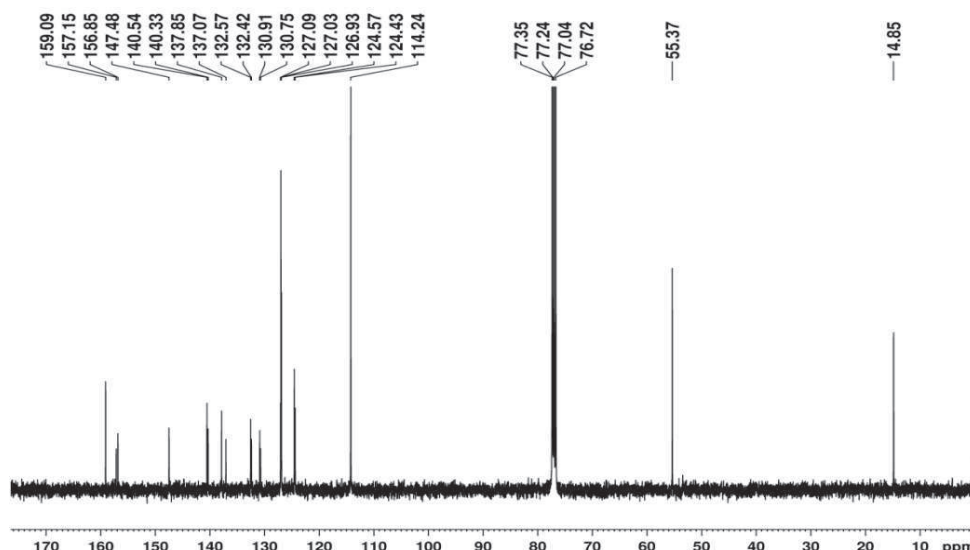


Fig. 3.17  $^{13}\text{C}$  NMR spectrum of BTTA in  $\text{CDCl}_3$

Figure 3.17 illustrates the  $^{13}\text{C}$  NMR of BTTA. Two signals are at high field and others are at low field. The total number of the signals is 20, which is in accordance with the total carbon species within the molecule.

#### Elemental Composition Report

Page 1

#### Single Mass Analysis

Tolerance = 5.0 mDa / DBE: min = -1.5, max = 100.0  
 Element prediction: Off  
 Number of isotope peaks used for i-FIT = 2

Monoisotopic Mass, Odd and Even Electron Ions  
 64 formula(e) evaluated with 1 results within limits (up to 1 closest results for each mass)

Elements Used:

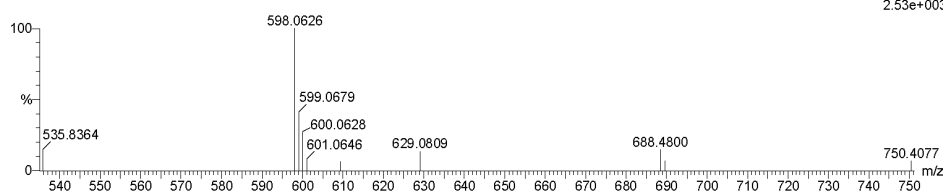
C: 0-30 H: 0-30 N: 0-4 O: 0-2 S: 0-4

ZHU-WH

ECUST institute of Fine Chem

02-Jul-2011  
 10:06:08  
 1: TOF MS ES+  
 2.53e+003

ZWH-YY-021 (0.128) Cm (1:4)



Minimum:

Maximum: 5.0 50.0 -1.5 100.0

Mass	Calc. Mass	mDa	PPM	DBE	i-FIT	i-FIT (Norm)	Formula
598.0626	598.0626	0.0	0.0	22.0	9.8	0.0	C30 H22 N4 O2 S4

Fig. 3.18 High resolution mass spectra of BTTA

HRMS of BTTA shows an apparent molecular ion peak corresponding to  $[\text{M}]^+$ . The

calculated value for  $[M]^+$  is 598.0626, which is in accordance with the observed value of 598.0626.

Figure 3.19 illustrates the  $^1\text{H}$  NMR spectrum of *c*-BTTA in  $d_6$ -benzene. Due to the lack of different conformers, and to the symmetric nature of central ethene bridge, only one set of signal was observed. Furthermore, due to the different structure between *c*-BTTA and BTTA, the corresponding protons are all shifted to some extent.

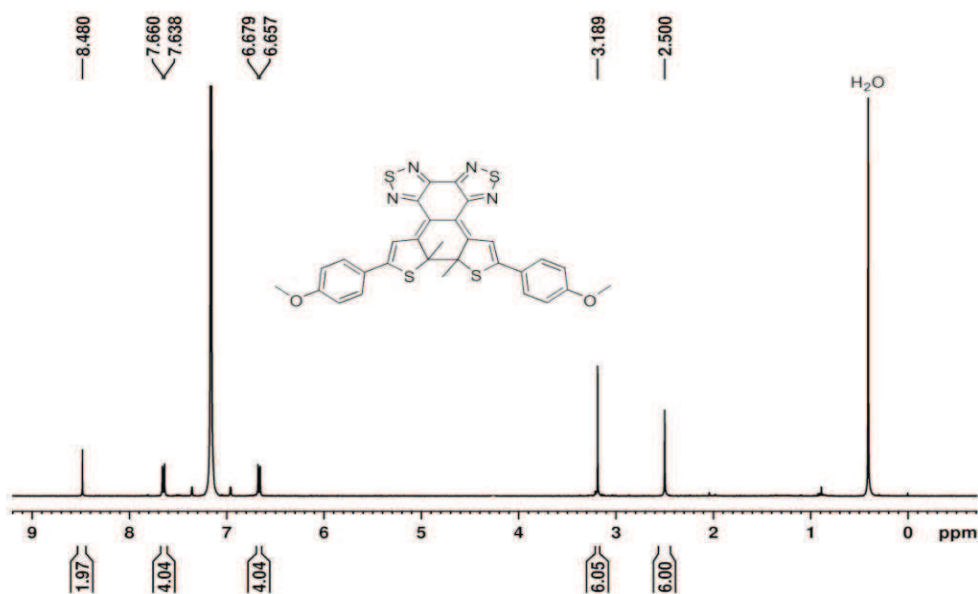


Fig. 3.19  $^1\text{H}$  NMR spectrum of *c*-BTTA in  $d_6$ -benzene.

### 3.3.3 UV-Vis absorption of BTE-NA, BTA and BTTA

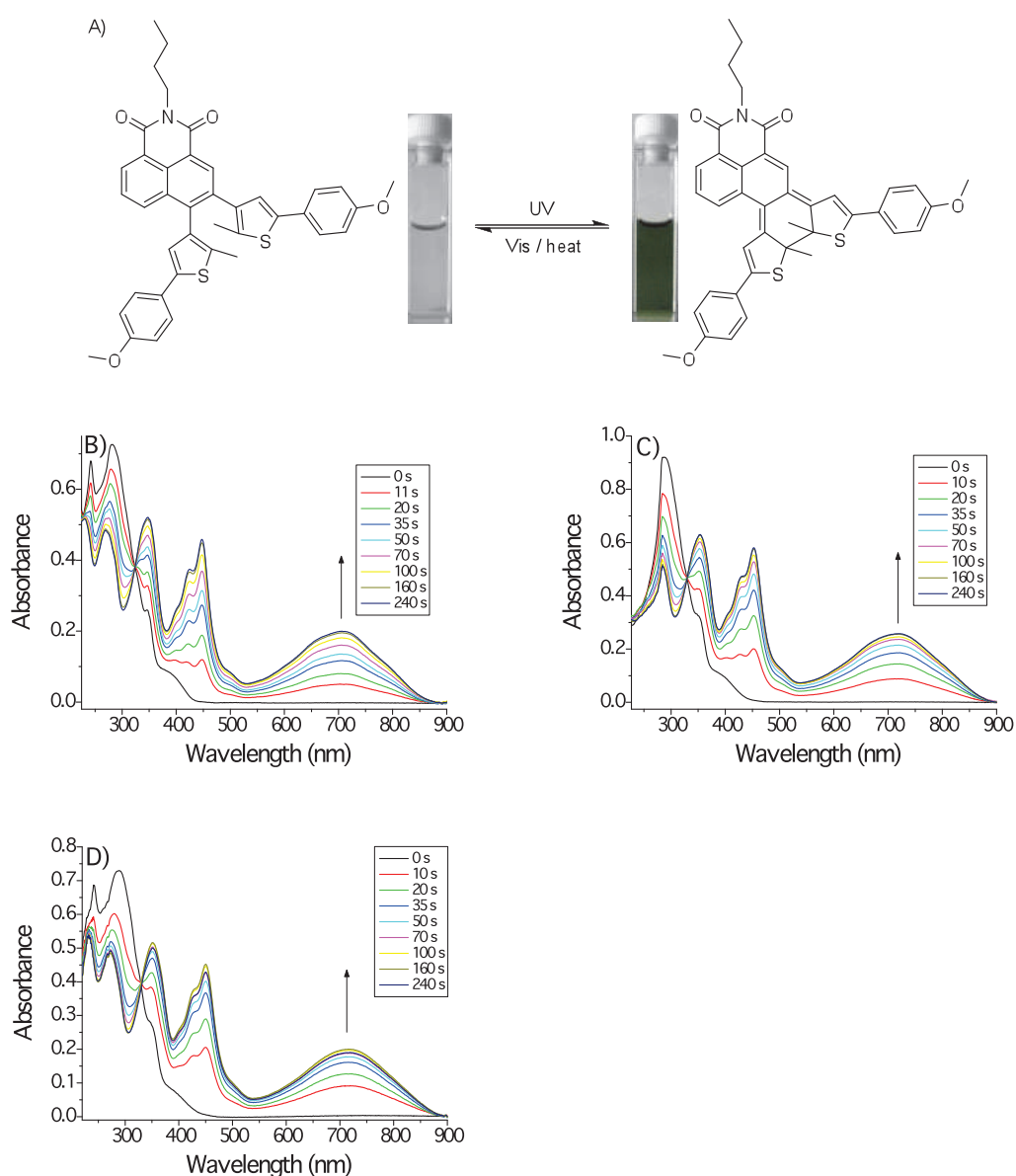
All three compounds are found to easily dissolve in toluene to give a colorless solution without any absorption bands in the visible range. In general, the electronic absorption spectra for the open forms of BTE-NA, BTA and BTTA in toluene at 298 K show an intense absorption band in the range of 290-350 nm and a moderately intense band at 378-430 nm (Figure 3.20-3.22). Upon UV irradiation at 365 nm, the corresponding closed forms (*c*-BTE-NA, *c*-BTA and *c*-BTTA) were produced by the typical photocyclization as the colorless solution changed to yellow green, bright green and dark green, respectively, resulting in broad absorption bands centered at 719 nm (*c*-BTE-NA), 657 nm (*c*-BTA), 655 nm (*c*-BTTA), in addition to bands in the 300-500 nm region. The significant bathochromic shift in absorption bands of the closed forms relative to their open forms is mainly due to the extended  $\pi$ -conjugation across the whole moiety. The longer wavelength of *c*-BTE-NA at the visible region than that of *c*-BTTA strongly indicates that the energy gap between the HOMO and LUMO orbitals of *c*-BTE-NA is smaller than that of *c*-BTTA, which results from the strong conjugation between 2-(4-methoxyphenyl)-5-methylthiophene and

*N*-butyl-1,8-naphthalimide units. The typical photochromic properties of BTE-NA, BTA, BTTA and their corresponding closed forms (*c*-BTE-NA, *c*-BTA and *c*-BTTA) are summarized in Table 3.1. Notably, the ring closure quantum yield of these molecules decreased with the loss of aromaticity of the ethene bridge. The ring closure quantum yields for BTE-NA, BTA and BTTA are 43.13%, 38.21% and 10.96% in cyclohexane, respectively. This may be ascribed to the difference in the competition between the photocyclization reaction from the excited state and the radiative pathway to the ground state.

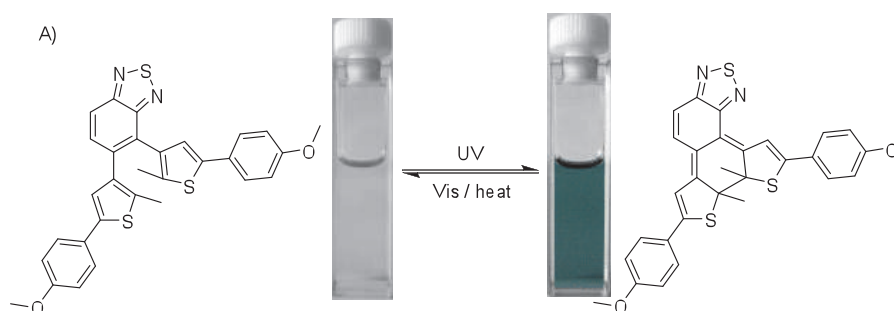
Table 3.1 Spectral data of open and closed form of BTE-NA, BTA and BTTA in various solvents

Compounds	cyclohexane	toluene	THF	acetonitrile
BTE-NA	281/36.27	288/39.84	289/38.61	--
$\varepsilon$ ( $10^3 \text{ M}^{-1} \text{ cm}^{-1}$ )	392/3.91	396/4.31	392/3.99	
<i>c</i> -BTE-NA	349/28.83	355/31.38	353/28.03	--
$\varepsilon$ ( $10^3 \text{ M}^{-1} \text{ cm}^{-1}$ )	424/22.58	428/26.06	427/21.13	
	447/27.91	453/32.60	450/25.62	
	709/12.14	717/14.50	716/11.33	
$\Phi_{\text{o-c}} / \Phi_{\text{c-o}} / \alpha_{\text{PSS}}$ (%)	43.13/2.61/82.1	35.11/3.22/76.8	26.98/1.19/88.4	--
BTA	251/27.42	309/36.34	251/27.43	246/30.08
$\varepsilon$ ( $10^3 \text{ M}^{-1} \text{ cm}^{-1}$ )	306/29.98	392/4.30	308/34.14	305/39.72
	384/3.65		391/3.68	380/3.93
<i>c</i> -BTA	333/30.60	338/33.48	336/31.13	329/32.64
$\varepsilon$ ( $10^3 \text{ M}^{-1} \text{ cm}^{-1}$ )	414/20.22	416/21.86	413/20.07	407/20.26
	650/13.68	657/15.13	655/14.01	648/14.50
$\Phi_{\text{o-c}} / \Phi_{\text{c-o}} / \alpha_{\text{PSS}}$ (%)	38.21/1.94/89.4	29.43/0.932/91.9	38.87/1.07/91.6	6.46/0.39/84.8
BTTA	293/63.47	298/57.4	294/59.5	290/50.8
$\varepsilon$ ( $10^3 \text{ M}^{-1} \text{ cm}^{-1}$ )	388/4.57	392/5.27	381/4.15	370/3.88
<i>c</i> -BTTA	276/29.12	329/29.4	277/23.8	280/22.3
$\varepsilon$ ( $10^3 \text{ M}^{-1} \text{ cm}^{-1}$ )	328/36.9	400/28.9	326/29.1	322/28.2
	400/36.2	420/55.7	397/31.1	393/26.6
	419/73.8	497/9.10	416/57.9	414/43.4
	485/11.2	655/10.5	495/9.27	492/7.61
	516/10.4		655/12.0	649/10.5
	655/12.8			
$\Phi_{\text{o-c}} / \Phi_{\text{c-o}} / \alpha_{\text{PSS}}$ (%)	10.96/0.43/93.2	14.03/0.97/99.2	16.62/0.47/91.7	14.95/0.14/98.8

<sup>[a]</sup> $\Phi_{\text{o-c}}$ ,  $\Phi_{\text{c-o}}$  and  $\alpha_{\text{PSS}}$  are depicted as the ring-closure quantum yield at 365nm, the ring-opening quantum yield at 575nm and the conversion yield at 365nm, respectively.



**Fig. 3.20** A) Structure and color variation of BTE-NA ( $2.31 \times 10^{-4} \text{ mol L}^{-1}$ ) in toluene before and after irradiation at 365 nm. Spectral changes of UV-Vis absorption of BTE-NA in B) cyclohexane ( $2.0 \times 10^{-5} \text{ mol L}^{-1}$ ); C) toluene ( $2.31 \times 10^{-5} \text{ mol L}^{-1}$ ) and D) THF ( $1.89 \times 10^{-5} \text{ mol L}^{-1}$ ) upon irradiation at 365 nm. The photostationary states (PSS) were obtained by irradiating solutions with 365 nm light until no further spectral changes were observed.



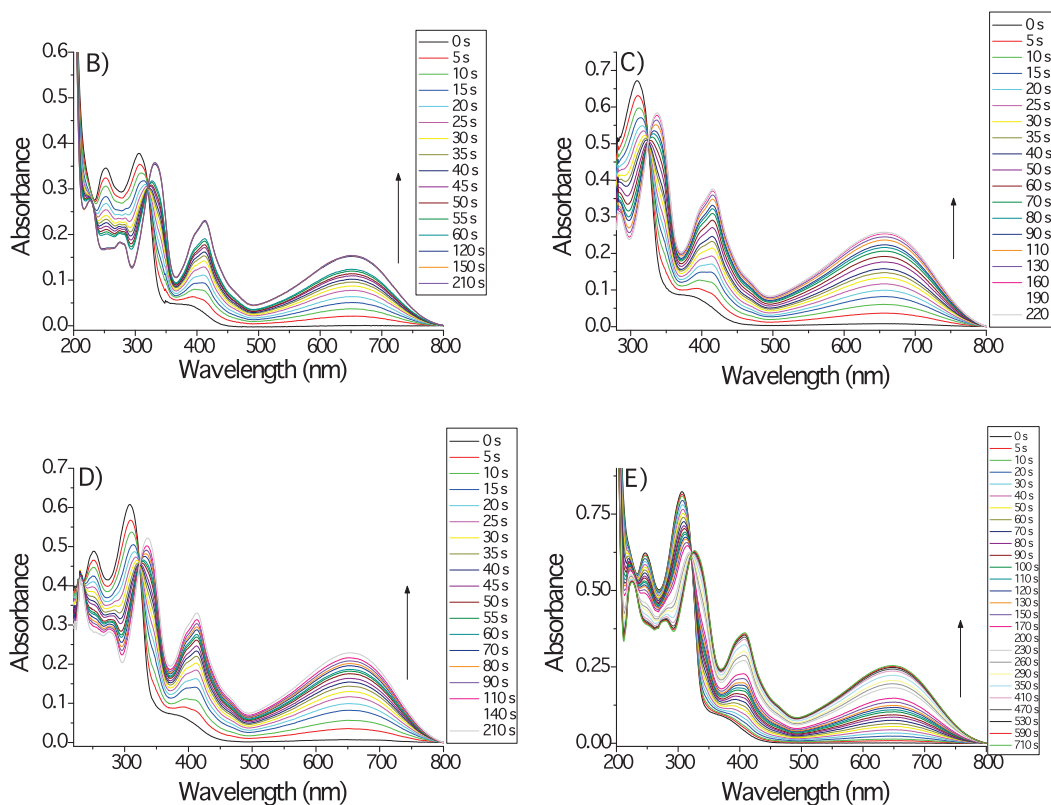
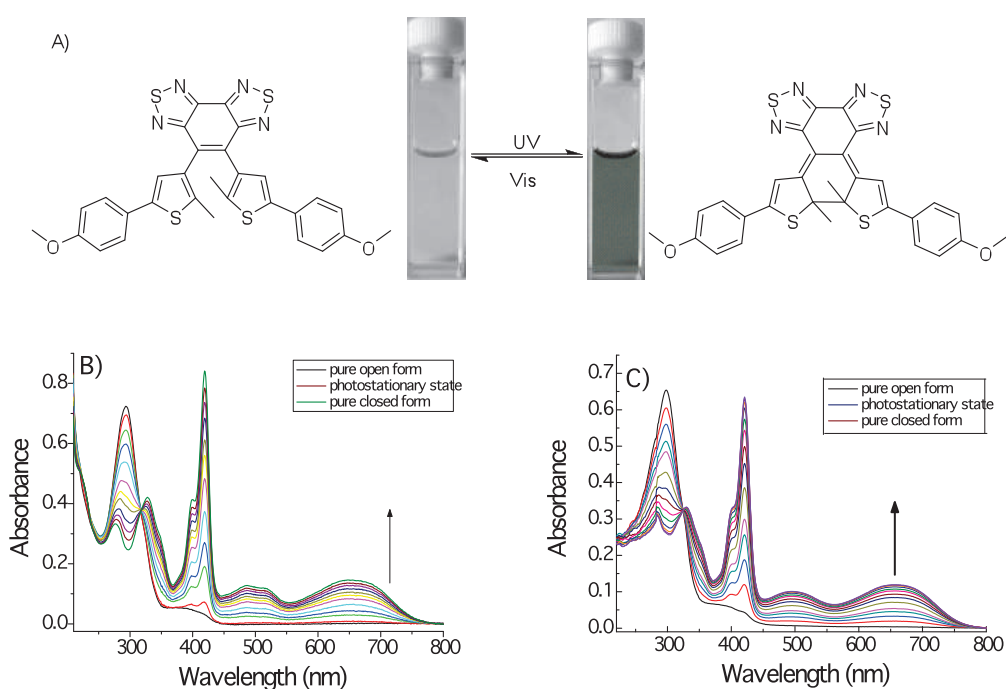


Fig. 3.21 A) Structure and color variation of BTA ( $1.85 \times 10^{-4} \text{ mol L}^{-1}$ ) in toluene before and after irradiation at 365 nm. Spectral changes of UV-Vis absorption of BTA in B) cyclohexane ( $1.26 \times 10^{-5} \text{ mol L}^{-1}$ ); C) toluene ( $1.85 \times 10^{-5} \text{ mol L}^{-1}$ ); D) THF ( $1.78 \times 10^{-5} \text{ mol L}^{-1}$ ) and E) acetonitrile ( $2.07 \times 10^{-5} \text{ mol L}^{-1}$ ) upon irradiation at 365 nm. The photostationary states (PSS) were obtained by irradiating solutions with 365 nm light until no further spectral changes were observed.



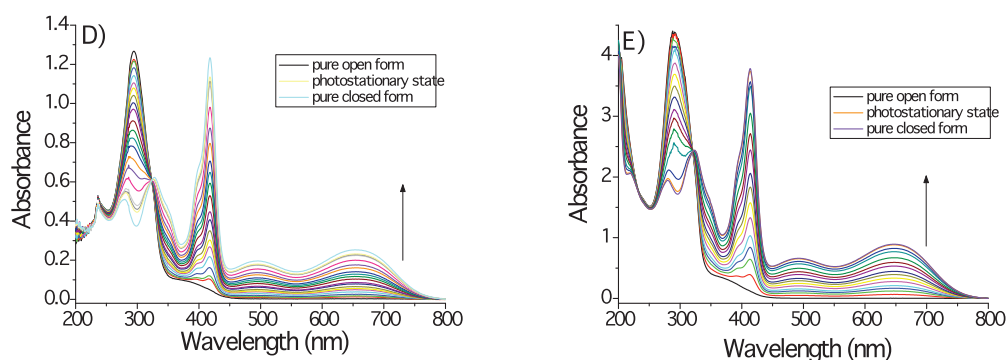


Fig. 3.22 A) Structure and color variation of BTTA ( $1.14 \times 10^{-4} \text{ mol L}^{-1}$ ) in toluene before and after irradiation at 365 nm. Spectral changes of UV-Vis absorption of BTTA in B) cyclohexane ( $1.14 \times 10^{-5} \text{ mol L}^{-1}$ ); C) toluene ( $1.14 \times 10^{-5} \text{ mol L}^{-1}$ ); D) THF ( $2.14 \times 10^{-5} \text{ mol L}^{-1}$ ) and E) acetonitrile ( $8.65 \times 10^{-5} \text{ mol L}^{-1}$ ) upon irradiation at 365 nm. The photostationary states (PSS) were obtained by irradiating solutions with 365 nm light until no further spectral changes were observed.

### 3.3.4 $^1\text{H}$ NMR changes of BTE-NA, BTA and BTTA before and after irradiation

In fact, great  $^1\text{H}$  NMR modifications can be observed in photochromic systems due to the large chemical environment changes between the open and closed forms. The  $^1\text{H}$  NMR spectra of BTE-NA and BTA show only one set of signals for the methyl protons on thiophene rings located at (1.82 and 2.13 ppm for BTE-NA; 1.98 and 2.03 ppm for BTA) in  $d_6$ -benzene (Figures 3.23-3.24). The different chemical shifts of two methyl protons are only due to the asymmetric organic framework of the central ethene bridge, while the  $^1\text{H}$  NMR spectrum of BTTA in  $d_6$ -benzene shows two well-resolved sets of signals for the methyl protons which correspond to the parallel ( $\delta = 2.04 \text{ ppm}$ ) and antiparallel ( $\delta = 1.98 \text{ ppm}$ ) conformers (Figure 3.25). In fact, the two conformations, parallel (photochromic inactive) and antiparallel (photochromic active) conformers, undergo very fast single-bond rotation in BTE-NA and BTA, thereby resulting in only one set of time-averaged signals in the  $^1\text{H}$  NMR spectra. Only in the cases of BTEs with large energy barrier between two conformers, the rotation of the aryl groups can be slowed down sufficiently to give two sets of signals.<sup>[18]</sup> As found by the area integration in  $^1\text{H}$  NMR spectra (Figure 3.25), the ratio between the parallel and antiparallel conformers of BTTA in  $d_6$ -benzene is 64:36. When irradiated at 365 nm, the open form was converted to the closed form (*c*-BTTA) with absorption bands in the visible region. The existence of *c*-BTE-NA, *c*-BTA and *c*-BTTA could also be evidenced by  $^1\text{H}$  NMR. For BTE-NA (Figure 3.23), the signals of  $H_a$ ,  $H_b$  and  $H_c$  on butyl group after photocyclization (in  $d_6$ -benzene) does not show any obvious changes with respect to the open form due to the distance from the  $\pi$ -delocalization of naphthalimide, while the methylene hydrogen signals ( $H_d$ ) attached to imide nitrogen shift by 0.07 ppm from 4.37 to 4.30 ppm.

The two groups of methyl protons ( $H_o$ ,  $H_p$ ) on thiophene ring in BTE-NA shift from 1.82 and 2.13 ppm to 2.37 and 2.50 ppm, respectively. The case is similar for the two methyl protons ( $H_i$ ,  $H_j$ ) on thiophene group of BTA (in  $d_6$ -benzene), which shifted from 1.98 and 2.03 ppm to the downfield at 2.46 and 2.50 ppm, respectively (Figure 3.24).

Generally speaking, the proton resonances on the thiophene heterocycles and six-membered ethene bridges shift upfield upon ring-closure of diarylethene,<sup>[124]</sup> which is due to the aromaticity loss of heterocycles in the ring-closure reaction. In the ring-open form, the resonances of the protons attached onto thiophene units and six-membered rings appear in the  $^1\text{H}$  NMR aromatic region. In contrast, the resonances for these protons in the ring-closed form appear in the region of alkenes characteristics. As expected, after the ring-closure of BTE-NA upon irradiation at 365 nm, the aromaticity of the naphthalimide and thiophene groups are disturbed, the protons ( $H_e$ ,  $H_f$ ,  $H_g$ , and  $H_h$ ) on the naphthalimide moiety shift remarkably to the high field upon photocyclization (Figure 3.23). A typical triplet peak corresponding to  $H_f$  moves from 7.14 to 6.98 ppm. The singlet peak of  $H_h$  shifts greatly from 8.91 to 8.24 ppm. Additionally, the two protons ( $H_i$  and  $H_v$ ) located on thiophene are 6.94 and 6.84 ppm for BTE-NA, while they shift to 6.86 and 6.61 ppm after photocyclization. Similarly in case of BTA, the chemical shifts of  $H_a$  and  $H_b$  on the benzothiadiazole (BTA) and  $H_c$  move to high field (Figure 3.24). Interestingly, in contrast to the two protons ( $H_c$  and  $H_p$ ) located on thiophene (6.95 and 7.16 ppm) for BTA,  $H'_c$  shifts upfield to 6.39 ppm while  $H'_p$  shifts downfield to 8.43 ppm for *c*-BTA. Also in the system of BTTA, the protons of  $H_b$  and  $H'_b$  on thiophene rings of BTTA shift downfield from 7.05 and 7.25 ppm in the open form to 8.48 ppm after photocyclization (Figure 3.25). The dramatic downfield shifts of  $H'_p$  for BTA could be attributed to the possible formation of intramolecular hydrogen bond between  $H'_p$  and the *N* atom on benzothiadiazole moiety (Figure 3.24). Similarly, the intramolecular hydrogen bonds between  $H_b$ ,  $H'_b$  and the *N* atom on benzobisthiadiazole units finally lead to the downfield shift of  $H_b$  and  $H'_b$  upon photocyclization (Figure 3.25).

Interestingly, in case of BTTA (in  $d_6$ -benzene), the two sets of well-resolved proton signals on thiophene and methyl groups of methoxy on the phenyl rings were converted into one set of protons signals (moved from 1.98 and 2.04 ppm to 2.50 ppm; 3.22 and 3.26 ppm to 3.19 ppm, respectively). It is the same case for the protons on phenyl rings after photocyclization. The simultaneous disappearance of the two sets of signals indicates that a slow interconversion between parallel and anti-parallel conformations takes place in the system, and that the chemical environment of the two sets of methyl groups becomes identical after photo-cyclization. It might be due to the small energy barrier between parallel and anti-parallel conformers between BTTA and *c*-BTTA that allows the full conversion from BTTA to *c*-BTTA as demonstrated by  $^1\text{H}$  NMR (Figure 3.25).

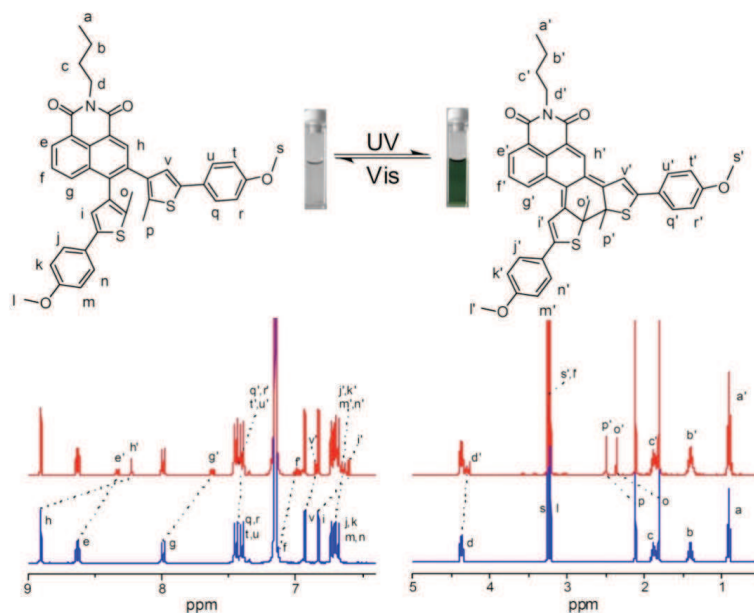


Fig. 3.23  $^1\text{H}$  NMR changes of BTE-NA in  $d_6$ -benzene. The signal of proton  $H_f$  overlaps with the solvent residual peak signals of  $d_6$ -benzene. Note: The corresponding inset photographic images of BTE-NA were taken at the concentration of  $2.31 \times 10^{-4} \text{ mol L}^{-1}$  in toluene upon irradiation at 365 nm.

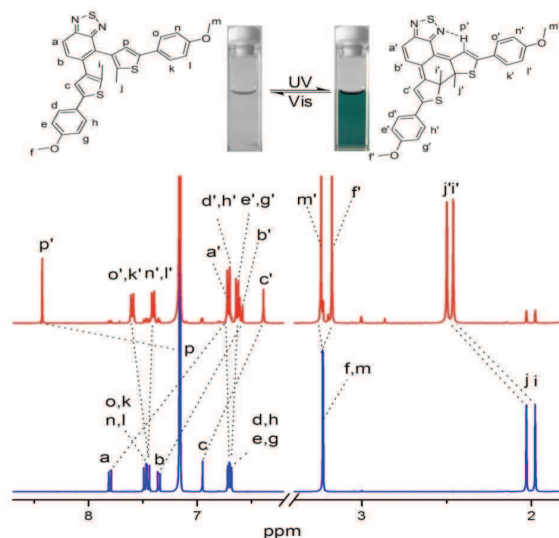


Fig. 3.24  $^1\text{H}$  NMR changes of BTA in  $d_6$ -benzene. The signal of proton  $H_p$  overlaps with the solvent residual peak signals of  $d_6$ -benzene. Note: The corresponding inset photographic images of BTA were taken at the concentration of  $1.85 \times 10^{-4} \text{ mol L}^{-1}$  in toluene upon irradiation at 365 nm.



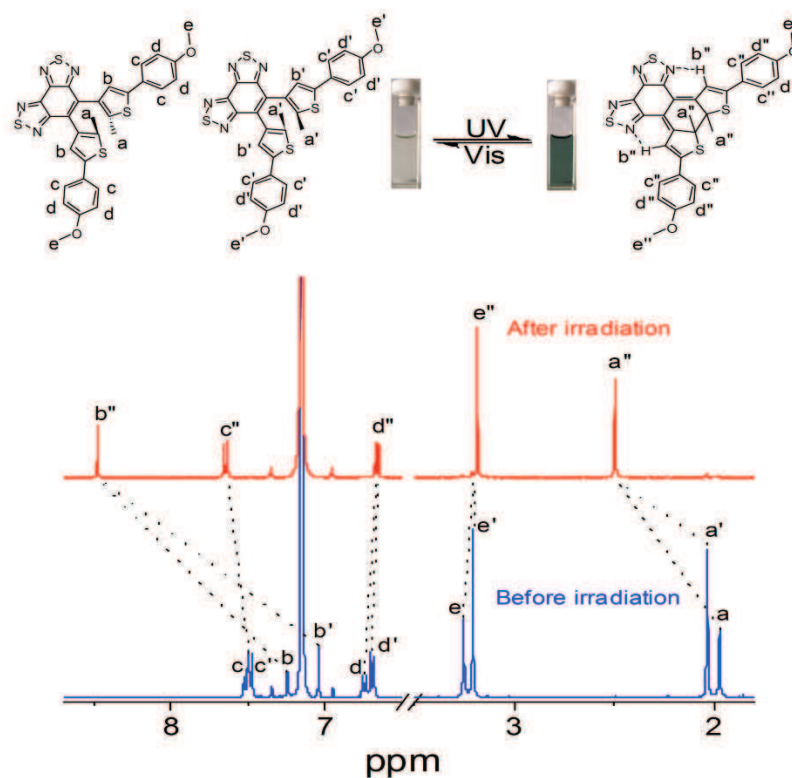
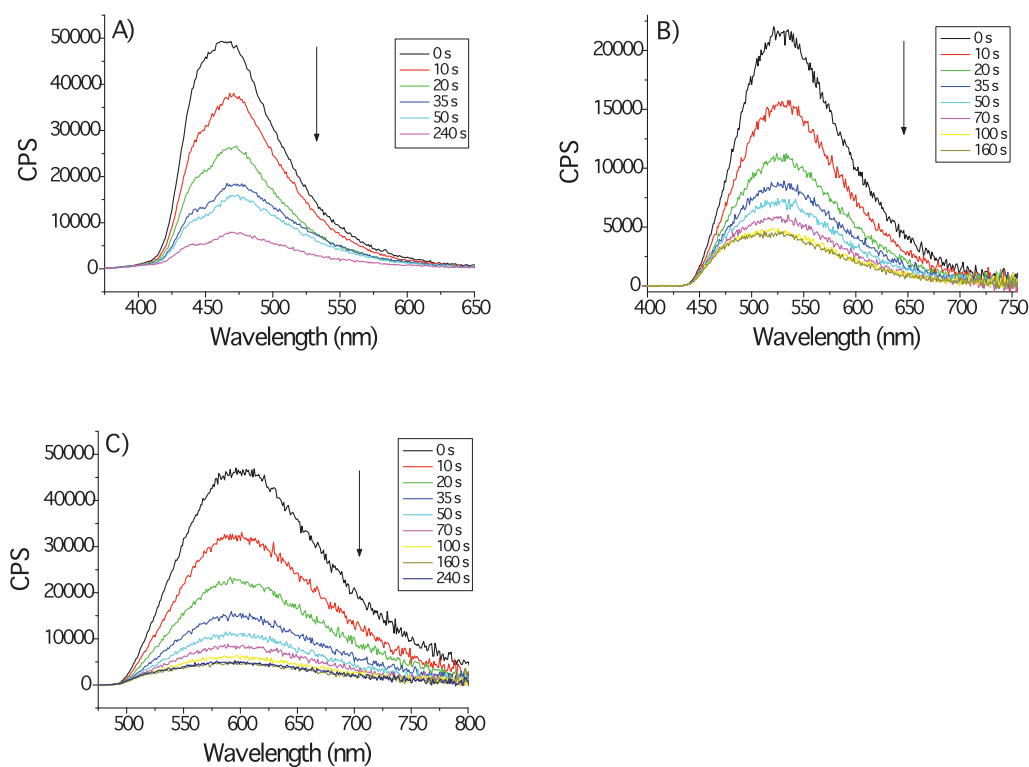


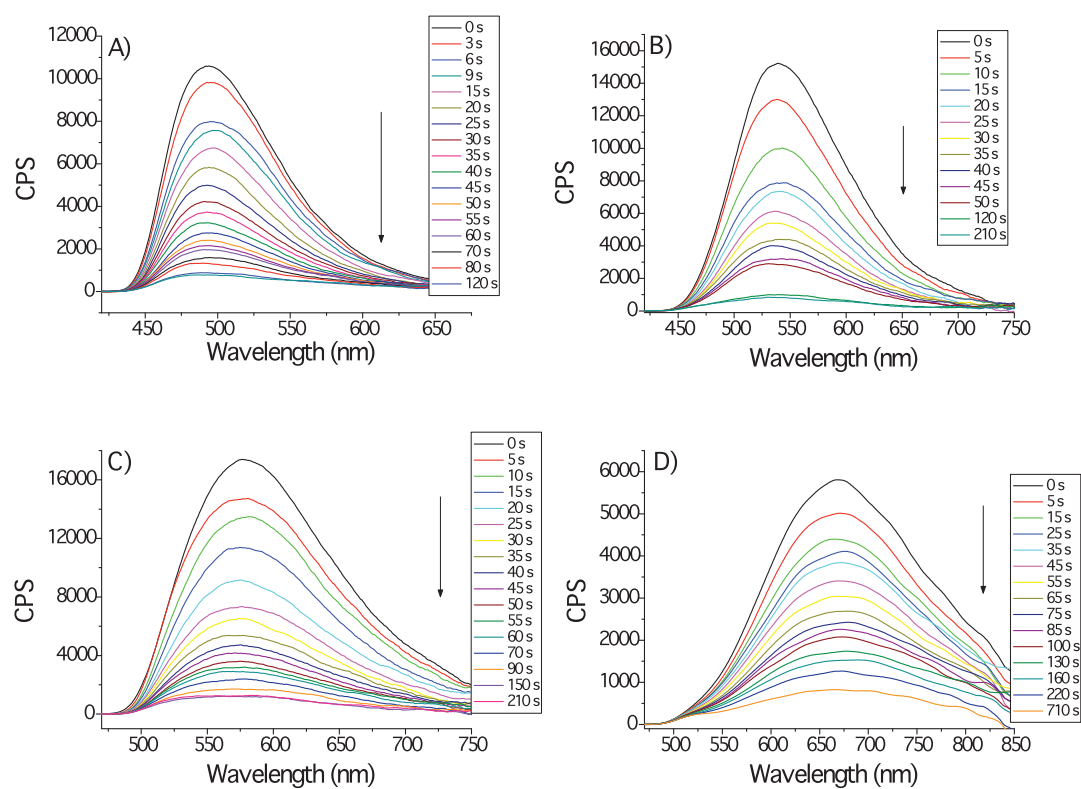
Fig. 3.25  $^1\text{H}$  NMR changes of BTTA in  $d_6$ -benzene. Note: the inset photographic images of BTTA were taken in toluene ( $1.14 \times 10^{-4}$  mol  $\text{L}^{-1}$ ) upon irradiation at 365 nm.

### 3.3.5 Fluorescence changes of BTE-NA, BTA and BTTA before and after irradiation

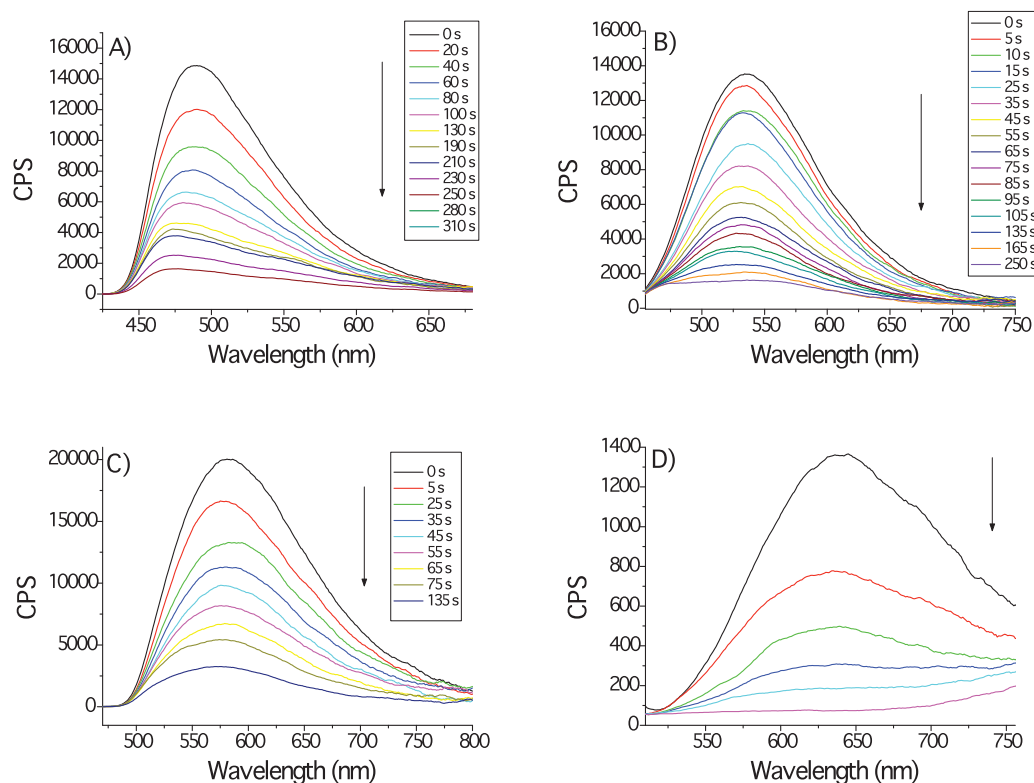
As shown in Table 3.1, the absorption bands of the open and closed forms of BTE-NA, BTA and BTTA in various solvents remain in the range of 378-430 nm and 650-719 nm, thus indicating that the solvent dependence of the absorption band is rather small. All three compounds show noticeable fluorescence, which could be well modulated by solvato- and photo-chromism. Indeed, upon excitation at 719 nm (BTE-NA), 657 nm (BTA) and 655 nm (BTTA), no significant fluorescence signals could be recorded from the closed form. The fluorescence quenched at photostationary state (PSS) in toluene is 77% for BTE-NA, 92% for BTA, and 94% for BTTA (excited at the isobestic points of 329, 324 and 324 nm, respectively), which are fully compatible with the conversion yield (Table 3.1). Thus, the fluorescence quenching of BTE-NA, BTA and BTTA is simply due to the disappearance of the open form upon photocyclization and non-fluorescent property of corresponding closed form (Figure 3.26-3.28).



**Fig. 3.26** Spectral changes of fluorescence of BTE-NA excited at isobestic points of 324, 329 and 331 nm in A) cyclohexane ( $2.0 \times 10^{-5} \text{ mol L}^{-1}$ ); B) toluene ( $2.31 \times 10^{-5} \text{ mol L}^{-1}$ ); C) THF ( $1.89 \times 10^{-5} \text{ mol L}^{-1}$ ) upon irradiation at 365 nm. The photostationary states (PSS) were obtained by irradiating solutions with 365 nm light until no further spectral changes were observed.



**Fig. 3.27** Spectral changes of fluorescence of BTA excited at isobestic points of 320, 324, 323 and 321 nm in A) cyclohexane ( $1.26 \times 10^{-5} \text{ mol L}^{-1}$ ); B) toluene ( $1.85 \times 10^{-5} \text{ mol L}^{-1}$ ); C) THF ( $1.78 \times 10^{-5} \text{ mol L}^{-1}$ ); D) acetonitrile ( $2.07 \times 10^{-5} \text{ mol L}^{-1}$ ) upon irradiation at 365 nm. The photostationary states (PSS) were obtained by irradiating solutions with 365 nm light until no further spectral changes were observed.



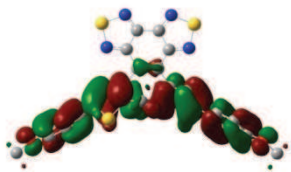
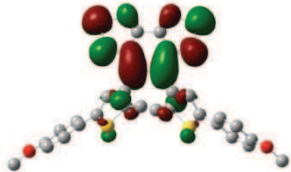
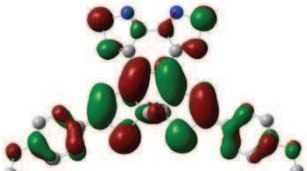
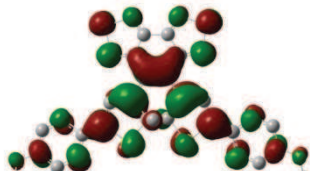
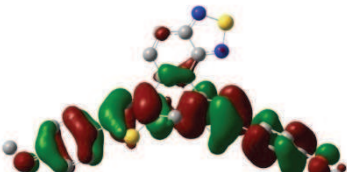
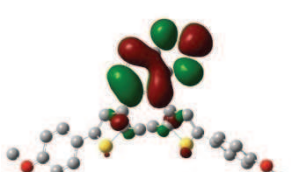
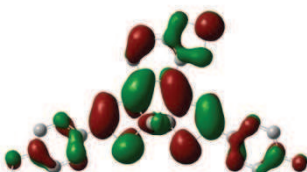

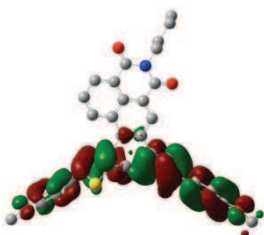
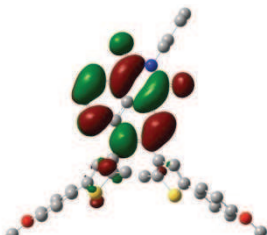
**Fig. 3.28** Spectral changes of fluorescence of BTTA excited at isobestic points of 317, 324, 323 and 321 nm in A) cyclohexane ( $1.14 \times 10^{-5} \text{ mol L}^{-1}$ ); B) toluene ( $1.14 \times 10^{-5} \text{ mol L}^{-1}$ ); C) THF ( $2.14 \times 10^{-5} \text{ mol L}^{-1}$ ); D) acetonitrile ( $8.65 \times 10^{-5} \text{ mol L}^{-1}$ ) upon irradiation at 365 nm. The photostationary states (PSS) were obtained by irradiating solutions with 365 nm light until no further spectral changes were observed.

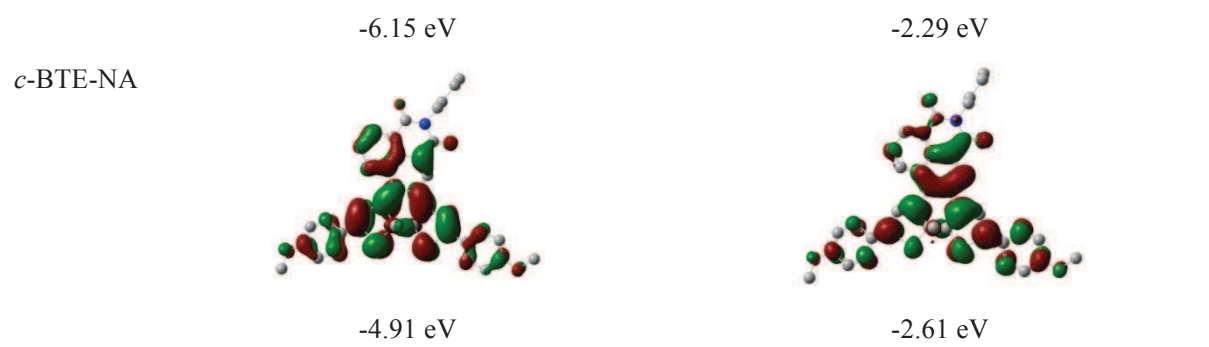
In general, emission from fluorophores generally occurs at wavelengths that are longer than those at which absorption occurs<sup>[93]</sup>.

Moreover, the solvent polarity is decisive in the emission wavelength due to the strong electron withdrawing nature of naphthalimide, benzothiadiazole and benzobisthiadiazole, and moderate donating ability of anisole rings. As illustrated in Table 3.2, the electronic densities of BTE-NA, BTA and BTTA are completely different between the HOMO and the LUMO, indicating a strong electron mobilization after excitation. When the three compounds are excited, the dipole moment is largely enhanced for all of them. In nonpolar solvents like cyclohexane, the dipole moments could not be stabilized, and hence, the emission wavelength was shorter. While in polar solvents like acetonitrile, the stabilized dipole moment yields

small energy gap between HOMO and LUMO, thus, longer emission wavelength was observed (Figure 3.29). The peak of the emission bands appear at 464 and 601 nm in cyclohexane and THF for BTE-NA, 494 and 670 nm in cyclohexane and acetonitrile for BTA, 488 and 636 nm in cyclohexane and acetonitrile for BTTA, respectively (Tables 3.3-3.5). Obviously, the solvatochromism of all three compounds is arisen from the possible photoinduced charge transfer from the donor anisole group to the electronegative central ethene bridge. The positive linearity of the Lippert–Mataga plots also illustrates that there is a higher dipole moment in the excited state than in the ground state (Figure 3.30).

Table 3.2 Molecular orbitals of BTE-NA, BTA and BTTA involved in the main electronic transitions

	HOMO	LUMO
BTTA	 -6.07 eV	 -2.26 eV
<i>c</i> -BTTA	 -4.98 eV	 -2.62 eV
BTA	 -5.96 eV	 -2.21 eV
<i>c</i> -BTA	 -4.55 eV	 -2.28 eV
BTE-NA	 -4.55 eV	 -2.28 eV



Note: Molecular orbitals were drawn with an iso-coefficient of 0.02

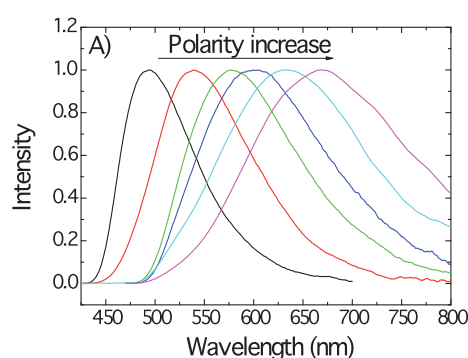


Fig. 3.29 A) Normalized fluorescence spectra of BTA in various solvents (from left to right, cyclohexane, toluene, THF, chloroform, acetone and acetonitrile)

To further investigate the effect of solvatochromism on the excited state of BTE-NA, BTA and BTTA, we studied the Lippert-Mataga plots of three compounds in various solvents. The interaction between BTE-NA, BTA and BTTA and solvents can affect the energy gap between HOMO-LUMO, which could be expressed in wavenumber ( $\text{cm}^{-1}$ ) as a function of dielectric constant ( $\epsilon$ ) and refractive index ( $n$ ) and described by Lippert-Mataga equation (Equation 2.1).

From the values reported in Table 3.3-3.5, the Lippert-Mataga plot of BTE-NA, BTA and BTTA was obtained (Figure 3.30). It could be evidenced from the plot that the excited BTE-NA, BTA and BTTA has a higher dipole moment than that of ground state BTTE, which is probably due to the photoinduced charge transfer from electron rich anisole rings to the electron deficient benzobisthiadiazole moiety. Hence, BTTE exhibits different emission spectra in various solvents.

Table 3.3 Spectral Properties of BTE-NA in Various solvents

Solvents	Absorption maximum (nm)	Emission maximum (nm)	Stokes shift (cm <sup>-1</sup> )	$\Delta f$
Cyclohexane	379	464	4833	0.001
Toluene	415	530	5228	0.015
THF	395	601	8678	0.209
Chloroform	394	585	8287	0.185

Table 3.4 Spectral Properties of BTA in Various solvents

Solvents	Absorption maximum (nm)	Emission maximum (nm)	Stokes shift (cm <sup>-1</sup> )	$\Delta f$
cyclohexane	379	494	6142	0.001
Toluene	400	539	6447	0.015
THF	374	577	9406	0.209
Chloroform	390	601	9002	0.185
Acetone	382	634	10405	0.287
Acetonitrile	389	670	10781	0.304

Table 3.5 Spectral Properties of BTTA in Various solvents

Solvents	Absorption maximum (nm)	Emission maximum (nm)	Stokes shift (cm <sup>-1</sup> )	$\Delta f$
Cyclohexane	362	488	7132	0.001
Toluene	379	527	7410	0.015
Chloroform	375	570	9122	0.185
THF	367	558	9327	0.209
Acetone	381	618	10075	0.287
Acetonitrile	385	636	10260	0.304

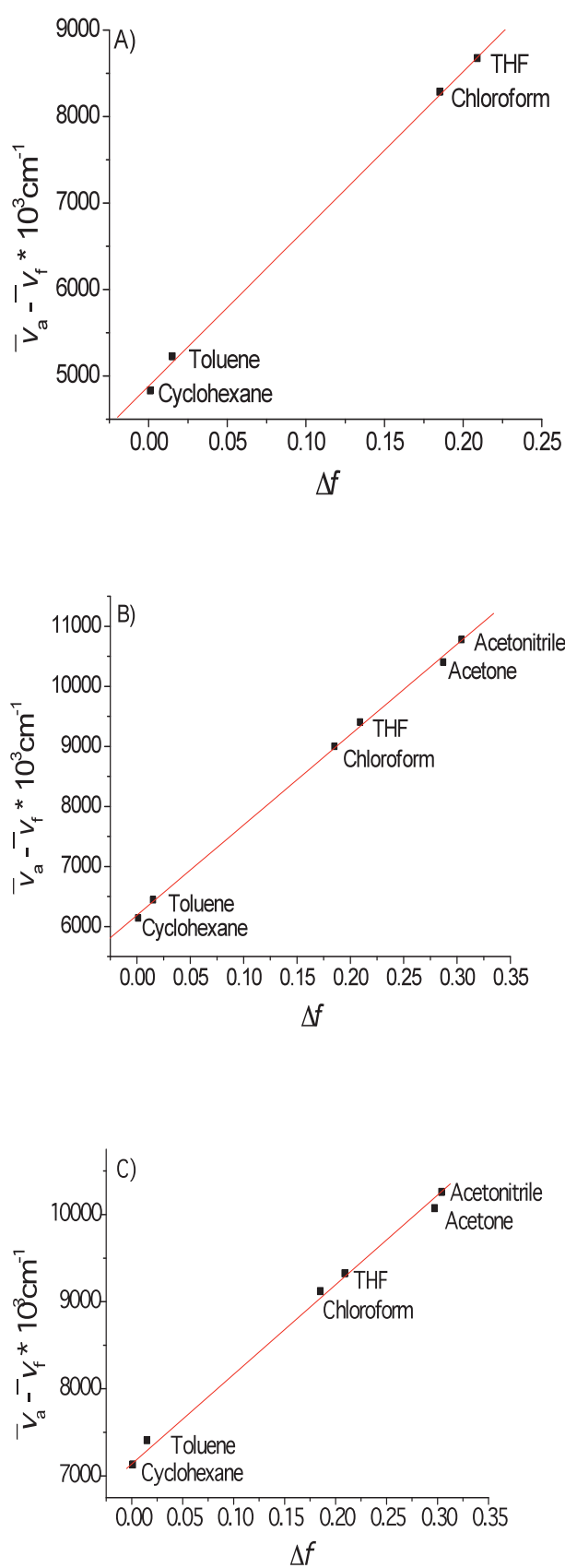


Fig. 3.30 Lippert-Mataga plots: A) BTE-NA, B) BTA and C) BTTA.

### 3.3.5 Thermal stability of BTE-NA, BTA and BTTA in various solvents

The energy barrier, which correlates with the ground-state energy difference between the open and the closed forms, contributes to the stability of the photogenerated closed-ring isomers. In fact, the change in aromatic character of six-membered ethene from open to closed form during the course of photocyclization can control the ground-state energy difference. With the strong aromaticity of the central ethene bridge, the energy barrier for the cyclo-reversion thus becomes smaller. Hence, the thermal back reaction is ready to take place.<sup>[19]</sup> As expected, *c*-BTE-NA is unstable even at 293 K due to the large difference in ground state energy before and after irradiation. As illustrated in Table 3.6, the absorbance at around 710 nm for BTE-NA could be completely bleached within 35 min, indicating the great loss of aromaticity after photocyclization reaction. The thermal back reaction rates for *c*-BTE-NA are  $1.01 \times 10^{-3}$ ,  $1.27 \times 10^{-3}$ ,  $3.10 \times 10^{-3}$  and  $3.71 \times 10^{-3} \text{ s}^{-1}$  in cyclohexane, toluene, THF and acetonitrile, respectively, monitored by CCD camera mounted on a spectrometer and CARY in kinetic mode (Figure 3.31). More impressively, the decay becomes much faster in chloroform ( $1.80 \times 10^{-1} \text{ s}^{-1}$ , Table 3.7). The experimental data were fitted with Equation 3.2.<sup>[125]</sup>

$$k\tau = -\ln[(A - A_\infty)/(A_0 - A_\infty)] \quad \text{Equation 3.2}$$

where  $A_0$ ,  $A_\infty$  and  $A$  are the initial, infinite absorbance and absorbance at  $\tau$ (s), respectively.

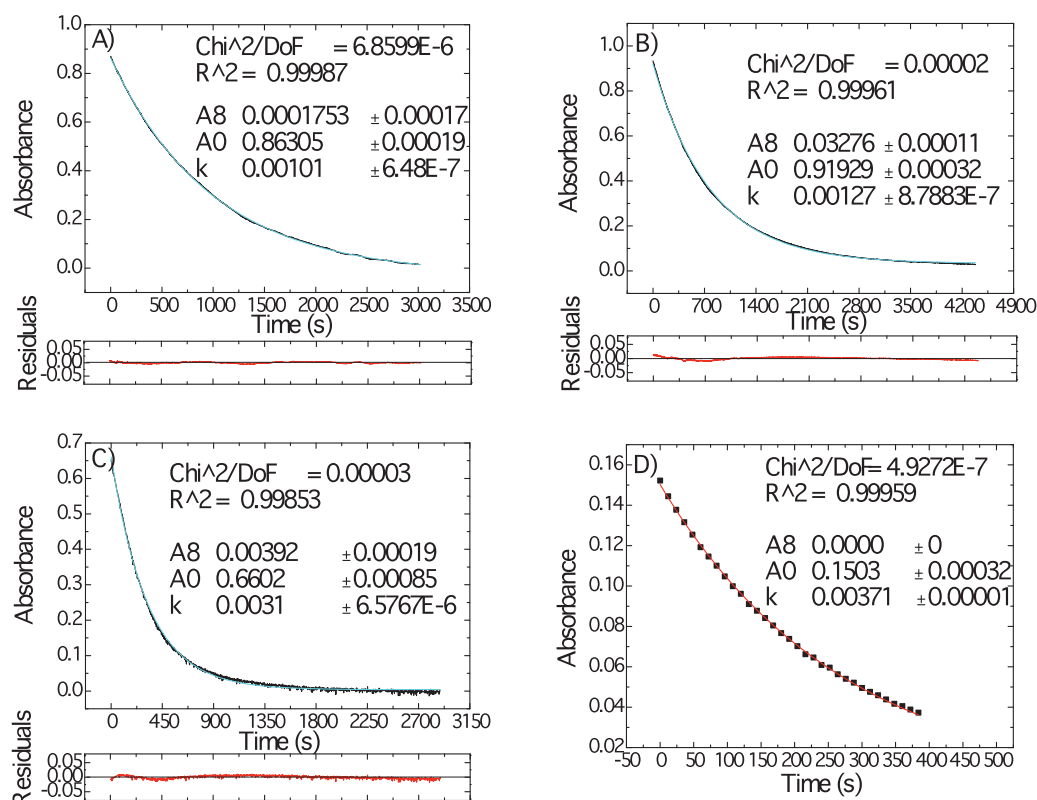


Fig. 3.31 The monoexponential (first order) decay model and experimental thermal fading kinetics monitored at 708, 717, 716, 719 nm in: A) cyclohexane ( $8.67 \times 10^{-5} \text{ mol L}^{-1}$ ), B) toluene ( $8.26 \times 10^{-5} \text{ mol}$



L<sup>-1</sup>), C) THF ( $6.23 \times 10^{-5}$  mol L<sup>-1</sup>), and D) acetonitrile ( $1.43 \times 10^{-5}$  mol L<sup>-1</sup>) at 293 K, respectively (black line: data measured; cyan line: the first order decay model fitted; red line: the absorbance residuals at testing time). Inset: the first order decay model parameters. Note: Due to the fast bleaching rate of BTE-NA in acetonitrile and low signal to noise ratio, the experiment of picture D was carried out on an absorption spectrophotometer (CARY) in scanning kinetic mode. Thus, the residuals were omitted due to the small amount of data points.

**Table 3.6** Spectrokinetic data of thermal bleaching for BTE-NA in various solvents at 293 K<sup>[a]</sup>

Solvents	$\lambda_{\max}$ (nm)	$\tau_{1/2}$ (s)	$k$ ( $10^{-3}$ s <sup>-1</sup> )	$A_0$
cyclohexane	708	647.5	1.01	0.863
toluene	717	581.4	1.27	0.919
THF	716	215.3	3.10	0.660
acetonitrile	719	182.2	3.71	0.150

[a]  $k$  and  $A_\infty$  are the fitted parameters from Equation 1;  $\lambda_{\max}$ ,  $\tau_{1/2}$  and  $A_0$  are obtained from the experimental data.

**Table 3.7** Spectrokinetic data of thermal bleaching for BTE-NA, BTA and BTTA in chloroform at 293 K

	$\lambda_{\max}$ (nm)	$\tau_{1/2}$ (s)	$k$ (s <sup>-1</sup> )	$A_0$
BTE-NA	719	3.89	$1.80 \times 10^{-1}$	0.28
BTA	657	$4.58 \times 10^4$	$1.52 \times 10^{-5}$	1.63
BTTA	655	-- <sup>[a]</sup>	-- <sup>[a]</sup>	0.87

[a] Data could not be obtained.

Generally, the decrease in aromaticity can greatly increase the bistability of BTE system. Due to the decrease of aromaticity, *c*-BTA shows no obvious thermal back reaction in non-polar solvents like toluene even at 328 K. However, *c*-BTA is not stable in polar solvents such as chloroform, which was found to follow similar first order decay with a constant of  $1.52 \times 10^{-5}$  s<sup>-1</sup> (Figure 3.32), four orders of magnitude slower than that of BTE-NA ( $1.80 \times 10^{-1}$  s<sup>-1</sup>). As shown in Figure 3.36 and Table 3.7, BTA exhibits first order decay in chloroform with a half-life ( $\tau_{1/2}$ ) of  $4.58 \times 10^3$  s, much slower than that of BTE-NA (3.89 s). The different thermal back rates in the system of BTE-NA and BTA are apparently due to the difference in activation energy of the thermal cyclo-reversion in various solvents.

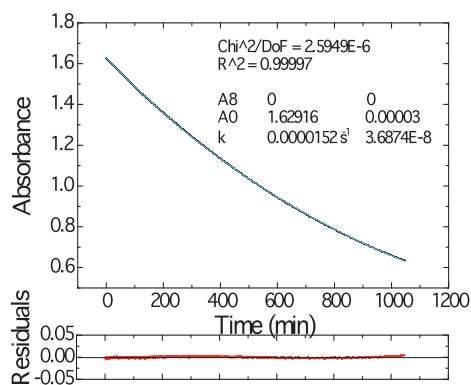


Fig. 3.32 Thermal stability of BTA in chloroform ( $1.67 \times 10^{-4} \text{ mol L}^{-1}$ ) at 293 K. The thermal back reaction rate was found to be  $1.52 \times 10^{-5} \text{ s}^{-1}$  by fitting the time profile into the first order decay.

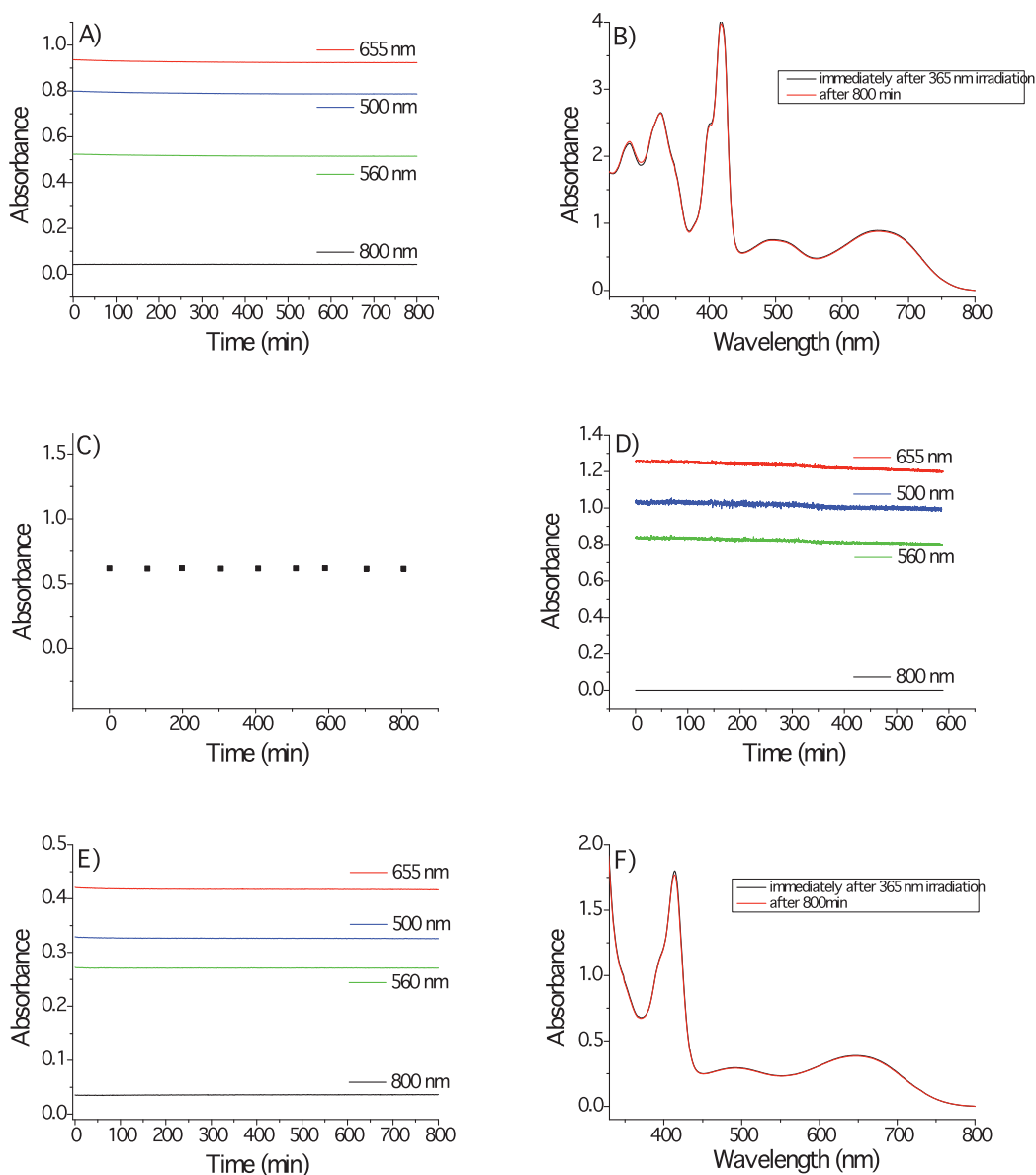


Fig. 3.33 A, B) Thermal stability of BTTA in cyclohexane ( $7.35 \times 10^{-5} \text{ mol L}^{-1}$ ) at 293 K; C) Thermal stability of BTTA in toluene ( $6.12 \times 10^{-5} \text{ mol L}^{-1}$ ) at 328 K; D) Thermal stability of BTTA in chloroform ( $1.27 \times 10^{-4} \text{ mol L}^{-1}$ ) at 293 K; E, F) Thermal stability of BTTA in acetonitrile ( $3.67 \times 10^{-5} \text{ mol L}^{-1}$ ) at 293 K.

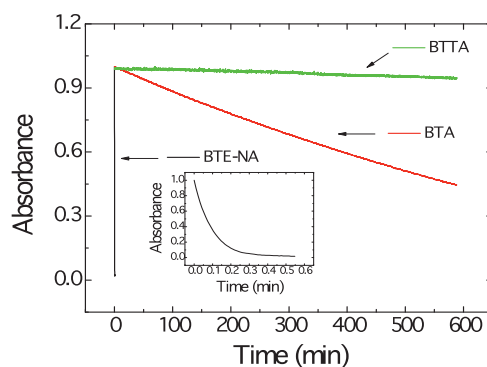


Fig. 3.34 Thermal back reaction of BTE-NA, BTA and BTTA in chloroform at 293 K. Inset: the enlarged graph is the thermal back reaction of BTE-NA in chloroform at 293 K.

In contrast, no obvious thermal back reaction could be observed for BTTA at dark and 273 K for a prolonged time. As a matter of fact, BTTA preserves very promising thermal stability with almost flat decays, and does not show any thermal back reaction in various solvents like cyclohexane, toluene, chloroform and even in acetonitrile at dark and 293 K (Figures 3.33). Even, the pure closed form was successfully separated on aluminum oxide eluted with  $\text{CCl}_4$  and dichloromethane (volume ratio = 4:1, Figure 3.19). At elevated temperature (328 K) in toluene, BTTA does not show any obvious decrease in its absorbance at 655 nm after 800 min (Figures 3.33 C).

Furthermore, the absorption bands of BTTA in the visible region could be gradually bleached as a result of the photochromic back reaction upon irradiation at 575 nm, showing a typical photo-responsive back reaction. However, for BTE-NA and BTA, the photochromic reaction could be reverted either by thermal back reaction at dark in polar solvents or on irradiation at 575 nm. Thus, considering the high polarity and electron-withdrawing tendency of the benzobisthiadiazole unit, the incorporation of an extremely high polar, low aromatic unit with benzobisthiadiazole as the center ethene bridging unit can finally lead to the thermally irreversible photochromic system, which can even be comparable to the photochromic performances of parent BTEs, such as the widely known five-membered hexafluorocyclopentene-based counterparts.

### 3.3.6 DFT calculation of BTE-NA, BTA and BTTA

To gain further insight into the aromaticity-controlled thermal stability, the calculations were performed with the Gaussian 09 program.<sup>[94]</sup> The geometries were optimized with PBE0

functional<sup>[95]</sup> and 6-31G(d,p) basis set. The energies obtained from the small basis set optimizations are not accurate enough. On the basis of the optimized structures, more accurate energy determinations can be achieved by performing single-point calculations with the larger basis set 6-311+G(d,p). The solvent effect is taken into account within the polarizable continuum model<sup>[96]</sup> in the single-point calculations.

For BTTA, BTA and BTE-NA, the open-ring isomers are more stable than the closed-ring isomers in both vacuum and solvents. Destabilization due to the destruction of the aromatic thiophene rings and central ethene bridges during the course of cyclization increases the ground-state energy of the closed-ring isomers.<sup>[97]</sup> Generally in BTE derivatives, the cyclo-reversion reaction in the ground states has to overcome the energy barriers correlating with the ground-state energy differences. The calculated values of ground-state energy difference between the open and closed isomers for BTTA, BTA and BTE-NA are -4.93, -10.16, and -20.44 kcal/mol in vacuum, respectively (Tables 3.2 and Table 3.8). When the ground-state energy difference is large, the energy barrier becomes small and the cyclo-reversion reaction readily takes place. On the other hand, the reaction barrier becomes large when the ground-state energy difference is small. In the case of *c*-BTTA, the cyclo-reversion reaction could not occur easily in the ground state compared to *c*-BTE-NA and *c*-BTA. Accordingly, the destabilization energy, which correlates with the decrease in aromaticity during the course of photocyclization, is lower in BTTA than in BTA, and much lower than in BTE-NA. The small energy difference between the open and closed forms results in excellent thermal stability of *c*-BTTA in a variety of solvents.

Table 3.8 Optimized ground state energies for the ring-open and ring-closed isomers of BTE-NA, BTA and BTTA

	vacuum
BTTA	-3116.7960 a.u.
<i>c</i> -BTTA	-3116.7881 a.u.
$\Delta E^a$	-4.93 kcal/mol
BTA	-2610.5194 a.u.
<i>c</i> -BTA	-2610.5033 a.u.
$\Delta E^a$	-10.16 kcal/mol
BTE-NA	-2695.5039 a.u.
<i>c</i> -BTE-NA	-2695.4713 a.u.
$\Delta E^a$	-20.44 kcal/mol

### 3.3.7 Photochromic behavior of BTE-NA, BTA and BTTA in bulky crystal and sol-gel system

Single crystals of the open forms of BTE-NA, BTA and BTTA were grown by slow evaporation of the corresponding solutions in mixed solvents of THF-MeOH, THF-H<sub>2</sub>O and CHCl<sub>3</sub>-MeOH, respectively. X-ray crystal structure analyses revealed that in all these crystals only parallel conformations are observed, indicating that all these three systems cannot undergo photocyclization in the single crystal state<sup>[126]</sup>. For the crystal of BTE-NA (Figure 3.35), two molecules are arranged in a head-to-tail fashion to afford a dimeric moiety by the intermolecular C-H...O hydrogen bonds with H...O distances of 2.43 Å, and C-H...O angles of 174°. Interestingly, weak O...C interactions are observed between naphthalimide and methoxy units, with the O...C distances of 3.120(2) Å, which is smaller than the sum of the van der Waals Radii for O and C atoms. These interactions may be understood as electrostatic interactions between the electron-rich O atom and the electron-deficient naphthalimide carbon atom. For the crystal of BTA (Figure 3.36), multiple intermolecular C-H...O hydrogen bonds are found involving the methoxy O atoms and phenyl C-H moieties, with H...O distances of 2.48 Å, and C-H...O angles of 160°. Thus, the interesting supramolecular linear structures are formed by these interactions.

For the crystal of BTTA (Figure 3.37), S...π interactions are observed with the shortest S...C distances of 3.412(5) Å. Similar to that observed in the crystal of BTE-NA, weak O...C interactions are also observed between benzobisthiadiazole and methoxy units, with the O...C distances of 3.12(5) Å. Thus, a linear structure is formed by these interactions (Figure 3.37). From these observations, it is reasonable to assert that the multiple intermolecular interactions stabilize and fix the conformations of the molecules. Thus, only the parallel conformations are observed. In contrast, the previously reported BTTE without methoxy groups adopt anti-parallel conformation due to the lack of wide occurrence of intermolecular interactions.<sup>[116]</sup> Obviously, the methoxy group plays an important role in these crystals due to the presence of the electron-rich O atoms. Moreover, BTTA forms a twin crystal. The asymmetric nature of the twin crystal and cooperative intermolecular interactions finally lead BTTA to form a three dimensional tube-like structure. Apparently, the variation in the six-membered ethene bridges from naphthalimide and benzothiadiazole to benzobisthiadiazole plays a key role in modulating intermolecular interactions, thus affecting the packing of these molecules.

Furthermore, the distance of the double bonds for central ethene bridges within naphthalimide (C3-C4), benzothiadiazole (C6-C11) and benzobisthiadiazole (C4-C5) are 1.398(2), 1.383(4) and 1.371(5) Å, respectively (Figure 3.35-3.37). Generally, the typical bond length is ca.1.54 Å for C-C single bond and 1.33 Å for double bond. Exactly, among

three compounds, the relative short bond length indicates that the C4-C5 bond in BTTA is closer to a typical double bond. It is consistent with the aromaticity tendency: benzobisthiadiazole < benzothiadiazole < naphthalimide.

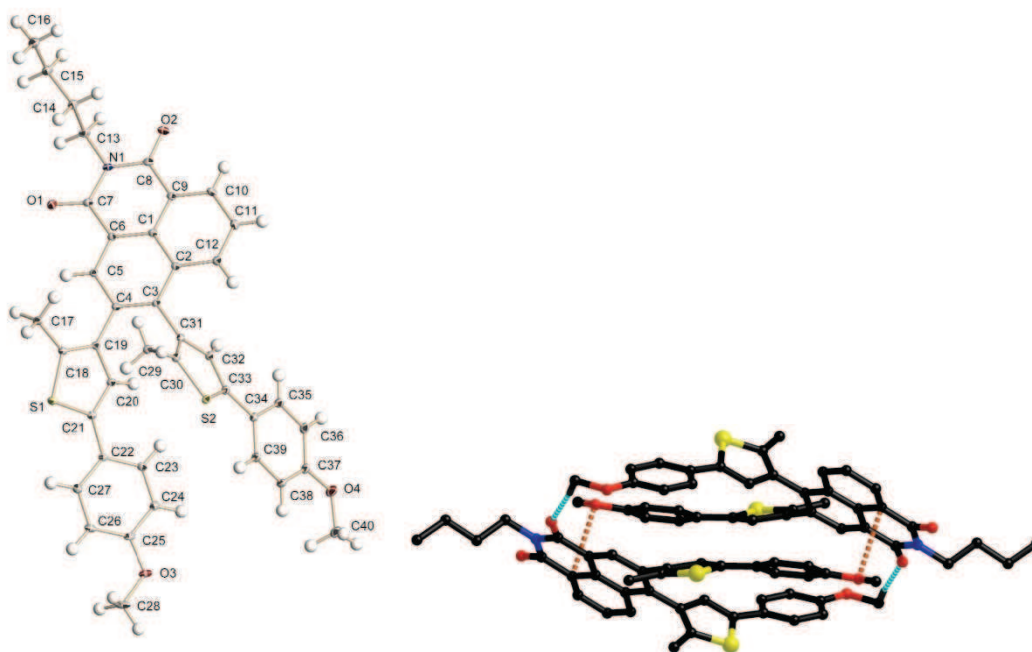
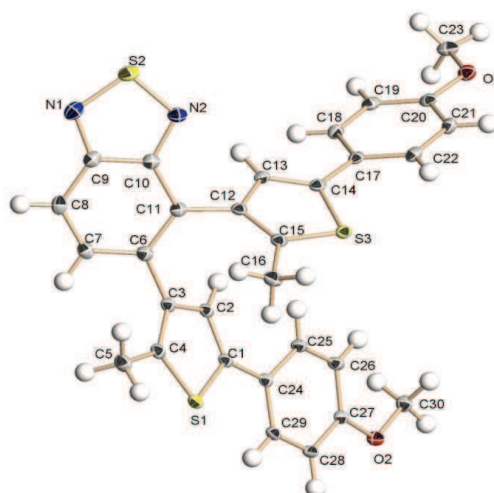


Fig. 3.35 Left) ORTEP representation of the crystal structure of BTE-NA with displacement ellipsoids shown at the 25% probability level. Selected bond lengths (Å): C2-C3, 1.426(2); C4-C5, 1.411(2); C3-C4, 1.398(2). Right) View of a dimeric unit in the crystal of BTE-NA, formed by C-H...O hydrogen bonds and O...C interactions.



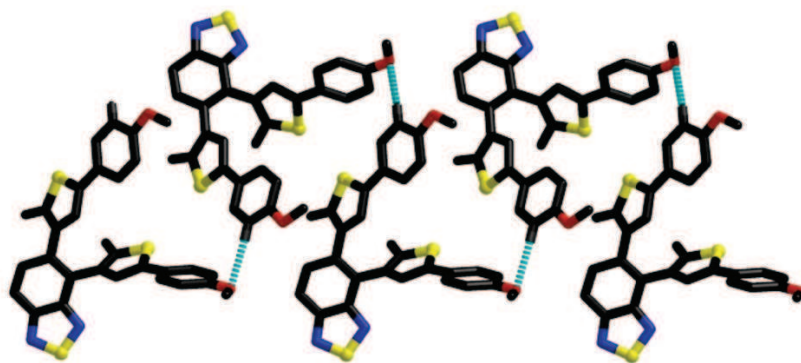


Fig. 3.36 Top) ORTEP representation of the crystal structure of BTA with displacement ellipsoids shown at the 25% probability level. Selected bond lengths (Å): C6-C7, 1.442(4); C10-C11, 1.435(4); C6-C11, 1.383(4). Down) View of a linear structure formed by multiple C-H...O hydrogen bonds in the crystal of BTA.

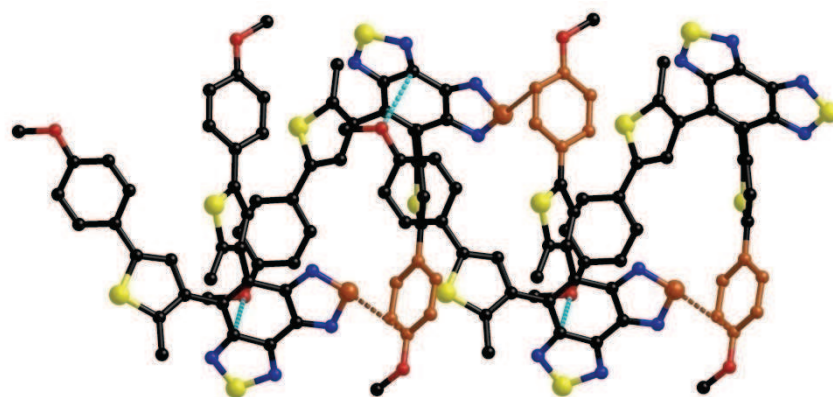
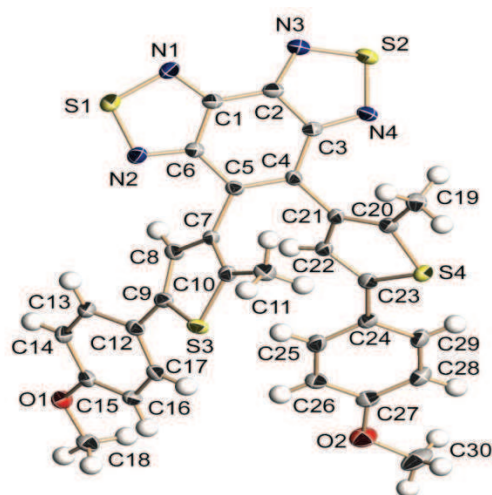


Fig. 3.37 Top) ORTEP representation of the crystal structure of BTTA with displacement ellipsoids shown at the 25% probability level. Selected bond lengths (Å): C5-C6, 1.452(5); C3-C4, 1.454(5); C4-C5, 1.371(5). Down) Side view of the linear structure of BTTA. Hydrogen atoms are omitted for clarity. Selected atom distances: S...C, 3.412(5) Å; O...C, 3.121(5) Å.

Table 3.24 Crystal Structure Determinations of BTE-NA, BTA and BTTA

Compounds	BTE-NA	BTA	BTTA
Empirical formula	C <sub>40</sub> H <sub>35</sub> NO <sub>4</sub> S <sub>2</sub>	C <sub>30</sub> H <sub>24</sub> N <sub>2</sub> O <sub>2</sub> S <sub>3</sub>	C <sub>30</sub> H <sub>22</sub> N <sub>4</sub> O <sub>2</sub> S <sub>4</sub>
Formula weight	657.81	540.69	598.76
Temp, K	133(2)	133(2)	293(2)
Crystal system	triclinic	monoclinic	triclinic
Space group	P-1	P2 <sub>1</sub> /n	P-1
<i>a</i> , Å	11.4898(12)	7.5004(9)	12.301(4)
<i>b</i> , Å	11.9884(13)	28.647(3)	12.559(4)
<i>c</i> , Å	14.1549(15)	12.1653(14)	19.099(6)
$\alpha$ , deg	106.272(2)	90.00	91.007(6)
$\beta$ , deg	111.923(2)	92.673(2)	103.522(6)
$\gamma$ , deg	101.837(2)	90.00	102.920(7)
Volume, Å <sup>3</sup>	1627.9(3)	2611.0(5)	2788.6(15)
<i>Z</i>	2	4	4
density(calc), mg/mm <sup>3</sup>	1.342	1.375	1.426
crystal size, mm <sup>3</sup>	0.35 × 0.15 × 0.05	0.40 × 0.20 × 0.18	0.23 × 0.11 × 0.09
index ranges	-14 ≤ <i>h</i> ≤ 14, -15 ≤ <i>k</i> ≤ 13, -17 ≤ <i>l</i> ≤ 18	-9 ≤ <i>h</i> ≤ 9, -36 ≤ <i>k</i> ≤ 35, -14 ≤ <i>l</i> ≤ 15	-14 ≤ <i>h</i> ≤ 14, -14 ≤ <i>k</i> ≤ 7, -22 ≤ <i>l</i> ≤ 22
reflections collected	12582	19898	13570
independent reflections	7033[R(int) = 0.0296]	5698[R(int) = 0.0307]	9518 [R(int) = 0.0306]
GOF on <i>F</i> <sup>2</sup>	1.088	1.158	1.011
final <i>R</i> indices [ <i>I</i> ≥ 2σ( <i>I</i> )]	R <sub>1</sub> = 0.0416, wR <sub>2</sub> = 0.1260	R <sub>1</sub> = 0.0533, wR <sub>2</sub> = 0.1374	R <sub>1</sub> = 0.0518, wR <sub>2</sub> = 0.1098
Largest diff. peak and hole / e Å <sup>-3</sup>	0.43 and -0.35	0.574 and -0.448	0.216 and -0.220

However, considering the good photochromic performance of BTE-NA, BTA and BTTA in organic solvents, it is expected that the parallel arrangements in the single-crystal state can shift to the anti-parallel conformation in solution due to the loss of the above-mentioned cooperative interactions in the well-ordered crystal state. Therefore, it is reasonable that the photochromic behavior can be distinctively different between the crystalline and solution phases. As a further case illustrated (Figure 3.38-3.40), BTE-NA, BTA and BTTA also exhibit excellent photochromic properties and defined thermoreversible properties in an



organogel system.<sup>[127-128]</sup> A stable gel with BTE-NA ( $1.66 \times 10^{-3}$  wt%), BTA ( $1.28 \times 10^{-3}$  wt%), BTTA ( $1.59 \times 10^{-3}$  wt%) dopants were formed around 20 w/w% Poloxamer 407 (Boluoshamu 407 with the molecular distribution of 9840-14600) in water, and showed an extraordinary sol-gel phase transition temperature around 28 °C. Irradiation of the thermoreversible organogel with UV 365 nm leads to the appearance of a new absorbance band around 719 nm for BTE-NA, 655 nm for BTA, and 497 and 655 nm for BTTA, which could be bleached by irradiating with visible light at 575 nm.

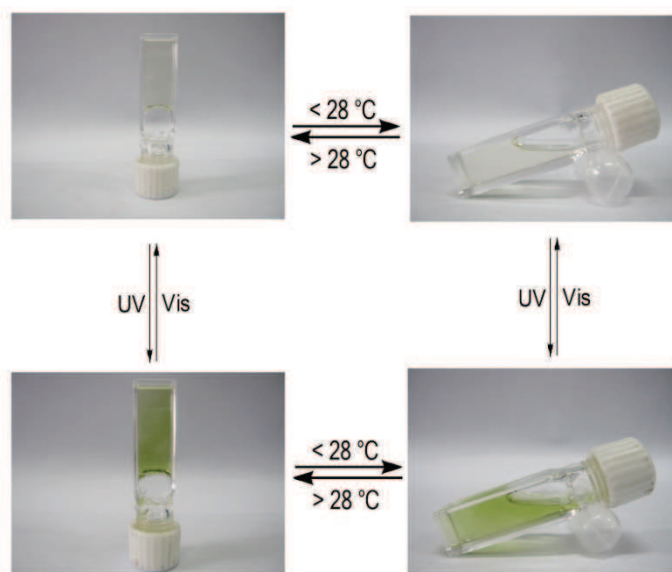


Fig. 3.38 Photography images of color changes and sol-gel phase transition of BTE-NA doped in thermosensitive organogel ( $1.66 \times 10^{-3}$  wt%) upon irradiation at UV (365 nm) and visible light (575 nm).

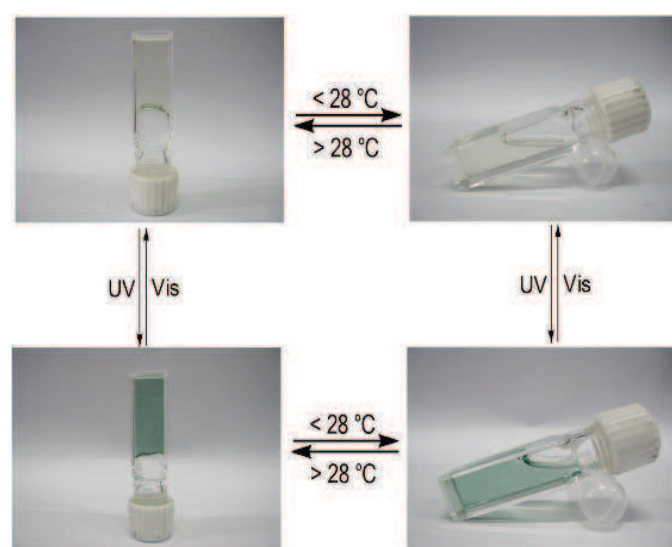


Fig. 3.39 Photography images of color changes and sol-gel phase transition of BTA doped in thermosensitive organogel ( $1.28 \times 10^{-3}$  wt%) upon irradiation at UV (365 nm) and visible light (575 nm).

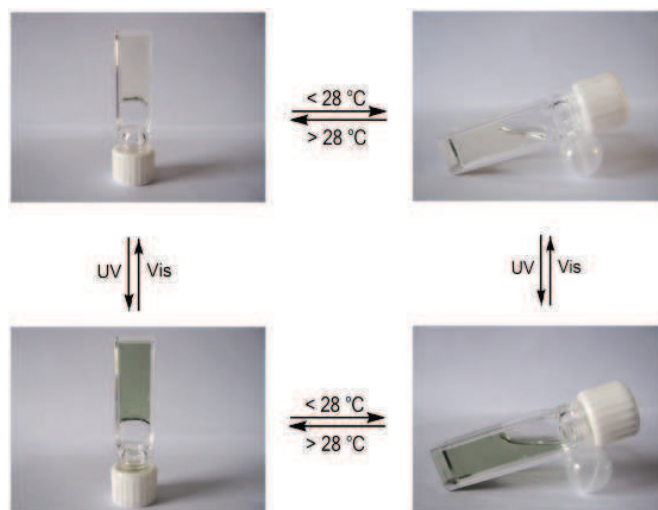


Fig. 3.40 Photography images of color changes and sol-gel phase transition of BTTA doped in thermosensitive organogel ( $1.59 \times 10^{-3}$  wt%) upon irradiation at UV (365 nm) and visible light (575 nm).

### 3.4 Conclusions

Three compounds BTE-NA, BTA and BTTA, containing electron withdrawing groups of naphthalimide, benzothiadiazole and benzobisthiadiazole as six-membered ring bridges, were specifically designed and synthesized. The three ethene bridges with different degree in aromaticity can give a systematical comparison in the thermal stability evolution for their corresponding closed forms. They show typical photochromic performance with considerably high cyclization quantum yields and high fatigue resistance in solution. The decrease of the aromaticity in ethene bridges can increase the thermal stability of closed form at room temperature. *c*-BTE-NA shows first order decay in various solvents, while *c*-BTA is only stable in nonpolar solvents. The less aromatic property of BTTA gives rise to the unprecedented thermal stability in various solvents even at elevated temperature in toluene. In well ordered crystal state, all three compounds adopt parallel conformer, and BTTA forms a three dimensional tube like structure due to the strong  $\pi \cdot \pi$  stacking interactions and weak electrostatic interactions between the electron-rich oxygen atom on methoxy and carbon atom on the electron-deficient benzobisthiadiazole moiety. Furthermore, the fluorescence of BTE-NA, BTA and BTTA could be modulated by photochromism and solvatochromism. This work contributes to the understanding of aromaticity controlled thermal stability of the ethene bridge and novel building blocks for the photochromic BTE systems.

## Chapter 4 Nonlinear Optical Materials Based on Benzothiadiazole

### 4.1 Introduction

A current challenge is the development of efficient strategies for the design of switchable nonlinear optical (NLO) materials.<sup>[129-132]</sup> As most molecules with large first hyperpolarizability values  $\beta$  comprise  $\pi$  systems that are asymmetrically endcapped with donor and acceptor moieties, various strategies have been explored to alter the electron-donor (or acceptor) capacity of the end groups using external stimuli such as redox methods and protonation/deprotonation reactions.<sup>[133-136]</sup> Another elegant approach to the reversible switching of NLO properties is the use of photochromic compounds.<sup>[137-144]</sup> Among them, BTEs derivatives are the most promising because of their good fatigue resistance, the remarkable thermal stability of both isomers, and the rapid response time, which are prerequisite conditions for practical applications. The design of the photoresponsive NLO switch has been mainly focused on the asymmetric synthesis by introducing donor and acceptor on the two sides of the aryl substituent to form a typical D- $\pi$ -A system after photocyclization. Thus, we introduced directly the acceptor of benzothiadiazole as central ethene bridge to form D- $\pi$ -A structure to circumvent the possible difficulty in organic synthesis, providing a new concept to the designing of the photoswitchable NLO materials (Figure 4.1).

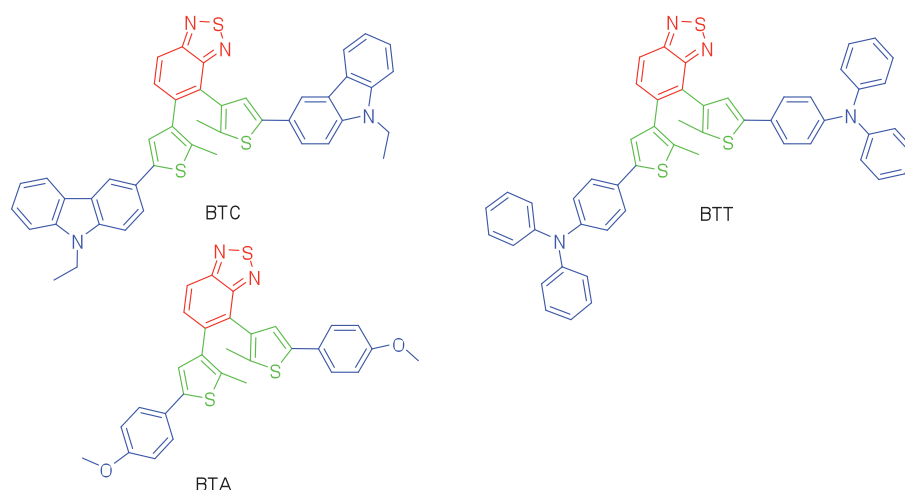


Fig. 4.1 Photochromic systems based on benzothiadiazole substituted by carbazole, triphenylamine and anisole. The blue, green and red parts are donor,  $\pi$  system and acceptor, respectively.

### 4.2 Experiment section

#### 4.2.1 Instruments and Reagents

$^1\text{H}$  NMR and  $^{13}\text{C}$  NMR spectra were recorded on Bruker Avance III 400 or 500 MHz with tetramethylsilane (TMS) as an internal reference recorded at room temperature. MS were recorded on a Waters ESI mass spectroscopy. Absorption and fluorescence spectra were recorded on UVIKON 933 (Kontron instruments) and FluoroMax-3 (Horiba Jobin-Yvon), respectively. Fluorescence lifetime measurements were measured (see Appendix I for detailed information). The photochromic property was evidenced and characterized by following *in situ* the absorption spectra under continuous irradiation (see Appendix I for detailed information).

#### 4.2.2 Synthetic route to the target and intermediate molecules

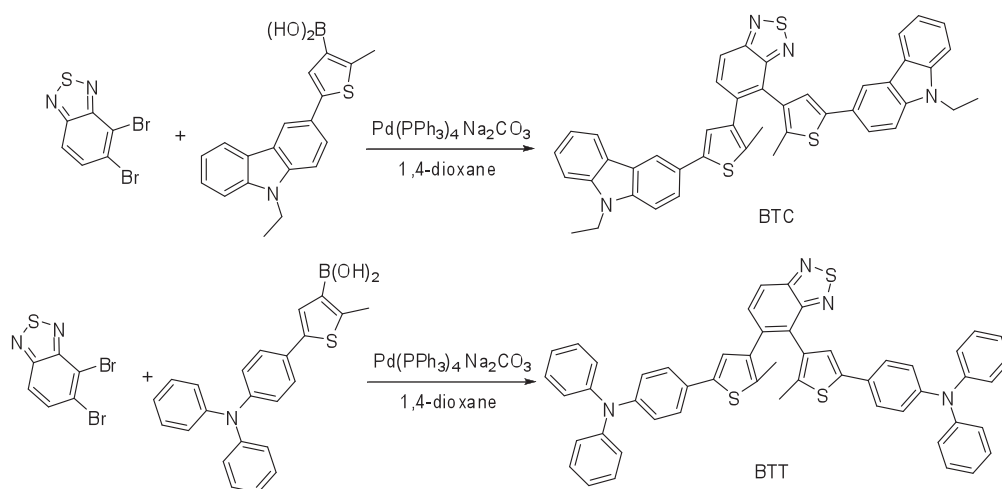
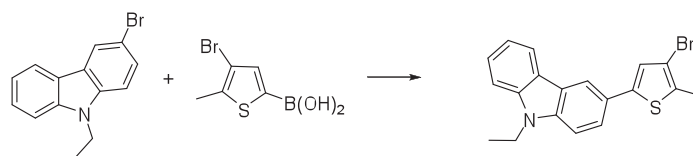


Fig. 4.2 Synthetic routes to novel BTEs with benzothiadiazole as ethene bridges, carbazole, triphenylamine and anisole as substituent.

#### 4.2.3 Preparation of target and intermediate molecules

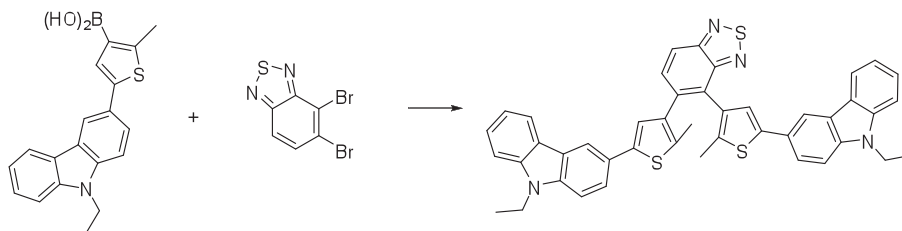
##### 4.2.3.1 3-(4-bromo-5-methylthiophen-2-yl)-9-ethyl-9H-carbazole



In a 100 mL single necked flask, 3-bromo-9-ethyl-9H-carbazole (1.52 g, 5.56 mmol), 4-bromo-5-methylthiophen-2-ylboronic acid (1.23 g, 5.56 mmol), 45 mL of THF, 30 mL of 2 M  $\text{Na}_2\text{CO}_3$  (aq), and  $\text{Pd}(\text{PPh}_3)_4$  (0.1 g) were introduced. The reactive mixture was refluxed under protection of argon for 12 h. The resulting mixture was poured into water and extracted with dichloromethane. The organic layer was separated and dried with  $\text{Na}_2\text{SO}_4$ . The solvent was removed under vacuum. The crude product was purified by chromatography eluted with petroleum ether to give a white solid 0.5 g. Yield: 25%.  $^1\text{H}$  NMR (500 MHz,  $\text{CDCl}_3$ , ppm):

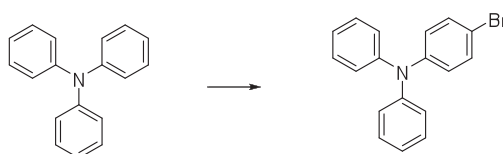
1.44 (t,  $J = 7.2$  Hz, 3 H, -CH<sub>3</sub>), 2.44 (s, 3 H, -CH<sub>3</sub>), 4.38 (m, 2 H, -CH<sub>2</sub>-), 7.13 (s, 1 H, Thiophene-H), 7.26 (m, 1 H, carbozole-H), 7.38 (m, 2 H, carbozole-H), 7.49 (m, 1 H, carbozole-H), 7.62 (dd,  $J_1 = 8.48$  Hz,  $J_2 = 1.6$  Hz, 1 H, carbozole-H), 8.11 (d,  $J = 7.7$  Hz, 1 H, carbozole-H), 8.22 (d,  $J = 1.38$  Hz, 1 H, carbozole-H).

#### 4.2.3.2 BTC



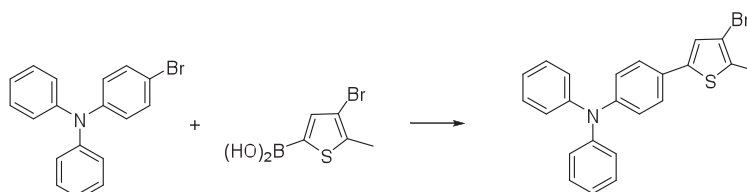
In a single necked flask, 4,5-dibromobenzo[*c*][1,2,5]thiadiazole (54 mg, 0.18 mmol), 5-(9-ethyl-9*H*-carbazol-3-yl)-2-methylthiophen-3-ylboronic acid (0.2 g, 0.59 mmol), 20 mL of dioxane, 20 mL of 2 M Na<sub>2</sub>CO<sub>3</sub>(aq), and Pd(PPh<sub>3</sub>)<sub>4</sub> (0.1 g) were introduced. The reactive mixture was allowed to reflux for 20 h. The resulting mixture was poured into water and extracted with dichloromethane. The organic layer was separated and dried with Na<sub>2</sub>SO<sub>4</sub>. The solvent was removed under vacuum. The crude product was purified by chromatography eluted with CCl<sub>4</sub>: ethyl acetate = 75:1 to give a yellow solid 20 mg. <sup>1</sup>H NMR (500 MHz, CDCl<sub>3</sub>, ppm): 1.41 (m, 6 H, -CH<sub>3</sub>), 2.14 (s, 3 H, -CH<sub>3</sub>), 2.33 (s, 3 H, -CH<sub>3</sub>), 4.33 (m, 4 H, -CH<sub>2</sub>-), 6.93 (m, 1 H, carbazole-H), 7.04 (m, 2 H, carbazole-H), 7.36 (m, 8 H, carbazole-H), 7.59 (dd,  $J_1 = 8.5$  Hz,  $J_2 = 1.6$  Hz, 1 H, carbazole-H), 7.67 (dd,  $J_1 = 8.47$  Hz,  $J_2 = 1.6$  Hz, 1 H, carbazole-H), 7.81 (s, 1 H, Thiophene-H), 7.83 (s, 1 H, Thiophene-H), 7.93 (d,  $J = 7.71$  Hz, 1 H, carbozole-H), 8.06 (d,  $J = 9.01$  Hz, 1 H, carbazole-H), 8.16 (d,  $J = 1.4$  Hz, 1 H, carbazole-H), 8.25 (d,  $J = 1.4$  Hz, 1 H, carbazole-H). <sup>13</sup>C NMR (CDCl<sub>3</sub>, 100 MHz): 13.83, 13.87, 14.29, 14.57, 37.64, 108.50, 108.71, 108.73, 117.65, 117.73, 118.93, 119.91, 120.60, 120.63, 122.80, 122.91, 123.36, 123.38, 123.98, 124.17, 124.45, 124.98, 125.52, 125.83, 125.86, 128.49, 133.26, 133.93, 135.06, 136.60, 136.81, 137.53, 139.37, 140.32, 140.35, 141.56, 154.32, 155.26. HRMS (TOF EI for M<sup>+</sup>): calcd. for C<sub>44</sub>H<sub>34</sub>N<sub>4</sub>S<sub>3</sub>Na, 737.1843; found 737.1840.

#### 4.2.3.3 4-bromo-*N,N*-diphenylaniline



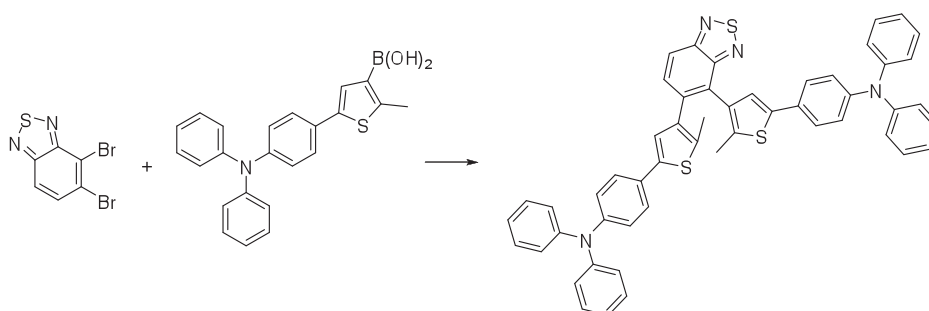
In a three necked flask, triphenylamine (2 g, 8.16 mmol) dissolved in 25 mL of DMF in an ice bath was introduced. NBS (1.45 g, 8.16 mmol) was then added by portion. The reactive mixture was allowed to warm to room temperature and stirred for 12 h. The resulting mixture was poured into water and recrystallized with hexane for several times until the purity is satisfactory evidenced by HPLC to yield a white solid 1.8 g. Yield: 68%.

#### 4.2.3.5 4-(4-bromo-5-methylthiophen-2-yl)-*N,N*-diphenylaniline



In a 250 mL single necked flask, 4-bromo-*N,N*-diphenylaniline (3 g, 9.28 mmol), 4-bromo-5-methylthiophen-2-ylboronic acid (2.05 g, 9.28 mmol), 70 mL of THF and 70 mL of 2 M  $\text{Na}_2\text{CO}_3$  (aq),  $\text{Pd}(\text{PPh}_3)_4$  (0.25 g) were introduced. The reactive mixture was refluxed under protection of argon for 24 h. The resulting mixture was poured into water and extracted with dichloromethane. The organic layer was separated and dried with  $\text{Na}_2\text{SO}_4$ . The solvent was removed under vacuum. The crude product was purified by chromatography eluted with petroleum ether to give a white solid 1.6 g. Yield: 44.8%.

#### 4.2.3.6 BTT



In a single necked flask, 4,5-dibromobenzo[*c*][1,2,5]thiadiazole (100 mg, 0.34 mmol), 5-(4-(diphenylamino)phenyl)-2-methylthiophen-3-ylboronic acid (0.3 g, 0.77 mmol), 40 mL of dioxane, 35 mL of 2 M  $\text{Na}_2\text{CO}_3$  (aq), and  $\text{Pd}(\text{PPh}_3)_4$  (0.1 g) were introduced. The reactive mixture was allowed to reflux for 15 h. The resulting mixture was poured into water and extracted with dichloromethane. The organic layer was separated and dried with  $\text{Na}_2\text{SO}_4$ . The solvent was removed under vacuum. The crude product was purified by chromatography

eluted with petroleum ether: ethyl acetate = 100:1 to give a yellow solid 150 mg.  $^1\text{H}$  NMR (500 MHz,  $\text{CDCl}_3$ , ppm): 2.06 (s, 3 H,  $-\text{CH}_3$ ), 2.22 (s, 3 H,  $-\text{CH}_3$ ), 6.88 (s, 1 H, Thiophene-H), 7.02 (m, 8 H, -Ph-H), 7.11 (m, 10 H, -Ph-H), 7.25 (m, 7 H, -Ph-H), 7.31 (d,  $J = 8.6$  Hz, 2 H, -Ph-H), 7.35 (d,  $J = 8.6$  Hz, 2 H, -Ph-H), 7.71 (d,  $J = 9$  Hz, 1 H, -Ph-H), 8.02 (d,  $J = 9$  Hz, 1 H, -Ph-H).  $^{13}\text{C}$  NMR ( $\text{CDCl}_3$ , 100 MHz): 13.27, 13.57, 118.93, 121.90, 122.00, 122.70, 122.74, 123.33, 123.40, 124.13, 125.30, 125.40, 127.16, 127.25, 127.63, 128.23, 128.26, 132.24, 132.79, 134.31, 135.47, 135.78, 136.52, 138.90, 139.15, 145.85, 146.04, 146.43, 146.49, 153.21, 154.11. HRMS (TOF EI for  $\text{M}^+$ ): calcd. for  $\text{C}_{52}\text{H}_{38}\text{N}_4\text{S}_3\text{Na}$ , 837.2156; found 837.2153.

### 4.3 Results and discussion

#### 4.3.1 Molecular design and synthesis

Figure 4.2 illustrates the synthetic route to the three target molecules. BTC, BTT and BTA were obtained via typical Suzuki coupling between 4,5-dibromo-2,1,3-benzothiadiazole and the corresponding boronic acid. The mono-substituted byproduct could be suppressed by controlling the ratio between 4,5-dibromo-2,1,3-benzothiadiazole and boronic acid. Dioxane was used for the Suzuki coupling instead of THF in order to increase the reactivity and temperature, which finally facilitates the separation process. Generally speaking, all the synthetic routes were classic organic reactions with cheap starting materials and reagents, mild conditions and comparatively high yields. 4-(4-bromo-5-methylthiophen-2-yl)-*N,N*-diphenylaniline has to be purified several times to remove the byproducts of 4-bromo-*N*-(4-bromophenyl)-*N*-phenylaniline and tris(4-bromophenyl)amine. The introduction of carbazole into the side aryl groups could greatly decrease the solubility of the target molecule BTC, thus,  $\text{CCl}_4$  was used instead of petroleum ether due to the excellent solubility and low polarity.

2,1,3-benzothiadiazole has been proven to be an excellent acceptor due to its wide application in solar cells and in sensors.<sup>[117-123]</sup> In general, the designing principle has been mainly confined to the asymmetric synthesis of the side aryl substituted by electron donor and acceptor respectively. The whole system should generate a relatively small  $\beta$  value before irradiation as the interruption of D- $\pi$ -A structure. The interrupted D- $\pi$ -A structure was restored after irradiation at 365 nm to yield an increased first hyperpolarizability values  $\beta$ . The principle has been proven to be effective in several cases, however, it costs tedious organic synthesis and steps. Hence, we directly link the donor to the central ethene bridge 2,1,3-benzothiadiazole due to its strong electron withdrawing ability, which could intrinsically form a D- $\pi$ -A structure. Usually, there exists parallel and anti-parallel conformer in the ring open form. The perpendicular conformer of thiophene rings to the central ethene

bridge could make the D- $\pi$ -A system less effective as evidenced by its strong ICT character. Thus, we anticipate the increased  $\beta$  after cyclization reaction due to the restored D- $\pi$ -A system.

#### 4.3.2 $^1\text{H}$ NMR, $^{13}\text{C}$ NMR and Mass characterization

Figure 4.3-4.4 and Figure 4.6-4.7 illustrate the  $^1\text{H}$  NMR spectrum of BTC and BTT. The chemical shifts of methyl groups on thiophene rings are similarly located at 2-2.5 ppm. The two signals corresponding to methyl groups are the result of asymmetric nature of 2,1,3-benzothiadiazole. No parallel and anti-parallel conformers are observable due to the fast rotation of single bond. The multiplets were the result of coupling between neighbouring protons. The chemical shift on ethyl of BTC was decided by the distance away from the cabazole ring. The closer to the ring, the lower field of the signal is. The signal of methylene directly connected with nitrogen was even at 4.30 ppm. Figure 4.5 and Figure 4.8 demonstrate the  $^{13}\text{C}$  NMR of BTC and BTT. For BTC, five are at high field and others are at low field. The total number of the signal is 38, which is in accordance with total carbon species within the molecule. For BTT, two are at high field and others are at low field. The total number of the signal is 31, which is in accordance with total carbon species within the molecule.

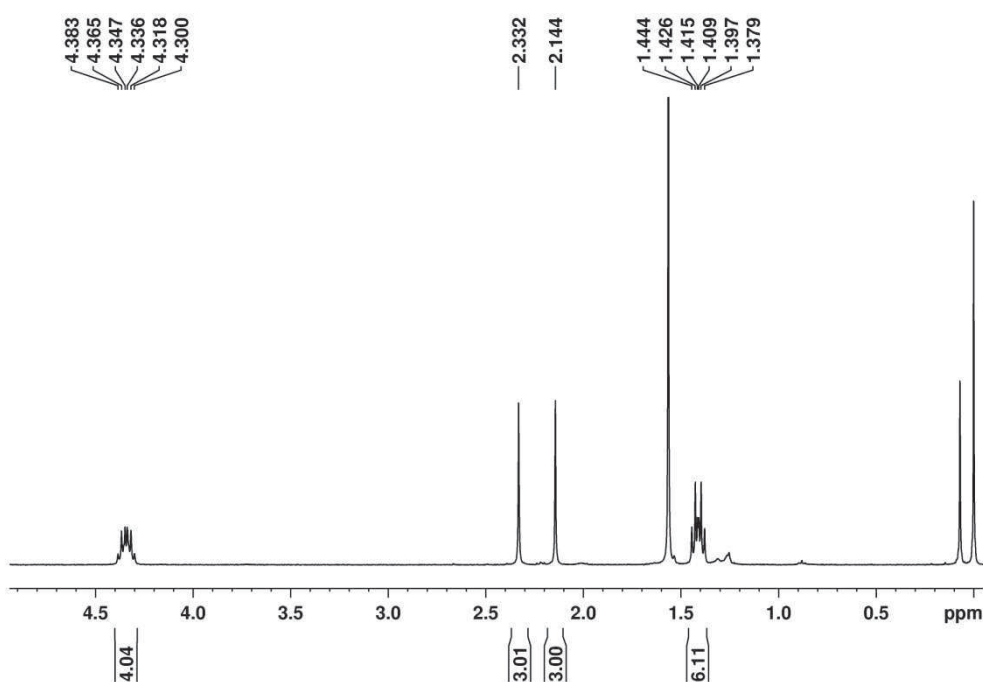


Fig. 4.3  $^1\text{H}$  NMR of BTC in  $\text{CDCl}_3$  (high field)



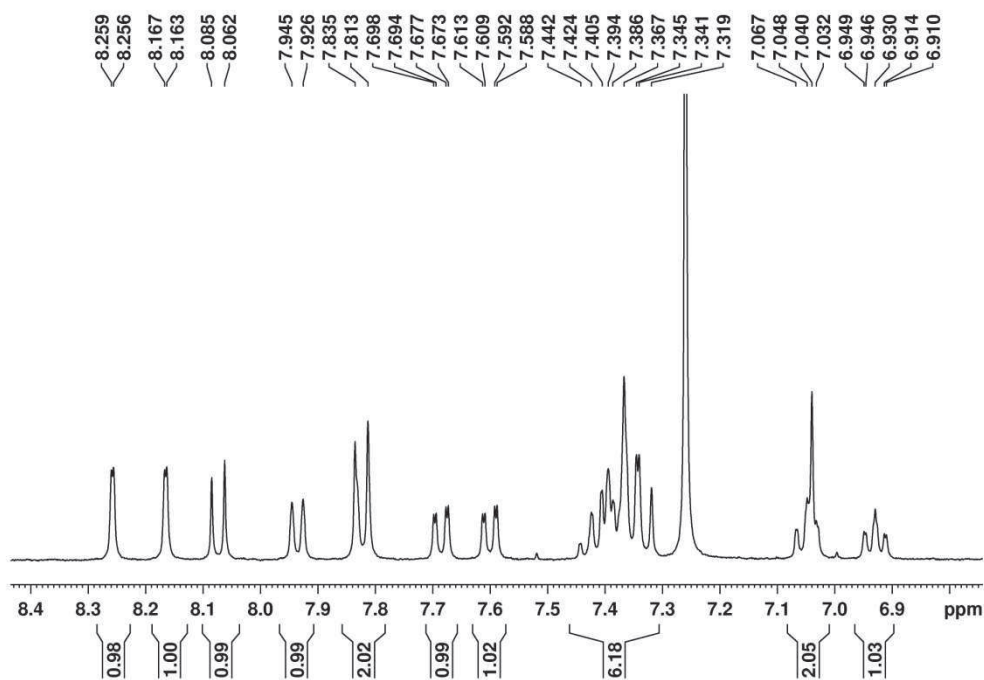


Fig. 4.4  $^1\text{H}$  NMR of BTC in  $\text{CDCl}_3$  (low field)

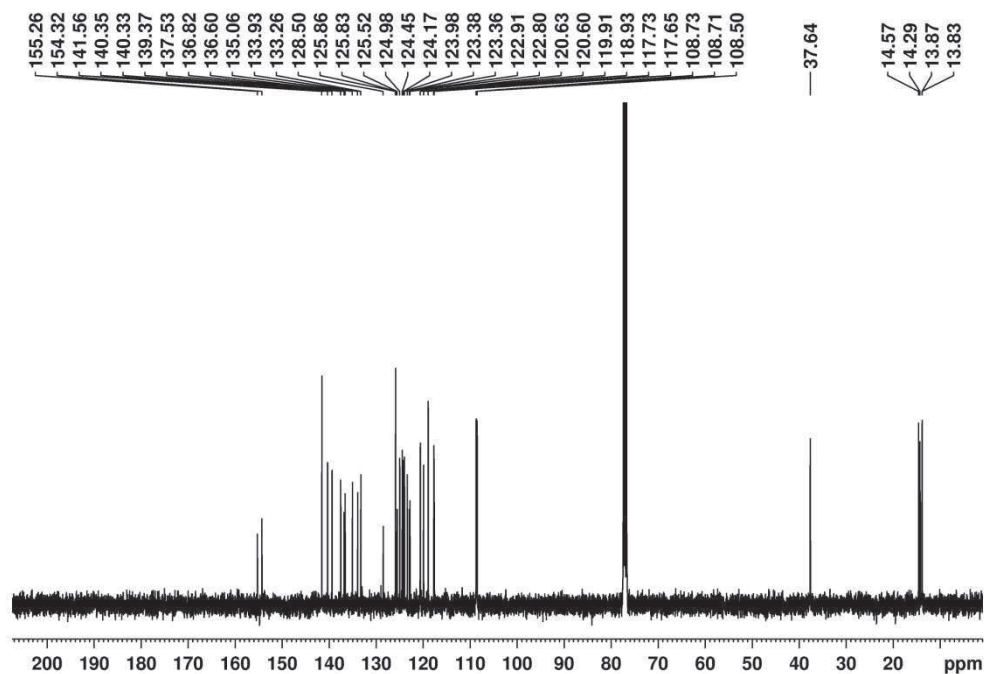


Fig. 4.5  $^{13}\text{C}$  NMR of BTC in  $\text{CDCl}_3$

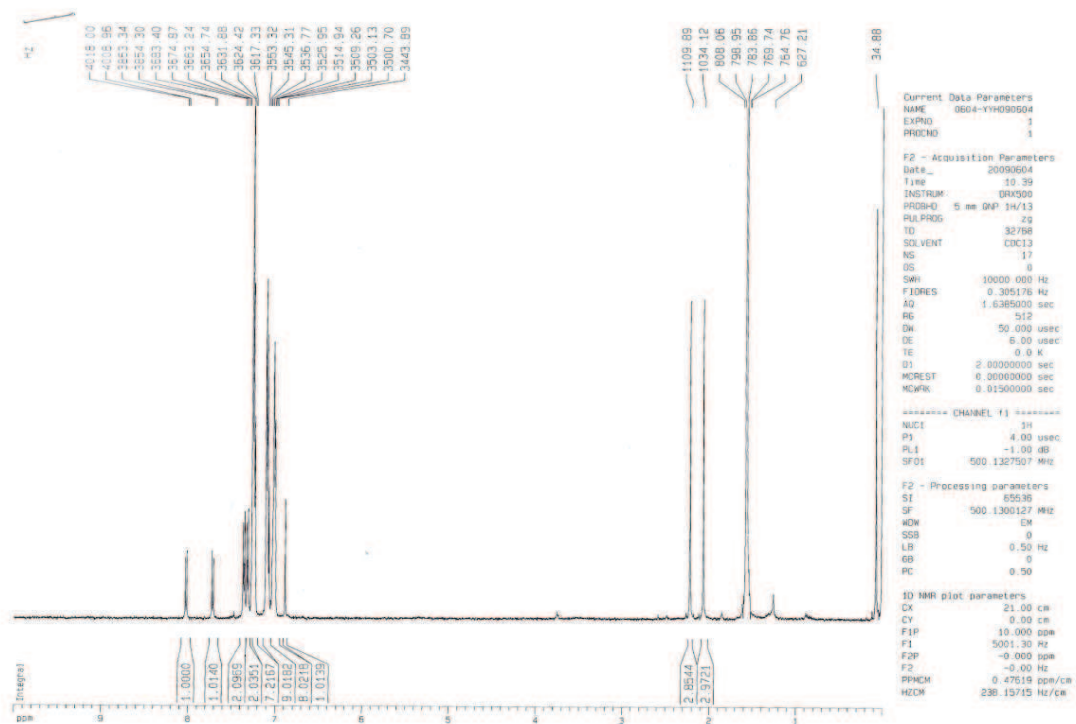


Fig. 4.6 <sup>1</sup>H NMR of BTT in CDCl<sub>3</sub> (high field)

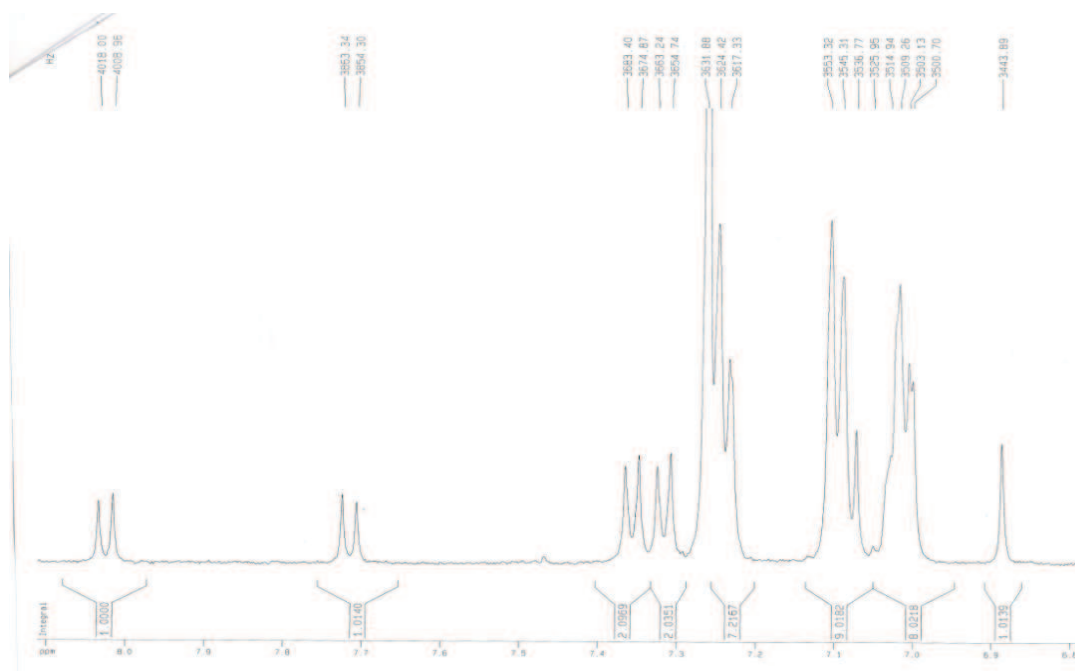


Fig. 4.7 <sup>1</sup>H NMR of BTT in CDCl<sub>3</sub> (low field)

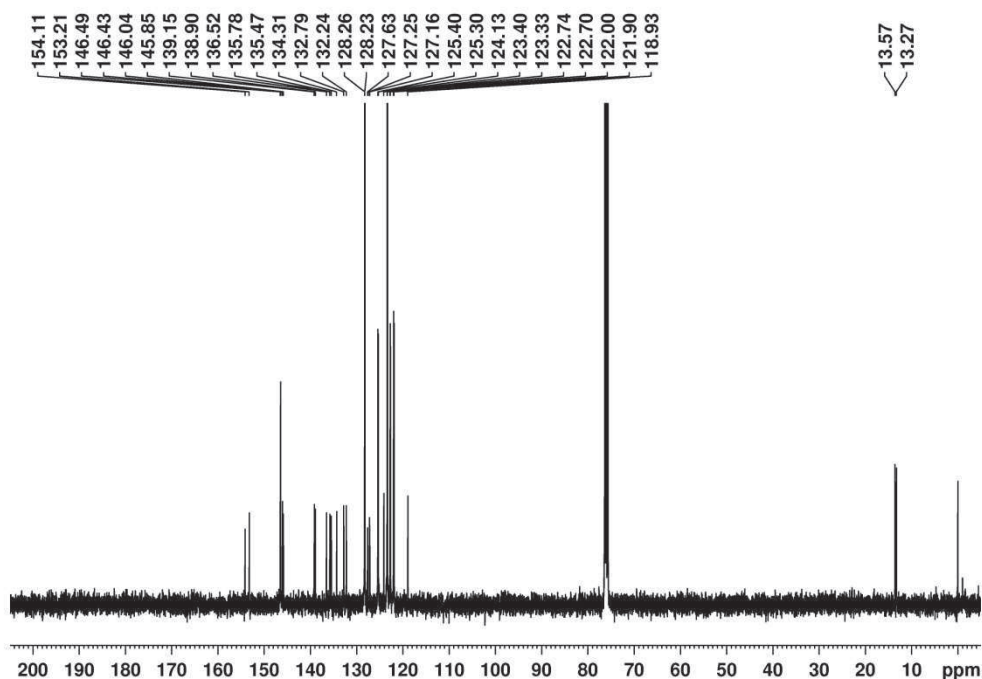


Fig. 4.8 <sup>13</sup>C NMR of BTT in CDCl<sub>3</sub>

Elemental Composition Report

Single Mass Analysis

Tolerance = 500.0 mDa / DBE: min = -1.5, max = 100.0

Element prediction: Off

Number of isotope peaks used for i-FIT = 2

Monoisotopic Mass, Even Electron Ions

47 formula(e) evaluated with 24 results within limits (up to 1 closest results for each mass)

Elements Used:

C: 0-50 H: 0-40 N: 0-4 S: 0-3 Na: 0-1

ZHU\_WH

LCT Premier

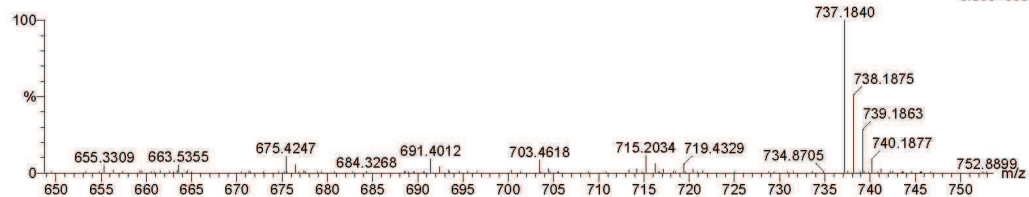
24-Nov-2009

16:14:31

1: TOF MS ES+

6.96e+003

YANGYH\_1 10 (0.371) Cm (9:16)



Minimum: -1.5  
Maximum: 500.0 50.0 100.0

Mass	Calc. Mass	mDa	PPM	DBE	i-FIT	i-FIT (Norm)	Formula
737.1840	737.1843	-0.3	-0.4	29.5	17.8	0.0	C44 H34 N4 S3 Na

Fig. 4.9 HRMS spectrum of BTC

## Elemental Composition Report

Page 1

## Single Mass Analysis

Tolerance = 500.0 mDa / DBE: min = -1.5, max = 100.0  
 Element prediction: Off  
 Number of isotope peaks used for i-FIT = 2

## Monoisotopic Mass, Even Electron Ions

80 formula(e) evaluated with 40 results within limits (up to 1 closest results for each mass)

## Elements Used:

C: 0-55 H: 0-40 N: 0-4 Na: 0-1 S: 0-5

ZHU\_WH

LCT Premier

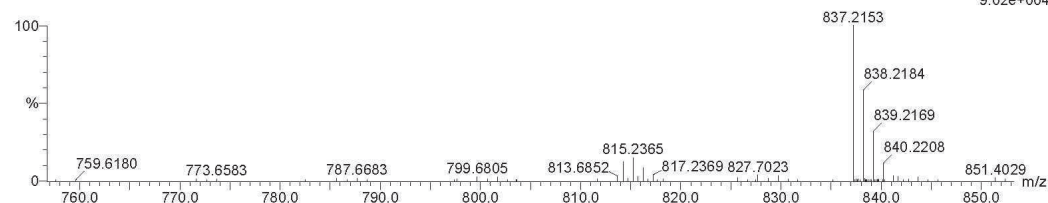
24-Nov-2009

16:48:41

1: TOF MS ES+

9.02e+004

YANGYH\_4.63 (0.625) Cm (44:71)



Mass	Calc. Mass	mDa	PPM	DBE	i-FIT	i-FIT (Norm)	Formula
837.2153	837.2156	-0.3	-0.4	35.5	147.1	0.0	C52 H38 N4 Na S3

Fig. 4.10 HRMS spectrum of BTT

## 4.3.3 UV-Vis absorption spectra of BTC, BTT and BTA

All three compounds can easily dissolve in a solvent mixture of hexane:THF = 4:1 to yield a pale yellow solution with an intense absorption band at *ca.* 300-350 nm and another moderate absorption band at *ca.* 380-490 nm in various solvents (Table 4.4 and Figure 4.11). From the comparison between TD-DFT calculation (Gaussian03, B3LYP, 6-31g(d,p)) and UV-Vis spectra, we could deduce that the UV absorption at *ca.* 300 nm for BTC is mainly composed of HOMO-2→LUMO, HOMO-3→LUMO, HOMO-4→LUMO, HOMO-4→LUMO, HOMO-3→LUMO; the absorption at *ca.* 400 nm is mainly composed of HOMO→LUMO, HOMO-1→LUMO transitions. The UV-Vis absorption of BTT at *ca.* 350 nm is mainly composed of HOMO→LUMO+1, HOMO-1→LUMO+1, HOMO→LUMO+2; *ca.* 425 nm is mainly composed of HOMO→LUMO, HOMO-1→LUMO, HOMO-2→LUMO. The UV-Vis absorption of BTT at *ca.* 300 nm is mainly composed of HOMO-2→LUMO; *ca.* 400 nm is mainly composed of HOMO→LUMO, HOMO-1→LUMO (Figure 4.10 and Table 4.1-4.3, Table 4.5). As expected, upon light irradiation at 365 nm, the solution of BTC, BTT and BTA quickly turns green with moderate low lying bands at 670 nm (*c*-BTC), 687 nm (*c*-BTT), 652 nm (*c*-BTA) (Figure 4.11), indicative of the appearance of the corresponding closed form produced by the characteristic photocyclization. The significant bathochromic shift in absorption bands of the closed forms relative to their open forms is mainly due to the extended  $\pi$ -conjugation across the whole moiety. The clear isobestic point strongly indicates that the photochromic reaction through excited state is simply composed of open and closed

isomers. The typical photochromic properties of BTC, BTT, BTA and their corresponding closed forms (*c*-BTC, *c*-BTT and *c*-BTA) are summarized in Table 4.4. Notably, the ring closure quantum yield of BTC, BTT and BTA increased with the increase of bulky substituent. The ring closure quantum yields for BTC, BTT and BTA in mixture solvents hexane: THF = 4:1 are 52.6%, 67.5% and 48.4% respectively. This may be ascribed to the dominance of anti-parallel conformer after the introduction of a large substituent.

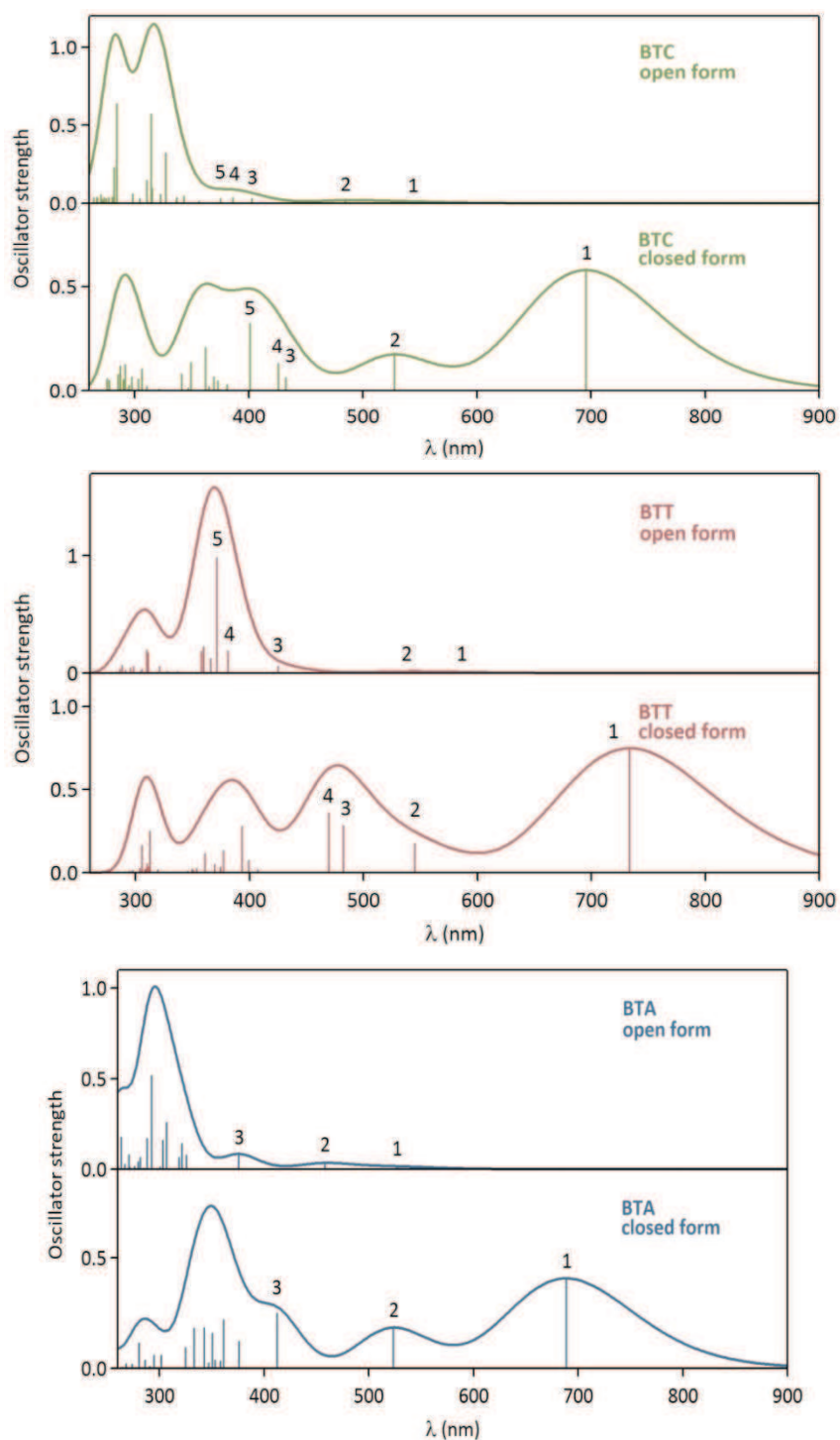


Fig. 4.11 Franck-Condon electronic transitions of BTC, BTT and BTA calculated by TD-DFT (using

3000 cm<sup>-1</sup> gaussian bandwidth)

Table 4.1 Composition of the main electronic transitions of the open and closed forms of BTC

	Open form	Closed form
	HOMO = 187 / LUMO = 188	HOMO = 187 / LUMO = 188
Transition 1	HOMO→LUMO 100%	HOMO→LUMO 100%
Transition 2	HOMO-1→LUMO 100%	HOMO→LUMO+1 90% HOMO-1→LUMO 7%
Transition 3	HOMO-2→LUMO 95%	HOMO→LUMO+2 78% HOMO-1→LUMO 18%
Transition 4	HOMO-3→LUMO 79% HOMO-4→LUMO 17%	HOMO-1→LUMO 63% HOMO→LUMO+2 24%
Transition 5	HOMO-4→LUMO 70% HOMO-3→LUMO 24%	HOMO→LUMO+3 97%

Table 4.2 Composition of the main electronic transitions of the open and closed forms of BTT

	Open form	Closed form
	HOMO = 213 / LUMO = 214	HOMO = 213 / LUMO = 214
Transition 1	HOMO→LUMO 100%	HOMO→LUMO 100%
Transition 2	HOMO-1→LUMO 100%	HOMO→LUMO+1 83% HOMO-1→LUMO 10%
Transition 3	HOMO-2→LUMO 98%	HOMO-1→LUMO 87% HOMO→LUMO+1 6%
Transition 4	HOMO-3→LUMO 92%	HOMO-2→LUMO 100%
Transition 5	HOMO→LUMO+1 46% HOMO-1→LUMO+1 21% HOMO→LUMO+2 18%	

Table 4.3 Composition of the main electronic transitions of the open and closed forms of BTA

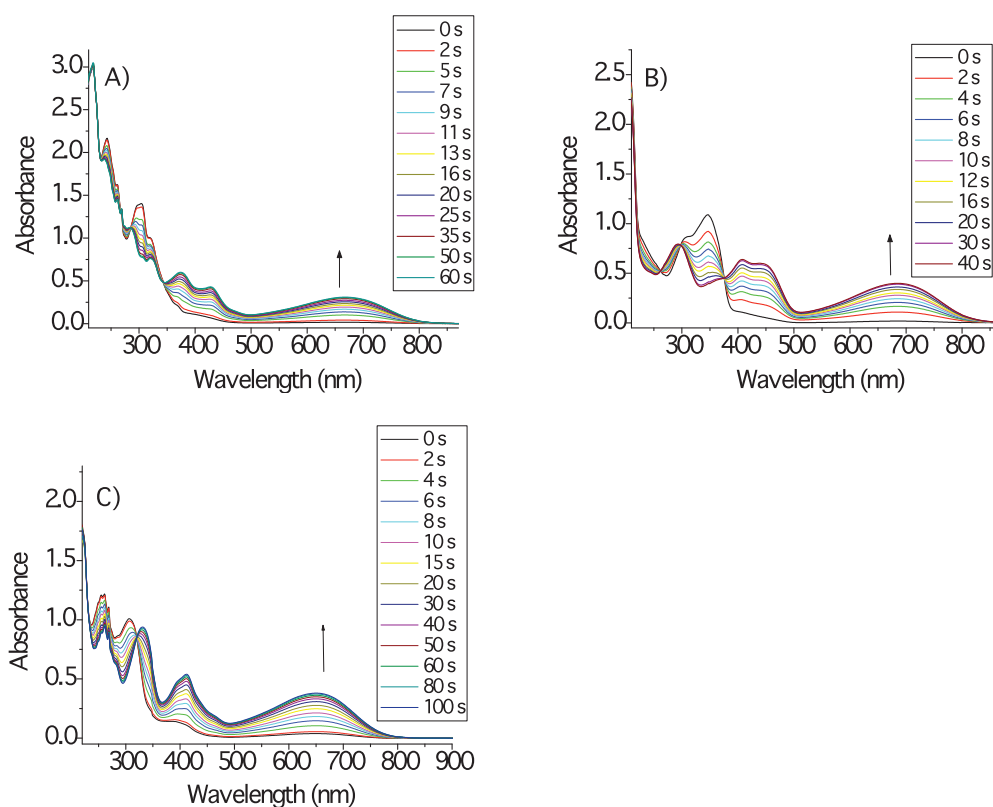
	Open form	Closed form
	HOMO = 141 / LUMO = 142	HOMO = 141 / LUMO = 142
Transition 1	HOMO→LUMO 100%	HOMO→LUMO 100%
Transition 2	HOMO-1→LUMO 100%	HOMO→LUMO+1 88% HOMO-1→LUMO 12%
Transition 3	HOMO-2→LUMO 100%	HOMO-1→LUMO 70% HOMO→LUMO+2 26%

**Table 4.4** Absorption properties of the open and closed forms of BTC, BTT and BTA in THF:Hexane = 1:4 and the reaction quantum yields

	$\Phi_{o \rightarrow c}^{a,b}$	$\Phi_{c \rightarrow o}^{a,b}$	Conversion at PSS(%)	$\lambda_{\max}(\text{nm})/\epsilon(10^3 \text{ M}^{-1} \text{ cm}^{-1})$	
				Open ring	Closed ring
BTC	52.6	0.347	95.23	303/66.1	373/28.9
					430/20.4
					670/14.6
BTT	67.5	0.085	99.76	345/52.7	407/31.3
					687/19.6
BTA	48.4	0.196	96.13	308/57.8	330/44.9
					411/26.1
					652/18.4

<sup>a</sup> Reaction quantum yields and conversion, measured under irradiation at 365 nm in THF:Hexane = 1:4.

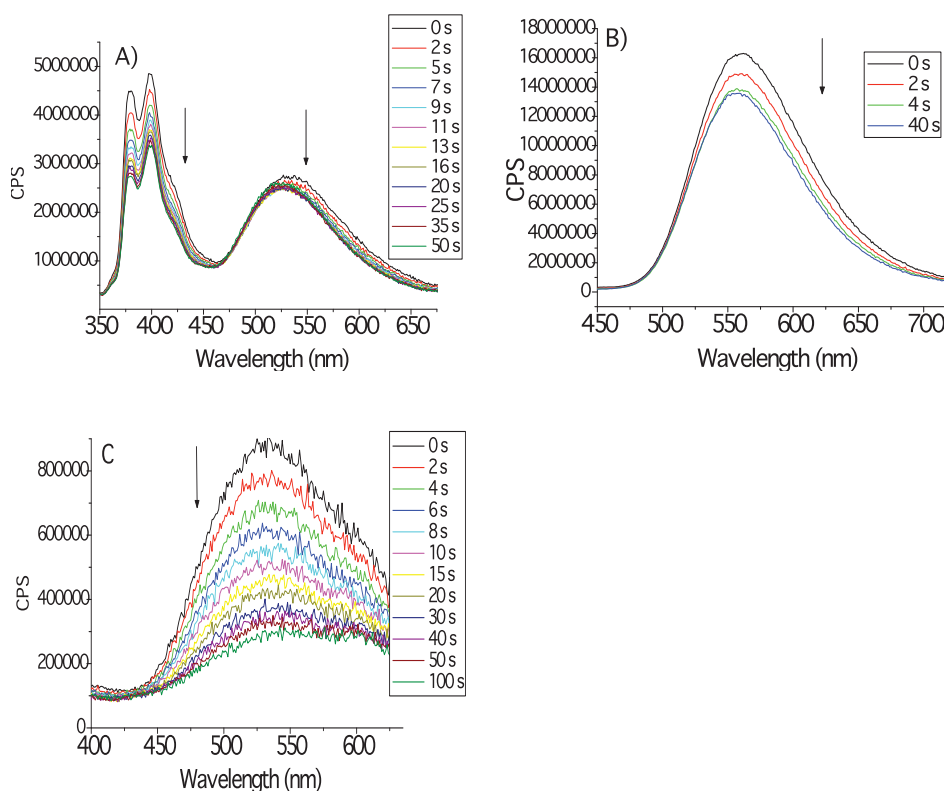
<sup>b</sup> Ring opening quantum yield in THF : Hexane = 1:4, measured at  $\lambda_{\max}$  of closed-ring isomer.



**Fig. 4.12** Spectral changes of UV-Vis absorption of A) BTC; B) BTT; C) BTA upon irradiation at 365 nm (in a mixture solvent of THF : Hexane = 1 : 4,  $2.12 \times 10^{-5} \text{ mol}\cdot\text{L}^{-1}$ ,  $2.06 \times 10^{-5} \text{ mol}\cdot\text{L}^{-1}$ ,  $2.09 \times 10^{-5} \text{ mol}\cdot\text{L}^{-1}$ ). The photostationary states were obtained by irradiating solutions with 365 nm light until no further spectral changes were observed.

#### 4.3.4 Emission spectra of BTC, BTT and BTA before and after irradiation

Generally speaking, the fluorescence quenching of photochromic compounds at low concentration is due to the disappearance of the fluorescent open form and the non-fluorescent property of the closed form. Thus, the conversion yield is usually compatible with the percentage of quenched fluorescence. Interestingly, the fluorescence of BTC and BTT were slightly quenched after photocyclization reaction, which is probably due to the existence of multi emission components. The emission peak at 400 nm for BTC is coming from the local excitation of carbazole due to the non co-planarity of carbazole with the central ethene bridge, while the emission at 528 nm is due to the typical ICT emission. To further investigate the origin of the fluorescence, TCSPC (Time-correlated single photon counting) method was used to measure the lifetime. As deduced from Figure 4.13, the lifetime analysis of BTC and BTT are both multi-exponential, indicating the existence of multi emission components. Interestingly, the lifetime decreased dynamically, indicating a possible energy transfer within the system.



**Fig. 4.13** Fluorescence changes of A) BTC; B) BTT; C) BTA excited at the isobestic point of 344 nm, 375 nm, 320nm upon irradiation at 365 nm (in a mixture solvent of THF : Hexane =1 : 4,  $2.12 \times 10^{-5}$  mol·L<sup>-1</sup>,  $2.06 \times 10^{-5}$  mol·L<sup>-1</sup>,  $2.09 \times 10^{-5}$  mol·L<sup>-1</sup>). The photostationary states were obtained by irradiating solutions with 365 nm light until no further spectral changes were observed.



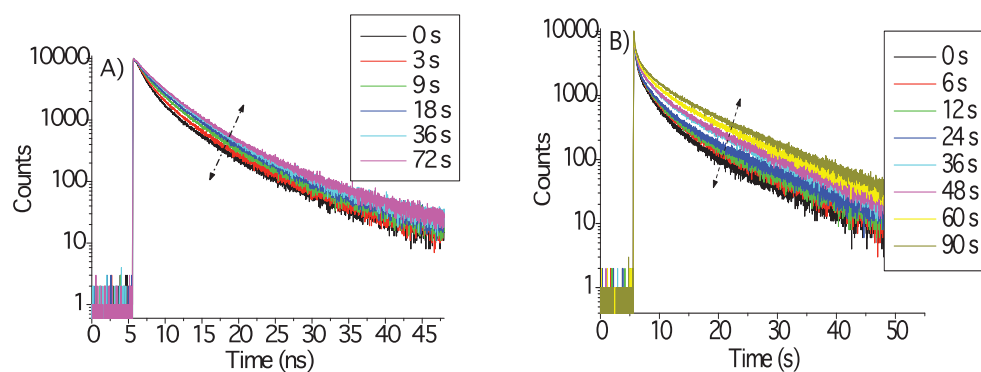
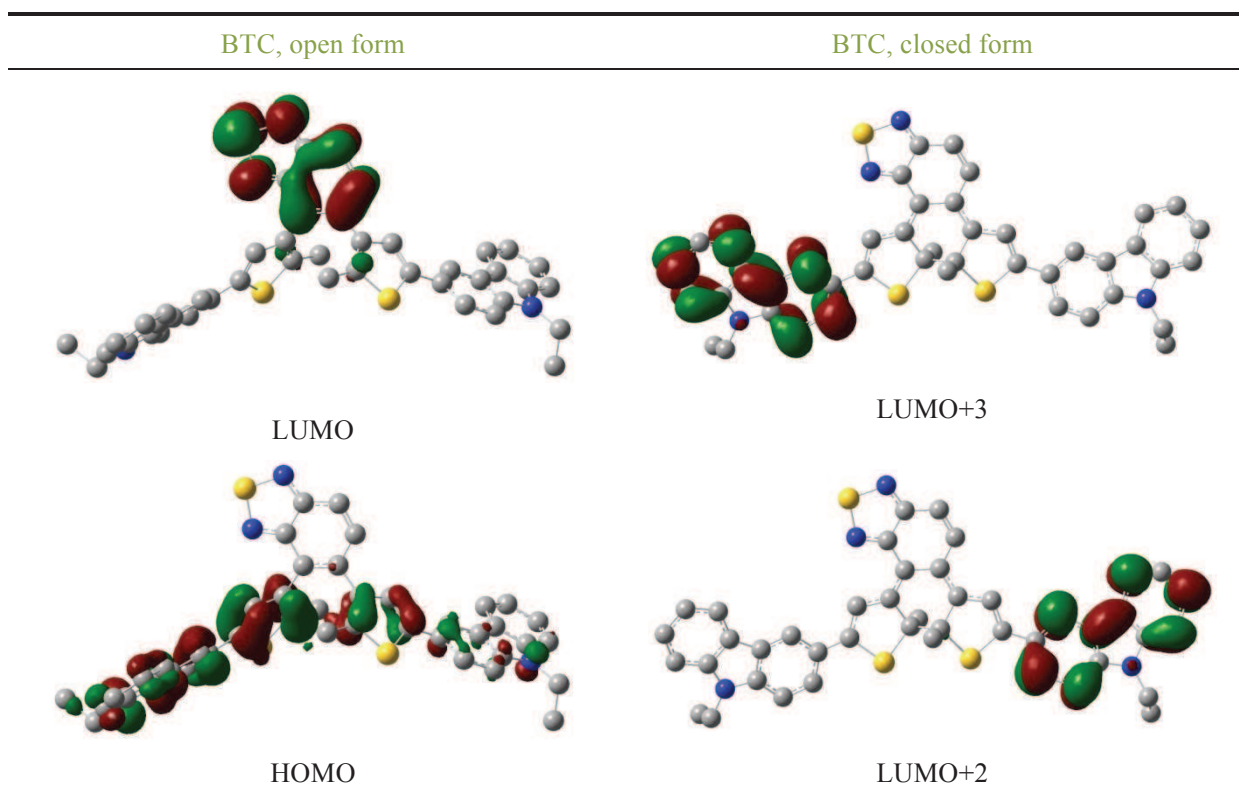
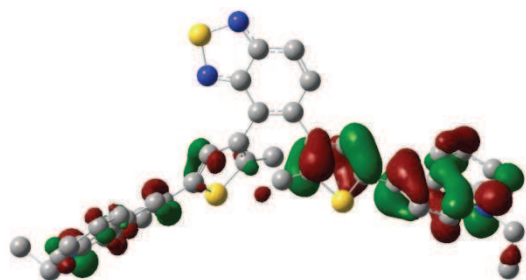


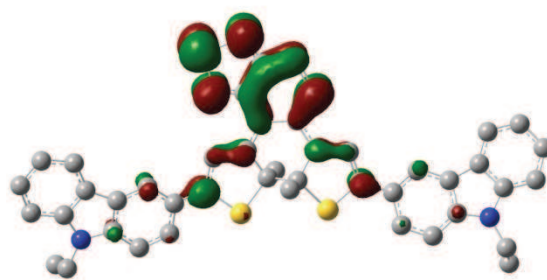
Fig. 4.14 The fluorescence decay of BTC in (A) THF excited at 360 nm and monitored at 587nm (B)  $\text{CCl}_4$ : hexane = 1: 9 excited at 360 nm and monitored at 500nm. The optical density was controlled below 0.1.

Table 4.5 Molecular orbitals of BTC and BTT involved in the main electronic transitions

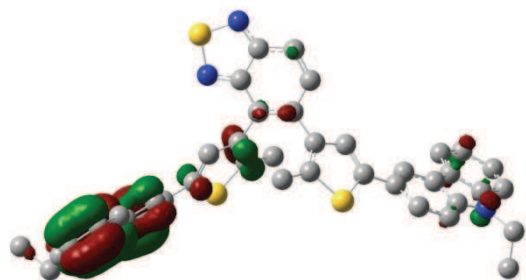




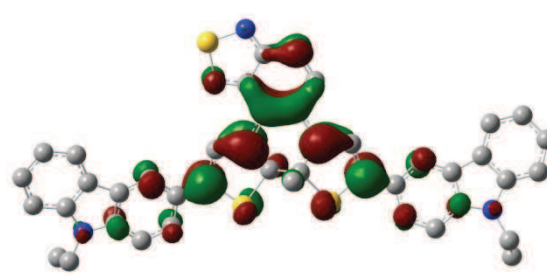
HOMO-1



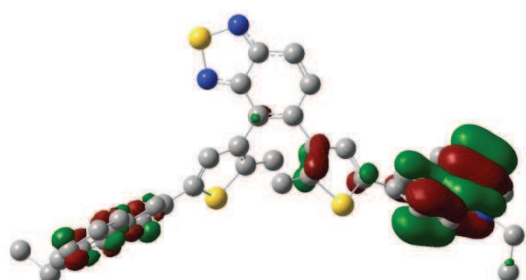
LUMO+1



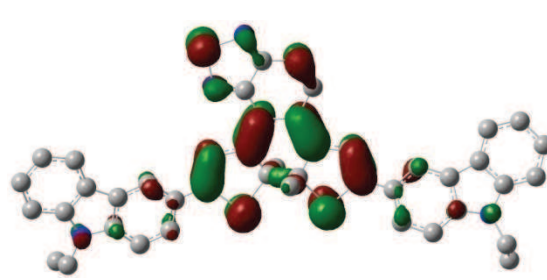
HOMO-2



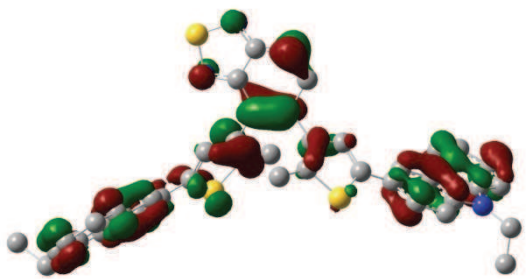
LUMO



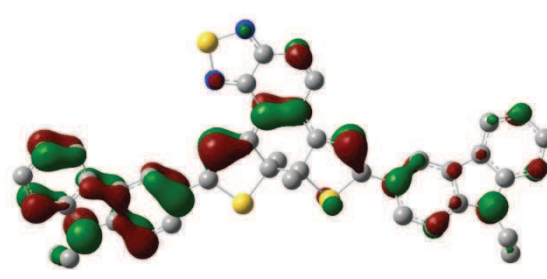
HOMO-3



HOMO



HOMO-4

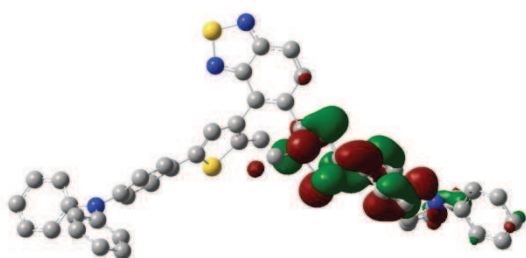


HOMO-1

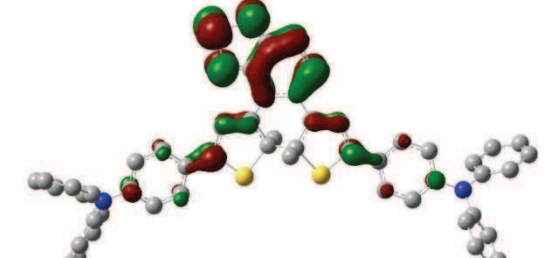
---

BTT, open form

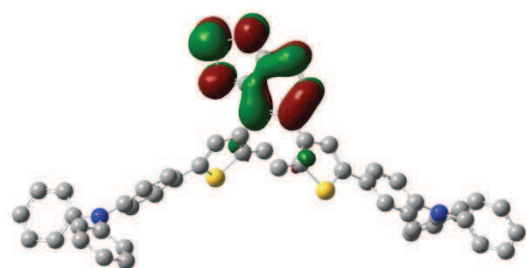
BTT, closed form



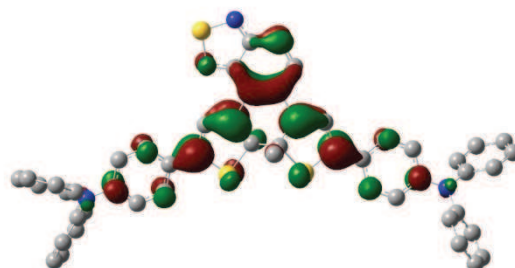
LUMO+1



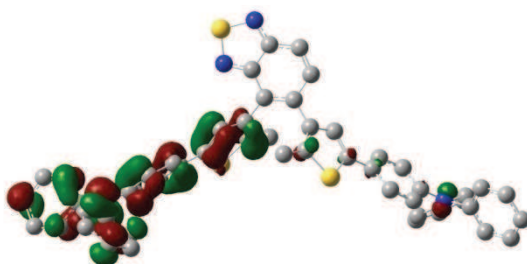
LUMO+1



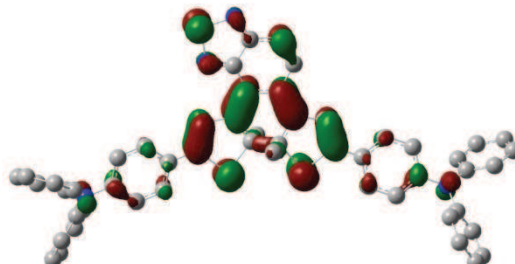
LUMO



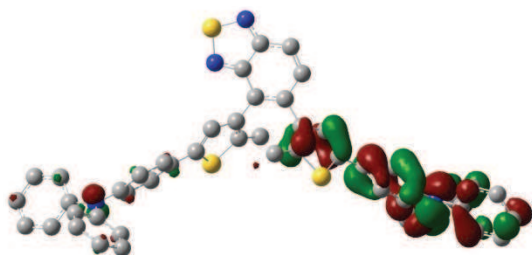
LUMO



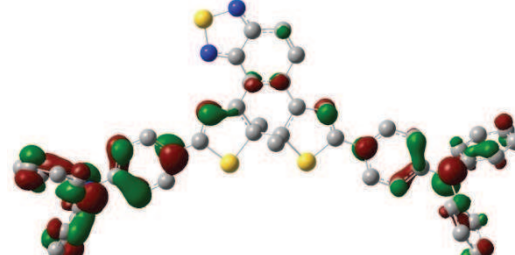
HOMO



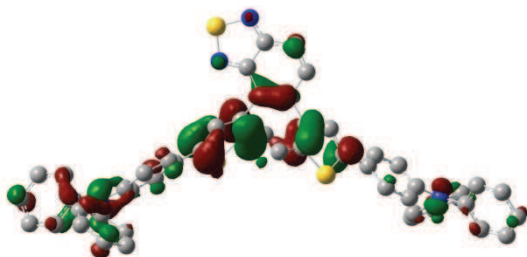
HOMO



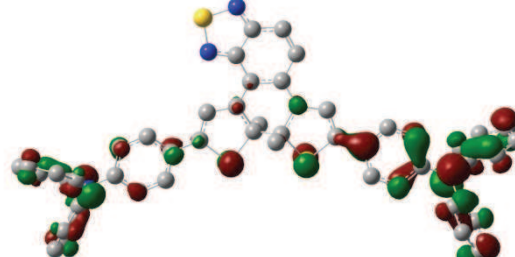
HOMO-1



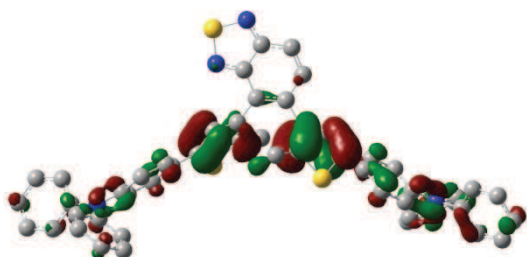
HOMO-1



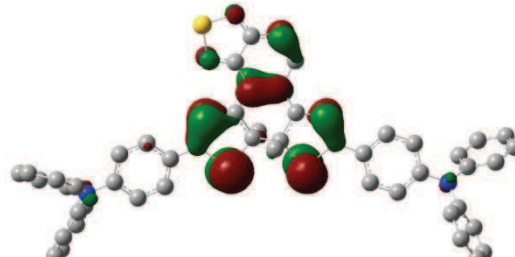
HOMO-2



HOMO-2



HOMO-3



HOMO-3

Note: Molecular orbitals were drawn with an iso-coefficient of 0.03

#### 4.3.5 Second harmonic generation (SHG) signal changes of BTC, BTT and BTA before and

after irradiation

#### 4.3.5.1 General introduction to SHG

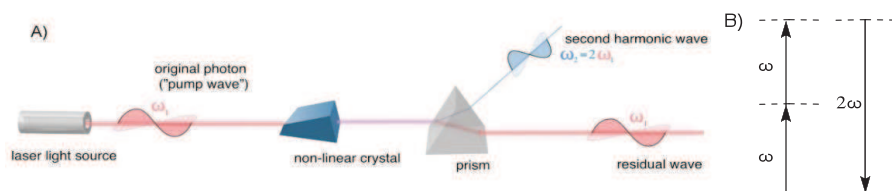


Fig. 4.15 A) Generation of SHG signal; B) Energy-level diagram describing second-harmonic generation

Nonlinear optics (NLO) is the study of optical phenomena that occur in the presence of a strong perturbation, for example light. In such a situation, the intensity of the response of a material system does not follow a linear law vs. the intensity of the light. Only laser light is sufficiently intense to induce such a response. The beginning of NLO is often taken to be the discovery of second-harmonic generation (SHG) by Franken et al. (1961),<sup>[145]</sup> shortly after the demonstration of the first laser by Maiman in 1960. As illustrated in Figure 4.14A, when an intense incident light goes through a nonlinear crystal,  $\omega_1$  is frequency-doubled to generate  $\omega_2$ , in which  $\omega_2 = 2\omega_1$ . SHG is modeled as follows equation 4.1:

$$P_i^{NL}(\omega_m + \omega_n) = N\epsilon_0 \sum \sum \beta_{ijk}(\omega_m + \omega_n, \omega_m, \omega_n) E_j^{loc}(\omega_m) E_k^{loc}(\omega_n) \quad \text{Equation 4.1}$$

$\beta_{ijk}$  is second-order hyperpolarizability of the molecules in the material, and  $P_i^{NL}$  is the polarization. In the case of SHG,  $m = n$ . In addition, nonlinear susceptibility  $\chi_{ijk}^{(2)}$  can be represented as follows equation 4.2:

$$\chi_{ijk}^{(2)}(\omega_m + \omega_n, \omega_m, \omega_n) = \zeta^{(2)}(\omega_m + \omega_n, \omega_m, \omega_n) N \beta_{ijk}(\omega_m + \omega_n, \omega_m, \omega_n) \quad \text{Equation 4.2}$$

In addition, we shall notice that second-order nonlinear optical interactions can practically occur only in non-centrosymmetric crystals: that is, in crystals that do not display inversion symmetry. Otherwise,  $\chi_{ijk}^{(2)} = 0$ .<sup>[146]</sup>

Under proper experimental conditions, the process of SHG can be so efficient that a large proportion of the power in the incident beam at frequency  $\omega_1$  is converted to radiation at the second-harmonic frequency  $2\omega_1$ . One common use of second-harmonic generation is to convert the output of a fixed-frequency laser to a different spectral region. For example, the Nd:YAG laser operates in the near infrared at a wavelength of  $1.06 \mu\text{m}$ . SHG is routinely used to convert the wavelength of the radiation to  $0.53 \mu\text{m}$ , in the middle of the visible spectrum. SHG can be visualized by considering the interaction in terms of the exchange of photons between the various frequency components of the field. According to this picture, which is illustrated in part (B) of Fig. 4.14, two photons of frequency  $\omega_1$  are converted to one photon of frequency  $2\omega_1$  in a single quantum mechanical process. The solid line in the figure

represents the atomic ground state, and the dashed lines represent what are known as virtual levels. These levels are not energy eigenlevels of the free atom but rather represent the energy of one or more photons of the radiation.

#### 4.3.5.2 SHG signals of BTC, BTT and BTA before and after irradiation

EFISH (Electric-Field Induced Second Harmonic Generation)<sup>[147]</sup> and HRS (Hyper-Rayleigh Scattering)<sup>[148]</sup> are common methods to determine the value of  $\mu\beta$  and  $\beta$ . As illustrated in Figure 4.15, the values of  $\mu\beta$  for the chromophores are measured using the electric-field induced second harmonic generation (EFISH) technique. The amplified nanosecond Nd<sup>3+</sup>:YAG laser at 1.06  $\mu\text{m}$  and 10 Hz repetition rate pumps a hydrogen Raman cell so as to obtain a larger wavelength (1.907  $\mu\text{m}$ ) for which both the fundamental and harmonic frequencies are far away from the resonance of the investigated molecule. A Schott RG 1000 filter is used to filter out any remaining visible light from the laser flash lamp. Suitable neutral density filters are used to control the power of the incident beam and a half wave plate and polarizer are used to set the incident polarisation along the direction of the applied electric field. In addition, a band pass filter is mounted in front of the detection photomultiplier (PMT) along with a filter to remove any remaining radiation at the fundamental wavelength. A high voltage (5 kV), synchronized with the 1.907  $\mu\text{m}$  laser pulse, is applied across the EFISH cell containing the solution. The EFISH cell consists of a stainless steel container with two quartz optical windows, which are fixed to form a wedge shaped cavity within the cell. The interelectrode distance is 2 mm, giving a static electric field around 25  $\text{kV}\cdot\text{cm}^{-1}$ . The cell is mounted on an electrically isolated translation stage. The whole cell is then translated horizontally relative to the incident beam to produce Maker fringes. Every measurement is referenced separately to the Maker fringes of the pure reference solvent (Hexane:THF = 13:12) used to dissolve the chromophores. A home made computer program is used to calculate the interfringe distance and the fringe amplitude. These data are then used to calculate the  $\mu\beta$  value of the chromophore.

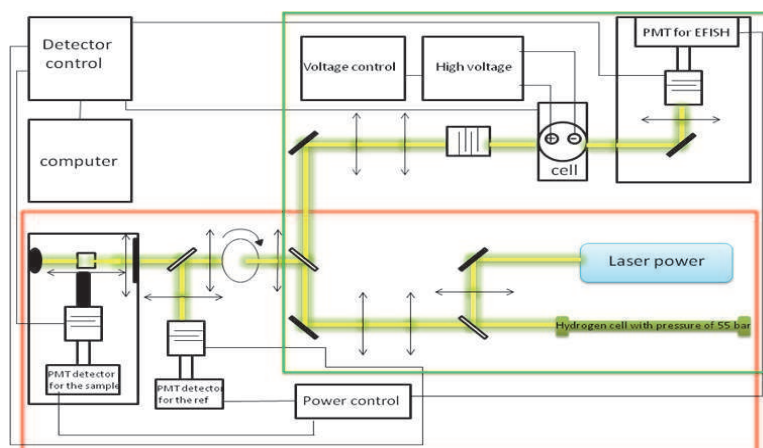


Fig. 4.16 Measurement of SHG signal. The red frame contains the setup of HRS, while the green frame

contains the setup of EFISH.

As illustrated in Figure 4.16, the SHG signal of BTA was recorded in Hexane:THF = 13:12 by EFISH. We can clearly find the Maker fringes from pure dichloromethane (Figure 4.16A). However, no Maker fringes could be distinguished from pure Hexane:THF = 13:12 and BTA in dissolved in Hexane:THF = 13:12 before and after irradiation at 365 nm for 16 h.

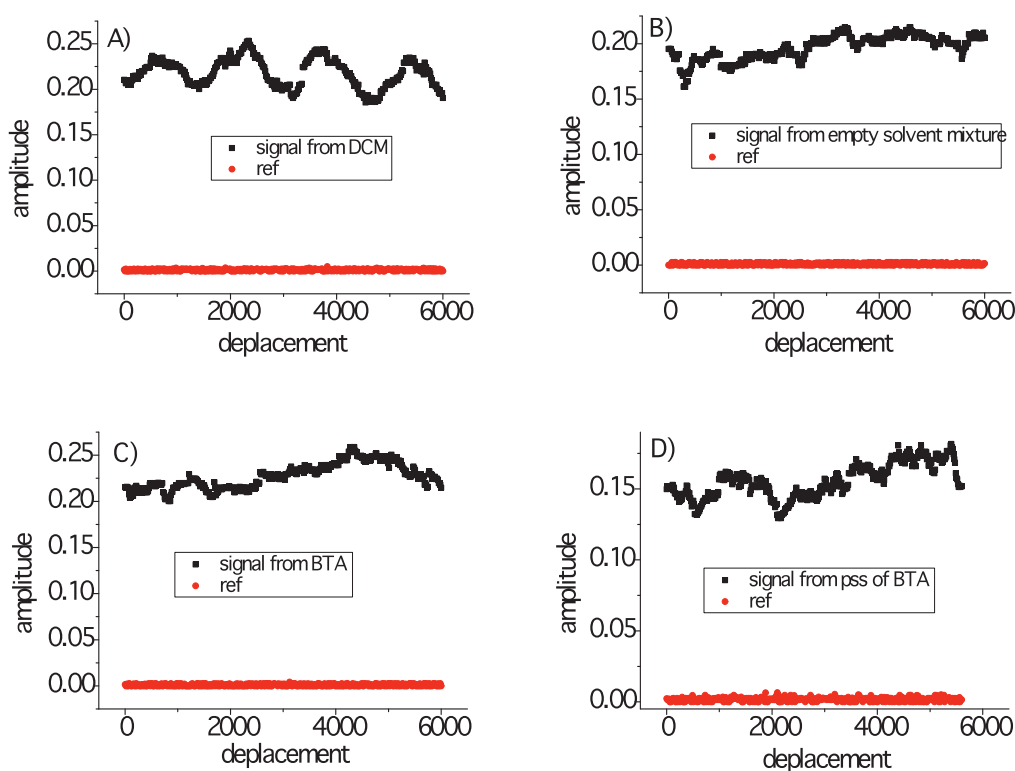


Fig. 4.17 EFISH measurement of A) signals of pure DCM; B) signals from a solvent mixture of THF:Hexane = 13:12; C) BTA ( $1.03 \times 10^{-2} \text{ mol}\cdot\text{L}^{-1}$ ) in a solvent mixture of THF: Hexane = 13: 12; D) PSS of BTA ( $1.03 \times 10^{-2} \text{ mol}\cdot\text{L}^{-1}$ ) in a solvent mixture of THF:Hexane = 13:12 after irradiation at 365 nm for 16 h.

To further investigate the SHG signals of BTA before and after irradiation, we obtained the single crystal of BTA from a solvent mixture of THF and water (Figure 4.17). BTA adopts a centrosymmetric packing form due to the strong  $\pi \cdots \pi$  interaction between benzothiadiazole rings. According to the abovementioned theory, second-order NLO phenomena can occur only in non-centrosymmetric crystals, that is, in crystals that do not display inversion symmetry. The centrosymmetric packing of BTA in crystal state provides a possible explanation to the absence of SHG signal of BTA in the bulk crystal state.

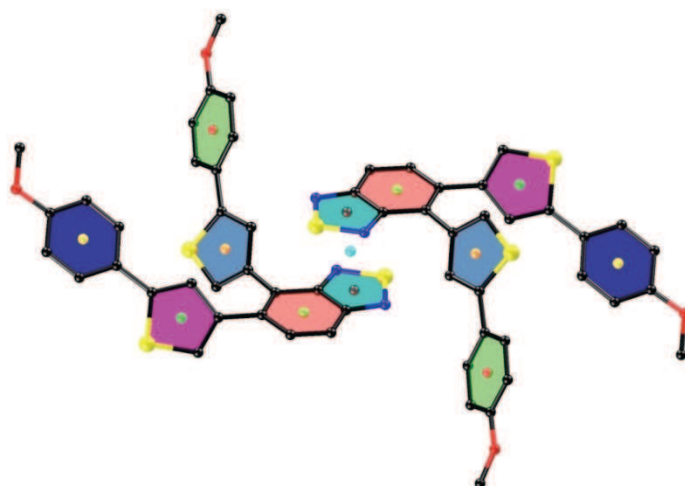


Fig. 4.18 Crystal structure of BTA obtained from the mixture solvents of THF and H<sub>2</sub>O. The crystal analysis reveals that BTA adopts a centrosymmetric packing, which makes it impossible to generate any SHG signals in crystal state. The methyl group was omitted for clarity.

#### 4.4 Conclusions

A novel photoswitchable NLO material has been synthesized based on 2,1,3-benzothiadiazole. The strategy for the designing of NLO switchable system was based on the difference in efficiency in D- $\pi$ -A structure before and after irradiation caused by the coplanarity between donor and benzothiadiazole ring. However, due to the strong  $\pi \cdots \pi$  interaction and planarity of benzothiadiazole ring, the compounds adopt central symmetric packing form in single crystal state. Thus, no signals could be recorded from powder test.

## Chapter 5 Photochromic System Based on 2,1,3-Benzothiadiazole

### 5.1 Iridium complex utilizing a 2,1,3-benzothiadiazole based photochromic unit as ligand

Nowadays, to improve photochromic properties and photoswitching functionality, exploitation of molecules involving the diarylethene moiety as ligand to form metal complexes has drawn much more attention, especially efforts on the investigation on phosphorescence involving triplet-excitation of the metal complexes.<sup>[149]</sup> These metal complex systems have shown novel properties that can be potentially applied as photosensitizers for the photochromic activity, since the perturbation of the photochromic properties of the diarylethene moiety upon coordination to the metal center has been observed.

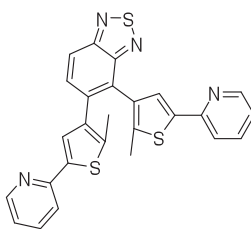


Fig. 5.1 2,1,3-benzothiadiazole based photochromic unit as complex ligand

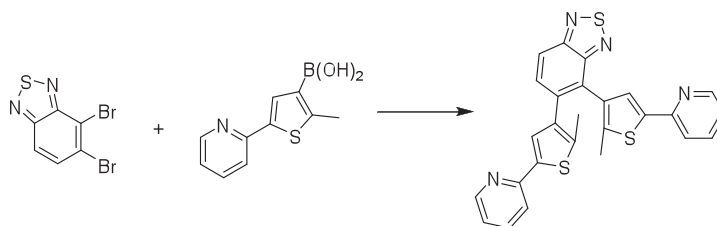
#### 5.1.1 Instruments and Reagents

<sup>1</sup>H NMR and <sup>13</sup>C NMR spectra were recorded on Bruker Avance III 400 MHz spectrometers with tetramethylsilane (TMS) as an internal reference recorded at room temperature. CDCl<sub>3</sub> was used as solvents. HRMS were recorded on a Waters LCT Premier XE spectrometer with methanol or acetonitrile as solvents. Absorption and fluorescence spectra were recorded on Varian Cary 500 and FluoroMax-3 (Horiba Jobin-Yvon), respectively. The photochromic property was evidenced and characterized by following *in situ* the absorption spectra under continuous irradiation (see Appendix I for detailed information).

#### 5.1.2 Synthetic route to the target and intermediate molecules

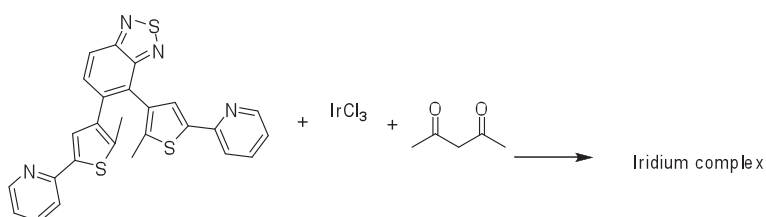
##### 5.1.2.1 BTP





4,5-dibromo-2,1,3-benzothiadiazole (0.2 g, 0.7 mmol) was dissolved in dioxane (35 mL),  $\text{Pd}(\text{PPh}_3)_4$  (0.10 g) was added, and the resulting mixture was stirred for 15 min at room temperature. Then aqueous  $\text{Na}_2\text{CO}_3$  (30 mL, 2.0 mol  $\text{L}^{-1}$ ) was added. The reactive mixture was heated and refluxed at a temperature of 60 °C and a solution of 2-methyl-5-(pyridin-2-yl)thiophen-3-ylboronic acid (0.6 g, 2.70 mmol) dissolved in 5 mL dioxane was added dropwise via a syringe. Subsequently the mixture was refluxed for 15 h, and cooled to room temperature. The reactive mixture was poured in  $\text{H}_2\text{O}$  and extracted with ether. The organic layer was separated and dried with  $\text{Na}_2\text{SO}_4$ . After concentration, the compound was purified by column chromatography on silica gel (Petroleum ether: ethyl acetate = 5: 1 v/v) to yield a yellow solid (70 mg, yield 57%).  $^1\text{H}$  NMR (500 MHz,  $\text{CDCl}_3$ , ppm): 2.10 (s, 3 H, - $\text{CH}_3$ ), 2.26 (s, 3 H, - $\text{CH}_3$ ), 7.11 (m, 2 H, -Pyridine-H), 7.29 (s, 1 H, Thiophene-H), 7.50 (m, 1 H, -Pyridine-H), 7.62 (m, 2 H, -Pyridine-H), 7.73 (d,  $J = 10$  Hz, 2 H, -Ph-H), 8.04 (d,  $J = 10$  Hz, 1 H, -Ph-H), 8.54 (m, 2 H, -Ph-H)

#### 5.1.2.2 BTP-Ir complex



A Schlenk flask was charged with anhydrous  $\text{IrCl}_3$  (10 mg, 0.033 mmol) and 2-ethoxyethanol (6 mL). The mixture was stirred at room temperature for 12h. Then BTP (50 mg, 0.103 mmol) was added to the flask. The mixture was refluxed for 24 h and cooled to room temperature. To the reaction mixture were added acetylacetone (3 mL, 0.072 mmol) and  $\text{Na}_2\text{CO}_3$  (10 mg, 0.096 mmol). The mixture was heated at 80 °C for 15 h. Then, after cooling to room temperature, the reaction mixture was poured into  $\text{H}_2\text{O}$  (5 mL) and extracted with dichloromethane. The TLC plate shows no products except for the two starting materials. The resulting reaction solution was diluted to the measurable concentration of UV, and the

resulting spectrum shows no difference compared to the BTP photochromic compound.

## 5.2 NLO photoswitchable system based on 2,1,3-benzothiadiazole as central ethene bridge with extended $\pi$ system

### 5.2.1 Molecule design and synthesis

Previously, we reported a novel NLO photoswitchable system based on 2,1,3-benzothiadiazole as central ethene bridge in Chapter 4. However, no obvious maker fringe could be recorded by EFISH method due to the centrosymmetric property of BTA in the crystal state. To further exploit the intrinsic acceptor property of 2,1,3-benzothiadiazole in a D- $\pi$ -A system, herein, we synthesized a photochromic compound with an extended  $\pi$  system and a large substituent, hoping to avoid the centrosymmetric property caused by strong  $\pi$ ... $\pi$  interaction between benzothiadiazole rings as well as to increase the NLO efficiency of D- $\pi$ -A structure.

### 5.2.2 Synthetic route to the target molecule

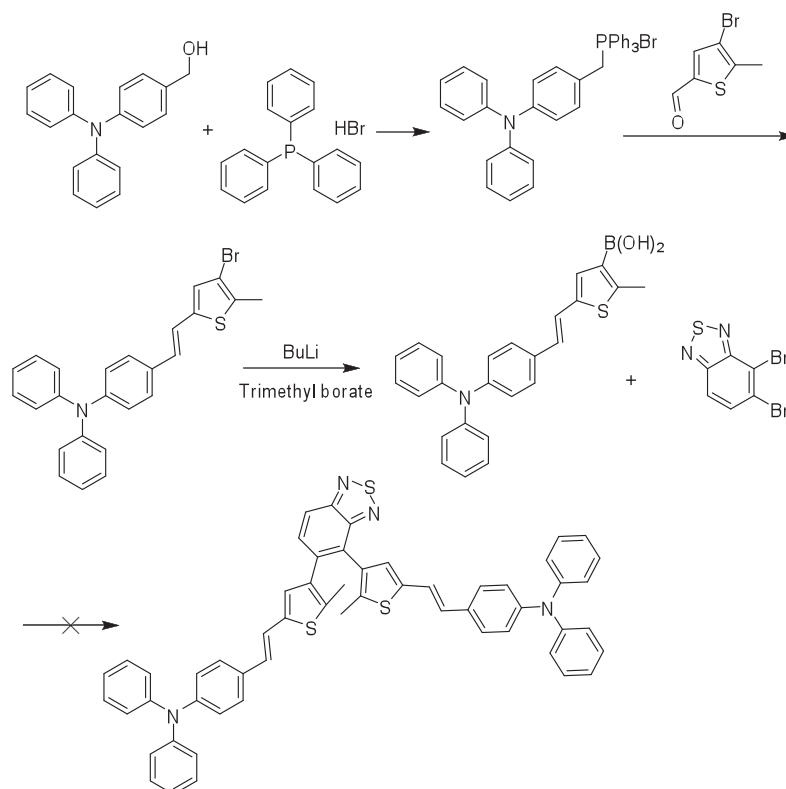


Fig. 5.2 Synthetic route1 to the target molecule

The target molecule DTPA was synthesized through two routes. As found during the synthetic manipulation, direct Suzuki coupling between 2,1,3-benzothiadiazole and (*E*)-5-(4-(diphenylamino)styryl)-2-methylthiophen-3-ylboronic acid as illustrated in synthetic

route1 could not yield any product due to the vulnerable property of the double bond between thiophene and triphenylamine when treated with BuLi. To circumvent the formation of double bond before the treatment of BuLi, 5-formyl-2-methylthiophen-3-ylboronic acid was prepared to couple with the ethene bridge. Unfortunately, the conversion yield is pretty low. However, after the protection of aldehyde as well as boronic acid before Suzuki coupling, the conversion yield could be greatly enhanced. Further Wittig reaction between 4,4'-(benzo[*c*][1,2,5]thiadiazole-4,5-diyl)bis(5-methylthiophene-2-carbaldehyde) and triphenylamine could give DTPA with a considerable yield.

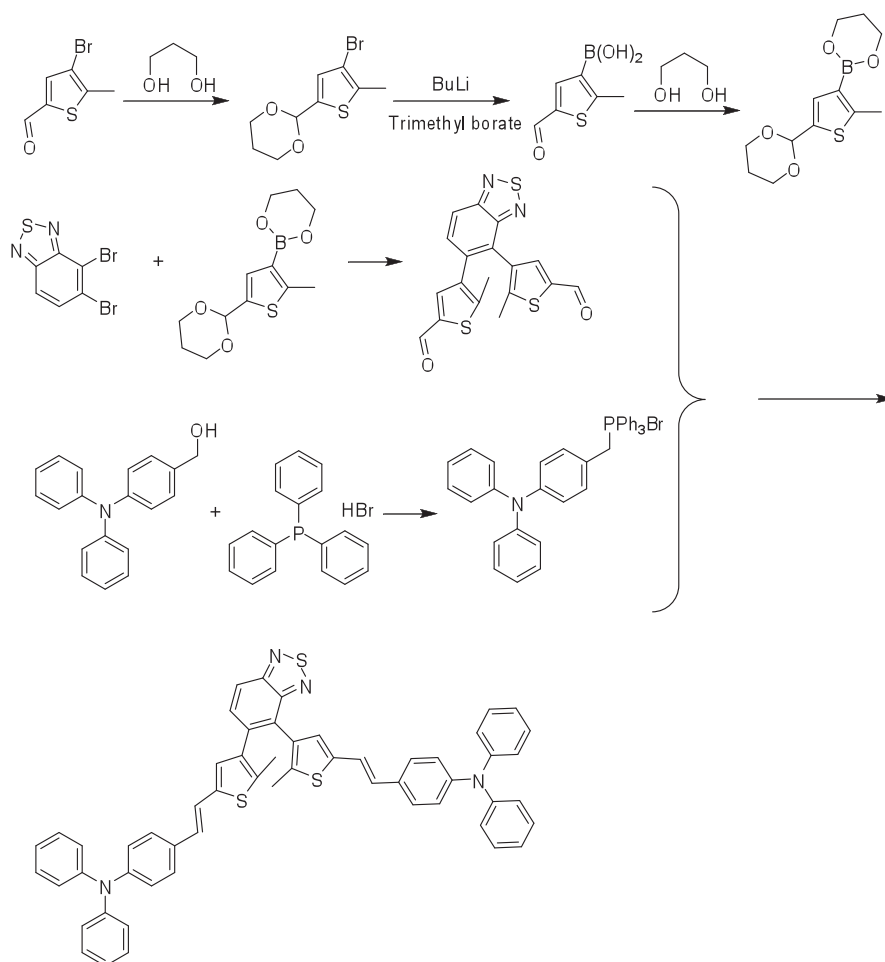
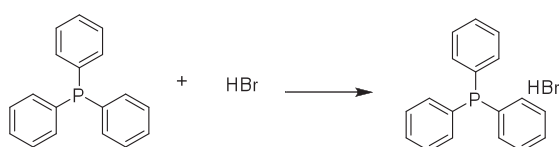


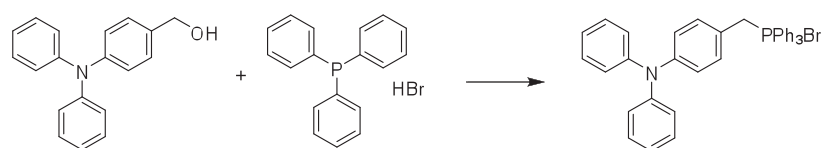
Fig. 5.3 Synthetic route2 to the target molecule

### 5.2.3.1 Triphenylphosphine hydrobromide



In a 100 mL flask with condenser, hydrobromic acid (13 mL, 48% wt aqueous) and triphenylphosphine (4 g, 15.26 mmol) were introduced. The temperature was slowly increased to 70 °C and then kept at the same condition for 5 min. Then, the reaction was cooled and extracted with chloroform. The solvent was removed under vacuum and the liquid was then solidified with EtOAc to yield 3.8 g of the product. M.p. 180°C.

### 5.2.3.2 Witting reagent



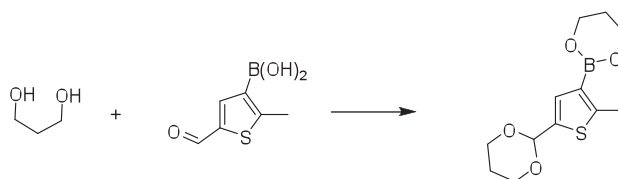
(4-(diphenylamino)phenyl)methanol (1.05 g, 3.8 mmol) and PPh<sub>3</sub>.HBr (1.37 g, 4 mmol) were dissolved in 20 mL chloroform and refluxed for 2 h. After removing the solvent, the residue was solidified with ether and filtrated to obtain 2.25 g of a white solid of TPA-PPh<sub>3</sub>.Br, yield 98.7%. M. p. > 250 °C.

### 5.2.3.3 5-formyl-2-methylthiophen-3-ylboronic acid



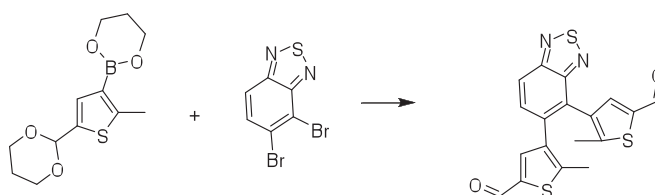
In a 250 mL schlenk tube, 2-(4-bromo-5-methylthiophen-2-yl)-1,3-dioxane (2.5 g, 9.5 mmol) and dried THF (40 mL) were introduced. Then, the mixture was cooled to -78 °C in an acetone-liquid nitrogen bath. *n*-butyllithium (7 mL, 1.6 mol·L<sup>-1</sup> in hexane) was added dropwise within few minutes. After an hour, trimethyl borate (2 mL) was added. The resulting mixture was allowed to react for another 2 h at -78 °C and 1 h at room temperature. The reaction was then quenched by 3 N HCl and stirred for another 2 h. The mixture was then extracted with ethyl acetate and separated by column chromatography (acetone: petroleum ether = 1: 1) to give a pale brown solid 0.9 g. Yield: 55.7%. <sup>1</sup>H NMR (400 MHz, DMSO, ppm): 2.66 (s, 3 H, -CH<sub>3</sub>), 8.08 (s, 1 H, Thiophene-H), 8.17 (s, 2 H, -OH), 9.78 (s, 1 H, -CHO). <sup>13</sup>C NMR (DMSO, 75 MHz): 16.72, 139.87, 145.11, 159.83, 183.62

### 5.2.3.4 2-(5-(1,3-dioxan-2-yl)-2-methylthiophen-3-yl)-1,3,2-dioxaborinane



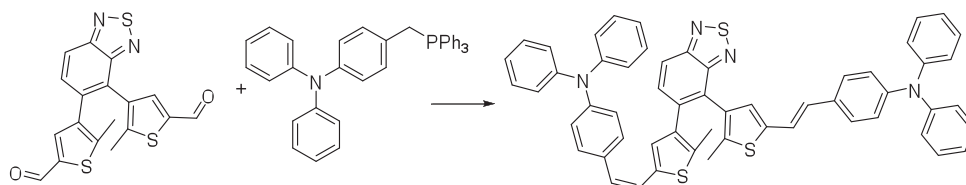
To a 50 mL single necked flask was added 5-formyl-2-methylthiophen-3-ylboronic acid (0.68 g, 4 mmol), 1, 3-propanediol (0.63 g, 8.4 mmol) dissolved in 25 mL toluene. The mixture was allowed to reflux for 3.5 h. After the reaction, toluene was removed by rotary evaporator to give pale yellow oil like product. The product was pure enough according to the TLC and was used directly without any purification and characterization.

### 5.2.3.5 Synthesis of 4,4'-(benzo[c][1,2,5]thiadiazole-4,5-diyl)bis(5-methylthiophene-2-carbaldehyde)



To 100 mL rounded flask was added boronic acid (1.4 g, 5.22 mmol), 4,5-dibromobenzothiadiazole (0.58 g, 2 mmol), Pd(PPh<sub>3</sub>)<sub>4</sub> (60 mg), dioxane (30 mL), 2 M Na<sub>2</sub>CO<sub>3</sub> (aq) (30 mL). The mixture was refluxed for 25 h. Then, the reactant was poured into 3N HCl and stirred for 3h. Subsequently, the resulting water phase was extracted with ethyl acetate, separated by column with a mixture of petroleum de ether: ethyl acetate = 2:1 to give 570 mg of the product. Yield: 57%. <sup>1</sup>H NMR (400 MHz, CDCl<sub>3</sub>, ppm): 2.14 (s, 3 H, -CH<sub>3</sub>), 2.29 (s, 3 H, -CH<sub>3</sub>), 7.37 (s, 1 H, Thiophene-H), 7.56 (s, 1 H, Thiophene-H), 7.63 (d, *J* = 9.2 Hz, 1 H, -Ph-H), 8.10 (d, 1 H, *J* = 9.2 Hz, -Ph-H), 9.73 (s, 1 H, -CHO), 9.78 (s, 1 H, -CHO)

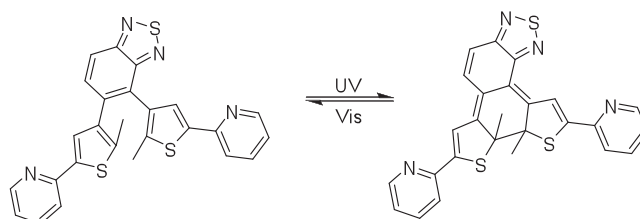
### 5.2.3.6 DTPA



To a 100 mL rounded flask was added aldehyde (100 mg, 0.26 mmol), 10 mL DMF and 10 mg 18-crown-6. TPA (0.45 mg, 0.78 mmol) dissolved in 10 mL DMF was added dropwise to the flask. After 6 h reaction at room temperature, the reactant was poured into water to give a mixture orange solid of *E* and *Z* form. The collected solid was dried in vacuum and dissolved in 40 mL THF with catalyst amount of iodine to be refluxed for 6 h. The reactant was poured into water, extracted with ethyl acetate, separated by column with a mixture of (petroleum ether: ethyl acetate = 15: 1 v/v) to give 36 mg.  $^1\text{H NMR}$  (400 MHz, DMSO, ppm): 1.97 (s, 3 H,  $-\text{CH}_3$ ), 2.15 (s, 3 H,  $-\text{CH}_3$ ), 6.68 (d,  $J = 4$  Hz, 1 H,  $-\text{CH}=\text{CH}-$ ), 6.72 (d,  $J = 4$  Hz, 1 H,  $-\text{CH}=\text{CH}-$ ), 6.81 (s, 1 H, Thiophene-H), 6.86 (dd,  $J_1 = 9$  Hz,  $J_2 = 2$  Hz, 4 H,  $-\text{Ph-H}$ ), 6.95 (s, 1 H, Thiophene-H), 6.98 (m, 12 H,  $-\text{Ph-H}$ ), 7.10 (d,  $J = 16$  Hz, 1 H,  $-\text{CH}=\text{CH}-$ ), 7.16 (d,  $J = 16$  Hz, 1 H,  $-\text{CH}=\text{CH}-$ ), 7.28 (t,  $J = 8$  Hz, 8 H,  $-\text{Ph-H}$ ), 7.38 (dd,  $J_1 = 8$  Hz,  $J_2 = 6$  Hz, 4 H,  $-\text{Ph-H}$ ), 7.74 (d,  $J = 9$  Hz, 1 H,  $-\text{Ph-H}$ ), 8.11 (d,  $J = 9$  Hz, 1 H,  $-\text{Ph-H}$ )

### 5.3 Optical properties and photochromism

BTP in hexane:THF = 4:1 and DTPA appeared to be pale yellow, which have absorption bands at 400 nm and 374 nm before irradiation, respectively. Upon UV irradiation at 365nm, the solution of BTP and DTPA quickly turned deep green and green yellow with new bands appearing in the visible region around 680 nm and 720 nm (Figures 5.4 and 5.7), which correspond to the intramolecular charge transfer (ICT) transition band of the closed form produced by photocyclization. Moreover, the *c*-BTP and *c*-DTPA can be bleached on irradiation of visible light ( $\lambda > 575$  nm, Figures 5.5 and 5.8). No obvious back reaction was observed for a prolonged time in the dark monitored at different wavelengths (Figure 5.6), but a slight thermal back reaction was observed for DTPA in hexane (Figure 5.9). The fatigue resistance test was carried out in the solvent ratio of hexane:THF = 4:1 for BTP and in hexane for DTPA. The compound can be toggled between the open form and closed form by alternating the UV lamp (365 nm) and visible lamp (575 nm) for at least ten cycles but *ca.* 12% and 5% degradation were observed for BTP and DTPA, respectively (Figures 5.5 and 5.8).



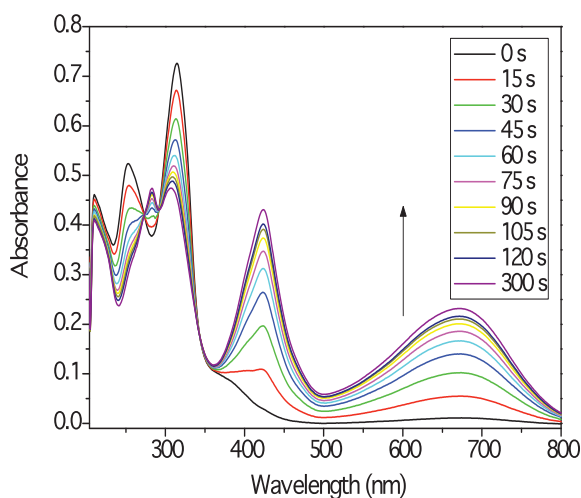


Fig. 5.4 Spectral changes of UV-Vis absorption of BTP upon irradiation at 365 nm. (in a mixture solvent of hexane:THF = 4:1,  $2 \times 10^{-5} \text{ mol}\cdot\text{L}^{-1}$ ) The photostationary state was obtained by irradiating BTP with 365 nm light until no spectral changes were observed.

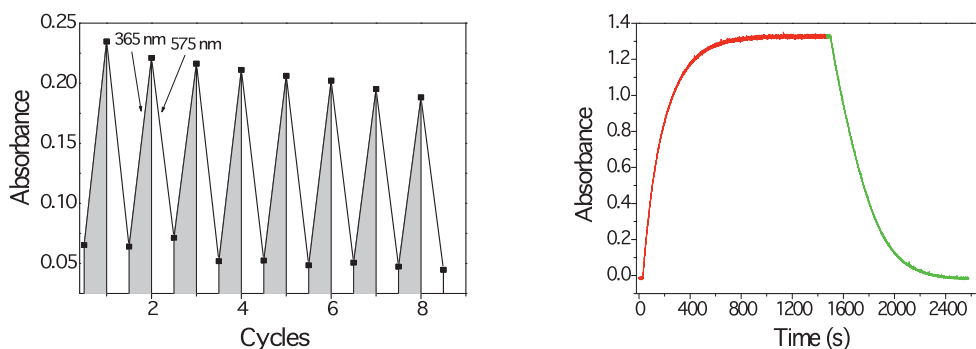


Fig. 5.5 Modulation of absorbance at 675 nm of BTP in a solvent mixture of hexane: THF = 4: 1 upon alternating illumination between UV (365 nm, shaded regions) and visible (575 nm, unshaded regions) light. Obvious degradation was observed within ten cycles.

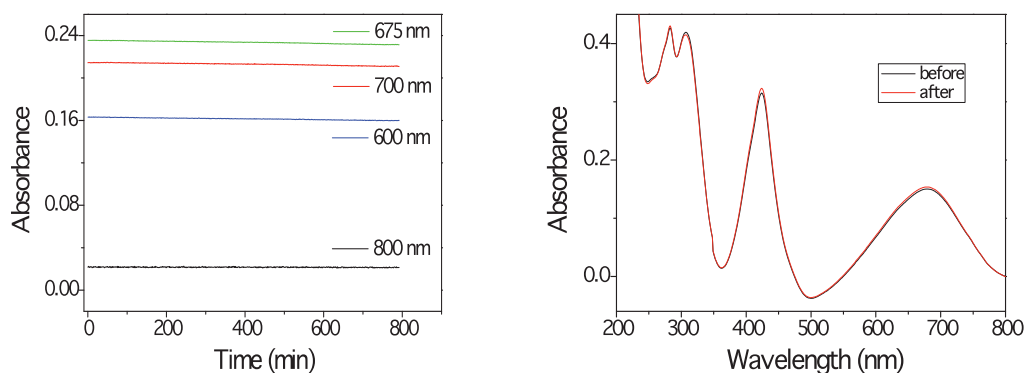
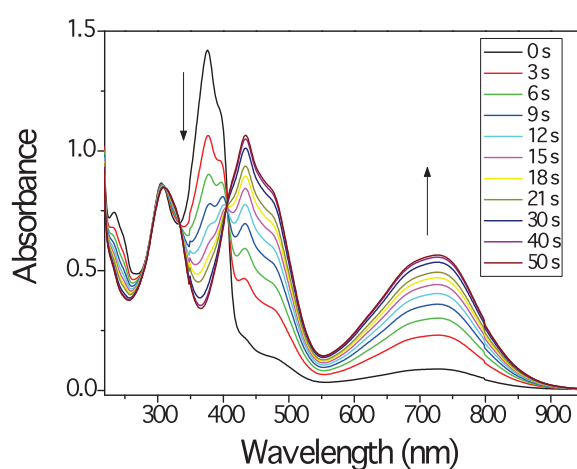
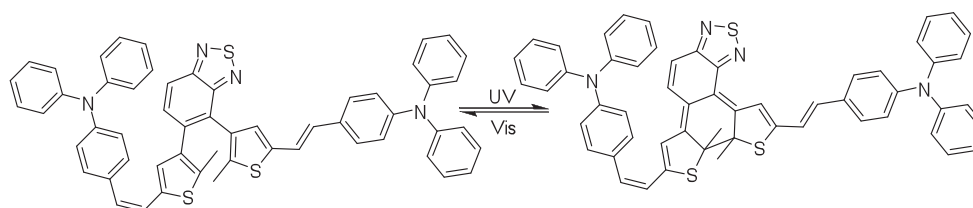
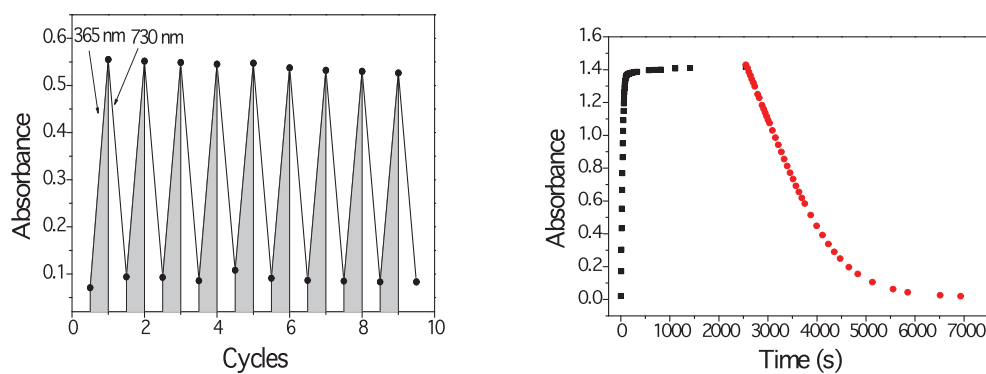


Fig. 5.6 Evolution of the absorbance (kinetic mode on CARY absorption spectrophotometer) overnight of BTP (in a mixture solvent of hexane: THF = 4:1,  $2 \times 10^{-5} \text{ mol}\cdot\text{L}^{-1}$ ) after stopping UV irradiation.

Absorption spectra upon UV irradiation: immediately after stopping the irradiation (before), and after leaving the sample in the dark for 800 min (after).



**Fig. 5.7** Spectral changes of UV-Vis absorption of DTPA upon irradiation at 365 nm (in hexane,  $2.07 \times 10^{-5} \text{ mol}\cdot\text{L}^{-1}$ ). The photostationary state was obtained by irradiating DTPA with 365 nm light until no spectral changes were observed.



**Fig. 5.8** Modulation of absorbance signals at 730 nm of DTPA in hexane upon alternating irradiation by UV lamp (365 nm, 3.02mW, shaded regions) and visible laser (730 nm with the input power of 900 mW for 25 min for each cycle, unshaded regions).



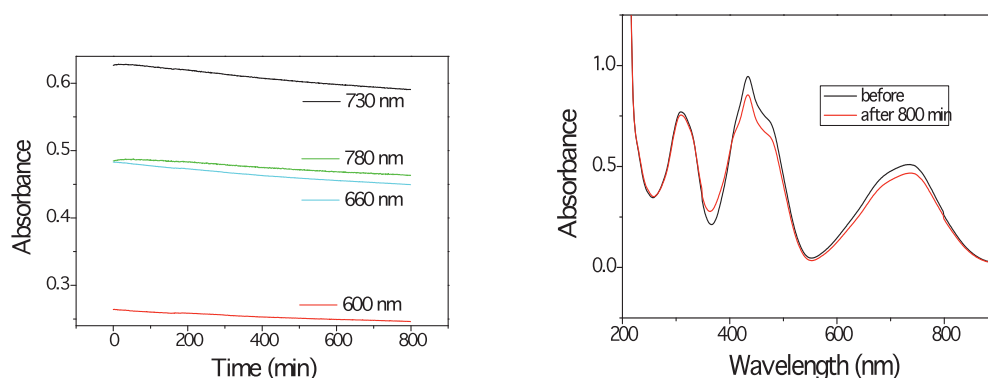


Fig. 5.9 Evolution of the absorbance (kinetic mode running on CARY absorption spectrophotometer) overnight of DTPA (in hexane,  $2.07 \times 10^{-5} \text{ mol}\cdot\text{L}^{-1}$ ) after stopping UV irradiation. Absorption spectra upon UV irradiation: immediately after stopping the irradiation (before), and after leaving the sample in the dark for 800 min (after).

#### 5.4 Conclusions

The main purpose of this chapter was to develop the photochromic compounds utilizing 2,1,3-benzothiadiazole to form photochromic complex and photoswitchable NLO materials. However, the complexation reaction could not be achieved in abovementioned conditions and the extended  $\pi$  system does not show any SHG before and after irradiation.

## Chapter 6 Conclusions

The dissertation is focused on the synthesis and study of novel BTEs with different central ethene bridges. The systems designed were carefully selected according to their difference in aromaticity realizing the evolution of thermal stability, thus demonstrating how the aromaticity of central ethene bridge affects the thermal stability of corresponding closed form.

In chapter 2, we incorporated high polar and electron-withdrawing chromophores of benzobisthiadiazole units as a novel family of six-membered ethene bridge to realize good photochromic performance with excellent fatigue resistance in solution as well as in crystal state. The fluorescence can be modulated by solvato- and photochromism due to the strong electron mobilization before and after irradiation. Additionally, a lower aromaticity of the central ethene moiety in BTEs leads to a higher thermal stability of the closed form. Since the ethene bridge with six-membered ring has its own advantages such as higher quantum yield in ring closure and longer absorption wavelength, we demonstrated that the six-membered ring with non-aromaticity as the center ethene bridge might widely extend the diversity in the thermally irreversible photochromic systems.

In chapter 3, we systematically reported the synthesis and photochromic properties of three ethene bridges with different degrees in aromaticity (BTE-NA, BTA and BTTA), which achieved obvious thermal stability evolution, and realizes the fluorescence modulation by solvato- and photo-chromism in the six-membered ethene bridged photochromic systems. An extremely low aromatic property of the central ethene bridge with benzobisthiadiazole unit finally leads to an unexpected thermally irreversible photochromic system (BTTA). Moreover, the small energy barrier between the parallel and anti-parallel conformers allows the full conversion from BTTA to *c*-BTTA. For the first time, the three ethene bridges with different degrees in aromaticity give a systematical comparison in the thermal stability evolution for their corresponding closed forms. This work contributes to the understanding of aromaticity-controlled thermal stability of photochromic systems based on six-membered rings as ethene bridges, and broadening novel building blocks for the photochromic BTE systems.

In chapter 4, benzothiadiazole was introduced directly as central ethene bridge as well as acceptor to form D- $\pi$ -A structure to achieve efficient photoswitchable nonlinear optical (NLO) materials. The strategy for the design of NLO switchable systems was based on the difference in efficiency in D- $\pi$ -A structure before and after irradiation caused by the coplanarity between

donor and benzothiadiazole ring. However, due to the strong  $\pi\cdots\pi$  interaction and planarity of benzothiadiazole ring, the compounds adopt a centrosymmetric packing in single crystal state.

In chapter 5, photochromic complex and photoswitchable NLO materials based on 2,1,3-benzothiadiazole were developed. However, the complexation reaction could not be finished in conventional conditions and the extended  $\pi$  system does not realize controllable Maker fringes before and after irradiation probably due to the centrosymmetric properties of DTPA.

## References

- [1] Ehrlich E., Flexner S. B., Carruth G., Hawkins J. H., Oxford American Dictionary, Oxford University Press: New York, 1980
- [2] Ballardini R., Balzani V., Credi A., Gandolfi M. T., Venturi M., Artificial Molecular-Level Machines: □ Which Energy To Make Them Work. *Acc. Chem. Res.*, 2001, 34(6): 445-455
- [3] Komura N., Zijlstra R. W., van Delden R. A., Harada N., Feringa B. L., Light-driven monodirectional molecular rotor. *Nature.*, 1999, 401(6749): 152-155
- [4] Clayden J., Pink J. H., Concerted Rotation in a Tertiary Aromatic Amide: Towards a Simple Molecular Gear. *Angew. Chem. Int. Ed.*, 1998, 37(13-14): 1937-1939
- [5] (a) Bissell R. A., Córdova E., Kaifer A. E., Stoddart J. F., A chemically and electrochemically switchable molecular shuttle. *Nature.*, 1994, 369(6476): 133-137 (b) Ashton P. R., Ballardini R., Balzani V., Baxter I., Credi A., Fyfe M. C. T., Spencer N., Stoddart F., Venturi M., White A. J. P., Williams D. J., Acid-Base Controllable Molecular Shuttles. *J. Am. Chem. Soc.*, 1998, 120(46): 11932-11942
- [6] Kelly T. R., Tellitu I., Sestelo J. P., In Search of Molecular Ratchets. *Angew. Chem. Int. Ed.*, 1997, 36(17): 1866-1868
- [7] (a) Guo Z. Q., Zhu W. H., Shen L. J., Tian H., A Fluorophore Capable of Crossword Puzzles and Logic Memory. *Angew. Chem. Int. Ed.*, 2007, 46(29): 5549-5553 (b) Guo Z. Q., Zhu W. H., Zhu M. M., Wu X. M., Tian H., Near-Infrared Cell-Permeable Hg<sup>2+</sup>-Selective Ratiometric Fluorescent Chemodosimeters and Fast Indicator Paper for MeHg<sup>+</sup> Based on Tricarbocyanines. *Chem. Eur. J.*, 2010, 16(48): 14424-14432 (c) Zhang K. D., Zhao X., Wang G. T., Liu Y., Zhang Y., Lu H. J., Jiang X. K., Li Z. T., Foldamer-Tuned Switching Kinetics and Metastability of [2]Rotaxanes. *Angew. Chem. Int. Ed.*, 2011, 50(42): 9866-9870
- [8] Schultz M., The end of the road for silicon. *Nature.*, 1999, 399(6738): 729-730
- [9] (a) *Supramolecular Chemistry*, Steed J. W., Atwood J. L., Eds.; John Wiley & Sons: New York, 2000, p463. (b) Lehn J. M., *Supramolecular Chemistry: Concepts and Perspectives*, VCH: New York, 1995, p139.
- [10] Griffiths J., Photochemistry of azobenzene and its derivatives. *Chem. Sov. Rev.*, 1972, 1(4): 481-493
- [11] (a) Lu X. Y., Guo Z. Q., Sun C. Y., Tian H., Zhu W. H., Helical Assembly Induced by Hydrogen Bonding from Chiral Carboxylic Acids Based on Perylene Bisimides. *J. Phys. Chem. B.*, 2011, 115(37): 10871-10876 (b) George S. J., Ajayaghosh A., Self-Assembled

- Nanotapes of Oligo(p-phenylene vinylene)s: Sol–Gel-Controlled Optical Properties in Fluorescent  $\pi$ -Electronic Gels. *Chem. Eur. J.*, 2005, 11(11): 3217-3227 (c) Ajayaghosh A., Varghese R., George S. J., Vijayakumar C., Transcription and Amplification of Molecular Chirality to Oppositely Biased Supramolecular  $\pi$  Helices. *Angew. Chem. Int. Ed.*, 2006, 45(7): 1003
- [12](a) Morimoto M., Irie M., A Diarylethene Cocrystal that Converts Light into Mechanical Work. *J. Am. Chem. Soc.*, 2010, 132(40): 14172-14178 (b) Uno K., Niikura H., Morimoto M., Ishibashi Y., Miyasaka H., Irie M., In Situ Preparation of Highly Fluorescent Dyes upon Photoirradiation. *J. Am. Chem. Soc.*, 2011, 133(34): 13558-13564 (c) Fukaminato T., Doi T., Tamaoki N., Okuno K., Ishibashi Y., Miyasaka H., Irie M., Single-Molecule Fluorescence Photoswitching of a Diarylethene–Perylenebisimide Dyad: Non-destructive Fluorescence Readout. *J. Am. Chem. Soc.*, 2011, 133(13): 4984-4990
- [13](a) Moriyama Y., Matsuda K., Tanifuji N., Irie Setsuko., Irie M., Electrochemical Cyclization/Cycloreversion Reactions of Diarylethenes. *Org. Lett.*, 2005, 7(15): 3315-3318 (b) Day J. H., Thermochromism. *Chem. Rev.*, 1963, 63(1): 65-80 (c) Peter A., Branda N. R., Electrochromism in Photochromic Dithienylcyclopentenes. *J. Am. Chem. Soc.*, 2003, 125(12): 3404-3405 (d) Yin M. F., Gong H. F., Zhang B. W., Liu M. H., Photochemical Reaction, Acidichromism, and Supramolecular Nanoarchitectures in the Langmuir–Blodgett Films of an Amphiphilic Styrylquinoxaline Derivative. *Langmuir*, 2004, 20(19): 8042-8048
- [14]Feringa B. L., Jager W. F., de Lange B., Organic materials for reversible optical data storage. *Tetrahedron*, 1993, 49(37): 8267-8310
- [15]Feringa B. L., Delden R. A., ter Wiel M. K. J., *Molecular Switches*; Feringa B. L., Ed.; Wiley-VCH: Weinheim, Germany, 2001; p 123
- [16]Fan M. G., Yu L., Zhao W., *Organic Photochromic and Thermochromic Compounds*, Vol 1, Crano J. C., Guglielmetti R. J., Eds.; Plenum Press: New York, 1999, p 141
- [17](a) Morimoto M., Kobatake S., Irie M., Multicolor Photochromism of Two- and Three-Component Diarylethene Crystals. *J. Am. Chem. Soc.*, 2003, 125(36): 11080-11087 (b) Ishow E., Brosseau A., Clavier G., Nakatani K., Pansu R. B., Vachon J. J., Tauc P., Chauvat D., Mendoça C. R., Piovesan E., Two-Photon Fluorescent Holographic Rewritable Micropatterning. *J. Am. Chem. Soc.*, 2007, 129(29): 8970-8971
- [18]Irie M., Mohri M., Thermally irreversible photochromic systems. Reversible photocyclization of diarylethene derivatives. *J. Org. Chem.*, 1988, 53(4): 803-808
- [19]Irie M., Diarylethenes for Memories and Switches. *Chem. Rev.*, 2000, 100(5): 1685-1716
- [20](a) Fischer E., Photosensitized isomerization of azobenzene. *J. Am. Chem. Soc.*, 1968, 90(3): 796–797 (b) Zimmerman G., Chow L. Y., Paik U. J., The Photochemical

- Isomerization of Azobenzene. *J. Am. Chem. Soc.*, 1958, 80(14): 3528–3531
- [21] Beharry A. A., Sadoski O., Woolley G. A., Azobenzene Photoswitching without Ultraviolet Light. *J. Am. Chem. Soc.*, 2011, 133(49): 19684–19687
- [22](a) Feringa B. L., van Delden R. A., Koumura N., Geertsema E. M., Chiroptical Molecular Switches. *Chem. Rev.*, 2000, 100(5): 1789–1816 (b) ter Wiel M. K. J., van Delden R. A., Meetsma A., Feringa B. L., Increased Speed of Rotation for the Smallest Light-Driven Molecular Motor. *J. Am. Chem. Soc.*, 2003, 125(49): 15076–15086
- [23](a) Yokoyama Y., Fulgides for Memories and Switches. *Chem. Rev.*, 2000, 100(5): 1717–1740 (b) Ishibashi Y., Murakami M., Miyasaka H., Kobatake S., Irie M., Yokoyama Y., Laser Multiphoton-Gated Photochromic Reaction of a Fulgide Derivative. *J. Phys. Chem. C*, 2007, 111(6): 2730–2737
- [24](a) Berkovic G., Krongauz V., Weiss V., Spiropyran and Spirooxazines for Memories and Switches. *Chem. Rev.*, 2000, 100(5): 1741–1754 (b) Tian Z. Y., Wu W. W., Wan W., Li A. D. Q., Single Chromophore Based Photoswitchable Nanoparticles Enable Dual Alternating Color Fluorescence for Unambiguous Live Cell Imaging. *J. Am. Chem. Soc.*, 2009, 131(12): 4245–4252
- [25] Irie M., Uchida K., Synthesis and Properties of Photochromic Diarylethenes with Heterocyclic Aryl Groups. *Bull. Chem. Soc. Jpn.*, 1998, 71(5): 985-996
- [26] Uchida K., Nakayama Y., Irie M., Thermally Irreversible Photochromic System. Reversible Photocyclization of 1,2-Bis(benzo[*b*]thiophene-3-yl)ethene Derivatives. *Bull. Chem. Soc. Jpn.*, 1990, 63(5): 1311-1315
- [27] Mechanism and Theory in Organic Chemistry, 3<sup>rd</sup> Edition, Lowry T. H., Richardson K. S., Eds.; Harper Collins Publishers: New York, 1987, p 1041
- [28] Spangenberg A., Perez J. A. P., Patra A., Piard J., Brosseau A., Métivier R., Nakatani K., Probing photochromic properties by correlation of UV-visible and infra-red absorption spectroscopy: a case study with cis-1,2-dicyano-1,2-bis(2,4,5-trimethyl-3-thienyl)ethene. *Photochem. Photobiol. Sci.*, 2010, 9(2): 188-193
- [29] Yumoto K., Irie M., Matsuda K., Control of the Photoreactivity of Diarylethene Derivatives by Quaternarization of the Pyridylethynyl Group. *Org. Lett.*, 2008, 10(10): 2051–2054
- [30] Takeshita M., Kato N., Kawauchi S., Imase T., Watanabe J., Irie M., Photochromism of Dithienylethenes Included in Cyclodextrins. *J. Org. Chem.*, 1998, 63(25): 9306–9313
- [31](a) Zhang J. J., Tan W. J., Meng X. L., Tian H., Soft mimic gear-shift with a multi-stimulus modified diarylethene. *J. Mater. Chem.*, 2009, 19(32): 5726-5729 (b) Yamaguchi T., Uchida K., Irie M., Asymmetric Photocyclization of Diarylethene Derivatives. *J. Am. Chem. Soc.*, 1997, 119(26): 6066–6071 (c) Ohsumi M., Fukaminato

- T., Irie M., Chemical control of the photochromic reactivity of diarylethene derivatives. *Chem. Commun.*, 2005(31): 3921-3923
- [32] Hohlneicher G., Mueller M., Demmer M., Lex J., Penn J. H., Gan L. X., Loesel P. D., 1,2-Diphenylcycloalkenes: electronic and geometric structures in the gas phase, solution, and solid state. *J. Am. Chem. Soc.*, 1988, 110(14): 4483-4494
- [33] Tian H., Chen B. Z., Tu H. Y., Müllen K., Novel Bisthiénylene-Based Photochromic Tetraazaporphyrin with photoregulating Luminescence. *Adv. Mater.*, 2002, 14(12): 918-923
- [34] Chen B. Z., Wang M. Z., Wu Y. Q., Tian H., Reversible near-infrared fluorescence switch by novel photochromic unsymmetrical-phthalocyanine hybrids based on bisthiénylene. *Chem. Commun.*, 2002(10): 1060-1061
- [35] Fukumoto S., Nakashima T., Kawai T., Intramolecular Hydrogen bonding in a Triangular Dithiazolyl-Azaindole for Efficient photoreactivity in Polar and Nonpolar solvents. *Eur. J. Org. Chem.*, 2011, 2011(26): 5047-5053
- [36] Li X. C., Ma Y. Z., Wang B. C., Li G. A., "Lock and key control" of Photochromic Reactivity by controlling the Oxidation/Reduction State. *Org. Lett.*, 2008, 10(16): 3639-3642
- [37] Jeong Y. C., Cao C. J., Lee I. S., Yang S. I., Ahn K. H., The considerable photostability improvement of photochromic tetrarylene by sulfone group. *Tetrahedron Lett.*, 2009, 50(37): 5288-5290
- [38] Chen S. J., Yang Y. H., Wu Y., Tian H., Zhu W. H., Multi-addressable photochromic terarylene containing benzo[*b*]thiophene-1,1-dioxide unit as ethene bridge: multifunctional molecular logic gates on unimolecular platform. *J. Mater. Chem.*, 2012, 22(12): 5486-5494
- [39] Li H. H., Chen Y., The Photochromism and Fluorescence of Diarylethenes with a Imidazole Bridge Unit: A Strategy for the Design of Turn-on Fluorescent Diarylethene System. *J. Phys. Chem. A.*, 2009, 113(19): 5550-5553
- [40] Duan G. P., Yam V. W. W., Syntheses and Photophysical Properties of *N*-Pyridylimidazol-2-ylidene Tetracyanoruthenates(II) and Photochromic Studies of Their Dithienylene-Containing Derivatives. *Chem. Eur. J.*, 2010, 16(42): 12642-12649
- [41] Duan G. P., Zhu N. Y., Yam V. W. W., Syntheses and Photochromic Studies of Dithienylene-Containing Imidazolium Derivatives and Their Reactivity towards Nucleophiles. *Chem. Eur. J.*, 2010, 16(44): 13199-13209
- [42] Duan G. P., Wong W. T., Yam V. W. W., Synthesis and photochromic studies of  $\eta^6$ -mesitylene ruthenium(II) complexes bearing *N*-heterocyclic carbene ligands with the dithienylene moiety. *New J. Chem.*, 2011, 35(10): 2267-2278

- [43] Lee P. H. M., Ko C. C., Zhu N. Y., Yam V. W. W., Metal Coordination-Assisted Near-Infrared Photochromic Behavior: A Large Perturbation on Absorption Wavelength Properties of N,N-Donor Ligands Containing Diarylethene Derivatives by Coordination to the Rhenium(I) Metal Center. *J. Am. Chem. Soc.*, 2007, 129(19): 6058-6059
- [44] Yam V. W. W., Lee J. K. W., Ko C. C., Zhu N. Y., Photochromic Diarylethene-Containing Ionic Liquids and N-Heterocyclic. *J. Am. Chem. Soc.*, 2009, 131(3): 912-913
- [45] Kawai S., Nakashima T., Atsumi K., Sakai T., Harigai M., Imamoto Y., Kamikubo H., Kataoka M., Kawai T., Novel Photochromic Molecules Based on 4,5-Dithienyl Thiazole with Fast Thermal Bleaching Rate. *Chem. Mater.*, 2007, 19(14): 3479-3483
- [46] Nakashima T., Atsumi K., Kawai S., Nakagawa T., Hasegawa Y., Kawai T., Photochromism of Thiazole-Containing Triangle Terarylenes. *Eur. J. Org. Chem.*, 2007, 2007(19): 3212-3218
- [47] Nakashima T., Fujii R., Kawai T., Regulation of Folding and Photochromic Reactivity of Terarylenes through a Host-Guest Interaction. *Chem. Eur. J.*, 2011, 17(39): 10951-10957
- [48] Nakagawa H., Kawai S., Nakashima T., Kawai T., Synthesis and Photochemical Reactions of Photochromic Terarylene Having a Leaving Methoxy Group. *Org. Lett.*, 2009, 11(7): 1475-1478
- [49] Ko C. C., Lam W. H., Yam V. W. W., Photochromic oligothienoacene derivatives with photo-switchable luminescence properties and computational studies. *Chem. Commun.*, 2008(41): 5203-5205
- [50] Wong H. L., Ko C. C., Lam W. H., Zhu N. Y., Yam V. W. W., Design and Synthesis of a New Class of Photochromic Diarylethene-Containing Dithieno[3,2-b:2',3'-d]pyrroles and Their Switchable Luminescence Properties. *Chem. Eur. J.*, 2009, 15(39): 10005-10009
- [51] Poon C. T., Lam W. H., Wong H. L., Yam V. W. W., A Versatile Photochromic Dithienylethene-Containing  $\beta$ -Diketonate Ligand: Near-Infrared Photochromic Behavior and Photoswitchable Luminescence Properties upon Incorporation of a Boron(III) Center. *J. Am. Chem. Soc.*, 2010, 132(40): 13992-13993
- [52] Chan J. C. H., Lam W. H., Wong H. L., Zhu N. Y., Wong W. T., Yam V. W. W., Diarylethene-Containing Cyclometalated Platinum(II) Complexes: Tunable Photochromism via Metal Coordination and Rational Ligand Design. *J. Am. Chem. Soc.*, 2011, 133(32): 12690-12705
- [53] Chen Y., Zeng D. X., Fan M. G., Synthesis and Photochromic Properties of Functional Diarylethene with a 2,5-Dihydrothiophene Bridging Unit. *Org. Lett.*, 2003, 5(9): 1435-1437
- [54] Poon C. T., Lam W. H., Yam V. W. W., Gated Photochromism in



- Triarylborane-Containing Dithienylethenes: A New Approach to a "Lock\_Unlock" System. *J. Am. Chem. Soc.*, 2011, 133(49): 19622-19625
- [55] Chen Y., Zeng D. X., Xie N., Dang Y. Z., Study on Photochromism of Diarylethenes with a 2,5-Dihydropyrrole Bridging Unit: A Convenient Preparation of 3,4-Diarylpyrroles from 3,4-Diaryl-2,5-dihydropyrroles. *J. Org. Chem.*, 2005, 70(13): 5001-5005
- [56] Belser P., Kühni J., Gated Photochromism of 1,2-Diarylethenes. *Org. Lett.*, 2007, 9(10): 1915-1918
- [57] Morinaka K., Ubukata T., Yokoyama Y., Structurally Versatile Novel Photochromic Bisarylindenone and Its Acetal: Achievement of Large Cyclization Quantum Yield. *Org. Lett.*, 2009, 11(17): 3890-3893
- [58] Yam V. W. W., Ko C. C., Zhu N. Y., Photochromic and Luminescence Switching Properties of a Versatile Diarylethene-Containing 1,10-Phenanthroline Ligand and Its Rhenium(I) Complex. *J. Am. Chem. Soc.*, 2004, 126(40): 12734-12735
- [59] Lemieux V., Branda N. R., Reactivity-Gated Photochromism of 1,2-Dithienylethenes for Potential Use in Dosimetry Applications. *Org. Lett.*, 2005, 7(14): 2969-2972
- [60] Suzuki K., Ubukata T., Yokoyama Y., Dual-mode fluorescence switching of photochromic bisthiazolylcoumarin. *Chem. Commun.*, 2012, 48(5): 765-767
- [61] Deng X. H., Liebeskind L. S., A Contribution to the Design of Molecular Switches: Novel Acid-Mediated Ring-Closing-Photochemical Ring-Opening of 2,3-Bis(heteroaryl)quinines (Heteroaryl = Thienyl, Furanyl, Pyrrolyl)., *J. Am. Chem. Soc.*, 2001, 123(31): 7703-7704
- [62] Evans R. A., Hanley T. L., Skidmore M. A., Davis T. P., Such G. K., Yee L. H., Ball G. E., Lewis D. A., The generic enhancement of photochromic dye switching speeds in a rigid polymer matrix. *Nature Mater.*, 2005, 4(3): 249-253
- [63] Tian H., Feng Y. L., Next step of photochromic switches. *J. Mater. Chem.*, 2008, 18(14): 1617-1622
- [64] Yagai S., Kitamura A., Recent advances in photoresponsive supramolecular self-assemblies. *Chem. Soc. Rev.*, 2008, 37(8), 1520-1529
- [65] Raymo F. M., Tomasulo M., Fluorescence Modulation with Photochromic Switches. *J. Phys. Chem. A.*, 2005, 109(33): 7343-7352
- [66] Kärnbratt J., Hammarson M., Li S. M., Anderson H. L., Albinsson B., Andréasson J., Photochromic Supramolecular Memory With Nondestructive Readout. *Angew. Chemie Int. Ed.*, 2010, 49(10): 1854-1857
- [67] Jiang G. Y., Song Y. L., Guo X. F., Zhang D. Q., Zhu D. B., Organic Functional Molecules towards Information Processing and High-Density Information Storage. *Adv.*

- Mater., 2008, 20(15): 2888-2898
- [68] Berberich M., Krause A. M., Orlandi M., Scandola F., Wurthner F., Switches Toward Fluorescent Memories with Nondestructive Readout: Photoswitching of Fluorescence by Intramolecular Electron Transfer in a Diaryl Ethene-Perylene Bisimide Photochromic System. *Angew. Chem. Int. Ed.*, 2008, 47(35): 6616–6619
- [69] Zhu M. Q., Zhu L. Y., Han J. J., Wu W. W., Hurst J. K., Li A. D. Q., Spiropyran-Based Photochromic Polymer Nanoparticles with Optically Switchable Luminescence. *J. Am. Chem. Soc.*, 2006, 128(13): 4303–4309
- [70] Arai R., Uemura S., Irie M., Matsuda K., Reversible Photoinduced Change in Molecular Ordering of Diarylethene Derivatives at a Solution–HOPG Interface. *J. Am. Chem. Soc.*, 2008, 130(29): 9371–9379
- [71] Irie M., Fukaminato T., Sasaki T., Tamai N., Kawai T., Organic chemistry: A digital fluorescent molecular photoswitch. *Nature.*, 2002(420): 759–760
- [72] Tian H., Data Processing on a Unimolecular Platform. *Angew. Chem. Int. Ed.*, 2010, 49(28): 4710–4712
- [73] Samachetty H. D., Branda N. R., Integrating molecular switching and chemical reactivity using photoresponsive hexatrienes. *Pure Appl. Chem.*, 2006, 78(12): 2351–2359
- [74] Andréasson J., Straight S. D., Moore T. A., Molecular All-Photonic Encoder–Decoder. *J. Amer. Chem. Soc.*, 2008, 130(33): 11122–11128
- [75] Yokoyama Y., Shiozawa T., Tani Y., Ubukata T., A Unified Strategy for Exceptionally High Diastereoselectivity in the Photochemical Ring Closure of Chiral Diarylethenes. *Angew. Chem. Int. Ed.*, 2009, 48(25): 4521–4523
- [76] Higashiguchi K., Matsuda K., Tanifuji N., Irie M., Full-Color Photochromism of a Fused Dithienylethene Trimer. *J. Am. Chem. Soc.*, 2005, 127(25): 8922–8923
- [77] Zou Y., Yi T., Xiao S. Z., Li F. Y., Li C. Y., Gao X., Wu J. C., Yu M. X., Huang C. H., Amphiphilic Diarylethene as a Photoswitchable Probe for Imaging Living Cells. *J. Am. Chem. Soc.*, 2008, 130(47): 15750–15751
- [78] Xie N., Chen Y., Construction and photoswitching properties of fluorescent diarylethenes. *J. Mater. Chem.*, 2007, 17(9): 861-865
- [79] de Jong J. J. D., Wegman T. D. T., van Esch J. H., Feringa B. L., Dynamic Chiral Selection and Amplification Using Photoresponsive Organogelators. *J. Am. Chem. Soc.*, 2005, 127(40): 13804–13805
- [80] Wang S., Shen W., Feng Y. L., Tian H., A multiple switching bisthienylethene and its photochromic fluorescent organogelator. *Chem. Commun.*, 2006, 2006(14): 1497-1499
- [81] Pu S. Z., Liu G., Shen L., Xu J. K., Efficient Synthesis and Properties of Isomeric Photochromic Diarylethenes Having a Pyrrole Unit. *Org. Lett.*, 2007, 9(11): 2139–2142

- [82] Ko C. C., Kwok W. M., Yam V. W. W., Phillips D. L., Triplet MLCT Photosensitization of the Ring-Closing Reaction of Diarylethenes by Design and Synthesis of a Photochromic Rhenium(I) Complex of a Diarylethene-Containing 1,10-Phenanthroline Ligand. *Chem. Eur. J.*, 2006, 12(22): 5840-5848
- [83] Meng X. L., Zhu W. H., Zhang Q., Feng Y. L., Tan W. J., Tian H., Novel Bisthiénylethenes Containing Naphthalimide as the Center Ethene Bridge: Photochromism and Solvatochromism for Combined NOR and INHIBIT Logic Gates. *J. Phys. Chem. B*, 2008, 112(49): 15636–15645
- [84] Zhu W. H., Meng X. L., Yang Y. H., Zhang Q., Xie Y. S., Tian H., Bisthiénylethenes Containing a Benzothiadiazole Unit as a Bridge: Photochromic Performance Dependence on Substitution Position. *Chem. Eur. J.*, 2010, 16(3): 899-906
- [85] Komin A. P., Carmack M., The chemistry of 1,2,5-thiadiazoles, IV. Benzo[1,2-c:3,4-c':5,6-c''] tris [1,2,5] thiadiazole. *J. Heterocyclic Chem.*, 1975, 12(5): 829–833
- [86] Irie M., Sayo K., Solvent effects on the photochromic reactions of diarylethene derivatives. *J. Phys. Chem.*, 1992, 96(19): 7671–7674
- [87] Ohsumi M., Hazama M., Fukaminato T., Irie M., Photocyclization reaction of a diarylmalimide derivative in polar solvents. *Chem. Commun.*, 2008(28): 3281-3283
- [88] Delbaere S., Vermeersch G., NMR spectroscopy applied to photochromism investigations. *J. Photochem. Photobiol. C. Photochem. Rev.*, 2008, 9(2): 61-80
- [89] Yamaguchi T., Irie M., Photochromism of 1,2-Bis(2-alkyl-1-benzofuran-3-yl)perfluorocyclopentene Derivatives. *Eur. J. Org. Chem.*, 2006, 2006(14): 3105-3111
- [90] Takeshita M., Irie M., Enhancement of the photocyclization quantum yield of 2,2'-dimethyl-3,3'-(perfluorocyclopentene-1,2-diyl)bis(benzo[b]-thiophene-6-sulfonate) by inclusion in a cyclodextrin cavity. *Chem. Commun.*, 1997, 1997(23): 2265-2266
- [91] Lippert V. E., Spektroskopische Bestimmung des Dipolmomentes aromatischer Verbindungen im ersten angeregten Singulettzustand., 1957, 61: 962-975
- [92] Mataga N., Kaifu Y., Koizumi M., Solvent effects upon fluorescence spectra and dipole moments of excited molecules. *Bull. Chem. Soc. Jpn.*, 1956, 29(4): 465-470
- [93] J. R. Lakowicz, *Principles of Fluorescence Spectroscopy*, Springer, 2006, pp. 205–216
- [94] Gaussian 09, Revision A.02, M. J. Frisch, G. W. Trucks, H. B. Schlegel, G. E. Scuseria, M. A. Robb, J. R. Cheeseman, G. Scalmani, V. Barone, B. Mennucci, G. A. Petersson, H. Nakatsuji, M. Caricato, X. Li, H. P. Hratchian, A. F. Izmaylov, J. Bloino, G. Zheng, J. L. Sonnenberg, M. Hada, M. Ehara, K. Toyota, R. Fukuda, J. Hasegawa, M. Ishida, T. Nakajima, Y. Honda, O. Kitao, H. Nakai, T. Vreven, J. A. Montgomery, Jr., J. E. Peralta,

- F. Ogliaro, M. Bearpark, J. J. Heyd, E. Brothers, K. N. Kudin, V. N. Staroverov, R. Kobayashi, J. Normand, K. Raghavachari, A. Rendell, J. C. Burant, S. S. Iyengar, J. Tomasi, M. Cossi, N. Rega, J. M. Millam, M. Klene, J. E. Knox, J. B. Cross, V. Bakken, C. Adamo, J. Jaramillo, R. Gomperts, R. E. Stratmann, O. Yazyev, A. J. Austin, R. Cammi, C. Pomelli, J. W. Ochterski, R. L. Martin, K. Morokuma, V. G. Zakrzewski, G. A. Voth, P. Salvador, J. J. Dannenberg, S. Dapprich, A. D. Daniels, O. Farkas, J. B. Foresman, J. V. Ortiz, J. Cioslowski, and D. J. Fox, Gaussian, Inc., Wallingford CT, 2009.
- [95] Adamo C., Barone V., Toward reliable density functional methods without adjustable parameters: The PBE0 model. *J. Chem. Phys.*, 1999, 110(13): 6158–6170
- [96] Cancès E., Mennucci B., A new integral equation formalism for the polarizable continuum model: Theoretical background and applications to isotropic and anisotropic dielectrics. *J. Chem. Phys.*, 1997, 107(8): 3032–3041
- [97] Nakamura S., Irie M., Thermally irreversible photochromic systems. A theoretical study. *J. Org. Chem.* 1988, 53(26): 6136–6138
- [98] Sheldrick G. M., A short history of SHELX. *Acta Crystallographica. Section. A.*, 2008, 64(1): 112-122
- [99] Dolomanov O. V., Bourhis L. J., Gildea R. J., Howard J. A. K., Puschmann H., OLEX2: a complete structure solution, refinement and analysis program. *J. Appl. Cryst.*, 2009, 42(2): 339-341
- [100] Kobatake S., Uchida K., Tsuchida E., Irie M., Single-crystalline photochromism of diarylethenes: reactivity–structure relationship. *Chem. Commun.*, 2002, 2002(23): 2804-2805
- [101] Morimoto M., Kobatake S., Irie M., Polymorphism of 1,2-Bis(2-methyl-5-p-methoxyphenyl-3-thienyl)perfluorocyclopentene and Photochromic Reactivity of the Single Crystals. *Chem. Eur. J.*, 2003, 9(3): 621-627
- [102] Andréasson J., Pischel U., Smart molecules at work—mimicking advanced logic operations. *Chem. Sov. Rev.*, 2010, 39(1): 174-188
- [103] Raymo F. M., Tomasulo M., Electron and energy transfer modulation with photochromic switches. *Chem. Sov. Rev.*, 2005, 34(4): 327-336
- [104] Darwish T. A., Evans R. A., James M., Malic N., Triani G., Hanley T. L., CO<sub>2</sub> Triggering and Controlling Orthogonally Multiresponsive Photochromic Systems. *J. Am. Chem. Soc.*, 2010, 132(31): 10748–10755
- [105] Zhu L. Y., Zhu M. Q., Hurst J. K., Li A. D. Q., Light-Controlled Molecular Switches Modulate Nanocrystal Fluorescence. *J. Am. Chem. Soc.*, 2005, 127(25): 8968–8970
- [106] Tian Z. Y., Wu W. W., Li A. D. Q., Photoswitchable Fluorescent Nanoparticles:

- Preparation, Properties and Applications. *ChemPhysChem*, 2009, 10(15): 2577-2591
- [107] Spangenberg A., Métivier R., Gonzalez J., Nakatani K., Yu P., Giraud M., Léaustic A., Guillot R., Uwada T., Asahi T., Multiscale Approach of Photochromism: Synthesis and Photochromic Properties of a Diarylethene in Solution, in Nanoparticles, and in Bulk Crystals. *Adv. Mater.*, 2009, 21(3): 309–313
- [108] Spangenberg A., Brosseau A., Métivier R., Sliwa M., Nakatani K., Asahi T., Uwada T., Fabrication of nanoscale photochromic materials by vapor deposition method. *J. Phys. Org. Chem.* 2007, 20(11): 985–991
- [109] Remónt P., Bälter M., Li S. M., Andréasson J., Pischel U., An All-Photonic Molecule-Based D Flip-Flop. *J. Am. Chem. Soc.* 2011, 133(51): 20742–20745
- [110] Yamamoto S., Matsuda K., Irie M., Absolute Asymmetric Photocyclization of a Photochromic Diarylethene Derivative in Single Crystals. *Angew. Chem. Int. Ed.* 2003, 42(14): 1636–1639
- [111] Yamaguchi T., Irie M., Photochromic and fluorescent properties of bisfurylethene derivatives. *J. Mater. Chem.*, 2006, 16(48): 4690-4694
- [112] Yagi K., Irie M., Fluorescence Property of Photochromic Diarylethenes with Indole Groups. *Bull. Chem. Soc. Jpn.*, 2003, 76(8): 1625-1628
- [113] Wu Y., Chen S. J., Yang Y. H., Zhang Q., Xie Y. S., Tian H., Zhu W. H., A novel gated photochromic reactivity controlled by complexation/dissociation with BF<sub>3</sub>. *Chem. Commun.*, 2012, 48(4): 528-530
- [114] Gorodetsky B., Branda N. R., Bidirectional Ring-Opening and Ring-Closing of Cationic 1,2-Dithienylcyclopentene Molecular Switches Triggered with Light or Electricity. *Adv. Funct. Mater.*, 2007, 17(5): 786–796
- [115] Tian H., Chen B. Z., Liu P. H., A Novel Photochromic Amorphous Molecular Material Based on Bisthiénylethene with a Spiro-linker. *Chem. Lett.*, 2001, 30(10): 990–991
- [116] Zhu W. H., Yang Y. H., Métivier R., Zhang Q., Guillot R., Xie Y. S., Tian H., Nakatani K., Unprecedented Stability of a Photochromic Bisthiénylethene Based on Benzobisthiadiazole as an Ethene Bridge. *Angew. chemie. Int. Ed.*, 2011, 50(46): 10986-10990
- [117] Zhu W. H., Wu Y. Z., Wang S. T., Li X., Chen J., Wang Z. S., Tian H., Organic D-A- $\pi$ -A Solar Cell Sensitizers with Improved Stability and Spectral Response. *Adv. Funct. Mater.*, 2011, 21(4): 756–763
- [118] Zou Q., Tian H., Chemodosimeters for mercury(II) and methylmercury(I) based on 2,1,3-benzothiadiazole. *Sensor Actuat B-Chem.* 2010, 149(1): 20–27
- [119] Zhong C. M., Duan C. H., Huang F., Wu H. B., Cao Y., Materials and Devices

- toward Fully Solution Processable Organic Light-Emitting Diodes. *Chem. Mater.*, 2011, 23(3): 326–340
- [120] Chen S. H., Li Y. J., Yang W. L., Chen N., Liu H. B., Li Y. L., Synthesis and Tuning Optical Nonlinear Properties of Molecular Crystals of Benzothiadiazole. *J. Phys. Chem. C*, 2010, 114(35): 15109–15115
- [121] Qian X. H., Xiao Y., Xu Y. F., Guo X. F., Qian J. H., Zhu W. P., “Alive” dyes as fluorescent sensors: fluorophore, mechanism, receptor and images in living cells. *Chem. Commun.*, 2010, 46(35): 6418-6436
- [122] Zhang L. J., He C., Chen J. W., Yuan P., Huang L., Zhang C., Cai W. Z., Liu Z. T., Cao Y., Bulk-Heterojunction Solar Cells with Benzotriazole-Based Copolymers as Electron Donors: Largely Improved Photovoltaic Parameters by Using PFN/Al Bilayer Cathode. *Macromolecules*, 2010, 43(23): 9771–9778
- [123] Li C., Liu M. Y., Pschirer N. G., Baumgarten M., Mullen K., Polyphenylene-Based Materials for Organic Photovoltaics. *Chem. Rev.*, 2010, 110(11): 6817–6855
- [124] Kawai S. H., Gilat S. L., Ponsinet R., Lehn J. L., A Dual-Mode Molecular Switching Device: Bisphenolic Diarylethenes with Integrated Photochromic and Electrochromic Properties. *Chem. Eur. J.*, 1995, 1(5): 285–293
- [125] Ko C. C., Wu L. X., Wong K. M. C., Zhu N. Y., Yam V. W. W., Synthesis, Characterization and Photochromic Studies of Spirooxazine-Containing 2,2'-Bipyridine Ligands and Their Rhenium(i) Tricarbonyl Complexes. *Chem. Eur. J.*, 10(3): 766-776
- [126] G. M. Sheldrick, SHELXS97 and SHELXL97 Programs for Crystal Structure Solution and Refinement; University of Göttingen, Göttingen, Germany, 1997
- [127] Wu J. C., Yi T., Shu T. M., Yu M. X., Zhou Z. G., Xu M., Zhou Y. F., Zhang H. J., Han J. T., Li F. Y., Huang C. H., Ultrasound Switch and Thermal Self-Repair of Morphology and Surface Wettability in a Cholesterol-Based Self-Assembly System. *Angew. Chem. Int. Ed.*, 2008, 47(6): 1063-1067
- [128] Ahmed S. A. M., Pozzo J. L., Photochromism of dihydroindolizines Part IX: First attempts towards efficient self-assembling organogelators based on photochromic dihydroindolizines and N-acyl-1, $\omega$ -amino acid units. *J. Photochem. Photobio. A-Chem.*, 2008, 200(1): 57–67
- [129] Delaire J. A., Nakatani K., Linear and Nonlinear Optical Properties of Photochromic Molecules and Materials. *Chem. Rev.*, 2000, 100(5): 1817–1846
- [130] Asselberghs I., Clays K., Persoons A., Ward M. D., McCleverty J., Switching of molecular second-order polarisability in solution. *J. Mater. Chem.*, 2004, 14(19): 2831-2839

- [131] Coe B. J., Molecular Materials Possessing Switchable Quadratic Nonlinear Optical Properties. *Chem. Eur. J.*, 5(9): 2464-2471
- [132] Samoc M., Gauthier N., Cifuentes M. P., Paul F., Lapinte C., Humphrey M. G., Electrochemical Switching of the Cubic Nonlinear Optical Properties of an Aryldiethynyl-Linked Heterobimetallic Complex between Three Distinct States. 45(44): 7376-7379
- [133] Cao B. J., Houbrechts S., Asselberghs I., Persoons A., Efficient, Reversible Redox-Switching of Molecular First Hyperpolarizabilities in Ruthenium(II) Complexes Possessing Large Quadratic Optical Nonlinearities. *Angew. Chemie. Int. Ed.*, 1999, 38(3): 366-369
- [134] Malaun M., Reeves Z. R., Paul R. L., Jeffery J. C., McCleverty J. A., Ward M. D., Asselberghs I., Clays K., Persoons A., Reversible switching of the first hyperpolarisability of an NLO-active donor-acceptor molecule based on redox interconversion of the octamethylferrocene donor unit. *Chem. Commun.*, 2001, 2001(1): 49-50
- [135] Paul F., Costuas K., Ledoux I., Deveau S., Zyss J., Halet J. F., Lapinte C., Redox-Switchable Second-Order Molecular Polarizabilities with Electron-Rich Iron  $\sigma$ -Aryl Acetylides. *Organometallics.*, 2002, 21(24): 5229-5235
- [136] Asselberghs I., Clays K., Persoons A., McDonagh A. M., Ward M. D., McCleverty J. A., In situ reversible electrochemical switching of the molecular first hyperpolarizability. 2003, 368(3-4): 408-411
- [137] Gilat S. L., Kawai S. H., Lehn J. M., Light-Triggered Molecular Devices: Photochemical Switching Of optical and Electrochemical Properties in Molecular Wire Type Diarylethene Species. *Chem. Eur. J.*, 1(5): 275-284
- [138] Nakatani K., Delaire J. A., Reversible Photoswitching of Second-Order Nonlinear Optical Properties in an Organic Photochromic Crystal. *Chem. Mater.*, 1997, 9(12): 2682-2684
- [139] Sanguinet L., Pozz J. L., Acido- and Phototriggered NLO Properties Enhancement. *J. Phys. Chem. B*, 2005, 109 (22): 11139-11150
- [140] Giraud M., Léaustic A., Guillot R., Yu P., Lacroix P. G., Nakatani K., Pansu R., Maurel F., Dithiazolylethene-based molecular switches for nonlinear optical properties and fluorescence: synthesis, crystal structure and ligating properties. *J. Mater. Chem.*, 2007, 17(41): 4414-4425
- [141] Bourgault M., Baum K., Le Bozec H., Pucetti G., Ledoux I., Zyss J., Synthesis and molecular hyperpolarisabilities of donor-acceptor bipyridyl metal complexes (M=Re, Zn, Hg). *New J. Chem.*, 1998, 22(5): 517-522

- [142] Maury O., Guégan J. P., Renouard T., Hilton A., Dupau P., Sandon N., Toupet L., Le Bozec H., Design and synthesis of 4,4' -  $\pi$  -conjugated[2,2' ]-bipyridines: a versatile class of tunable chromophores and fluorophores. *New J. Chem.*, 2001, 25(12): 1553-1566
- [143] Maury O., Viau L., Sénéchal K., Corre B., Guégan J. P., Renouard T., Ledoux I., Zyss J., Le Bozec H., Synthesis, Linear, and Quadratic-Nonlinear Optical Properties of Octupolar D3 and D2d Bipyridyl Metal Complexes. *Chem. Eur. J.*, 2004, 10(18): 4454-4466
- [144] Maury O., Le Bozec H., Molecular Engineering of Octupolar NLO Molecules and Materials Based on Bipyridyl Metal Complexes. *Acc. Chem. Res.*, 2005, 38(9): 691-704
- [145] Franken P.A., Hill A.E., Peters C.W., Weinreich G., Generation of optical harmonics. *Phys. Rev. Letters.*, 1961, 7(4): 118-119
- [146] Zyss J., Oudar J.-L., Relation between microscopic and macroscopic lowest-order optical nonlinearities of molecular crystals with one- or twodimensional units. *Phys. Rev. A.*, 1982, 26, p. 2028.
- [147] Levine B. F., Bethea C. G., Absolute signs of hyperpolarizabilities in the liquid state. *J. Chem. Phys.*, 1974, 60(10): 3856-3858
- [148] Zyss J., Ledoux I., Nonlinear optics in multipolar media: theory and experiments. *Chem. Rev.*, 1994, 94(1): 77-105
- [149] Youngmin Y., Jangwon S., Se H. K., Kil S. K., Tae K. A., Dongho K. Soo Y. P., Highly Phosphorescent Iridium Complexes with Chromophoric 2-(2-Hydroxyphenyl)oxazole-Based Ancillary Ligands: Interligand Energy-Harvesting Phosphorescence. *Inorg. Chem.*, 2008, 47 (5): 1476-1487



## Appendix I

**Fluorescence lifetimes** were measured by the time-correlated single-photon counting (TCSPC) method with femtosecond laser excitation using a Spectra-Physics set-up composed of a Titanium Sapphire Tsunami laser pumped by a doubled YAG laser Millennia, pumped itself by two laser diode arrays. Light pulses at 700 nm were selected by optoacoustic crystals at a repetition rate of 4 MHz, and then frequency-doubled at 350 nm. Fluorescence photons were detected through a monochromator by means of a Hamamatsu MCP R3809U photomultiplier, connected to a constant-fraction discriminator. The time-to-amplitude converter was purchased from Tennelec. The fluorescence data were analyzed by a nonlinear least-squares global method using the Globals software package developed at the Laboratory for Fluorescence Dynamics at the University of Illinois at Urbana-Champaign. POPOP was used as reference compound for lifetime measurements.

**Photochromic reaction** was induced *in situ* by a continuous wavelength irradiation Hg/Xe lamp (Hamamatsu, LC6 Lightningcure, 200 W) equipped with narrow band interference filters of appropriate wavelengths (Semrock Hg01 for  $\lambda_{\text{irr}} = 365$  nm, Semrock BrightLine FF01-575/25-25 for  $\lambda_{\text{irr}} = 575$  nm). The irradiation power was measured using a photodiode from Ophir (PD300-UV). The photochromic quantum yields were determined by probing the sample with a xenon lamp during the photochromic reaction. Absorption changes were monitored by a CCD camera mounted on a spectrometer (Princeton Instruments). Kinetic profiles were analyzed by an Igor-implemented home-made software. All chemicals are commercially available and analytical grade. All solvents used in organic synthesis were dried before use.

## Appendix II

**Table II\_1** Fractional Atomic Coordinates ( $\times 10^4$ ) and Equivalent Isotropic Displacement Parameters ( $\text{\AA}^2 \times 10^3$ ) for BTTE.  $U_{\text{eq}}$  is defined as 1/3 of the trace of the orthogonalised  $U_{\text{ij}}$  tensor.

Atom	x	y	z	U(eq)
S1	7346(4)	6073(3)	4541.4(16)	19.4(5)
S2	8573(3)	6128(3)	188.2(18)	20.0(5)
S3	2013(3)	-553(3)	-995.5(16)	19.9(5)
S4	947(3)	734(3)	3310.2(16)	17.3(5)
N1	7077(10)	4422(10)	-499(6)	19.9(16)
N2	8029(11)	5906(9)	1202(6)	19.4(16)
N3	3741(11)	1006(10)	-1113(5)	20.1(16)
N4	2226(11)	-115(9)	156(5)	17.3(15)
C1	7124(14)	2902(11)	3722(7)	20.1(18)
C2	6856(13)	4425(11)	3569(6)	17.1(17)
C3	6282(13)	4862(11)	2743(6)	16.9(17)
C4	6246(13)	6518(11)	2893(6)	16.5(17)
C5	6764(12)	7319(10)	3844(6)	15.7(16)
C6	6820(14)	9021(11)	4247(7)	23(2)
C7	5654(12)	3792(10)	1775(6)	14.1(11)
C8	6601(13)	4424(11)	1025(7)	17.9(17)
C9	6093(13)	3578(11)	56(7)	16.4(17)
C10	4558(12)	1966(11)	-226(6)	15.0(16)
C11	3690(13)	1340(11)	485(6)	15.4(16)
C12	4204(12)	2227(10)	1510(6)	14.1(11)
C13	3097(13)	1459(11)	2152(6)	17.6(17)
C14	2950(13)	-176(11)	2291(6)	18.8(18)
C15	1851(13)	-725(11)	2909(7)	19.5(18)
C16	2083(12)	2089(10)	2673(6)	14.2(16)
C17	1473(14)	-2308(11)	3236(7)	21.1(19)
C18	1869(13)	3743(11)	2727(7)	18.9(18)

**Table II\_2** Anisotropic Displacement Parameters ( $\text{\AA}^2 \times 10^3$ ) for BTTE. The Anisotropic displacement factor exponent takes the form:  $-2\pi^2[h^2a^*U_{11} + \dots + 2hka \times b \times U_{12}]$

Atom	U <sub>11</sub>	U <sub>22</sub>	U <sub>33</sub>	U <sub>23</sub>	U <sub>13</sub>	U <sub>12</sub>
S1	28.1(12)	11.2(10)	14.7(10)	1.7(7)	2.6(8)	3.7(9)
S2	18.6(11)	15.7(11)	28.3(12)	10.4(9)	9.9(9)	5.1(9)
S3	19.8(11)	17.9(11)	14.7(11)	-2.4(8)	-1.3(8)	3.1(9)
S4	20.1(11)	12.9(10)	18.5(11)	4.5(7)	7.5(8)	4.0(8)
N1	11(3)	24(4)	27(4)	12(3)	8(3)	6(3)
N2	21(4)	12(4)	23(4)	4(3)	7(3)	3(3)
N3	18(4)	28(4)	10(3)	1(3)	2(3)	5(3)
N4	18(4)	15(4)	16(4)	-3(3)	3(3)	4(3)
C1	22(4)	13(4)	21(5)	0(3)	-3(3)	6(3)
C2	21(4)	10(4)	18(4)	4(3)	2(3)	3(3)
C3	23(4)	13(4)	14(4)	3(3)	3(3)	6(3)
C4	19(4)	15(4)	15(4)	1(3)	2(3)	7(3)
C5	18(4)	8(4)	18(4)	3(3)	2(3)	3(3)
C6	26(5)	11(4)	25(5)	-3(3)	5(4)	1(4)
C7	19(3)	5(2)	17(3)	4.1(18)	3(2)	2(2)
C8	16(4)	18(4)	22(4)	7(3)	7(3)	5(3)
C9	18(4)	13(4)	22(4)	9(3)	9(3)	6(3)
C10	13(3)	15(4)	17(4)	4(3)	7(3)	3(3)
C11	19(4)	11(4)	17(4)	5(3)	4(3)	5(3)
C12	19(3)	5(2)	17(3)	4.1(18)	3(2)	2(2)
C13	25(4)	12(4)	16(4)	5(3)	11(3)	4(3)
C14	21(4)	9(4)	17(4)	-2(3)	-1(3)	-3(3)
C15	19(4)	14(4)	22(5)	2(3)	5(3)	3(3)
C16	18(4)	12(4)	10(4)	0(3)	0(3)	6(3)
C17	27(5)	11(4)	22(5)	3(3)	4(4)	6(4)
C18	22(4)	11(4)	22(5)	5(3)	10(4)	1(3)

Table II\_3 Bond Lengths for BTTE.

Atom	Atom	Length/Å	Atom	Atom	Length/Å
S1	C5	1.723(9)	C5	C6	1.503(12)
S1	C2	1.748(9)	C5	C4	1.377(12)
S2	N2	1.620(8)	<b>C7</b>	<b>C12</b>	<b>1.395(11)</b>
S2	N1	1.603(9)	C7	C3	1.470(12)
S3	N4	1.628(8)	<b>C8</b>	<b>C7</b>	<b>1.483(12)</b>

S3	N3	1.610(8)	C8	C9	1.411(13)
S4	C15	1.721(10)	C10	C9	1.451(12)
S4	C16	1.719(9)	C10	C11	1.405(12)
N1	C9	1.336(11)	<b>C12</b>	<b>C11</b>	<b>1.491(12)</b>
N2	C8	1.346(12)	C12	C13	1.457(12)
N3	C10	1.346(11)	C14	C13	1.454(13)
N4	C11	1.340(11)	C15	C17	1.495(13)
C2	C1	1.468(12)	C15	C14	1.364(13)
C3	C2	1.371(12)	C16	C13	1.354(12)
C3	C4	1.449(12)	C16	C18	1.511(12)

Table II\_4 Bond Angles for BTTE.

Atom	Atom	Atom	Angle/°	Atom	Atom	Atom	Angle/°
N1	S2	N2	100.3(4)	C7	C12	C13	124.3(8)
N1	C9	C8	114.2(8)	C8	N2	S2	106.4(6)
N1	C9	C10	128.0(8)	C8	C9	C10	117.8(8)
N2	C8	C7	122.8(8)	C9	N1	S2	106.5(7)
N2	C8	C9	112.6(8)	C9	C8	C7	124.6(8)
N3	S3	N4	100.9(4)	C10	N3	S3	105.7(6)
N3	C10	C9	128.0(8)	C10	C11	C12	124.8(8)
N3	C10	C11	113.9(8)	C11	N4	S3	105.4(6)
N4	C11	C10	114.1(8)	C11	C10	C9	117.9(8)
N4	C11	C12	121.0(8)	C12	C7	C8	117.7(8)
C1	C2	S1	120.2(7)	C12	C7	C3	124.2(8)
C2	C3	C7	125.9(8)	C13	C12	C11	118.4(7)
C2	C3	C4	113.9(8)	C13	C16	S4	111.6(6)
C3	C7	C8	118.0(7)	C13	C16	C18	127.8(8)
C3	C2	S1	109.0(7)	C14	C15	S4	109.5(7)
C3	C2	C1	130.8(8)	C14	C15	C17	127.6(9)
C4	C5	S1	110.1(6)	C14	C13	C12	121.3(8)
C4	C5	C6	126.6(8)	C15	C14	C13	114.1(9)
C4	C3	C7	120.2(8)	C16	S4	C15	93.5(4)
C5	S1	C2	94.1(4)	C16	C13	C12	127.3(8)
C5	C4	C3	113.0(8)	C16	C13	C14	111.4(8)
C6	C5	S1	123.4(7)	C17	C15	S4	122.9(7)

C7	C12	C11	117.2(8)	C18	C16	S4	120.6(6)
----	-----	-----	----------	-----	-----	----	----------

**Table II\_5** Hydrogen Atom Coordinates ( $\text{\AA}\times 10^4$ ) and Isotropic Displacement Parameters ( $\text{\AA}^2\times 10^3$ ) for BTTE.

Atom	x	y	z	U(eq)
H1A	6020	2194	3887	30
H1B	8217	3179	4233	30
H1C	7311	2338	3147	30
H4	5909	6990	2399	20
H6A	8111	9795	4417	35
H6B	6302	9007	4806	35
H6C	6082	9349	3777	35
H14	3551	-794	1985	23
H17A	1970	-3001	2869	32
H17B	128	-2871	3148	32
H17C	2078	-2069	3900	32
H18A	2612	4482	3327	28
H18B	557	3593	2675	28
H18C	2302	4206	2213	28

**Table II\_6** Fractional Atomic Coordinates ( $\times 10^4$ ) and Equivalent Isotropic Displacement Parameters ( $\text{\AA}^2\times 10^3$ ) for BTE-NA.  $U_{\text{eq}}$  is defined as 1/3 of the trace of the orthogonalised  $U_{\text{ij}}$  tensor.

Atom	x	y	z	U(eq)
S1	-2753.1(4)	3442.8(4)	1322.0(4)	20.62(13)
S2	158.9(4)	1471.3(4)	-267.9(4)	19.58(13)
N1	5086.4(15)	8070.6(14)	6320.9(12)	20.3(3)
O1	2973.2(14)	7976.7(13)	6011.6(11)	26.7(3)
O2	7189.2(13)	8167.9(14)	6610.2(12)	30.9(3)
O3	-5238.4(14)	1216.4(13)	-4224.9(11)	28.3(3)
O4	1087.4(16)	2470.7(15)	-4466.7(12)	32.9(3)
C1	4037.8(17)	6049.4(16)	4262.1(14)	16.7(3)
C2	3505.6(17)	5049.8(15)	3218.4(14)	16.5(3)
C3	2094.8(17)	4538.9(15)	2524.5(14)	16.2(3)
C4	1245.3(17)	5026.7(16)	2865.4(14)	16.5(3)
C5	1795.5(17)	6003.8(16)	3912.1(14)	17.1(3)

---

C6	3160.7(17)	6514.5(16)	4601.1(14)	17.0(3)
C7	3699.3(18)	7560.2(16)	5679.7(15)	18.9(4)
C8	5993.5(18)	7646.3(17)	6016.2(15)	20.7(4)
C9	5432.6(18)	6571.9(16)	4951.1(15)	18.5(4)
C10	6285.5(18)	6101.4(17)	4635.1(16)	21.7(4)
C11	5771.0(19)	5094.6(18)	3617.3(16)	22.6(4)
C12	4413.8(18)	4584.7(16)	2921.8(15)	19.3(4)
C13	5644.8(19)	9135.2(16)	7387.1(15)	23.7(4)
C14	5939(2)	8748.3(17)	8360.9(16)	24.3(4)
C15	6446(2)	9852.6(18)	9446.0(16)	27.0(4)
C16	6687(2)	9476(2)	10425.8(17)	32.8(5)
C17	-1013(2)	4241(2)	3569.6(16)	25.7(4)
C18	-1179.2(18)	4158.4(17)	2446.8(15)	19.2(4)
C19	-225.4(17)	4528.1(16)	2131.4(14)	17.3(3)
C20	-796.2(18)	4262.3(16)	972.7(14)	18.4(4)
C21	-2147.1(18)	3654.3(16)	407.6(14)	18.6(4)
C22	-2998.4(18)	3105.6(16)	-798.1(15)	18.4(4)
C23	-2414.3(18)	2882.3(17)	-1511.7(15)	20.8(4)
C24	-3187.5(19)	2282.2(16)	-2643.7(15)	21.4(4)
C25	-4574.5(19)	1861.0(16)	-3103.0(15)	21.8(4)
C26	-5187.1(19)	2093.7(18)	-2422.5(16)	24.5(4)
C27	-4391.8(19)	2717.0(18)	-1280.1(16)	23.3(4)
C28	-6648(2)	609(2)	-4707.4(18)	34.3(5)
C29	113.7(19)	1856.0(16)	1763.0(15)	19.9(4)
C30	678.1(18)	2357.5(16)	1110.1(15)	17.7(3)
C31	1556.1(17)	3507.8(16)	1425.0(14)	17.1(3)
C32	1821.8(18)	3668.9(16)	553.3(15)	19.0(4)
C33	1116.5(18)	2655.0(16)	-427.9(15)	18.8(4)
C34	1089.7(18)	2528.6(16)	-1500.8(15)	18.9(4)
C35	2173.3(19)	3281.6(18)	-1534.0(16)	23.6(4)
C36	2140(2)	3237.8(19)	-2531.7(17)	25.7(4)
C37	1022(2)	2432.9(18)	-3526.2(16)	23.7(4)
C38	-49(2)	1671.6(19)	-3513.7(16)	25.0(4)
C39	-7.8(19)	1721.7(18)	-2505.6(16)	23.2(4)
C40	13(2)	1600(2)	-5509.6(17)	32.5(5)

---

Table II\_7 Anisotropic Displacement Parameters ( $\text{\AA}^2 \times 10^3$ ) for BTE-NA. The Anisotropic displacement factor exponent takes the form:  $-2\pi^2[h^2a^{*2}U_{11}+\dots+2hka \times b \times U_{12}]$

Atom	U <sub>11</sub>	U <sub>22</sub>	U <sub>33</sub>	U <sub>23</sub>	U <sub>13</sub>	U <sub>12</sub>
S1	14.7(2)	25.3(2)	17.0(2)	6.31(18)	5.84(18)	3.21(17)
S2	22.5(2)	15.8(2)	16.7(2)	3.39(16)	9.27(18)	3.03(17)
N1	19.7(8)	16.3(7)	14.4(7)	2.4(6)	2.5(6)	1.5(6)
O1	24.4(7)	23.7(7)	23.2(7)	0.5(5)	9.8(6)	5.8(6)
O2	17.7(7)	32.2(8)	25.4(8)	4.4(6)	1.3(6)	1.7(6)
O3	28.9(7)	24.0(7)	15.3(7)	3.8(5)	0.3(6)	1.8(6)
O4	37.3(8)	42.1(9)	21.6(7)	13.5(6)	17.6(7)	8.6(7)
C1	16.7(8)	16.8(8)	16.0(8)	8.6(7)	6.4(7)	4.1(6)
C2	17.1(8)	16.4(8)	16.1(8)	8.3(7)	7.0(7)	4.7(6)
C3	18.2(8)	15.3(8)	13.6(8)	6.2(6)	6.5(7)	4.0(6)
C4	14.9(8)	16.6(8)	14.7(8)	6.4(6)	4.5(7)	3.3(6)
C5	16.7(8)	18.1(8)	15.9(8)	6.9(7)	6.8(7)	5.8(7)
C6	17.4(8)	15.0(8)	15.3(8)	5.7(6)	5.6(7)	3.4(6)
C7	19.2(9)	17.1(8)	17.0(9)	6.8(7)	6.0(7)	4.2(7)
C8	19.0(9)	20.6(9)	17.4(9)	8.4(7)	4.3(7)	3.5(7)
C9	17.3(8)	19.0(8)	16.7(8)	9.0(7)	5.0(7)	4.0(7)
C10	14.9(8)	25.3(9)	22.7(9)	12.0(8)	5.8(7)	4.5(7)
C11	21.3(9)	25.7(9)	26.7(10)	13.3(8)	13.5(8)	10.8(7)
C12	21.1(9)	18.7(8)	19.1(9)	8.3(7)	10.3(7)	5.4(7)
C13	23.5(9)	15.0(8)	19.1(9)	1.5(7)	2.7(8)	1.7(7)
C14	26.4(10)	19.5(9)	21.3(9)	5.0(7)	8.7(8)	5.5(7)
C15	26.8(10)	23.4(9)	21.5(10)	2.9(8)	8.2(8)	5.2(8)
C16	30.5(11)	39.8(12)	23.2(10)	8.4(9)	12.4(9)	8.1(9)
C17	21.9(9)	34(1)	16.7(9)	8.1(8)	8.2(7)	4.9(8)
C18	16.3(8)	20.8(8)	15.8(8)	4.8(7)	5.4(7)	4.6(7)
C19	16.9(8)	15.7(8)	16.4(8)	4.5(6)	6.3(7)	5.4(6)
C20	17.7(8)	17.3(8)	16.1(8)	5.5(7)	6.0(7)	3.5(7)
C21	17.8(8)	18.4(8)	15.8(8)	5.5(7)	5.6(7)	5.0(7)
C22	18.5(8)	15.6(8)	17.0(9)	6.5(7)	4.9(7)	4.0(7)
C23	18.4(8)	19.3(8)	20.7(9)	8.0(7)	6.4(7)	3.7(7)
C24	25.7(9)	19.1(9)	17.1(9)	8.0(7)	8.0(8)	5.9(7)
C25	25.1(9)	16.2(8)	15.6(9)	6.8(7)	2.1(7)	3.9(7)
C26	18.5(9)	24.4(9)	21.6(9)	8.2(7)	2.2(7)	4.4(7)

C27	21.4(9)	24.6(9)	21.8(9)	8.4(7)	8.5(8)	7.5(7)
C28	27.9(11)	30.0(11)	21.8(10)	10.2(8)	-3.8(8)	-4.8(8)
C29	22.4(9)	17.9(8)	17.2(9)	6.5(7)	8.9(7)	3.8(7)
C30	18.0(8)	18.9(8)	16.4(8)	6.6(7)	8.3(7)	6.5(7)
C31	16.2(8)	18.4(8)	15.7(8)	5.9(7)	6.8(7)	6.0(7)
C32	18.7(8)	18.8(8)	19.1(9)	7.2(7)	9.3(7)	4.9(7)
C33	19.2(8)	19.7(8)	18.3(9)	7.4(7)	9.9(7)	6.1(7)
C34	22.0(9)	18.9(8)	17.2(9)	6.5(7)	10.3(7)	7.9(7)
C35	22.8(9)	22.9(9)	20.7(9)	5.1(7)	10.1(8)	3.8(7)
C36	27(1)	26.8(10)	26.1(10)	10.4(8)	16.5(8)	6.5(8)
C37	28.6(10)	28.2(10)	20.6(9)	10.6(8)	15.5(8)	12.5(8)
C38	23.3(9)	29.6(10)	16.6(9)	5.3(7)	8.4(8)	5.6(8)
C39	21.4(9)	26.5(9)	18.9(9)	6.4(7)	10.2(8)	4.3(7)
C40	41.6(12)	40.8(12)	19.9(10)	13.7(9)	16.4(9)	16.6(10)

Table II\_8 Bond Lengths for BTE-NA.

Atom	Atom	Length/Å	Atom	Atom	Length/Å
S1	C18	1.7290(18)	C11	C12	1.378(3)
S1	C21	1.7347(19)	C13	C14	1.518(3)
S2	C30	1.7318(18)	C14	C15	1.525(3)
S2	C33	1.7325(18)	C15	C16	1.523(3)
N1	C7	1.395(2)	C17	C18	1.500(3)
N1	C8	1.400(3)	C18	C19	1.369(3)
N1	C13	1.476(2)	C19	C20	1.428(2)
O1	C7	1.224(2)	C20	C21	1.365(2)
O2	C8	1.215(2)	C21	C22	1.471(2)
O3	C25	1.366(2)	C22	C23	1.404(3)
O3	C28	1.425(2)	C22	C27	1.395(3)
O4	C37	1.374(2)	C23	C24	1.380(3)
O4	C40	1.428(3)	C24	C25	1.389(3)
C1	C2	1.423(2)	C25	C26	1.392(3)
C1	C6	1.414(3)	C26	C27	1.396(3)
C1	C9	1.411(2)	C29	C30	1.495(2)
<b>C2</b>	<b>C3</b>	<b>1.426(2)</b>	C30	C31	1.366(2)
C2	C12	1.418(3)	C31	C32	1.429(2)
<b>C3</b>	<b>C4</b>	<b>1.398(2)</b>	C32	C33	1.368(2)



C3	C31	1.491(2)	C33	C34	1.471(2)
<b>C4</b>	<b>C5</b>	<b>1.411(2)</b>	C34	C35	1.405(3)
C4	C19	1.490(2)	C34	C39	1.392(3)
C5	C6	1.384(2)	C35	C36	1.384(3)
C6	C7	1.480(2)	C36	C37	1.394(3)
C8	C9	1.481(2)	C37	C38	1.382(3)
C9	C10	1.375(3)	C38	C39	1.394(3)
C10	C11	1.407(3)			

Table II\_9 Bond Angles for BTE-NA.

Atom	Atom	Atom	Angle/°	Atom	Atom	Atom	Angle/°
N1	C7	C6	117.49(16)	C18	S1	C21	92.72(9)
N1	C8	C9	117.39(15)	C18	C19	C4	124.92(16)
N1	C13	C14	112.57(15)	C18	C19	C20	111.90(16)
O1	C7	N1	120.26(16)	C19	C18	S1	111.14(14)
O1	C7	C6	122.25(16)	C19	C18	C17	129.28(17)
O2	C8	N1	119.98(17)	C20	C19	C4	122.89(16)
O2	C8	C9	122.61(18)	C20	C21	S1	109.63(13)
O3	C25	C24	115.30(17)	C20	C21	C22	127.80(17)
O3	C25	C26	124.84(17)	C21	C20	C19	114.55(16)
O4	C37	C36	115.34(17)	C22	C21	S1	122.21(13)
O4	C37	C38	124.82(18)	C22	C27	C26	121.88(18)
C1	C2	C3	119.50(16)	C23	C22	C21	119.77(16)
C1	C6	C7	120.22(15)	C23	C24	C25	120.29(18)
C1	C9	C8	120.18(16)	C24	C23	C22	121.36(17)
C2	C3	C31	118.80(15)	C24	C25	C26	119.85(17)
C3	C4	C5	119.33(15)	C25	O3	C28	117.05(17)
C3	C4	C19	120.54(15)	C25	C26	C27	119.17(18)
C4	C3	C2	120.09(15)	C27	C22	C21	122.74(17)
C4	C3	C31	121.10(15)	C27	C22	C23	117.37(17)
C5	C4	C19	120.13(15)	C29	C30	S2	120.44(13)
C5	C6	C1	119.82(16)	C30	S2	C33	92.87(8)
C5	C6	C7	119.95(16)	C30	C31	C3	124.27(16)
C6	C1	C2	119.57(15)	C30	C31	C32	113.04(15)
C6	C5	C4	121.67(16)	C31	C30	S2	110.47(13)
C7	N1	C8	124.28(15)	C31	C30	C29	129.01(16)

C7	N1	C13	118.30(15)	C32	C31	C3	122.46(15)
C8	N1	C13	117.41(15)	C32	C33	S2	110.09(13)
C9	C1	C2	120.05(16)	C32	C33	C34	127.80(17)
C9	C1	C6	120.37(16)	C33	C32	C31	113.49(16)
C9	C10	C11	120.08(17)	C34	C33	S2	122.08(13)
C10	C9	C1	120.47(17)	C34	C39	C38	121.52(18)
C10	C9	C8	119.34(16)	C35	C34	C33	119.83(16)
C11	C12	C2	121.02(17)	C35	C36	C37	120.06(18)
C12	C2	C1	117.92(16)	C36	C35	C34	121.10(18)
C12	C2	C3	122.57(16)	C37	O4	C40	117.63(16)
C12	C11	C10	120.43(17)	C37	C38	C39	119.76(18)
C13	C14	C15	111.76(16)	C38	C37	C36	119.84(18)
C16	C15	C14	112.56(17)	C39	C34	C33	122.38(17)
C17	C18	S1	119.50(14)	C39	C34	C35	117.72(17)

Table II\_10 Hydrogen Atom Coordinates ( $\text{\AA} \times 10^4$ ) and Isotropic Displacement Parameters ( $\text{\AA}^2 \times 10^3$ ) for BTE-NA.

Atom	x	y	z	U(eq)
H5	1214	6319	4150	20
H10	7223	6457	5105	26
H11	6363	4764	3408	27
H12	4082	3911	2233	23
H13A	5002	9578	7355	28
H13B	6482	9717	7504	28
H14A	6620	8346	8420	29
H14B	5114	8134	8229	29
H15A	7293	10448	9592	32
H15B	5783	10278	9371	32
H16A	5852	8885	10286	49
H16B	6991	10212	11098	49
H16C	7371	9087	10524	49
H17A	-128	4223	4002	39
H17B	-1707	3538	3488	39
H17C	-1096	5017	3952	39
H20	-278	4490	624	22
H23	-1467	3150	-1209	25

H24	-2769	2156	-3111	26
H26	-6135	1831	-2732	29
H27	-4811	2881	-817	28
H28A	-6840	80	-4329	51
H28B	-6992	99	-5494	51
H28C	-7081	1230	-4631	51
H29A	656	2385	2553	30
H29B	124	1012	1638	30
H29C	-809	1841	1526	30
H32	2429	4408	646	23
H35	2942	3830	-861	28
H36	2880	3757	-2539	31
H38	-809	1116	-4190	30
H39	-746	1193	-2504	28
H40A	-98	758	-5536	49
H40B	214	1681	-6107	49
H40C	-815	1765	-5602	49

**Table II\_11** Fractional Atomic Coordinates ( $\times 10^4$ ) and Equivalent Isotropic Displacement Parameters ( $\text{\AA}^2 \times 10^3$ ) for BTA.  $U_{\text{eq}}$  is defined as 1/3 of of the trace of the orthogonalised  $U_{ij}$  tensor.

Atom	x	y	z	U(eq)
S1	11593.3(9)	2564.8(2)	331.7(5)	31.48(17)
S2	12204.9(11)	-447.5(3)	1047.9(7)	43.2(2)
S3	10158.3(9)	1441.1(2)	3946.7(5)	31.92(17)
N1	12740(3)	-252.6(9)	-140(2)	42.2(6)
N2	11645(3)	31.2(8)	1657(2)	36.5(5)
O1	3037(3)	502.1(7)	6221.5(17)	37.7(4)
O2	4306(3)	3456.6(6)	2525.3(16)	35.5(4)
C1	9710(3)	2319.6(9)	880.7(19)	27.1(5)
C2	9800(3)	1843.7(9)	815.4(19)	27.1(5)
C3	11376(3)	1670.1(9)	340.6(19)	28.2(5)
C4	12478(4)	2026.1(10)	33(2)	31.0(5)
C5	14273(4)	2005.7(11)	-452(2)	39.3(6)
C6	11787(3)	1164.5(9)	250(2)	30.5(5)
C7	12436(4)	994.1(10)	-773(2)	34.4(6)
C8	12769(4)	537.1(11)	-967(2)	36.9(6)

C9	12485(3)	214.1(9)	-106(2)	32.7(6)
C10	11846(3)	375.7(9)	917(2)	30.7(5)
C11	11491(3)	860.6(9)	1105(2)	29.2(5)
C12	10761(3)	1005.1(8)	2168(2)	27.6(5)
C13	9141(3)	817.5(8)	2563(2)	27.8(5)
C14	8626(3)	1018.4(8)	3511(2)	28.9(5)
C15	11493(4)	1341.9(9)	2853(2)	30.9(5)
C16	13150(4)	1622.3(10)	2747(2)	39.9(7)
C17	7112(3)	900.9(8)	4186(2)	27.3(5)
C18	5600(4)	670.7(9)	3731(2)	31.8(6)
C19	4209(4)	535.0(9)	4372(2)	32.5(6)
C20	4307(3)	624.3(8)	5497(2)	30.3(5)
C21	5787(4)	855.1(9)	5963(2)	33.7(6)
C22	7158(4)	993.1(9)	5315(2)	31.6(5)
C23	1439(4)	292.5(10)	5767(3)	40.2(7)
C24	8324(3)	2612.1(9)	1337.5(19)	26.6(5)
C25	7027(3)	2417.2(9)	1991(2)	30.4(5)
C26	5672(3)	2685.1(9)	2398(2)	29.6(5)
C27	5601(3)	3161.9(9)	2179(2)	28.5(5)
C28	6926(4)	3364.9(9)	1578(2)	32.7(6)
C29	8247(4)	3094.8(9)	1158(2)	31.0(5)
C30	2847(4)	3252.2(10)	3066(2)	34.6(6)

Table II\_12 Anisotropic Displacement Parameters ( $\text{\AA}^2 \times 10^3$ ) for BTA. The Anisotropic displacement factor exponent takes the form:  $-2\pi^2[h^2a^*2U_{11}+\dots+2hka \times b \times U_{12}]$

Atom	U <sub>11</sub>	U <sub>22</sub>	U <sub>33</sub>	U <sub>23</sub>	U <sub>13</sub>	U <sub>12</sub>
S1	37.1(4)	32.1(3)	25.2(3)	2.7(2)	0.7(2)	-8.8(3)
S2	44.7(4)	29.7(4)	54.6(5)	-0.1(3)	-2.9(3)	5.5(3)
S3	42.2(4)	24.9(3)	27.9(3)	0.0(2)	-6.6(3)	-6.0(3)
N1	37.3(13)	38.7(13)	49.9(15)	-8.6(11)	-6.0(11)	7.4(10)
N2	36.6(12)	29.8(11)	42.6(13)	4.5(10)	-3.3(10)	1.8(9)
O1	36.3(10)	33(1)	44.4(11)	-3.0(8)	7.7(8)	0.5(8)
O2	40.2(11)	28.9(9)	37.5(10)	3.2(8)	1.2(8)	0.5(8)
C1	30.8(13)	29.9(12)	20.0(11)	4.5(9)	-4.5(9)	-5.1(10)
C2	29.1(12)	30.3(12)	21.5(11)	4.2(9)	-3.1(9)	-3.5(10)
C3	30.1(13)	31.6(13)	22.2(11)	2.4(9)	-4.6(10)	-1.5(10)

C4	33.8(13)	37.3(14)	21.6(11)	3.3(10)	-2.4(10)	-4.5(11)
C5	35.2(15)	48.3(17)	34.5(14)	2.7(12)	4.7(12)	-5.1(12)
C6	27.9(12)	32.6(13)	30.5(13)	2.4(10)	-3.5(10)	-0.1(10)
C7	29.6(13)	43.5(15)	29.6(13)	3.6(11)	-2.6(10)	0.1(11)
C8	31.6(14)	47.6(16)	31.2(14)	-5.4(12)	0.0(11)	1.9(12)
C9	25.5(12)	34.1(14)	38.2(14)	-4.3(11)	-4.4(11)	2.4(10)
C10	26.1(12)	31.5(13)	34.2(13)	1.3(10)	-2.9(10)	-0.2(10)
C11	27.2(12)	28.3(12)	31.4(13)	0.9(10)	-5.5(10)	-0.6(10)
C12	32.6(13)	22.2(11)	27.6(12)	5.1(9)	-3.3(10)	-0.4(9)
C13	32.4(13)	21.2(11)	29.3(12)	0.7(9)	-2.9(10)	-1.5(9)
C14	31.8(13)	21.8(11)	32.3(13)	2.3(9)	-7(1)	0.0(9)
C15	36.6(14)	26.4(12)	28.9(13)	6.2(10)	-6.9(10)	-2.3(10)
C16	43.9(16)	38.8(15)	35.7(15)	7.2(12)	-11.1(12)	-14.1(13)
C17	32.1(12)	19.0(11)	30.6(12)	-1.3(9)	-2.7(10)	6.5(9)
C18	37.2(14)	27.8(13)	29.7(13)	-0.7(10)	-5.9(11)	4.9(10)
C19	31.0(13)	23.6(12)	42.2(15)	-1.1(10)	-5.2(11)	2(1)
C20	31.0(13)	19.8(11)	40.3(14)	-1.5(10)	4.5(11)	6.4(10)
C21	36.5(14)	32.7(14)	31.9(13)	-7.6(11)	1.8(11)	5.4(11)
C22	29.8(13)	28.0(12)	36.6(14)	-6.2(10)	-2.1(10)	3.5(10)
C23	35.2(15)	28.1(13)	57.5(18)	3.7(12)	3.8(13)	0.6(11)
C24	31.7(13)	29.0(12)	18.4(11)	2.5(9)	-6.1(9)	-6(1)
C25	34.7(13)	25.8(12)	30.0(13)	4.7(10)	-3.6(10)	-7(1)
C26	30.0(13)	28.4(12)	30.0(13)	4.9(10)	-2.6(10)	-7.6(10)
C27	34.4(13)	28.1(12)	22.4(11)	0.5(9)	-5.9(10)	-3.3(10)
C28	48.1(16)	22.6(12)	27.0(12)	4.5(9)	-3.1(11)	-4.4(11)
C29	40.5(14)	29.9(13)	22.5(12)	5.0(9)	-0.8(10)	-7.2(11)
C30	35.2(14)	37.4(14)	30.9(13)	-1.6(11)	-1.3(11)	0.5(11)

Table II\_13 Bond Lengths for BTA.

Atom	Atom	Length/Å	Atom	Atom	Length/Å
S1	C1	1.738(3)	C8	C9	1.421(4)
S1	C4	1.725(3)	C9	C10	1.431(4)
S2	N1	1.617(3)	<b>C10</b>	<b>C11</b>	<b>1.435(4)</b>
S2	N2	1.623(2)	C11	C12	1.487(4)
S3	C14	1.735(3)	C12	C13	1.432(4)
S3	C15	1.725(3)	C12	C15	1.373(4)

N1	C9	1.351(4)	C13	C14	1.361(4)
N2	C10	1.349(3)	C14	C17	1.472(4)
O1	C20	1.373(3)	C15	C16	1.491(4)
O1	C23	1.429(4)	C17	C18	1.403(4)
O2	C27	1.368(3)	C17	C22	1.398(4)
O2	C30	1.428(3)	C18	C19	1.387(4)
C1	C2	1.367(4)	C19	C20	1.391(4)
C1	C24	1.465(4)	C20	C21	1.390(4)
C2	C3	1.429(4)	C21	C22	1.382(4)
C3	C4	1.375(4)	C24	C25	1.401(4)
C3	C6	1.486(4)	C24	C29	1.401(3)
C4	C5	1.496(4)	C25	C26	1.383(4)
<b>C6</b>	<b>C7</b>	<b>1.442(4)</b>	C26	C27	1.392(4)
<b>C6</b>	<b>C11</b>	<b>1.383(4)</b>	C27	C28	1.389(4)
C7	C8	1.355(4)	C28	C29	1.374(4)

Table II\_14 Bond Angles for BTA.

Atom	Atom	Atom	Angle/°	Atom	Atom	Atom	Angle/°
N1	S2	N2	101.32(13)	C12	C15	S3	110.7(2)
N1	C9	C8	126.5(3)	C12	C15	C16	129.6(3)
N1	C9	C10	113.6(3)	C13	C12	C11	122.7(2)
N2	C10	C9	113.3(2)	C13	C14	S3	110.1(2)
N2	C10	C11	125.0(2)	C13	C14	C17	129.3(2)
O1	C20	C19	125.3(2)	C14	C13	C12	113.8(2)
O1	C20	C21	115.1(2)	C15	S3	C14	92.81(13)
O2	C27	C26	124.6(2)	C15	C12	C11	124.8(2)
O2	C27	C28	116.1(2)	C15	C12	C13	112.5(2)
C1	C2	C3	114.5(2)	C16	C15	S3	119.6(2)
C2	C1	S1	109.74(19)	C17	C14	S3	120.41(19)
C2	C1	C24	129.0(2)	C18	C17	C14	121.2(2)
C2	C3	C6	123.2(2)	C18	C19	C20	119.7(2)
C3	C4	S1	111.3(2)	C19	C18	C17	121.7(2)
C3	C4	C5	129.9(3)	C20	O1	C23	117.0(2)
C4	S1	C1	92.68(12)	C21	C20	C19	119.6(2)
C4	C3	C2	111.8(2)	C21	C22	C17	121.4(2)
C4	C3	C6	125.0(2)	C22	C17	C14	121.4(2)

C5	C4	S1	118.7(2)	C22	C17	C18	117.3(2)
C6	C11	C10	116.9(2)	C22	C21	C20	120.3(2)
C6	C11	C12	123.9(2)	C24	C1	S1	121.23(18)
C7	C6	C3	118.3(2)	C25	C24	C1	120.8(2)
C7	C8	C9	117.7(3)	C25	C24	C29	117.2(2)
C8	C7	C6	123.3(3)	C25	C26	C27	119.9(2)
C8	C9	C10	119.9(2)	C26	C25	C24	121.5(2)
C9	N1	S2	105.8(2)	C27	O2	C30	117.3(2)
C9	C10	C11	121.6(2)	C28	C27	C26	119.3(2)
C10	N2	S2	105.9(2)	C28	C29	C24	121.5(2)
C10	C11	C12	119.1(2)	C29	C24	C1	122.0(2)
C11	C6	C3	121.1(2)	C29	C28	C27	120.4(2)
C11	C6	C7	120.6(2)				

Table II\_15 Hydrogen Atom Coordinates ( $\text{\AA} \times 10^4$ ) and Isotropic Displacement Parameters ( $\text{\AA}^2 \times 10^3$ ) for BTA.

Atom	<i>x</i>	<i>y</i>	<i>z</i>	U(eq)
H2	8889	1645	1065	33
H5A	14883	1718	-214	59
H5B	14983	2276	-202	59
H5C	14128	2010	-1256	59
H7	12640	1213	-1340	41
H8	13179	436	-1655	44
H13	8485	575	2196	33
H16A	13932	1465	2241	60
H16B	13770	1653	3471	60
H16C	12838	1933	2461	60
H18	5527	606	2965	38
H19	3194	382	4044	39
H21	5857	918	6730	40
H22	8154	1154	5645	38
H23A	882	501	5212	60
H23B	611	239	6354	60
H23C	1728	-6	5423	60
H25	7079	2093	2159	36
H26	4792	2544	2825	36

H28	6919	3692	1456	39
H29	9129	3239	736	37
H30A	2256	3021	2580	52
H30B	1992	3496	3245	52
H30C	3293	3099	3745	52

Table II\_16 Fractional Atomic Coordinates ( $\times 10^4$ ) and Equivalent Isotropic Displacement Parameters ( $\text{\AA}^2 \times 10^3$ ) for BTTA.  $U_{\text{eq}}$  is defined as 1/3 of of the trace of the orthogonalised  $U_{ij}$  tensor.

Atom	x	y	z	U(eq)
C1	8465(3)	10818(3)	3947.0(18)	43.3(9)
C2	9165(3)	10026(3)	4045.5(19)	46.2(9)
C3	8628(3)	8925(3)	4160.4(17)	39.8(9)
C4	7426(3)	8572(3)	4166.9(17)	38.7(8)
C5	6756(3)	9336(3)	4061.2(17)	37.1(8)
C6	7279(3)	10453(3)	3952.8(17)	38.6(8)
C7	5501(3)	9031(3)	4024.6(17)	36.9(8)
C8	4651(3)	8993(3)	3375.1(18)	42.3(9)
C9	3550(3)	8537(3)	3422.1(18)	41.7(9)
C10	5060(3)	8667(3)	4592.7(18)	41.6(9)
C11	5679(3)	8585(3)	5362.3(18)	54.2(11)
C12	2492(3)	8235(3)	2843.0(19)	42.8(9)
C13	2301(3)	8847(3)	2231(2)	51.8(10)
C14	1358(3)	8496(3)	1660(2)	50.2(10)
C15	550(3)	7519(3)	1672(2)	46.0(9)
C16	701(3)	6927(3)	2276.4(18)	44.5(9)
C17	1648(3)	7284(3)	2843.7(19)	45.7(9)
C18	-1125(3)	6178(3)	1032(2)	59.0(11)
C19	8275(3)	7093(3)	5438(2)	58.0(11)
C20	7303(3)	6778(3)	4775.6(19)	44.0(9)
C21	6898(3)	7387(3)	4223.4(19)	40.1(9)
C22	5900(3)	6785(3)	3715.7(19)	40.7(9)
C23	5544(3)	5734(3)	3867.8(19)	43.6(9)
C24	4505(3)	4903(3)	3474.6(19)	45.0(9)
C25	3513(4)	5207(3)	3123(2)	51.9(10)
C26	2535(4)	4451(3)	2771(2)	55.3(10)
C27	2503(4)	3342(3)	2767(2)	51.4(10)



---

C28	3490(4)	3015(3)	3108(2)	57.4(11)
C29	4469(4)	3787(3)	3454(2)	55.3(11)
C30	1374(5)	1503(4)	2486(3)	92.7(17)
C31	1674(3)	4662(3)	941(2)	49.5(10)
C32	881(3)	3610(3)	810(2)	48.8(10)
C33	1328(3)	2666(3)	760.8(18)	43.7(9)
C34	2542(3)	2720(3)	829.7(18)	43.4(9)
C35	3297(3)	3727(3)	970.4(18)	41.3(9)
C36	2868(3)	4702(3)	1036.5(19)	45.4(9)
C37	4563(3)	3882(3)	1056.4(19)	41.7(9)
C38	5387(3)	4231(3)	1718(2)	45.0(9)
C39	6485(3)	4202(3)	1702(2)	44.2(9)
C40	5039(3)	3623(3)	509(2)	47.7(10)
C41	4439(4)	3231(4)	-259(2)	65.9(13)
C42	7536(3)	4444(3)	2293(2)	44.1(9)
C43	7660(3)	5178(3)	2880(2)	51.8(10)
C44	8634(4)	5418(3)	3446(2)	54.8(11)
C45	9528(3)	4915(3)	3444(2)	49.7(10)
C46	9419(3)	4162(3)	2879(2)	52.4(10)
C47	8452(3)	3945(3)	2313(2)	51.4(10)
C48	10785(4)	5978(4)	4505(2)	75.8(14)
C49	2949(3)	1704(3)	772.1(19)	43.7(9)
C50	3928(3)	1499(3)	1291.3(19)	47(1)
C51	4257(3)	586(3)	1117(2)	47.9(10)
C52	2527(3)	907(3)	208(2)	47.2(10)
C53	1587(4)	830(4)	-464(2)	62.4(12)
C54	5241(3)	173(3)	1481.9(19)	46.7(10)
C55	6313(4)	896(4)	1800(2)	59.3(11)
C56	7255(4)	509(4)	2106(2)	60.7(12)
C57	7191(4)	-590(4)	2118(2)	61.3(13)
C58	6151(4)	-1337(4)	1817(2)	64.2(13)
C59	5208(4)	-936(3)	1495(2)	57.5(11)
C60	8194(5)	-1999(5)	2390(3)	113(2)
N1	8794(3)	11874(3)	3831.2(18)	58.0(9)
N2	6717(3)	11256(2)	3843.8(16)	48.9(8)
N3	10268(3)	10188(3)	4031.2(17)	55.4(9)

N4	9358(3)	8262(3)	4215.2(16)	49.9(8)
N5	3535(3)	5717(3)	1184.5(19)	61.3(10)
N6	1435(3)	5637(3)	1012(2)	67.9(10)
N7	-255(3)	3405(3)	743(2)	64.1(10)
N8	505(3)	1734(3)	668.0(18)	56.8(9)
O1	-336(2)	7219(2)	1067.6(13)	57.0(7)
O2	1470(3)	2651(2)	2430.8(15)	71.3(9)
O3	10539(3)	5100(2)	3974.0(16)	68.2(8)
O4	8208(3)	-881(3)	2425.6(16)	85.7(11)
S1	7640.9(10)	12345.9(9)	3734.5(6)	61.3(3)
S2	10581.2(9)	9000.4(10)	4137.8(6)	60.3(3)
S3	3576.1(8)	8233.8(9)	4311.2(5)	48.9(3)
S4	6430.1(9)	5471.0(8)	4661.5(5)	51.5(3)
S5	2663.6(12)	6520.9(10)	1195.8(8)	80.5(4)
S6	-700.6(10)	2084.7(11)	634.8(8)	76.5(4)
S7	6501.7(9)	3790.8(9)	830.0(6)	53.8(3)
S8	3352.1(10)	-52.9(9)	306.9(6)	56.3(3)

Table II\_17 Anisotropic Displacement Parameters ( $\text{\AA}^2 \times 10^3$ ) for BTTA. The Anisotropic displacement factor exponent takes the form:  $-2\pi^2[h^2a^{*2}U_{11}+\dots+2hka \times b \times U_{12}]$

Atom	U <sub>11</sub>	U <sub>22</sub>	U <sub>33</sub>	U <sub>23</sub>	U <sub>13</sub>	U <sub>12</sub>
C1	41(2)	44(2)	43(2)	6.9(17)	8.8(18)	5.9(19)
C2	41(2)	51(2)	46(2)	5.2(18)	15.1(19)	5(2)
C3	39(2)	43(2)	36.7(19)	2.2(16)	10.3(17)	7.3(18)
C4	39(2)	40(2)	42(2)	7.6(16)	16.4(17)	12.3(18)
C5	36(2)	45(2)	31.9(18)	4.8(16)	9.5(16)	10.9(18)
C6	40(2)	40(2)	35.4(19)	2.3(16)	10.1(17)	8.4(18)
C7	38(2)	34(2)	41.0(19)	3.9(16)	11.4(17)	13.1(17)
C8	43(2)	47(2)	39(2)	6.7(17)	12.1(18)	13.3(19)
C9	39(2)	43(2)	44(2)	0.2(17)	11.0(18)	11.7(18)
C10	45(2)	39(2)	43(2)	5.0(17)	11.5(18)	14.1(18)
C11	55(3)	72(3)	41(2)	8(2)	16.1(19)	21(2)
C12	43(2)	44(2)	47(2)	-0.1(18)	17.8(18)	14(2)
C13	49(3)	42(2)	65(3)	12(2)	15(2)	12(2)
C14	45(3)	48(3)	56(2)	16.8(19)	4(2)	14(2)
C15	42(2)	47(2)	53(2)	2.6(19)	10.8(19)	20(2)

---

C16	37(2)	48(2)	49(2)	8.1(18)	11.8(19)	10.4(19)
C17	43(2)	55(3)	45(2)	10.2(18)	14.4(19)	18(2)
C18	46(3)	60(3)	63(3)	1(2)	6(2)	5(2)
C19	57(3)	61(3)	55(2)	12(2)	13(2)	13(2)
C20	45(2)	45(2)	49(2)	6.9(18)	19.3(19)	15.7(19)
C21	41(2)	39(2)	47(2)	6.2(17)	19.3(18)	14.6(18)
C22	43(2)	38(2)	47(2)	7.4(17)	17.6(18)	15.0(19)
C23	45(2)	44(2)	49(2)	5.4(18)	21.7(19)	13.5(19)
C24	53(3)	36(2)	49(2)	6.1(17)	20(2)	9(2)
C25	56(3)	41(2)	65(3)	6(2)	24(2)	14(2)
C26	47(3)	55(3)	59(2)	5(2)	7(2)	9(2)
C27	59(3)	50(3)	44(2)	2.7(19)	18(2)	4(2)
C28	74(3)	37(2)	57(2)	5(2)	19(2)	2(2)
C29	64(3)	46(3)	58(2)	9(2)	16(2)	16(2)
C30	107(5)	54(3)	86(3)	3(3)	-3(3)	-19(3)
C31	50(3)	51(3)	53(2)	-0.8(19)	22(2)	16(2)
C32	43(3)	55(3)	51(2)	0.3(19)	14.1(19)	15(2)
C33	43(2)	49(2)	41(2)	-0.6(18)	14.5(18)	9(2)
C34	46(2)	46(2)	42(2)	2.2(17)	14.5(18)	13(2)
C35	40(2)	44(2)	43(2)	-0.2(17)	17.6(18)	9.8(19)
C36	48(2)	41(2)	48(2)	0.0(18)	18.9(19)	6(2)
C37	41(2)	37(2)	49(2)	0.3(17)	17.2(19)	6.6(18)
C38	48(3)	44(2)	46(2)	-5.8(17)	19.2(19)	9.5(19)
C39	43(2)	40(2)	53(2)	0.0(18)	17.9(19)	11.6(19)
C40	44(2)	46(2)	54(2)	0.2(19)	20(2)	5(2)
C41	66(3)	81(3)	51(2)	-8(2)	25(2)	9(3)
C42	45(2)	39(2)	53(2)	3.7(18)	19(2)	10.0(19)
C43	50(3)	49(3)	64(3)	1(2)	20(2)	20(2)
C44	56(3)	51(3)	59(3)	-7(2)	15(2)	16(2)
C45	46(3)	45(2)	59(2)	12(2)	18(2)	7(2)
C46	44(3)	45(2)	76(3)	8(2)	25(2)	15(2)
C47	49(3)	44(2)	64(3)	-3(2)	21(2)	11(2)
C48	80(4)	69(3)	69(3)	2(3)	13(3)	5(3)
C49	46(2)	37(2)	49(2)	5.4(18)	17.2(19)	7.5(19)
C50	54(3)	44(2)	45(2)	-2.7(18)	14(2)	13(2)
C51	47(2)	43(2)	53(2)	3.4(19)	13(2)	8(2)

C52	45(2)	43(2)	50(2)	0.0(19)	8.6(19)	8(2)
C53	68(3)	58(3)	61(3)	3(2)	7(2)	25(2)
C54	52(3)	45(2)	47(2)	2.1(18)	15(2)	14(2)
C55	62(3)	49(3)	61(3)	3(2)	4(2)	13(2)
C56	56(3)	68(3)	54(2)	3(2)	5(2)	15(3)
C57	61(3)	93(4)	41(2)	4(2)	7(2)	46(3)
C58	87(4)	56(3)	55(3)	-2(2)	13(3)	34(3)
C59	60(3)	51(3)	60(3)	-2(2)	10(2)	14(2)
C60	153(6)	145(6)	72(3)	-10(3)	8(4)	120(5)
N1	54(2)	46(2)	70(2)	15.8(17)	12.0(18)	5.6(18)
N2	53(2)	42.2(19)	56.4(19)	8.8(15)	18.8(17)	14.6(17)
N3	40(2)	56(2)	70(2)	12.7(17)	15.3(17)	7.8(17)
N4	42(2)	54(2)	60(2)	5.3(16)	21.0(16)	15.5(17)
N5	60(2)	45(2)	87(3)	-4.3(18)	38(2)	11.3(19)
N6	54(2)	55(2)	101(3)	-5(2)	25(2)	21(2)
N7	39(2)	68(3)	86(3)	-7(2)	16.4(19)	12.8(19)
N8	42(2)	54(2)	73(2)	-1.5(18)	16.4(18)	4.5(18)
O1	45.5(17)	61.9(19)	55.0(16)	12.6(14)	-1.6(14)	8.5(15)
O2	70(2)	59(2)	67.8(18)	-6.8(15)	4.4(16)	-7.3(17)
O3	58(2)	66(2)	75(2)	1.3(17)	1.5(17)	19.0(17)
O4	92(3)	103(3)	70(2)	6.1(19)	4.4(19)	54(2)
S1	59.7(7)	41.5(6)	81.8(8)	13.0(5)	16.9(6)	9.9(6)
S2	42.0(6)	67.1(8)	78.0(7)	8.0(6)	23.7(6)	15.8(6)
S3	38.9(6)	63.5(7)	48.3(6)	9.0(5)	18.0(5)	11.9(5)
S4	54.0(7)	43.5(6)	58.5(6)	14.2(5)	16.0(5)	11.2(5)
S5	73.5(9)	44.2(7)	136.6(12)	-4.7(7)	47.9(9)	17.3(7)
S6	43.9(7)	74.8(9)	107(1)	-9.8(7)	21.4(7)	4.1(6)
S7	45.0(6)	59.7(7)	59.4(6)	-9.3(5)	24.8(5)	6.1(5)
S8	61.5(7)	44.4(6)	61.0(6)	-5.8(5)	7.1(6)	17.2(6)

Table II\_18 Bond Lengths for BTTA.

Atom	Atom	Length/Å	Atom	Atom	Length/Å
C1	N1	1.335(5)	C32	C33	1.425(5)
C1	C6	1.431(5)	C33	N8	1.343(5)
C1	C2	1.442(5)	C33	C34	1.454(5)
C2	N3	1.333(5)	C34	C35	1.372(5)

C2	C3	1.438(5)	C34	C49	1.483(5)
C3	N4	1.343(4)	C35	C36	1.452(5)
<b>C3</b>	<b>C4</b>	<b>1.449(5)</b>	C35	C37	1.494(5)
<b>C4</b>	<b>C5</b>	<b>1.387(4)</b>	C36	N5	1.337(5)
C4	C21	1.501(5)	C37	C40	1.378(5)
<b>C5</b>	<b>C6</b>	<b>1.447(5)</b>	C37	C38	1.414(5)
C5	C7	1.489(5)	C38	C39	1.367(5)
C6	N2	1.338(4)	C39	C42	1.473(5)
C7	C10	1.365(4)	C39	S7	1.740(4)
C7	C8	1.416(5)	C40	C41	1.498(5)
C8	C9	1.371(5)	C40	S7	1.723(4)
C9	C12	1.467(5)	C42	C43	1.397(5)
C9	S3	1.741(4)	C42	C47	1.401(5)
C10	C11	1.506(5)	C43	C44	1.385(5)
C10	S3	1.733(4)	C44	C45	1.385(5)
C12	C17	1.396(5)	C45	O3	1.378(5)
C12	C13	1.413(5)	C45	C46	1.384(5)
C13	C14	1.375(5)	C46	C47	1.379(5)
C14	C15	1.400(5)	C48	O3	1.415(5)
C15	O1	1.369(4)	C49	C52	1.378(5)
C15	C16	1.383(5)	C49	C50	1.445(5)
C16	C17	1.375(5)	C50	C51	1.359(5)
C18	O1	1.433(5)	C51	C54	1.455(5)
C19	C20	1.500(5)	C51	S8	1.741(4)
C20	C21	1.378(5)	C52	C53	1.500(5)
C20	S4	1.728(4)	C52	S8	1.728(4)
C21	C22	1.422(5)	C54	C59	1.385(5)
C22	C23	1.353(5)	C54	C55	1.415(6)
C23	C24	1.487(5)	C55	C56	1.366(5)
C23	S4	1.732(4)	C56	C57	1.366(6)
C24	C25	1.385(5)	C57	O4	1.383(5)
C24	C29	1.393(5)	C57	C58	1.395(6)
C25	C26	1.374(5)	C58	C59	1.384(5)
C26	C27	1.384(5)	C60	O4	1.400(6)
C27	O2	1.374(5)	N1	S1	1.630(3)
C27	C28	1.389(6)	N2	S1	1.623(3)

C28	C29	1.381(6)	N3	S2	1.627(3)
C30	O2	1.428(5)	N4	S2	1.622(3)
C31	N6	1.334(5)	N5	S5	1.632(3)
C31	C36	1.426(5)	N6	S5	1.621(4)
C31	C32	1.434(5)	N7	S6	1.619(4)
C32	N7	1.339(5)	N8	S6	1.626(3)

Table II\_19 Bond Angles for BTTA.

Atom	Atom	Atom	Angle/°	Atom	Atom	Atom	Angle/°
N1	C1	C6	114.9(3)	C35	C34	C49	121.2(3)
N1	C1	C2	127.0(3)	C33	C34	C49	120.4(3)
C6	C1	C2	118.1(3)	C34	C35	C36	119.6(3)
N3	C2	C3	115.0(3)	C34	C35	C37	123.1(3)
N3	C2	C1	127.5(4)	C36	C35	C37	117.3(3)
C3	C2	C1	117.6(3)	N5	C36	C31	113.3(3)
N4	C3	C2	111.6(3)	N5	C36	C35	124.2(4)
N4	C3	C4	124.7(3)	C31	C36	C35	122.5(4)
C2	C3	C4	123.5(3)	C40	C37	C38	113.1(3)
C5	C4	C3	118.4(3)	C40	C37	C35	123.2(3)
C5	C4	C21	120.8(3)	C38	C37	C35	123.6(3)
C3	C4	C21	120.5(3)	C39	C38	C37	114.4(3)
C4	C5	C6	119.2(3)	C38	C39	C42	129.2(3)
C4	C5	C7	121.9(3)	C38	C39	S7	109.1(3)
C6	C5	C7	118.9(3)	C42	C39	S7	121.7(3)
N2	C6	C1	112.5(3)	C37	C40	C41	128.1(4)
N2	C6	C5	124.3(3)	C37	C40	S7	110.0(3)
C1	C6	C5	123.2(3)	C41	C40	S7	121.9(3)
C10	C7	C8	113.5(3)	C43	C42	C47	116.1(4)
C10	C7	C5	123.5(3)	C43	C42	C39	121.2(3)
C8	C7	C5	122.8(3)	C47	C42	C39	122.8(3)
C9	C8	C7	114.4(3)	C44	C43	C42	122.5(3)
C8	C9	C12	129.0(3)	C43	C44	C45	119.8(4)
C8	C9	S3	108.8(3)	O3	C45	C46	116.2(3)
C12	C9	S3	122.0(3)	O3	C45	C44	124.7(4)
C7	C10	C11	129.2(3)	C46	C45	C44	119.1(4)
C7	C10	S3	109.9(3)	C47	C46	C45	120.5(4)

C11	C10	S3	120.9(3)	C46	C47	C42	122.0(4)
C17	C12	C13	116.1(4)	C52	C49	C50	112.4(3)
C17	C12	C9	121.7(3)	C52	C49	C34	125.5(3)
C13	C12	C9	122.1(4)	C50	C49	C34	121.9(3)
C14	C13	C12	121.4(4)	C51	C50	C49	114.1(3)
C13	C14	C15	120.7(4)	C50	C51	C54	129.2(4)
O1	C15	C16	124.9(4)	C50	C51	S8	109.6(3)
O1	C15	C14	116.3(3)	C54	C51	S8	121.1(3)
C16	C15	C14	118.8(4)	C49	C52	C53	130.4(3)
C17	C16	C15	120.1(4)	C49	C52	S8	110.2(3)
C16	C17	C12	122.9(3)	C53	C52	S8	119.1(3)
C21	C20	C19	131.0(4)	C59	C54	C55	116.4(4)
C21	C20	S4	109.8(3)	C59	C54	C51	122.3(4)
C19	C20	S4	119.0(3)	C55	C54	C51	121.1(4)
C20	C21	C22	113.0(3)	C56	C55	C54	121.2(4)
C20	C21	C4	124.1(3)	C57	C56	C55	121.0(4)
C22	C21	C4	122.9(3)	C56	C57	O4	115.7(5)
C23	C22	C21	114.0(3)	C56	C57	C58	120.0(4)
C22	C23	C24	127.9(3)	O4	C57	C58	124.3(4)
C22	C23	S4	110.1(3)	C59	C58	C57	118.5(4)
C24	C23	S4	121.8(3)	C58	C59	C54	122.9(4)
C25	C24	C29	116.7(4)	C1	N1	S1	105.2(3)
C25	C24	C23	121.2(3)	C6	N2	S1	106.7(3)
C29	C24	C23	122.1(4)	C2	N3	S2	105.7(3)
C26	C25	C24	122.2(4)	C3	N4	S2	107.3(3)
C25	C26	C27	120.5(4)	C36	N5	S5	105.8(3)
O2	C27	C26	116.1(4)	C31	N6	S5	105.8(3)
O2	C27	C28	125.4(4)	C32	N7	S6	105.5(3)
C26	C27	C28	118.5(4)	C33	N8	S6	106.8(3)
C29	C28	C27	120.2(4)	C15	O1	C18	118.1(3)
C28	C29	C24	121.9(4)	C27	O2	C30	117.3(4)
N6	C31	C36	114.3(4)	C45	O3	C48	119.0(3)
N6	C31	C32	127.4(4)	C57	O4	C60	117.0(4)
C36	C31	C32	118.2(3)	N2	S1	N1	100.73(17)
N7	C32	C33	115.0(4)	N4	S2	N3	100.43(17)
N7	C32	C31	126.9(4)	C10	S3	C9	93.32(17)

C33	C32	C31	118.1(3)	C20	S4	C23	93.06(18)
N8	C33	C32	112.0(3)	N6	S5	N5	100.74(18)
N8	C33	C34	124.7(3)	N7	S6	N8	100.52(18)
C32	C33	C34	123.2(4)	C40	S7	C39	93.34(18)
C35	C34	C33	118.3(3)	C52	S8	C51	93.54(18)

Table II\_20 Hydrogen Atom Coordinates ( $\text{\AA} \times 10^4$ ) and Isotropic Displacement Parameters ( $\text{\AA}^2 \times 10^3$ ) for BTTA.

Atom	x	y	z	U(eq)
H8	4824	9255	2952	51
H11A	5228	8744	5681	81
H11B	6411	9102	5475	81
H11C	5793	7858	5422	81
H13	2825	9501	2213	62
H14	1256	8912	1262	60
H16	162	6287	2299	53
H17	1730	6875	3246	55
H18A	-1717	6084	592	88
H18B	-1466	6149	1437	88
H18C	-722	5605	1042	88
H19A	8089	6667	5825	87
H19B	8397	7857	5576	87
H19C	8963	6955	5337	87
H22	5525	7086	3315	49
H25	3509	5946	3124	62
H26	1889	4687	2534	66
H28	3491	2275	3105	69
H29	5123	3554	3679	66
H30A	1911	1275	2259	139
H30B	607	1111	2250	139
H30C	1539	1352	2985	139
H38	5197	4460	2130	54
H41A	4925	3527	-569	99
H41B	3734	3469	-390	99
H41C	4273	2445	-309	99
H43	7065	5519	2892	62



---

H44	8689	5915	3827	66
H46	10002	3801	2882	63
H47	8407	3451	1933	62
H48A	10818	6655	4275	114
H48B	11511	6003	4835	114
H48C	10191	5872	4763	114
H50	4300	1952	1708	56
H53A	1777	481	-855	94
H53B	1504	1553	-582	94
H53C	877	409	-386	94
H55	6378	1648	1800	71
H56	7951	1001	2310	73
H58	6093	-2086	1833	77
H59	4523	-1433	1277	69
H60A	8008	-2273	1894	170
H60B	7627	-2388	2622	170
H60C	8938	-2101	2630	170

---

### Appendix III

1. **Yuheng Yang**, Yongshu Xie, Qiong Zhang, Keitaro Nakatani, He Tian, Weihong Zhu\*, Aromaticity-Controlled Thermal Stability of Photochromic Systems Based on Six-Membered Ring as Ethene Bridges: Photochemical and Kinetic Studies, *Chem. Eur. J.* 2012. Accepted.
2. Weihong Zhu\*, **Yuheng Yang**, Rémi Métivier, Qiong Zhang, Régis Guillot, Yongshu Xie, He Tian, Keitaro Nakatani, Unprecedented Stability of a Photochromic Bisthiénylene Based on Benzobisthiadiazole as an Ethene Bridge, *Angew. Chem. Int. Ed.* 2011, **50**, 10986-10990.
3. Liwen Song, **Yuheng Yang**, Qiong Zhang, He Tian, Weihong Zhu, Synthesis and Photochromism of Naphthopyrans Bearing Naphthalimide Chromophore: Predominant Thermal Reversibility in Color-Fading and Fluorescence Switch, *J. Phys. Chem. B.* 2011, **115**, 14648-14658.
4. Shangjun Chen, **Yuheng Yang**, Yue Wu, He Tian, Weihong Zhu\*, Multi-addressable photochromic terarylene containing benzo[*b*]thiophene-1,1-dioxide unit as ethene bridge: multifunctional molecular logic gates on unimolecular platform, *J. Mater. Chem.* 2012, **22**, 5486-5494.
5. Yue Wu, Shangjun Chen, **Yuheng Yang**, Qiong Zhang, Yongshu Xie, He Tian, Weihong Zhu\*, A novel gated photochromic reactivity controlled by complexation/dissociation with BF<sub>3</sub>, *Chem. Commun.* 2012, **48**, 528-530.
6. Weihong Zhu\*, Xianle Meng, **Yuheng Yang**, Qiong Zhang, Yongshu Xie, He Tian\*, Bisthiénylenes Containing a Benzothiadiazole Unit as a Bridge: Photochromic Performance Dependence on Substitution Position, *Chem. Eur. J.* 2010, **16**, 899-906.
7. **Yuheng Yang**, Shangjun Chen, Liwen Song, He Tian, Weihong Zhu\*, Novel photochromic systems based on six-membered ethene bridge: photochromic reactivity in solutions and in single crystals, 5<sup>th</sup> East Asia Symposium on Functional Dyes & Advanced Materials Hangzhou, China, September 26-29, 2011. (The Best Poster Paper Award)
8. Weihong Zhu\*, **Yuheng Yang**, Shangjun Chen, Liwen Song, He Tian, Aromaticity-Controlled Thermal Stability of Photochromic Systems Based on Six-Membered Ring as Ethene Bridges, International Symposium on Electronic/Optic Functional Molecules, March 11-13, 2012.
9. Weihong Zhu, Liwen Song, **Yuheng Yang**, Shangjun Chen, He Tian. Novel photochromic naphthopyrans containing naphthalimide units: high colorability,

- reversibility and fatigue resistance. 6<sup>th</sup> International Symposium on Organic Photochromism. Yokohama/Japan, October 17–21, **2010**.
10. Weihong Zhu, Shangjun Chen, **Yuheng Yang**, Liwen Song, He Tian. Novel photochromic systems based on benzothiadiazole or benzothiophene unit: photochromic reactivity in solutions and in single crystals. 6<sup>th</sup> International Symposium on Organic Photochromism. Yokohama/Japan, October 17–21, **2010**.
11. 朱为宏, 孟宪乐, 马哨庆, **杨玉衡**, 田禾, 含萘酰亚胺单元的二噻吩乙烯类化合物, 中国发明专利, ZL200710172531.9 (2007年12月19日申请; 公开日2008年8月13日, 公开号CN101239976A; 授权日2010年6月9日, 授权公告号CN101239976B)
12. 朱为宏, 孟宪乐, 张晓民, **杨玉衡**, 徐敏, 甘家安, 兰文田, 田禾, 含2,1,3-苯并噻二唑单元的二噻吩乙烯类化合物, 中国发明专利, ZL200910047158.3 (2009年3月6日申请, 公开号: CN101497610, 公开日: 2009.08.05; 授权日2011年5月11日, 授权公告号774839)

## Acknowledgements

I would like to extend my gratitude to Prof. Weihong ZHU and Prof. Keitaro NAKATANI for their enduring support and patience throughout my rewarding five years. Their rigorous attitude of scholarship and profound understanding in functional materials has created an excellent atmosphere of learning, which have helped me a lot with setting clear purpose in experiment and thought in a scientific way. Their passion and aspiration for scientific research have encouraged me to analyze and solve the problem alone with suitable methods and technology. The thesis presented here could not be finished without their valuable and detailed suggestions.

In addition, China Scholarship Council has covered my expenditures throughout the 18 months in École Normale Supérieure de Cachan Paris, France. Thank Prof. Academician He TIAN and Dr. Rémi MÉTIVIER for their valuable suggestions and discussion.

I have been lucky to be surrounded by intelligent and dedicated lab mates. In particular, I have benefited immensely from Dr. Bo LIU for the organic synthesis, from Rémi MÉTIVIER and Qiong ZHANG for the fundamental and profound optical knowledge and theoretical calculation, from Prof. Keitaro NAKATANI, Prof. Ledoux ISABELLE, Castro Beltran RIGOBERTO, ANU for their continuous support in the measurement of EFISH and HRS, from Prof. Yongshu XIE for his kindness to resolve the crystal structure, from Technician Brosseau ARNAUD and Stéphan for numerous knowledge in the building up and insight structure and specific function of TCSPC, vapor deposition, photolysis continue and NMR technology.

I'd like to thank Patra ABHIJIT, yibin RUAN, Piard JONATHAN, Liwen SONG, Shangjun CHEN, Yue WU, Wenlong LI for being such pleasant and dedicated collaborators and their abundant discussion as well as my evolving scientific ideas.

Greatest gratitude should be extended to Qin ZHOU, Xiaoqian XU, Jian CHEN, Yao WANG, Zhenzhen YI, Fangzhou ZHANG, Zongwei TANG and those who helped me greatly during my 18 months in Paris for their continuous support in my daily life.

Finally, my family has been supportive throughout my entire five years that should be remembered and cherished.

The thesis presented has been supported by NSFC/China (20976049, 61077085), National 973 Program (2011CB808400), the Oriental Scholarship, SRFDP 200802510011, and the Fundamental Research Funds for the Central Universities (WK1013002). China Scholarship Council and PHENICS international network (CNRS GDRI93) gave financial support for the collaboration

Author: Yuheng YANG

2012. 4. 20